THE STRUCTURE AND PROPERTIES OF QUENCHED IRON-NITROGEN ALLOYS.

by

T. BELL

A thesis submitted in partial fulfilment of the requirements for the degree of Doctor in Philosophy in the University of Liverpool.

ACKNOWLEDGEMENTS.

The author would like to thank Professor W.S. Owen for his overall supervision of the project and in the preparation of this thesis.

The author also wishes to thank his colleagues Messrs D. Atkinson, D. Brough, R.G. Bryans, M.J. Roberts and E.A. Wilson for their critical comments and helpful discussions at various stages of the work.

Thanks are also extended to all the members of the technical staff, especially to Mr. B. Wynne of the Photographic Section, for their assistance.

The tenure of a B.I.S.R.A. financial award is gratefully acknowledged.

Finally the author would like to express his sincere thanks to his family, in particular his mother, for their encouragement over the years.

ABSTRACT

A series of homogeneous martensitic iron-nitrogen alloys containing up to 2.7 w/o nitrogen have been prepared in the form of 0.010" diameter wires and 0.010" thick strip by nitriding in the austenite phase field and subsequently quenching into brine.

Optical metallographic studies have shown that at low nitrogen contents a cubic massive martensite is formed and at high nitrogen concentrations mixtures of acicular martensite and retained austenite result. By transmission electron microscopy it has been shown that the massive martensite has a substructure consisting of packets of parallel laths with a high dislocation density, while the high-nitrogen martensite has mainly an internally twinned substructure. Lattice parameter measurements of the austenite and martensite phases as functions of composition have been made. The variation of the volume fraction of austenite retained in the alloys has been carried out using an X-ray technique. Thermal analysis and resistivity techniques have been applied to the iron-nitrogen alloys to find the variation of the experimental M_s temperature with nitrogen concentration. The hardness and strength of

the quenched products have been studied also.

The experimental data are compared with parallel data for iron-carbon alloys. They are discussed in terms of Zener ordering, the lattice strains associated with the interstitial atoms, the current ideas about the classification of martensite morphologies, the thermodynamic models of Zener and of Fisher, and the more recent models of Kaufman, Radcliffe and Cohen.

LIST OF SYMBOLS.

The following list is of the symbols used throughout the thesis. Deviations from the list or additional symbols are specifically defined in the text.

a or a_o	.....Lattice cell dimension in 100
C or C_o	.....Lattice cell dimensions in 001
α	.....Ferrite
α'	.....Martensite
γ	.....Austenite
γ'	.....Gamma iron nitride
ε	.....Epsilon iron nitride
i	.....Component 1,2,3 etc usually carbon or nitrogen.
C_i	..... Atom fraction of component i.
$^a/_o$	..... Atom percent.
$^w/_o$	..... weight percent
$^a/_{100}$	..... Interstitial atoms per 100 iron atoms.
x	..... Concentration of interstitials expressed in $^a/_{100}$
$\bar{x}$	..... ratio of interstitial atoms to iron atoms.
$\bar{n}$	..... number of nitrogen atoms per unit volume.

n	.....	number of interstitial sites per host iron atom.
k	.....	Boltzman's constant.
H_m	.....	Reichart Microhardness number.
V.H.N.	.....	Vickers Hardness Number.
D	.....	Density of X-ray film
Φ	.....	Galvanometer scale deflection.
I_+	.....	Intersity of X-radiation.
I_γ	.....	Integrated intensity of an austenite reflection.
$I_{\alpha'}$	.....	Integrated intensity of a martensite reflection.
"R"	.....	Factor used in evaluation of integrated intensities.
t	.....	Time.
T	.....	Temperature
K	.....	Internal friction conversion factor
Q^{-1}	.....	Internal friction
δ	.....	Logarithmic decrement.
A_f	.....	Thermal arrest in a cooling curve at the onset of fine pearlite formation.
A_r''	.....	Martensite transformation start temperature M_s.
M_s	.....	Martensite transformation start temperature

T_o	..... Temperature at which the free energy of austenite and martensite are equal.
ΔE	..... Elastic strain energy term in Zener thermodynamic analysis.
G_*	..... Decrease in free energy on ordering of martensite from a b.c.c. to a b.c.t. lattice.
γ_N^γ	..... Activity coefficent of nitrogen in austenit
γ_N^α	.... in ferrite
γ_C^α	.... carbon .. ..
γ_C^γ	.... austenite
H_N^γ	..... Heat of solution of nitrogen in austenite
$\Delta G^{\gamma \to \alpha}$	..... Free energy change accompanying the austenite to ferrite transformation.
$\Delta G^{\gamma \to \alpha'}$	..... Free energy change accompanying the austenite to martensite transformation.
σ_f	..... Flow stress
σ	..... applied tensile stress.
$\bar{z}$	..... Number of iron atoms per unit cell
z^γ	..... Exclusion parameter of austenite
z^α	..... Exclusion parameter of ferrite.
z	..... Zener ordering parameter.
T_c	..... Critical temperature for Zener ordering.

CONTENTS.

INTRODUCTION

A vast amount of both theoretical and experimental research into the nature and structure of interstitial ferrous martensites has been carried out over the last 50 years. The major part of this work has been concerned with carbon as the interstitial alloying element. There has been some work done on iron-boron alloys, but because of its limited solubility in the face centred cubic austenite phase, these investigations have necessarily been restricted. Even less work has been done with nitrogen as the interstitial alloying element and most of this has been restricted to work with iron-nitrogen; the only reliable work on bulk specimens being confined to that reported by Bose and Hawkes[1] and some unpublished work by Maxwell and Jack[2]. Some good electron diffraction analyses of iron-nitrogen martensite have been carried out by Pitsch[3,4] on a few nitrided evaporated thin foils.

The major deterent to work on nitrogen alloys has been the difficulty of systematically and reproducibly obtaining homogeneous alloys over a wide range of nitrogen content in a form suitable for physical metallurgy experiments.

The object of the work described in the thesis was to investigate several aspects of the properties of quenched iron-nitrogen alloys with a view to establishing the general crystallographic, morphological and kinetic features of iron-nitrogen martensites. It was then possible to obtain some understanding of the role of the interstitial atom, in the formation and properties of martensite by comparing the iron-nitrogen and iron-carbon systems.

The detailed objectives were:

1. The preparation of quenched homogeneous iron-nitrogen alloys in a form suitable for the measurement of certain physical and mechanical properties.
2. The determination of the crystal structure and lattice parameters of the quenched alloys by X-ray diffraction.
3. A limited study of the hardness and strength of the quenched alloys.
4. A morphological study of the alloys by optical and electron microscopy over a wide range of nitrogen contents.
5. The determination of the variation of transformation temperatures with nitrogen content by high-speed thermal analysis and electrical-resistance methods.
6. The determination of the effect of nitrogen on the volume fraction of retained austenite.

7. A thermodynamic study of the iron-nitrogen martensite transformation.

It is proposed to depart from the perhaps more generally accepted sequence of presentation. In the first part of the thesis a complete but necessarily short review of all previous work on iron-nitrogen martensite and related structures is presented. Each of the objectives mentioned previously are dealt with in individual sections. Each section covers the appropriate previous work on iron-carbon martensite and contains sections on (a) experimental techniques, (b) results, (c) discussion of the results and (e) detailed conclusions. After the section on Thermodynamics there is a general discussion followed by an overall conclusions section.

1. REVIEW OF IRON-NITROGEN LITERATURE

1.1 Introduction

It was Fry[5] in 1923 who first showed that iron-nitrogen austenite, when cooled sufficiently rapidly to prevent diffusional decomposition, transforms to martensite similar to that found in quenched carbon steels. The product martensite had been identified in steels about thirty years earlier by A. Martens, after whom Osmond[6] named the product in 1895.

1.2 Iron-Nitrogen Phase diagram

A serious interest in the iron-nitrogen system was taken in the 1930's in Germany, when several workers[7-10] including Lehrer,[11] attempted to establish the metastable iron-nitrogen phase diagram. In 1950 Paranjpe, Bever, Floe and Cohen[12] studied the iron-nitrogen phase diagram using an X-ray diffraction technique with iron-nitrogen powder alloys. Their results, which resemble in form those of Lehrer, are given in Figure 1. The main differences compared with the Lehrer work are in the composition limits of the various phases. The diagram given in Figure 1 is today still thought to be essentially correct.

Atkinson[13] has shown very recently that slight alterations of the $\alpha+\gamma/\gamma$ boundary are necessary in view of his activity measurements of nitrogen in austenite. Rawlings and Tambini[14] using an internal friction method have shown that the limits of the $\alpha/\alpha+\gamma$ boundary occur at somewhat lower nitrogen concentrations that those obtained by Paranjpe et al[12] using a gas equilibrium method. The maximum solubility of nitrogen in ferrite was found to be 0.10^{W}/o by the internal friction method compared with 0.11^{W}/o by the gas equilibrium method. The points of interest in relation to the transformations from the gamma phase are;

(a) The eutectoid temperature is 591^{o}C

(b) The eutectoid composition is 2.35^{W}/o nitrogen

(c) The maximum solubility of nitrogen in austenite is about 2.8^{W}/o at 650^{o}C.

1.3 Previous X-Ray Diffraction and Morphological Studies

Jack[15] in 1951 produced a few martensitic iron nitrogen powder alloys by nitriding with ammonia hydrogen mixtures. With these he carried out a detailed structural X-ray diffraction analysis and showed that iron-nitrogen martensite containing about 2.2^{W}/o nitrogen was structurally analogous to high-carbon iron martensites.

Jack[16] also showed that when these alloys are tempered a structure with an expanded body centred tetragonal cell is formed. This is a transition nitride $Fe_{16}N_2$. The stable nitride is face centred cubic Fe_4N.

Morphological studies of phase transformations in high nitrogen alloys have been undertaken by Kontorovich and Yemel' Ianova[17]. However their alloys were extremely inhomogeneous, consequently they were not able to study iron-nitrogen martensites in a satisfactory manner. The only other work is that of Bose and Hawkes[1] who studied phase transformations in the eutectoid alloy. They studied mainly the "braunitic" eutectoid transformation, using metallographic techniques, on strip specimens 0.125 mms thick. In addition to the eutectoid alloy (2.35^W/o nitrogen), they also quenched a 1.85^W/o nitrogen alloy from the austenite region to produce mixtures of acicular martensite and retained austenite. They deduced that the M_s temperature of the 1.85^W/o nitrogen alloy was higher than the M_s temperature of the 2.35^W/o nitrogen alloy, which was about 35^{o}C. They also showed that the $\frac{c}{a}$ ratio of the lattice parameters for the 1.85^W/o nitrogen martensite alloy was 1.07, while that for the 2.35^W/o nitrogen alloy was 1.09.

The average hardness of the lower nitrogen alloy was 700 Knoop and that of the more concentrated alloy 640 Knoop.

Pitsch[3,4] has looked at the products of the martensitic transformation in thin films of iron-based alloys and included in this work was an iron-nitrogen alloy. He carried out no systematic work to determine the exact conditions to produce the martensite. The alloy examined contained 1.5 w/o nitrogen. It was prepared by nitriding an evaporated polycrystalline iron foil at 670°C with a 5% ammonia-hydrogen mixture. During nitriding the alloy was just in the austenitic region and on quenching a mixture of marteniste and retained austenite was produced. The martensite formed in irregular volumes, made up of parallel plates or laths (called "fibre crystals" by Pitsch) which were twin related to each other. Figure 2 shows the structure of the martensite and Figure 3 is the corresponding electron diffraction pattern. The twin plane was $\{112\}_{\alpha'}$ and the major axis of each plate was parallel to $<111>_{\alpha'}$ and normal to $\{110\}_{\alpha'}$. The orientation relationships deduced from the electron diffraction data were $[\bar{1}10]_{\gamma} \parallel [11\bar{1}]_{\alpha'}$ and $(110)_{\gamma} \parallel (112)_{\alpha'}$. These are different from the orientation relationships found in other martensites thinned from bulk specimens.

He explained the difference by supposing that the crystallography of the transformation is modified by the reduced elastic constraint to the growth of a plate in a thin foil compared with a bulk specimen. There are no electron microscopy reports in the literature of the internal structure of acicular martensite plates in bulk specimens of quenched iron-nitrogen alloys.

2. SPECIMEN PREPARATION

2.1 Starting Material

To ensure that the effects of nitrogen were not marked by the presence of another interstitial, carbon the starting material was decarburised to as low a carbon concentration as possible. The initial materials were two "pure"irons supplied by B.I.S.R.A.

Material 1 ACN 2 in the form of 0.100" diameter wire containing 0.015^{W}/o C.

Material 2 ACN 2 in the form of 0.040" strip containing 0.0177^{W}/o C.

They were both decarburised in wet hydrogen in an impervious alumina tube, (1) at 700^{o} C for 110 hours while (2) was at 950^{o} C for 170 hours[18]. The resulting carbon contents were,

Material 1 0.008^{W}/o C analized by B.I.S.R.A.

Material 2 0.0047^{W}/o C analized by L. Messulam of this department using an oxidation technique. The iron is heated at 1400^{o} C with litharge in a porcelain boat. The carbon is oxidized to carbon dioxide which is dried and then solidified in glass coils immersed in liquid air. The carbon dioxide is then allowed to gasefy and its volume is measured at constant temperature and pressure.

The weight percent carbon is then deduced by comparison with standard low carbon steels. Material (1) was drawn to 0.010" diameter wire for X-ray diffraction, resistivity and thermal analysis experiments; while material (2) was cold rolled to 0.010" thick for the morphological studies. Two further supplies of pure iron were later obtained from B.I.S.R.A. and fabricated to the above dimensions. The analyses of all four "pure" irons together with their initial heat treatment are listed in Table 1.

2.2. The Nitriding Process.

There are two gas-solid equilibria in the iron-nitrogen system which have to be considered, the equilibrium between nitrogen gas and the metal,

$$N_2 \rightleftharpoons 2N \text{ in Fe} \qquad (2.1)$$

and the equilibrium between ammonia gas and the metal.

$$NH_3 \rightleftharpoons N \text{ in Fe} + \tfrac{3}{2} H_2 \qquad (2.2)$$

The first equilibrium, at one atmosphere of nitrogen, is shown as a function of temperature in Figure 4. The solubility of nitrogen under these conditions is very small and is much less than the concentration needed to saturate iron at any temperature. Ammonia has a greater nitriding potential than nitrogen gas and by varying the partial pressure of ammonia from 0 to 0.8 atmospheres

the solubility of the phases occuring between 0-12^{w}/o nitrogen at temperatures up to 900^{o} C can be determined. As mentioned previously, Lehrer[11] and later Paranjpe et al[12] determined a substantial part of the iron nitrogen metastable phase diagram. (0-12^{w}/o N: 450-700^{o} C) The phases delineated being metastable with respect to nitrogen gas at one atmosphere pressure. Figure (1).

In order to produce a range of iron-nitrogen alloys in the austenitic condition by nitriding with hydrogen/ ammonia mixtures, temperatures in the range 600-910^{o} C are required. However above 600^{o} C the thermal dissociation of ammonia becomes appreciable,

$$2NH_3 \rightleftharpoons 3H_2 + N_2 \qquad (2.3)$$

and at 700^{o} C for example, the partial pressure of ammonia in equilibrium with nitrogen and hydrogen is only 10^{-5} atmospheres in a closed system and hence the nitriding potential is very small. However, with a straight-through system, such that a continuous stream of gas is passed over the heated specimens, the gas does not reach internal equilibrium and a higher partial pressure of ammonia over the specimen can be achieved. The extent of the thermal dissociation can be reduced by increasing the flow rate, but too high a gas flow cannot be used since it would cool the specimens below the furnace temperature.

Initial experiments with 1¼ inch diameter furnace tube showed that the optimumim flow rate is about 11 litres per hour and this flow rate was used in all subsequent experiments.

2.3 The Nitriding Apparatus and Procedure.

The nitriding apparatus is illustrated diagramatically in Figure 5. The hydrogen and ammonia gases were dried with silica Gel and metered seperately to enable the composition of the mixture to be controlled accurately. The excess pressure was bubbled off through oil reservoirs placed before the flow meters. The sensitive control of the rate of flow, ± 0.01%, was achieved by varying the depth of oil in the blow off bottles. The gases were mixed by passing them through a glass bulb packed with silica gel crystals, which also completed the drying of the gases. The nitriding mixture was then led down through a vertical quartz furnace tube held in a three part Vacrome wound furnance. The furnace had a hot zone 12 cms long in which the temperatures up to 910° C could be maintained to ± 2° C, using an external Chromel-Alumel thermocouple down the side of the furnace tube. This was calibrated for each run by means of an internal Platinum- Platimum 13% Rhodium thermocouple adjacent to the specimens.

The pure iron specimens, either in the form of wires or strip up to 0.010" diameter or thickness respectively, after degreasing and cleaning were suspended from a 0.125" diameter stainless steel rod which passed through a rotary vacuum seal at the top of the tube. Loading of the specimens took place from the bottom of the furnace in an atmosphere of pure nitrogen. After sealing the bottom of the tube with the quenching liquid, the nitrogen gas was allowed to flow for a further five minutes in order to completely purge the furnace and glass assembly of any traces of oxygen. After this time the nitrogen was switched off and the hydrogen admitted. The specimens were then raised on the bottom of the rod and suspended in the hot zone in hydrogen for ten minutes, to remove any trace of surface oxide since this impairs the nitriding procedure[19]. Then the ammonia gas was admitted to give the predetermined ammonia-hydrogen mixture. After leaving the bottom of the furnace the gas mixture was analized for ammonia to give the ammonia concentration in equilibrium with the specimens. The nitriding process took up to 12 hours. When completed the specimens were plunged to the bottom of the furnace into the quenching liquid, the quench taking less than two seconds. In order to obtain specimens over a wide range of nitrogen content two routes were explored:

1. The gamma phase is unstable below 590° C (Lehrer 1930 Figure 1) and nitriding at lower temperatures produces a shell rich in γ' (Fe_4N) with a ferritic matrix, characteristic of commercial nitriding treatments. Alloys containing 1.7 w/o nitrogen were prepared by exposure to a 20% ammonia/hydrogen mixture at 580° C. The specimens were not homogeneous and it was necessary to remove the steep nitrogen gradient between the γ' shell and the core. No satisfactory homogenising treatment was found. For example, annealing the 1.7 w/o nitrogen alloy in sealed evacuated quartz capsules at 1050°C resulted in an alloy with only 0.18 w/o nitrogen. As a result of these initial experiments this method was abandoned.

2. The second route, which was completely successful, consisted of nitriding in the γ phase field in the temperature range 650-910° C and quenching directly from the nitriding atmosphere. This more direct method resulted in martensitic specimens which could be used immediately for further experiments without reaustenitising and quenching.

2.4 Results and Discussion.

The degree of dissociation of the ammonia depends not only upon temperature and flow rates as discussed earlier but also upon the prevailing catalytic conditions.

Quartz the material of the furnace tube is not a catalyst for the dissociation[12] and the specimens themselves and the steel suspension rod provide the only catalytic surfaces. It is therefore reasonable to assume that no more dissociation occurs after the gas has passed the specimens and consequently that the composition of the exhaust gas is that of the nitriding gas over the specimens. For constant experimental conditions the composition of the exhaust gas, though different from the composition of the inlet gas is controlled by the inlet composition. The composition of the inlet nitriding mixture is decided by the relative flow rates of the individual gases. Therefore it is essential to control carefully these individual flow rates. In the present situation it was found that the usual combination of needle valve and pressure reducer unit on the gas cylinders did not give adequate pressure control, because, especially with the ammonia, the pressure varied somewhat with variations in the ambient temperature. The difficulty was overcome by using pressures in excess of those required and bubbling off the excess pressure through oil to exhaust.

The composition of the exit gas indicates the nitriding potential which is represented by

$$r = \frac{PNH_3}{(PH_2)^{3/2}} \times 10^2 \qquad 2.4$$

In figure 6 the parameter γ is plotted as a function of the nitrogen concentration in the alloy for two nitriding temperatures 660° C and 810° C, (Figure 6 has been reproduced from the technical note by D. Atkinson, T. Bell and D. Brough in Journal of the Iron and Steel Institute, August, 1965.) From these data any iron-nitrogen alloy in the austenite range can be reproduced by control of the exit gas composition. The 660° C data shows a discontinuity at $\gamma = 12$ and the 810° C data at $\gamma = 9$. At these values of the gas is in equilibrium with the $\gamma + \varepsilon$ and a rim of ε - iron nitride is formed on the surface of the specimen.

After some practice it was found possible with the present apparatus to prepare alloys of approximately the desired composition with just a knowledge of the inlet composition and furnace temperature. The higher temperatures around 900° C and fairly low ammonia concentrations were used to produce the low nitrogen alloys, while temperatures of 650° C were required for the high alloy concentrations. In all the experiments care had to be taken to use the correct combinations of ammonia-hydrogen mixtures and temperature to avoid two phase regions.

In the initial experiments the specimens were quenched into oil, but the rate of cooling was insufficient to prevent some diffusional transformation taking place at the grain boundaries.

Figure 7 shows this grain boundary transformation product in a 1.8^{W}/o N_2 alloy. Carbon replicas were prepared of the surface of such oil quenched alloys but whether the diffusionally transformed regions are of either a braunitic or bainitic nature could not be determined. Figure 8 is a single stage carbon replica of the grain boundary transformation product. (At present a detailed investigation in to the existance of a nitrogen bainite and its morphology is being undertaken in the department.)

A satisfactory quench producing a diffusionless transformation was obtained by replacing the oil with brine covered with di-n-butyl phthalate to prevent absorption of the ammonia. Quenching into the liquid resulted in a fully martensitic structure in the low nitrogen alloys and a mixture of martensite and retained austenite in the higher nitrogen alloys up to about 2.4^{W}/o nitrogen. Alloys containing more than 2.4^{W}/o nitrogen were fully austenitic on quenching to room temperature.

In order to ensure homogeneity the temperature must be kept constant along the length of the specimen during the time of nitriding. Only when all the variables, flow rate, temperature and gas composition are carefully controlled can homogeneous specimens be obtained reproducibly. The homogeneity of the specimens was checked by metallography, by microhardness measurements along the length and across a transverse section, by analysis for nitrogen, by the

Kjehdal method, of successive layers of the specimen dissolved in hydrochloric acid, and by X-ray diffraction analysis of successive layers.

The nitrogen content of the specimens was calculated from the weight gain and checked by the Kjehdal steam - distillation method, which is estimated to be accurate to $\pm$ 2%.

2.5 Chemical Analysis for Nitrogen

The method used is that developed by Kjehdal for the determination of nitrogen in organic compounds. It depends on the conversion of nitrogen to the ammonium salt during solution of the metal in acid, followed by distillation of ammonia from the salt in the boiling alkali and determination of ammonia in standard acid. There are 3 main steps:

1. Solution of sample. The iron-nitrogen alloys analysed by this method contained no appreciable amount of strong nitride formers such as silicon and boran, and they were in the hardened condition. It is therefore sufficent to use 1:1 hydrochloric acid as a solvent to ensure the conversion of all the nitrogen available to an ammonium salt.

Depending on the nitrogen content 0.05 to 0.3 gm of clean grease-free alloy are weighed and transfered

to a small round bottomed flask. 10 mls of HCl are added and the sample is dissolved with the minimum of heating, a long reflux air condenser being fitted to the flask. All the nitrogen in the alloy is converted to ammonium chloride and retained in solution.

2. Separation of ammonia. The ammonia is separated by steam distillation from a boiling alkali solution. Ground glass joints are fitted throughout, sealed with water not grease. Deionised water is used for all solutions and washing.

A 3 litre glass boiler heated by two 500 watt immersion heaters sheathed in silica, feeds steam to two distillation flasks. When required the steam can be directed to the atmosphere by the hollow glass tubes shown in Figure 9. The distillation flasks are each set in 750 watt mantle heaters. All heaters are connected to the mains via variacs so that the rate of distillation can be controlled with precision. All 3 glass flasks are fitted with dropping funnels providing entry for reagents and, in the case of the boiler, also acting as safety valves against pressure build up. Water cooling jackets condense the ammonia and as it is steam distilled off it is collected in the titration flasks via the guard tubes. The steam distillation apparatus is illustrated in Figure 9.

The standard procedure adopted for the separation of ammonia is as follows:

Each distillation flask is half filled with 40% sodium hydroxide solution and the glassware is cleaned internally by passing steam through the apparatus until no ammonia is distilled over as indicated by Nesler's reagent.

The acid solution of alloy and washing is added to the sodium hydroxide solution in one of the distillation flasks via the dropping funnel, while the steam flow is temporarily diverted. Distillation is now carried out at a rate such that 100-150 ml of the distillate are collected in 45 minutes. Transfer of caustic soda to the distillate is largely avoided by the inclusion of a three bulb air condenser before the water condenser. It has been reported that using this technique no trace of caustic soda appears in the distillate until the volume of distillate exceeds 150 mls. (20)

Distillation using 10 ml of standard ammonium chloride solution dissolved in 10 ml 1:1 HCl and then distillation using 20 mls of standard ammonium chloride solution disolved in 10 ml 1:1 HCl is carried out before and after each batch of specimens as a check on the blank distillation value and the accuracy of the method.

3. Determination of Nitrogen. Four drops methyl red screened with methylene blue are added to the distillate which is then titrated against standard (0.005N) hydrochloric acid. From this titre, the blank titre is deducted. The weight of nitrogen in the specimen can be calculated directly from the corrected titre using the fact that 1 ml of 0.005N HCl is equivalent to 7×10^{-5} grams of nitrogen. By subtracting the titre due to the distillation of 10 ml of standard ammonium chloride solution from that due to the distillation of 20 ml of the standard ammonium chloride solution, the true titre corresponding to 10 ml of the standard solution is found. This is a check on the accuracy of the method. By subtracting this resultant titre from that actually obtained with 10 Ml of standard solution the blank is obtained. The blank is always in the range 0.05 to 0.15 ml of standard hydrochloric acid. The accuracy and reproducibility of the method was found to be $\pm$ 2%.

2.6 Chemical Analysis for Ammonia.

To determine the ammonia content of the exit gas a known volume was entrapped in a calibrated glass vessel, About 200 mls of a 4% solution of boric acid was introduced into the calibrated volume to absorb the ammonia gas. Separate 10 ml lots of the solution were then passed

from the calibrated volume into flasks, these were each titrated against a standardised solution of hydrochloric acid using Bromcresol Green indicator. The ammonia concentration was obtained by dividing the number of millilitres of standard acid used in the titration by the number of millilitres calculated for 100% ammonia using the perfect gas law. By this method the percentage ammonia was analysed reproducibly to $\pm$ 0.1% in the range of 0-15% ammonia. As a check, occasional tests were taken on pure ammonia, obtained by by-passing the furnace, and it was always found that these samples analysed 99.5 $\pm$ .05% nitrogen.

3. LATTICE PARAMETER MEASUREMENTS.

3.1 Introduction

X-ray diffraction studies of the crystal structure and lattice parameters of iron-nitrogen austenite and martensite have been carried out by K.H. Jack[15] on a limited number of alloys prepared as powders. He showed that iron-nitrogen austenite is isostructural with iron-carbon austenite. Petch[21] showed that in iron-carbon austenite the carbon atoms occupy the octahedral interstices in gamma iron in a statistically random manner. The octahedral sites in gamma iron are illustrated in Figure 10. These $\frac{1}{2}$, 0, 0 and $\frac{1}{2}\frac{1}{2}\frac{1}{2}$ type positions are therefore, also randomly occupied by nitrogen atoms in iron-nitrogen austenite. At the limit of solubility of carbon in gamma iron only one in twelve of the octahedral sites are occupied, but for the most concentrated iron-nitrogen austenite ($\simeq 2.7^{w}/o$ nitrogen) one in nine sites are occupied by nitrogen atoms. Jack[15] also showed that concentrated iron-nitrogen martensites in powder form are structurally analogous to high carbon martensites. Petch[22] in 1943 deduced from spatial considerations that the observed tetragonality of iron-carbon martensite is consistent with the occupation by carbon atoms of the octahedral interstices at the mid

points of the C edges and at the centres of the C faces of the body centred tetragonal cell. In 1944 Lipson and Parker[23] interpreted intensity measurements of X-ray diffraction patterns of bulk specimens as indicating that the iron atoms are displaced from their lattice points by 0·18A° in the C. direction, the displacements being due to the presence of carbon atoms located in precisely the positions suggested by Petch[22]. The structure of tetragonal martensite is shown in Figure 11.

If the carbon and nitrogen atoms do not occupy a specific set of the octahedral interstices but are randomly distributed in all three sets of octahedral sites then a body-centred cubic lattice structure results. Cubic martensite has been observed by Honda[24] in iron-carbon alloys with up to 0.5 w/o C while a similar highly supersaturated body-centred cubic iron-nitrogen martensite has been shown to exist by Dijkstra[25]. Maxwell[2] has also found some low nitrogen alloys, to be cubic. The lattice parameter measurements made by Jack[15] on iron-nitrogen austenitic and martensitic powders are presented in Figures 12, 13, & 14. The results by Bose and Hawkes[1] for two high nitrogen alloys in bulk form are also presented. All the martensitic alloys studied by Jack[15] and by Bose and Hawkes[1] were tetragonal.

3.2 Experimental Method

A series of iron-nitrogen alloys containing between 0 and 2.7 w/o nitrogen were prepared in the form of 0.010" diameter wires, quenched from the nitriding atmosphere into brine at room temperature and further quenched to -196° C.

After pickling in hydrochloric acid to remove any trace of oxide the specimens were irradiated, at room temperature, for up to 12 hours, with iron-filtered Cobalt K radiation, in a Phillips 114.83 mm diameter Debye-Scherrer camera. The Straumanis unsymmetrical film loading technique was used and the specimen, which had been carefully centred, was rotated to enable the maximum number of crystals to be irradiated. The film, which was Ilford 'Industrial G', was developed for five minutes in a fine-grain developer, then fixed washed and dried.

The films showed negligible shrinkage and the lines on the films were measured with a standard vernier slider accurate to ± 0.005 mm. High angle doublets could not usually be resolved because of line broadening due to internal lattice strains and so a weighted Cobalt $K\alpha_1$ and $K\alpha_2$ radiation wavelength of 1.79021A° was used. The design of the camera was such that 2 mms on the film corresponded to 1° of Bragg angle.

3.3 Results and Discussion

The line positions were analysed by standard methods. The "pure" iron was body-centred cubic with fairly sharp lines. The lines broadened, but there was no line shift as the nitrogen content was increased. Line profile studies using a Hilger micro-photometer showed that at 0.7^{W}/o nitrogen a transition to a tetragonal structure occurred. The $110\alpha'$ reflection split to give the tetragonal doublet $101\alpha'$ and $110\alpha'$ and the intense $211\alpha'$ reflection split to give a weak $112\alpha'$ and an intense $211\alpha'$ line. As the interstitial content was further increased splitting was observed for all the lines. At about 1.1^{W}/o nitrogen face centred cubic lines corresponding to retained austenite were detected. A further increase of the nitrogen content resulted in an increased intensity of the retained austenite lines and at the same time the degree of tetragonality of the martensite increased. The transition from the b.c.c. phase to the b.c.t. and f.c.c. phases can be seen in the series of diffraction patterns reproduced in Figure 15. In Figure 16 a series of diffractometer tracings of the $\{110\}$, $\{200\}$ and $\{211\}$ martensite reflections are reproduced for alloys containing 0.0^{W}/o, 0.30^{W}/o, 0.64^{W}/o and 0.71^{W}/o nitrogen. It is clearly shown that as the nitrogen content is increased the line profiles broaden considerably

but there is no trace of line splitting at all in the first three alloys and then in the 0.71^{w}/o alloy the splitting of the lines can readily be seen. The $\frac{c}{a}$ ratio of this alloy is 1.027. If the lower nitrogen alloys were b.c.t. it should have been possible to detect the tetragonality. For example, if the 0.64^{w}/o nitrogen alloy had been tetragonal the $\frac{c}{a}$ ratio would have been 1.023, which is well within the range of values detectible by the technique used.

The lattice parameters of the body centred tetragonal martensite were deduced as accurately as possible. The limitation to the accuracy was set by the diffuseness of the lines and the lack of clear high angle lines. Using the method described below, the accuracy was $\pm$ .002A^{o}. An approximate $\frac{c}{a}$ ratio was obtained from the d spacings of the 002α' and 200α' reflections and this value was used in the equation

$$\sin^2\theta_{hkl} = \frac{\lambda^2}{4a^2}\left\{(h^2 + k^2) + \left(\frac{a}{c}\right)^2 l^2\right\} \qquad 3.1$$

for all hkl lines. The values of a so obtained were plotted against the Nelson-Riley function[27]

$$\frac{1}{2}\left\{\frac{\cos^2\theta}{\theta} + \frac{\cos^2\theta}{\sin\theta}\right\}$$ to give a_o at $= 90^{o}$

The value of C_o was obtained in a similar fashion from the equation

$$\sin^2 \theta_{hkl} = \frac{\lambda^2}{4c^2} \left\{ (h^2 + k^2) \left(\frac{c}{a}\right)^2 + l^2 \right\} \qquad 3.2$$

Figure 17 illustrates the application of the Nelson-Riley extrapolation technique for the determination of the lattice parameters of martensite and austenite in an alloy containing 2.35^{W}/o nitrogen. The data for this graph are given in Table 2 and the results are $C_o = 3.102 \pm .002A^o$ and $a_o = 2.849 \pm .002A^o$ for the martensite, and $a = 3.635 \pm .002A^o$ for the austenite.

The variation of the iron-nitrogen martensite lattice parameters a_o and C_o as a function of intersitial content is shown in Figure 13. The straight lines in Figure 13 corresponds to the average lattice parameters of iron-carbon martensites taken from the collected data of C.S. Roberts[28]. These data were converted from Kx units to Angstroms by using the factor 1.00202. All the lattice parameters are expressed in Angstroms. The abscissa of Figure 13 is labelled "Interstial atoms per 100 Iron atoms". (In the text the abbreviation $^{a}/_{100}$ is used). This method of indicating interstitial concentrations is preferred to weight or atomic percent, when considering cell dimensions. This is because the number of available interstices is a simple multiple of the number of iron atoms.

The equation of the lines corresponding to the variation of the lattice parameters of the carbon martensite with interstial content are,

$$C_o = 2.866 + 0.0246x \quad 3.3$$

$$a_o = 2.866 - 0.0026x \quad 3.4$$

where x is $^a/_{100}$. These fit the carbon data in the range $2.8^a/_{100}$ to $8^a/_{100}$.

The least squares equations of the present results on iron-nitrogen martensites for the C and a parameters as a function of interstitial content are,

$$C_o = 2.868 + 0.024x \quad 3.5$$

$$a_o = 2.865 - 0.0019x \quad 3.6$$

They fit the nitrogen data in the range $2.8^a/_{100}$ to $11^a/_{100}$. By comparison of equations 3.3 and 3.4 with equations 3.5 and 3.6 it can be seen that the nitrogen data follow virtually the same linear relations, between lattice parameters and interstitial content as do the iron-carbon martensites. Because of the greater solubility of nitrogen, the linearity can be tested to appreciably greater interstitial content than in the iron-carbon case and, as can be seen from Figure 13, the linearity was found to hold up to the maximum concentration of nitrogen that could be achieved experimentally ($2.7^w/o$ nitrogen).

In both the iron-carbon and the iron-nitrogen system the transition from a body centred cubic to a body-centred tetragonal structure occurs at about $2.8^{a}/100$.

Figure 14 shows the variation of the ratio of the lattice parameters of the iron-nitrogen martensite with increasing nitrogen content as well as the data of C.S. Roberts[28] on iron-carbon martensites and it can be seen that they both fit the equation

$$\frac{c}{a} = 1 + 0.0093\ x \qquad 3.7$$

in the ranges of nitrogen and carbon contents specified above.

The lattice parameters of the austenite phase were determined in the range $1.2^{w}/o$ to $2.7^{w}/o$ nitrogen using the extrapolation technique of Nelson and Riley, and the variation of the austenite lattice parameter for this range of nitrogen contents is given in Figure 12. The data for iron-carbon austenites from C.S. Roberts[28] is plotted in terms of $^{a}/_{100}$ on the same graph. The iron-carbon austenite data extends only to about $\frac{7a}{100}$ and the straight line relation between the lattice parameter and the carbon content is

$$a_{o} = 3.555 + 0.0092\ x \qquad 3.8$$

The nitrogen data obey approximately the same linear relation, but on even better fit to the present nitrogen-austenite results is obtained with the least squares equation,

$$a_o = 3.564 + 0.0077\,x \qquad 3.9.$$

for the variation of the austenite lattice parameter with increasing nitrogen concentration. Equation 3.9 extrapolates to 3.56A° at zero nitrogen. This is very close to 3.57A° the value obtained for the lattice parameter of pure gamma iron when high temperature lattice parameter measurements of gamma iron are extrapolated to room temperature.(26)

3.4 Effective Diameters of carbon and nitrogen in iron.

The experimental results show clearly that the linear variation of lattice parameter with interstitial content is virtually the same for both iron-nitrogen and iron-carbon martensites. It must therefore be concluded that the average distortion per interstitial atom produced by nitrogen in the martensite lattice is the same as that produced by carbon. This contradicts the assertion, made by Cohen(29) in the 1963 Hatfield Memorial Lecture, that interstitial nitrogen creates less disturbance in the martensite lattice than does interstitial carbon. This statement was probably based on the covalent values of atomic radii given in Goldschmidt's tables. The Goldschmidt radius for carbon is 0.77A° while for nitrogen it is 0.71A°.

3.4.1 Atomic radii of carbon and nitrogen in martensite.

Lipson and Parker in 1944[23] pointed out that a maximum of 1 in 12 octahedral interstices are occupied by carbon atoms in iron carbon martensite and because of the presence of the carbon atoms the structure factor of the martensite will be altered. From a calculation of the structure factor using prescise intensity measurements of the martensite tetragonal doublets Lipson and Parker[23] deduced that the mean displacement of the iron atoms was 0.17A° to 0.20A°. Jack[15] similarly showed that the mean square displacements of the iron atoms in an <001> direction due to the presence of nitrogen atoms, in iron-nitrogen martensite was 0.167A° with a probable error of ± 0.004A°. Using observed lattice parameters of nitrogen martensite or a function of concentration and the above value for the root-mean-square displacement of the iron atoms. Jack[15] calculated values for the maximum and minimum nitrogen atom radius in martensite, these are 0.79A° and 0.61A° respectively.

With the present lattice parameter results given in Equations 3.5 + 3.6 and using the value of 0.167A° for the root mean square displacement of the iron atom it is possible to derive, in a manner similar to Jack, upper and lower limits for the nitrogen atom radius.

For nitrogen martensite containing $10\frac{a}{100}$ the C dimension is $3.108A^{o}$. This is the average of the actual cell dimensions of all unit cells; some expanded by nitrogen atoms and some unexpanded. Thus assuming that each nitrogen atom displaces mainly the two neighbouring iron atoms, there will be 80 iron atoms out of the basis of 100 iron atoms with a displacement.

$$(\overline{U}^2)^{\frac{1}{2}} \leq \frac{C\alpha' - C\alpha}{2} \qquad 3.10$$

$$(\overline{U}^2)^{\frac{1}{2}} \leq \frac{3.108 - 2.866}{2}$$

Hence for 80 iron atoms the root mean square displacement in the [001] direction is

$$(\overline{U}^2)^{\frac{1}{2}} \leq 0.121A^{o}$$

$$\overline{U}^2 \leq 0.01464 \qquad 3.11$$

Because some of the unit cells containing no nitrogen may be distorted by neighbouring cells, the displacement values are probably less than given in Equation 3.11. From the results of Jack[15], the total of 100 atoms have a mean square displacement

$$\overline{U}^2 = 0.0280 \pm .0012A^{o} \qquad 3.12$$

Hence for the 20 iron atoms in expanded cells

$$\sum \overline{U}^2 \geq 100\ (0.0280) - 80(0.01464)$$

$$\sum \overline{U}^2 \geq 1.63 \qquad 3.13$$

Thus for each of these iron atoms.

$$(\overline{U}^2)^{\frac{1}{2}} \geq \frac{1.63}{20}^{\frac{1}{2}} \geq 0.286 \qquad 3.14$$

The distance between two iron atoms Δ_{fe} separated by a nitrogen atom is therefore

$$\Delta_{fe} \geq C_o + 2(0.286)$$

$$\Delta fe \geq 3.680A^o \qquad 3.15$$

Therefore the iron-nitrogen minimum distance is 1.84A°. Assuming the iron radius to be that for a co-ordination number 8 (1.24A°) then the nitrogen atom radius is greater than 0.60A°. This is a minimum value for the radius. The maximum value for the nitrogen atom radius may be determined by another approach, again taking 100 iron atoms as the basis.

50 unit cells have an average C dimension 3.108A°
while 40 unit cells have an average C dimension 2.866A°

Thus for 10 expanded unit cells.

$$\sum C \leq 50(3.108) - 40\ (2.866) \qquad 3.16$$

$$\sum C \leq 40.8\ A^o \qquad 3.16$$

For each of these 10 cells

$$C \leq 4.08A^o$$

The maximum iron-nitrogen distance is therefore $\leq$ 2.04A°
Hence the maximum nitrogen atom radius $\leq$ 0.80A°.

By these two methods of approach it is found that the minimum value of the nitrogen atom radius is 0.6A° and the maximum value is 0.8A°. The average value is 0.7 $\pm$ 0.1A°

which is the same value as found by Jack[15].

Jack[15] also estimated the maximum radius for a carbon atom in martensite to be 0.79A° and by a different method found a minimum radius of 0.86A°, using the results of Lipson and Parker[23]. The latter limit is obviously incorrect and Jack ascribed this to the inaccuracy of Lipson and Parker's intensity measurements, this is because they had not used crystal monochromated radiation.

3.4.2. Effective diameter of carbon and nitrogen atoms in austenite.

The effective diameters of carbon and nitrogen in austenite can be determined using a different method suggested by Speiser, Spretnak and Taylor[31]. They estimated the carbon atom radius in austenite to be 0.68A° and that of nitrogen 0.73A°. The lattice parameter data used in these calculations was not as accurate as that now available consequently the calculations are repeated here, using the present results for iron-nitrogen and the average results for iron-carbon collected by C.S. Roberts[28].

It is assumed that the iron lattice can be replaced by a continuous perfectly elastic isotropic medium and that the solution is sufficiently diluted so that the effects of the interstitial atoms in expanding the lattice are additive.

Each interstitial atom occupies a hole and in enlarging this hole the lattice is strained. To calculate the strains in the lattice due to a given interstitial, the effects of discontinuities in the lattice such as other interstices or interstitials are neglected.
Let $\bar{x}$ equal the ratio of interstitial atoms to iron atoms. Let $\bar{z}$ equal the number of iron atoms per unit cell, in the case of the face-centred cubic austenite lattice $\bar{z} = 4$ Therefore, the number of interstitial atoms per unit cell is $\bar{z}\bar{x}$. From the X-ray data, the change in volume per unit cell is

$$\Delta V_o = (a_o + \Delta a_o)^3 - a_o^3 \simeq 3a_o^2 \Delta a_o \qquad 3.17$$

This ΔV_o is effectively produced by $\bar{z}\bar{x}$ interstitials, therefore the increase in volume per interstitial atom is

$$\Delta V = \frac{\Delta V_o}{\bar{z}\bar{x}} \qquad 3.18$$

Now consider an isolated interstitial atom producing ΔV overall expansion of the crystal as in equation 3.18. At relatively large radii, the crystal acts like a continuum and the radial displacement ΔR is inversely proportional to R^2. This aysmptotic form of ΔR follows from elastic theory[32] and shows that at large R an elastic medium subject to spherically symmetric stresses behaves like an incompressible fluid. The volume of the material displaced through a spherical shell of radius R is

$$\Delta V = 4\pi R^2 \Delta R \qquad 3.19$$

and approaches asymptotically to a constant value as R increases.

From equations 3.17, 3.18 and 3.19

$$\Delta R = \frac{\Delta V}{4\pi R^2} = \frac{3a_o^2 \Delta a_o}{4\pi \bar{Z} \bar{x} R^2} \qquad 3.20$$

This expression represents an approximation for ΔR for small R in cubic crystals, and it is assumed that it can be extrapolated to obtain the displacement of the lattice atoms which are nearest neighbours of the interstitial atom in a face-centred cubic lattice. $R = \frac{a_o}{2}$ the nearest neighbour distance to the interstice.

The diameter of an interstitial solute atom is now set equal to the diameter of the vacant octahedral hole in the austenite plus twice the radial displacement of the nearest neighbour atom. For an f.c.c. lattice the diameter of an octahedral hole is $(1 - \frac{1}{\sqrt{2}})\, a_o$ and hence $(1 - \frac{1}{\sqrt{2}})\, a_o + 2\Delta R$ is the interstial atom diameter in a f.c.c. lattice.

In Table 3 the values of $\bar{x}$, a_o, and Δa_o used in the computation of the diameter of carbon and nitrogen atoms in austenite are given, together with the results obtained by substitution in equation 3.21.

$$\text{Diameter of interstial} = (1-\tfrac{1}{\sqrt{2}})a_o + \tfrac{3}{2}\left[\frac{a_o^2}{\pi \overline{ZX}}\,\frac{\Delta a_o}{R^2}\right] \qquad 3.21$$

The value of 0.71A° for the atom radius of nitrogen is the same as the calculated values for the radius of the nitrogen atom in martensite and it is the same as the Goldschmidt covalent radius. It is not possible in this calculation to estimate the exact error in determining the value of 0.71A° as the nitrogen atom radius in austenite; because the validity of the assumption that the lattice is a continuous isotropic medium is not really known. The value of 0.74A° for the radius of the carbon atom in austenite is rather less than the Goldschmidt radius and, as shown earlier, an exact value of the radius of the carbon atom in martensite is not know, but is less than 0.79A°.

3.4.3. Derivation of the internal friction conversion factor K.

An interesting and completely independent way of checking the accuracy of the estimate of the distortion produced by a nitrogen atom in an iron lattice is to compare the internal friction conversion factor K calculated from the estimated nitrogen atom radius with the measured value of K.

Fast and Verrijp [33] have measured K for nitrogen in iron.

From standard internal friction theory of b.c.c. metals containing interstitials,

$$\text{w/o Nitrogen} = K \delta_{max} \qquad 3.22$$

where K is a conversion factor and δ is the logarithmic decrement, which can be defined as the natural logarithm of successive amplitudes of the vibration

$$\delta = \ln \frac{A_1}{A_2} \qquad 3.23$$

can also be correlated with phase angle α by which the strain lags behind the stress [34]

$$\tan \alpha = \frac{1}{\pi} \ln \frac{A_1}{A_2} = \frac{\delta}{\pi} \qquad 3.24$$

where $\frac{\delta}{\pi}$ is usually called the internal friction Q^{-1}, which is analogous to damping or energy loss in an electrical system.

Smit and Van Bueren [35] following the experiments of Snoek [36] and Polder [37] on stress induced diffusion, were able to relate the maximum damping to the modulus of rigidity and the strains produced by solute atoms

$$\delta_{max} = 3 \pi b G \qquad 3.25$$

where

$$b = 0.26 \bar{n} \bar{V}^2 / 9kT \qquad 3.26$$

$$G = 8.2 \times 10^{11} \text{ dynes/cm}^2$$

b is a constant and $\bar{n}$ in this case is the number of nitrogen atoms per unit volume. $\bar{V}$ is proportional to

the strains produced by solute atoms taking part in the relaxation process and k is the Boltzman constant, $\bar{n}$ may be converted to weight precent using the relation

$$\bar{n} = \frac{N \rho \ (^{w}/_{o}N)}{100\ M} \qquad 3.27$$

ρ density of iron = 7.9 grams / cc.

N Avogadros number = 6.02×10^{23}

M Atomic weight of iron = 55.85

Substituting and rearranging equations 3.25, 3.26 and 3.27

$$^{w}/_{o} \text{ Nitrogen} = \left(\frac{367\ MkT}{N\rho\ \bar{V}^{2}G}\right) \delta_{max} \qquad 3.28$$

from equation 3.22 and 3.28

$$K = \frac{367\ Mkt}{N\rho\ \bar{V}^{2}G} \qquad 3.29$$

To calculate K for iron-nitrogen it is necessary to know $\bar{V}$. Snoek[36] has shown that the magnitude of the after-effect is directly related to the tetragonal deformation ε_m of martensite and is inversely proportional to the concentration of nitrogen atoms. Hence at low concentrations

$$\bar{V} = \frac{\varepsilon_m}{\bar{n}} \qquad 3.30$$

$\varepsilon_m = 9.25 \times 10^{-2}$ for martensite of nitrogen content $10\frac{a}{100}$

$$\bar{n} = \frac{\rho N}{M} \bar{x} \qquad \text{where } \bar{x} \text{ is atom fraction 0.1}$$

$$\bar{n} = 8.3 \times 10^{22} \bar{x}$$

$$\bar{V} = 1.12 \times 10^{-23} \text{ cm}^3 \qquad 3.30$$

Substituting $\bar{V}$ in equation 3.29 and assuming $T = 295^{\circ}$ K

$$\underline{K = 0.415}$$

Fast and Verrijp[33] have measured very accurately, with torsion experiments, the dependence of the after-effect on the concentration of solute nitrogen atoms in polycrystalline iron, and found that

$$^{W}/_{o} \text{ Nitrogen} = 1.26Q^{-1} \quad \text{at } 295^{\circ}K$$

giving a value of $K = 0.40$

Hence the calculated value of $K = 0.415$ is in excellent agreement with the experimental value of 0.40.

3.5 Conclusions

1. Iron-nitrogen alloys quenched from the gamma phase to -196° C and containing up to approximately 0.7 W/o nitrogen form body-centred cubic martensite. Those containing more nitrogen are mixtures of body-centred tetragonal martensite and face-centred cubic austenite.
2. There is a linear variation of the c and a lattice parameters of tetragonal iron-nitrogen martensite with nitrogen content expressed as interstitial atoms per 100 iron atoms.

3. There is a linear increase of the lattice parameter of austenite with increasing nitrogen concentration. This linear relationship extrapolated to zero nitrogen predicts correctly the room temperature lattice parameter of pure gamma iron.

4. At the same interstitial concentration the values of the cell dimensions c and a are essentially the same for iron-nitrogen and iron-carbon martensite.

5. At the same interstial concentration the value of the cell dimension a, is very nearly the same for iron-nitrogen and iron-carbon austenite.

6. The average lattice distortion produced by nitrogen in martensite and austenite is virtually the same as that produced by carbon in the equivalent structures in iron-carbon alloys.

7. The atomic radius of the nitrogen atom in martensite and in austenite is the same, the best estimate of the radius being $0.71A^{o}$.

8. There is excellent agreement between the experimental value of the conversion factor K in internal friction, and the value calculated from the present lattice parameter results.

4. THE HARDNESS AND STRENGTH OF IRON-NITROGEN MARTENSITE.

4.1 Introduction

The high hardness that can be attained in high carbon steels by quenching austenite to produce martensite was thought for several years following the discovery of martensite by Martens to be an essential part of the martensite reaction. We now realise that in general martensites are not necessarily hard and strong, and hence the mere occurrence of a martensitic transformation does not automatically confer very high strength upon the product of the transformation. It is now known that the strength of martensite cannot be ascribed to one factor alone but it must be due to a combination of several strengthening influences. P.M. Kelly and J. Nutting[38] have recently discussed the relative magnitudes of the possible strengthening mechanisms in martensite. The factors which seem likely to contribute to the strength of martensite in binary iron-carbon alloys are

1. Grain Size
2. Substructure of the martensite
3. Precipitation or segregation of carbon
4. Carbon in interstitial solid solution.

1. Grain size effects.

The martensite grain size is primarily determined by the original austenite grain size since the first plates of martensite to form from the austenite cannot be larger than the austenite grain diameter. Cohen[29] has shown that the yield strength of martensite in iron-nickel-carbon alloys is inversely proportional to the square root of the original austenite grain diameter. It is found that for the normal range of sizes, the effect on the total hardness (about 900 V.H.N.) is about 170 VHN, which is relatively small.

2. Substructure effects.

It has been suggested by Kelly[39] that the twin substructure found in both iron-carbon and in iron-nickel-carbon acicular martensites, is responsible for much of the strength of martensite. He attributed a large part of the increase in hardness with increasing carbon content to an increasing proportion of twinned plates. The hardening is considered to be due to the alternating twin plates reducing the available deformation systems by four. This idea has to a considerable extent been disproved by the work of Radcliffe and Schatz[40] and by the work at Liverpool[41]. Here the hardness of a series of cubic martensites containing up to 32 W/o nickel was measured using the microhardness technique described later

in this section. The results are shown in Figure 18. The hardness increases with nickel content up to about 5^{w}/o nickel and then remains reasonable constant. The transition from a densely dislocated massive martensite structure, to an internally twinned acicular structure takes place at 29^{w}/o nickel[41], yet there is no discontinuity at this composition in the hardness curve. Therefore, the hardening effect of the internal twinning must be negligible. It is interesting to note that up to 5^{w}/o nickel the structure of the quenched iron-nickel alloys would in fact be equiaxed or massive ferrite[41] and not martensite and it is in this region that the hardness increases rapidly.

3. Precipitation or segregation of carbon

The effects of precipitation or segregation of interstitials may be subdivided into a). precipitation during the quench and b). aging after the quench.

a). It is well known that precipitation can occur in low carbon steels during a quench from the austenitizing temperature[42,43,44] and reports of precipitates up to 1000A^{o} long[43] from electron microscopy investigations are available. However these observations have only been reported when the quenching rate was slow or when specimens of relatively large section size have been used.

It has been clearly shown by Aborn[44] with his excellent extraction electron metallography that the outer regions of rapidly cooled iron-carbon martensite specimens contained no trace of precipitates, but at the centre of the 0.125" diameter specimens there was evidence of carbide precipitation. Although recognising precipitation during the quench as a possible source of strength in commercially produced steels, it is clearly improbable that any contribution from this cause will be made to the hardness of the thin rapidly quenched specimens studied in the present investigation.

b). Winchell and Cohen[45] have shown that room temperature aging after the quench of iron-carbon-nickel alloys for 3 hours can result in an increase in hardness of up to 100 VHN over the as quenched hardness.

4. Solution hardening by interstials.

Since the effects of grain size, aging during and after the quench and of substructure are not usually major contributors to the hardness of interstitial martensites, solid solution hardening by interstitials is probably the main source of strength. In fact the solid-solution hardening effect of iron due to carbon is between 6000 and 7500 p.s.i. per 0.01 w/o carbon increase, in very dilute iron carbon alloys[46,47]. A.J. McEvily, H.C. Ku and T.L. Johnston[48] have shown that 50% of the total

flow stress of a 0.39 w/o carbon steel can be attributed to solid solution hardening by carbon. The theories of the mechanisms of interstitial solid solution hardening by Cohen, Fleischer and Friedel have been reviewed recently by M.J. Roberts and W.S. Owen[49].
The role played by interstitial carbon in producing high hardness in martensite has been the subject of many investigations, while experiments into the exact manner in which nitrogen effects the hardness and strength of martensite have been very few.

It has been popularly considered that nitrogen is less effective than carbon in hardening steel because the distortion produced by carbon in the martensite lattice was thought to be greater than the distortion produced by nitrogen. This idea arose from a knowledge of the relative covalent sizes of the carbon and nitrogen atoms, where carbon is about 15% longer than the nitrogen atom. From the previous section on X-ray diffraction it was seen that carbon and nitrogen have effectively the same atom radius when in solution in martensite. It is therefore expected that all other things being equal nitrogen hardens martensite to just about the same extent as carbon.

4.2 Experimental procedure.

A series of 0.005" strip specimens containing up to 2.35 W/o nitrogen were quenched to -196° C and mounted on aluminuim blocks with cold setting Araldite. The specimens were polished and microhardness impressions were taken across the surface using a Reichart micro hardness indenter. A load of 80 grams was used and the average of 20 occular readings was converted into micro hardness for each of the specimens as follows. The micro-hardness of a material H_m is

$$Hm = 1.8544 \times 10^3 \frac{P}{d^2} \quad Kg / mm^2 \qquad 4.1$$

for a square pyramidal diamond indenter with an apex angle of 136°

P = load in Grams

d = diagonal of base indentation in microns

d = m xq

m = length constant = 0.1628

q = number of divisions

$$Hm = 6.996 + 10^4 \frac{P}{q^2}$$

where P = 80 grams $Hm = \frac{5.5968 + 10^5}{2}$ 4.2

Equation 4.2 was plotted for values of " θ " in the range 80 to 180 and is given in Figure 19. The micro-hardness value of the maximum and minimum occular readings were al so taken for each specimen. These microhardness values were then converted into Vickers Hardness Numbers using a conversion scale which was obtained from a series of iron-carbon alloy martensite specimens in the form of $\frac{1}{4}$" cubes on which both micro and Vickers hardness measurements had been taken. This conversion scale is also plotted in Figure 19.

4.3 Results and discussion

The hardness results for the series of iron-nitrogen alloys in terms of V.H.N. as a function of nitrogen content are given in Figure 20. The limits of the error bars indicate the maximum and minimum hardness values found in each specimen. The results of hardness measurements for a series of rapidly quenched binary iron-carbon martensites obtained by Radcliffe[40] are also given in Figure 20. These results on carbon martensite are in goodagreement with the results of other workers[39,50] particularly at carbon concentrations greater than $1.5\frac{a}{100}$. The hardness results of Kelly[39] show an inflexion in the curve for lower carbon martensites in the range 0.1^{W}/o to 0.2^{W}/o C and his hardness values

in this range tend to fall rather higher than the Radcliffe data. It is possible that Kelly obtained aging of the low carbon martensites during the quench resulting in rather higher hardness figures at these low concentrations.

From Figure 20 it can be seen that for both iron-carbon and iron-nitrogen massive martensites there is a rapid increase in hardness H with the first $2.5\frac{a}{100}$ and as anticipated the initial rate of hardening in this range, $\frac{dH}{dc}$, is the same for both iron-carbon and iron-nitrogen martensites. After the first $2.5\frac{a}{100}$ the rate of hardening for both systems decreases but it continues to rise to a maximum at about $5\frac{a}{100}$. Then in the more concentrated nitrogen alloys the hardness decreases with increasing nitrogen content. After about $2.5\frac{a}{100}$ the curves separate, the carbon martensites being rather harder. At the maximum hardness, carbon martensites are about 100 V.H.N. points greater than the maximum hardness of the iron-nitrogen martensite. The slope $\frac{dH}{dc}$ starts to decrease between 2 and $3\frac{a}{100}$ because at this composition retained austenite appears. Measurements of the microhardness of the accicular plates suggest that in these concentrated alloys the rate of hardening is less than in the massive martensite range and the effect is not only due to retained austenite. This has been clearly

shown by Winchell and Cohen[51]. By measuring the flow stress of a series of iron-nickel-carbon alloys with various retained austenite content and extrapolating to zero retained austenite, they obtained the variation of the flow stress of 100% martensite with carbon content. The solution hardening effects of substitutional nickel are small compared with the effects of carbon[41]. The extrapolated flow stress σ_f is plotted as a function of the square root of the atom fraction of carbon in Figure 21. When the carbon concentration is greater than $1\frac{a}{100}$ there is very little increase of σ_f with carbon concentration. It is difficult to explain the disappearance of the solution hardening effect in such dilute alloys other than by the assumption that the alloys are so brittle that they fracture at stresses lower than that at which appreciable plastic flow could be produced. Such quenched alloys probably contain some microscopic quench cracks which would result in erroneous measurement of the flow stress in compression tests. The fact that the apparent fall off in solution hardening with increasing interstitial content is not detected by hardness test until at about $3\frac{a}{100}$ is also compatable with this assumption. It would therefore seem that the apparent fall off of the solid solution hardening and of the hardness is not related to a morphological or structural change in the martensite.

Similar interstitial contents of nitrogen and carbon produce the same hardening effect of massive martensite. To test whether they have similar affects on the flow stress of massive martensite, a few low nitrogen martensitic alloys were produced. The tensile tests at room temperature as a function of composition were carried out by M.J. Roberts[52]. The variation of 0.2% flow stress as a function of the square root of composition for these nitrogen alloys is given in Figure 22. There is no direct data on the flow stress of iron-carbon martensites to compare with the results in Figure 22, but from the experiments by Roberts[52] it is possible to obtain an estimate of the effect of carbon on the flow stress. These iron-nickel-carbon martensite results are also given in Figure 22. It can be seen that the rate of increase of the 0.2% flow stress as a function of the square root of interstitial content for the iron-nickel-carbon martensites and the iron-nitrogen martensites, over the more limited composition range, are very nearly the same. The absolute magnitude of the 0.2% flow stress at any specific interstitial content for an iron-nickel-carbon alloy is greater than for the corresponding iron-nitrogen alloy because of the additional strengthening effect of the nickel. A much more comprehensive and detailed study of the relative effects of carbon and

nitrogen on solid solution strengthening is being carried out at Liverpool by M.J. Roberts[52].

The conclusion that equal interstitial contents of carbon and nitrogen have essentially the same hardening and strengthening effect in massive martensite is contary to the result of work by Nehrenberg, Payson and Lillys[53] who report that nitrogen is less effective than carbon in hardening steel. They derived the following equation for the hardness of martensite in terms of carbon and nitrogen concentrations for carbon contents up to 0.5^{W}/o carbon and nitrogen contents up to 0.3^{W}/o nitrogen.

$$\text{Log Rockwell C} = 2.182 + 0.469\,(\text{Log}^{W}/o\text{C}) + 0.108(\log^{W}/o\text{C})^{2} + 0.164(\log^{W}/o\text{N}) + 0.025(\log^{W}/o\ \text{N})^{2} \qquad 4.3$$

This equation however, was based on nitrogen analyses of the as forged material prior to austenitising at about 1050°C. It is almost certain that considerable nitrogen loss would have occurred during austenitising and hence the ascribed contribution to the hardness of the martensite by nitrogen would be much too low. If it is assumed that the minimum of the error bars given in Figure 20 correspond to the hardness of a region of retained austenite then it would seem that the hardness of the retained austenite associated with the transformed nitrogen martensite can be quite high.

In the medium nitrogen range 5 to $7\frac{a}{100}$ the austenite will have undergone considerable strain hardening because of almost complete transformation to martensite and the hardness of pockets of retained austenite may be as high as 650 V.H.N. As the nitrogen content is increased there is more retained austenite present and therefore it will be less strain hardened and the hardness drops to 500 V.H.N. Hardness measurements prior to transformation of 100% austenite containing 2.5 w/o nitrogen showed it to be relatively soft, about 200 V.H.N.

4.4. Conclusions

1. The initial rates of hardening of massive martensite by carbon and nitrogen are the same.
2. At high interstitial contents, carbon is a more effective hardener of martensite, than is nitrogen.
3. The maximum hardness of iron-nitrogen and iron-carbon martensite occurs at the same intersititial content.
4. Iron carbon martensite has a maximum hardness of about 900 V.H.N. relative to a maximum of about 800 V.H.N. in the iron-nitrogen system.
5. The flow stresses of iron-carbon and iron-nitrogen massive martensites are similar for the same interstitial content.

6. One of the main factors causing a decrease in the rate of hardening of martensite at about $3\frac{a}{100}$ is due to the appearance of retained austenite. It is not due to a change of morphology or structure of the martensite.

7. It is suggested that the other major factor in the fall off, of solid solution hardening by interstitials is the presence of micro quench cracks which result in erroneous measurements.

8. The hardness of relatively strain free iron-nitrogen austenite is about 200 V.H.N.

5. THE EFFECT OF NITROGEN ON THE RETENTION OF AUSTENITE AT -196° C.

5.1 Introduction

The effects of carbon on the retention of austenite in binary iron-carbon alloys, after cooling to -196° C, have been studied by several workers[28,54] using the measurement technique of intergrated intensities devised byB.L. Averbach and M. Cohen[55] in 1948. The results of these studies have been collectively presented by C.S. Roberts[28] and may be seen in Figure 23. A parallel investigation of the effects of nitrogen on the volume fraction of retained austenite in iron-nitrogen martensitic alloys, after cooling to -196° C, was undertaken and the results are presented in Figure 23. The theory of the X-ray determination of retained austenite by the integrated intensities method is presented in Appendix 1.

5.2 Experimental Procedure

A series of iron-nitrogen alloys containing up to 2.6^{w}/o nitrogen were quenched from the nitriding atmosphere to room temperature and after ten minutes were removed from the apparatus and transferred to liquid nitrogen, resulting in a further transformation of austenite to martensite.

At the start of the series of experiments a diffractometer was not available and so the more tedious film technique had to be used. Later, when a diffractometer was available, some more alloys were prepared in the form of both wire and strip. The percentage retained austenite after cooling to -196° C was then determined for comparison purposes using both the film and diffractometer techniques.

5.2.1 Debye Sherrer film technique

Debye Sherrer X-ray diffraction patterns were produced from the alloys using the procedure described in detail in Section 3. The radiation used was cobalt K_{α} and care was taken to ensure as far as possible uniformity of developing and drying procedure.

The patterns of alloys containing up to 0.8 w/o nitrogen showed no trace of retained austenite lines. Alloys with higher concentrations of nitrogen gave faint austenite lines up to about 1.2 w/o nitrogen. At high concentrations the austenite lines were sharp and readily discernable. Several X-ray diffraction patterns were taken using the Helium Path Technique[56], which gives better peak to background ratio. The specimen selected contained about 0.8 w/o nitrogen. The helium was passed through the camera at a rate of about 0.5 litres/hour.

Because helium has a lower absorption and scattering affect than air, considerably improved films were obtained but the improvement of the peak to background ratio was not as great as the 300% claimed by the exponents of the procedure[56].

5.2.2. Intensity Measurements using a Hilger microphotometer

When a photographic emulsion is activated by radiation, the density D is a function of the wavelength, the intensity of the radiation I_* and the exposure time t.

$$D = k_1 I_* t^h \qquad 5.1$$

k_1 is a constant h Schwartzchild's constant and is a function of the wavelength. In the X-ray region of the spectrum h = 1

$$D = k_1 I_* t \qquad 5.2$$

Now with the hand operated Hilger micro-photometer used in these experiments the light transmitted through the film is proportional to the current produced in the receiving photocell, which is in turn proportional to the scale deflection Φ . The instrument can be calibrated for a particular film by using a sectored wheel which allows a stepped exposure of the film to the X-ray source by varying the exposure time for a constant X-ray intensity. The steps used were in the ratio 1, 2, 3, ...18.

The deflection corresponding to each step can be plotted against step number, thus giving a relationship between density and deflection.

Provided a sufficiently wide range of densities are produced in this fashion to cover the range of densities produced by the experiment, the graph can be used to convert deflections to densities. The densities in turn are proportional to intensities, for a constant exposure time, up to densities of about 1.0 corresponding to 10% light transmission through the film. Using this calibration curve, the intensity was measured as a function of Bragg angle and the integrated intensity I in arbitary units for a particular reflection was obtained by measuring the area under a peak using a planimeter.

In theory it is necessary to compare the intensities of only one austenite line and one martensite line in order to obtain the volume fraction of retained austenite, but in practice several lines close together in θ value, were measured and the results were averaged. The lines measured were $002\alpha'$; $200\alpha'$; 220γ ; $112\alpha'$; $211\alpha'$. When the martensite tetragonal doublets were too diffuse to permit good resolution of the individual lines, both the structure factor and the multiplicity factor were calculated on the basis of a body centred cubic structure. This introduced no error because in each case the total

diffracted power for each set of doublets was combined in the measurement of the integrated intensity.

Diffractometer Technique. The diffractometer method is essentially similar to the film technique but is rather simpler and quicker since the integrated intensity can be measured directly from the recording chart. A Phillips vertical circle diffractometer was used in conjection with a Phillips current and voltage stabilised power unit. The diffracted beam was measured using an amplified Geiger counter unit and the output was continuously recorded on a Phillips high speed recorder.

The X-ray diffraction unit settings consisted of the following.

1. Co $K\alpha$ radiation operated at 35 Kv and 13 ma. This gives good resolution of the $200\alpha'$; 220γ ; $211\alpha'$ reflections
2. No crystal monochrometer was used, but the radiation was filtered of $K\beta$ with an iron foil 0.001" thick, at the receiving slit.
3. The following slit system was used; Divergence 4^{o}, Receiving 1^{o}, Scatter 4^{o}.
4. The scan rate was 1^{o}/ minute and the chart speed 1 inch / minute.

The specimens used were flat strips $\frac{1}{4}$" square and 0.010" thick.

5.3 Calculation of volume percent retained austenite.

To illustrate the procedure for calculating the percentage retained austenite, the results of a 2.1^{W}/o alloy, by both the film and diffractometer techniques, will be analysed.

5.3.1. Debye Sherrer film method.

The microphotometer trace of the $002_{\alpha'}$; $200_{\alpha'}$; 220_{γ} ; $112_{\alpha'}$; $211_{\alpha'}$ reflections from the X-ray diffraction pattern of specimen N 63 containing 2.1^{W}/o nitrogen where changed into an intensity versus Bragg angle a curve (Figure 24) by using the sectored disc conversion curve given in Figure 25. The areas under the peaks over the background were measured several times using a planimeter and the average value taken, giving the integrated intensities. The "R" factors for each of the four martensite lines and the one austenite line were calculated from the equations.

$$R_{\alpha'} = \frac{1}{V_{\alpha}^2} \left\{2(f_o - 4)\right\}^2 m\left[\frac{1 + \cos^2\theta}{\sin^2\theta \cos\theta}\right] \quad 5.3$$

$$R_{\gamma} = \frac{1}{V_{\alpha}^2} \left\{4(f_o - 4)\right\}^2 m\left[\frac{1 + \cos^2\theta}{\sin^2\theta \cos\theta}\right] \quad 5.4.$$

and the results are given in Table 4 together with all the data used to derive their values. The average integrated intensity measurements are also given. From Equation A1.5 in Appendix 1.

$$\frac{C_\gamma}{C_{\alpha'}} = \frac{I_\gamma R_{\alpha'}}{I_{\alpha'} R_\gamma} \qquad 5.5$$

Substituting the values of I and R from Table 4 to give

a). $220_\gamma/002_{\alpha'}$ $\frac{C_\gamma}{C_{\alpha'}} = 0.503$

b). $220_\gamma/200_{\alpha'}$ $\frac{C_\gamma}{C_{\alpha'}} = 0.388$

c). $220_\gamma/112_{\alpha'}$ $\frac{C_\gamma}{C_{\alpha'}} = 0.475$

d). $220_\gamma/211_{\alpha'}$ $\frac{C_\gamma}{C_{\alpha'}} = 0.515$

average $\frac{C_\gamma}{C_{\alpha'}} = 0.465$

now $C_{\alpha'} + C_\gamma = 1$

$C_{\alpha'} = 0.684$

percentage retained austenite 31.6% $\simeq$ 32 $\pm$ 2%

5.3.2. Diffractometer method.

The diffractometer tracing of the 220_γ peak and the $211_{\alpha'}$ and $112_{\alpha'}$ peaks of the same alloy as above N 63 is given in Figure 26. The integrated intensity was measured directly from the chart using a planimeter andthe result togather with the "R" values from Table 4 are given in Table 5. The absorption is assumed to be negligible and since it is a flat specimen account must be taken of the

of the Debye Waller Temperature factor,

Equation 5.5 is

$$\frac{C_\gamma}{C_{\alpha'}} = \frac{I_\gamma R_{\alpha'}}{R_{\alpha'} I_\gamma}$$

a). 220_γ and $112_{\alpha'}$ gives 31% retained austenite.

b). 220_γ and $211_{\alpha'}$ gives 35% retained austenite.

Therefore average retained austenite content is $33 \pm 2\%$

5.4 Results.

The accuracy of the above calculations by both methods is within 2% retained austenite. Cohen[55] et al have shown that there is good agreement between the results obtained by integrated intensity methods and metallographic linear analysis. Consequently the results in these experiments have not been systematically checked by metallagraphic analysis. However, some metallographic measurements of retained austenite were made on alloys with high nitrogen content and in each case the results were within 2% of those obtained by X-ray technique.

The volume percent retained austenite for all the alloys in the range 0.85 to 2.65 w/o nitrogen ($3.5\frac{a}{100}$ to $11.0\frac{a}{100}$), together with the collected results of C.S. Roberts[28] for iron-carbon alloys are given in Figure 23 as a function of interstitial content. Up to about $3\frac{a}{100}$ there is virtually no retained austenite in either the

iron-carbon or iron-nitrogen alloys. In the range $3\frac{a}{100}$ to $7\frac{a}{100}$ the volume fraction of retained austenite increases with increasing interstitial content, but over the whole range the iron-nitrogen alloys contain 4 to 5 volume percent more retained austenite than the iron-carbon alloys. At $7\frac{a}{100}$ the iron-carbon alloy contain about 15% retained austenite and this is the maximum amount of austenite that can be retained at -196° C in the binary iron-carbon system. However, in the iron-nitrogen system the interstitial solubility is much greater and the retained austenite continues to increase rapidly with further increase in the nitrogen content. The maximum volume fraction of austenite that can be retained at -196° C is 60%, in an alloy with a nitrogen content of $10\frac{a}{100}$.

5.5. Discussion

When ferrous alloys which produce athermal martensites are quenched from the austenite region to below M a certain volume fraction of the austenite transforms to martensite immediately[57]. No more transformation occurs until the temperature is lowered still further to provide the thermodynamic driving force necessary to bring about

the transformation. Hence in many iron-carbon alloys there are considerable amounts of retained austenite even after cooling to room temperature. Further cooling below room temperature results in further transformation but in some alloys austenite can still be retained at -196° C.

One of the important reasons why complete transformation to martensite is rarely achieved is that the retained austenite is severely work hardened by the transformation strains and the austenite then presents a strong barrier to the propagation of a martensite plate. This severe strain hardening of the austenite has been clearly shown By M.G.H. Wells[58] in an iron-nickel alloy which by electron microscropy was shown to have a very high dislocation density in the austenite between the martensite plates.

Furthermore Zener[59] and Crussard[60] have pointed out that in the absence of plastic relaxation a martensite plate can impose elastic strains of the order of 10^6 p.s.i. but because of plastic relaxation, which is usually present the stresses momentarily achieved in the austenite are of the order of 10^5 p.s.i. Stabilisation by strengthening of the retained austenite is the same effect as the

mechanical stabilisation of austenite by cold working the specimen prior to initial transformation. In some alloy systems, particularly those with low stacking fault energies, deformation of the parent austenite stimulates the transformation and it is only after a large amount of deformation that retardation or stabilisation of the austenite is observed. A reasonable explanation of this transition is provided by P. Kelly and J. Nutting[61] in terms of the presence of stacking faults.

In iron-carbon alloys austenite can be stabilised thermally be holding the partially transformed alloy at room temperature and above. Then subsequent cooling to lower temperatures results in less transformation for a specimen of the same alloy content, quenched directly from the austenitising temperature. The mechanism of thermal stabilisation has been the subject of considerable controversy. It is probable that all the examples of stabilisation quoted in the literature cannot be attributed to the same cause.

J. Philibert[62] has shown that for thermal stabilisation to occur it is essential that some interstitial alloying element is present and several theories of stabilisation[63,64] suppose that the essential mechanism is a diffusional aging process whereby

dislocations are locked by interstitials. Das Gupta and B.S. Lement[65] have investigated thermal stabilisation effects in a 15^{W}/o chromium, 0.7^{W}/o carbon steel and have discussed their results in terms of the reactionpath theory. It was assumed that stabilisation is a result of the relaxation of strain embryos. They postulated that the embryos are present at the austenitising temperature in the form of dislocations or lattice imperfections in the austenite. Martensite plates are generated during the cooling below M_s from embryos possessing energies greater than the activation energy for martensite formation at the temperature at which the cooling is stopped. Relaxation of some of the remaining embryos can take place by diffusion of interstitials into strain embryo regions, resulting in a degree of stabilisation. On this theory however, it would be expected that some stabilisation should occur by the locking of possible nucleation sites even above M_s . Klier and Troiano and De Lazaro[67] et al have reported that stabilisation can be induced if the cooling is interrupted above M_s , but the results of Das Gupta[65] on the same steels, show that thermal stabilisation only occurred if some prior transformation had taken place. Morgan and Ko[64], studying iron-nickel-carbon alloys

showed that stabilisation of austenite above M_s did occur without prior transformation but that it was slow at temperatures below 150° C. They also said that the activation energy of diffusion of carbon is austenite was of the same order as the estimated order of magnitude of the activation energy for the stabilisation of austenite. From this it would appear that the controlling factor of thermal stabilisation is the diffusion of carbon in the austenite to the martensitic embryos. However more recent work, which would appear to be more reliable, by Woodilla, Winchell and Cohen[68] has shown that the activation energy for the stabilisation of austenite by carbon is between 15 and 18 Kilocals which is of the same order of magnitude as the activation energy for the diffusion of carbon in ferrite and is much less than the value for the diffusion in austenite. Hence it seems that the interstitial diffusion producing the stabilisation occurs within the martensite plates and embryos and not in the matrix of the parent phase. The kinetics of the stabilisation process further suggest that the interstitial atoms tend to diffuse from within the embryos towards the surroundings, thereby immobilising the interface. A possible reason for the segregation to the interface has been suggested by Woodilla[68] et al. The carbon in

the martensitic embryos and plates has a higher thermodynamic activity than the same concentration of carbon in the austenite and hence there is a driving force for diffusion towards the austenite. Because the diffusion rate is much faster in the martensitic then in the austenite there will be a time-temperature-dependent build up of interstitial atoms at the interface, which will then become progressively immobilised. This hypothesis for stabilisation would seem particularly attractive in the case of a dislocation interface, such as has been postulated by Knapp and Dehlinger[69] and by Frank[70]. This concept is also compatable with the previously discussed ideas of mechanical stabilisation and stabilisation due to prior deformation where the interface is impeded by a strain hardened austenite. It is also in agreement with the experimental observation that in ferrous athermal martensites, the initially formed plates do not continue to grow after cooling following isothermal holding, instead new plates are formed producing partitioning of the austenite.

From Figure 23 it can be seen that the volume fraction of retained austenite is greater, for a given interstital content, in iron-nitrogen than in iron-carbon alloys. Two possible explanations, both concerned with the immobilisation of the austenite - martensite interface

will be considered.

The first possibility is that the locking is provided by hydrogen. Very little work has been done on this point but Ramachandran and Dasarathy[71] have considered the possibility of hydrogen deactivating martensitic embryos in the austenite. They came to the conclusion that even though hydrogen will diffuse rapidly,* at room temperature both in ferrite and austenite very large quantities must be present before it could be effective to any degree in producing stabilisation. This is because the solubility of hydrogen is low and is more or less the same in both phases, hence there is no strong tendency for hydrogen to segregate at the interface when the transformatic occurs. Under normal austenitising conditions, in air or in a vacuum, the extent to which steel is supersaturated with respect to hydrogen is only about 4:1, compared with 40:1 relative to carbon.

*Table 6 gives the diffusivities of carbon, nitrogen and hydrogen in both austenite and ferrite as a function of temperature. The diffusivities at 20° C for each of the elements both in ferrite and austenite are also given. These were obtained by extrapolation of the high temperature data.

However under the conditions by which the iron-nitrogen alloys were produced it is possible that the degree of supersaturation could be considerably greater than normal. It has not been possible to determine the amount of hydrogen absorbed during the nitriding process, because in order to analyse for hydrogen it is necessary to use 30 grams of alloy for each analysis. This is considerably greater than the weight of the specimens which could be produced.

The second possibility and perhaps the more probable one, is that the enhanced stabilisation in the iron-nitrogen alloys is due to segregation of nitrogen to the martensite - austenite interface. Nitrogen diffuses faster than carbon at lower temperatures, both in the austenite and ferrite. (Table 6). Hence, it is probable that the amount of segregation and hence the degree of locking will be greater in the nitrogen case.

5.6. Conclusions

1. Both the Debye Sherrer and X-ray diffractometer methods of integrated intensity give the same results for the retained austenite content of iron-nitrogen alloys quenched to -196° within 2 percent.

2. With nitrogen concentrations less than $3\frac{a}{100}$ virtually no austenite is retained after transforming at -196° C.

3. In the range $3\frac{a}{100}$ to $7\frac{a}{100}$ about 5% more austenite is retained with nitrogen alloys than with the corresponding carbon alloys, after cooling to -196° C.

4. Up to 60% austenite can remain untransformed at the very high nitrogen contents, after cooling to -196° C.

5. The reason why nitrogen is a more effective austenite stabiliser than carbon may be due to a). diffusion of hydrogen, and more probably b). the diffusion of nitrogen to the interfaces of martensitic embryos and plates at a rate greater than that found with carbon.

6. MORPHOLOGY OF IRON-NITROGEN MARTENSITE I

6.1 Optical metallographic fractures.

6.11 Introduction.

No comphrehensive metallographic studies of iron-nitrogen martensite have been published. This is because most of the previous work on iron-nitrogen alloys has been concerned with alloys prepared as powders. There are two photographs by Bose and Hawkes[1] of a high-nitrogen alloy which show a structure very similar to high carbon martensite; that is, acicular platelike martensite in a matrix of retained austenite.

Nitrogen with its extensive solubility in gamma-iron produces a variety of morphologies when the austenitic alloys are quenched to room temperature. The basic forms of this range of structures has been observed previously in several other ferrous alloy systems and it is in the light of these previous observations that the morphology of quenched iron-nitrogen alloys will be discussed.

6.1.2. Massive structure.

The term "massive" was introduced by Greninger[78] in 1939 to describe a micro constitient in a Copper -9.3% Aluminium

alloy quenched from 1020° C. Volumes of the α phase which appeared in the microsection as shapeless areas with jagged and irregular boundaries were described as areas of massive-α . Many similar structures have been observed since in other non-ferrous and in ferrous systems. Relevant observations include those of Hull and Garwood[79] on β brass, Massalski[80] on copper-gallium and Gilbert and Owen[81] on iron-nickel alloys. Following Massalski[80] a massive transformation is defined in 'Perspectives in metals research'[82] as one which is essentially diffusionless but in which, unlike the martensite transformation there is no shape change or surface relief. It has since been recognised[41,83] that all microstructures containing a massive constituent do not form by the same transformation mechanism. Two extreme forms can be recognised; those formed by short range diffusion across an incoherent or possibly semi-coherent interface with no resulting shape change and those produced by a martensitic process involving shear and surface relief. Kurdjumov[84] had described the former transformation as one of 'disorderly growth' but Owen and Wilson[83] have suggested that the term short-range diffusional (S.R.D.) transformation is better. A product of such a transformation has been called by Owen, Wilson and Bell[41], equiaxed

or massive ferrite, while the product involving surface relief has been termed massive-martensite. The equiaxed alpha grains grow by the movement of incoherent grain boundaries which are not restricted or impeded by the boundaries of the parent grains,[41,80] through which they move. Figure 27 shows the microstructure of an iron -4% nickel alloy annealed in vacuum, where the austentite grain boundaries were thermally grooved, and then cooled to room temperature. The boundaries of the massive-α have been revealed by etching and it is clear that these boundaries cross the ausentite boundaries without restriction. The diffusionless type of transformation is represented by the gamma to alpha transformation which occurs over a wide range of cooling rates in iron-nickel alloys containing between 8-29.5 nickel. The block like appearance of this massive structure is illustrated in Figure 28[41], which is the microstructure of an 23.8% iron-nickel alloy. It is evident from the surface relief that these blocks of ferrite (Figure 29) are made up of packets each containing a large number of parallel or in some places interlacing shear plates[41]. It can be seen that the shear plates do not cross the original austenite grain boundaries and the volumes of martensite are smaller than the volume of the parent gamma grain.

6.1.3. Acicular martensite.

Although massive alpha and massive-martensite have some similarities both structures are strikingly different from the more familiar form of martensite, here called acicular martensite found in iron-nickel-carbon alloys (Figure 30[49]) and in high carbon, iron-carbon alloys. Acicular martensite consists of singular or connected lenticular plates embedded in a matrix of retained austenite.

6.2 Experimental procedure.

Several different methods of metallographic preportion were used because of the wide variety of structures which were examined. In general the specimens were in the form of thin strip and the low nitrogen alloys were usually cold mounted and mechanically polished. Alcoholic ferric chloride was used to etch the very low nitrogen alloys and picral-nital mixtures for compositions up to 0.7 W/o nitrogen. To examine the higher nitrogen series the specimens were usually tempered at about 220° C prior to mounting in order to darken the martensite plates on etching with 2% nital. The high nitrogen alloys, which were mainly austenitic, were best prepared by electropolishing and etching using 5% Perchloric/acetic acid or 5% perchloric/isopropyl alcohol mixtures at about 25 volts

and 20° C. Interferograms of prepolished surfaces were taken of several specimens after transformation to examine the form of the martensite plates using a two beam interferometer employing light of wavelength 5,640A°. The method of metallographic preparation, the etchant, the temperature to which the specimen was quenched are noted for each of the photomicrographs.

6.3 Results and Discussion

The optical photomicrographs of a complete series of quenched iron-nitrogen alloys containing up to 2.5^{W}/o nitrogen are given in Figures 31-54.

Figure 31 is of a 0.08^{W}/o nitrogen alloy which was quenched into brine from 915° C. The grains are essentially equiaxed and there is no trace of substructure. Oblique illumination of prepolished surfaces after transformation of these low nitrogen alloys revealed no surface tilts. Hence the structure is similar to that found in very low iron-nickel alloys and is of massive ferrite a short range diffusional product. The quenching rate must have been too slow to produce martensite.

Figure 32 is a low magnification photomicrograph of a 0.17^{W}/o nitrogen alloy quenched from 900° C into brine. The structure is essentially the same as the massive martensite found in iron-nickel alloys. Prior to this

observation in the iron-nitrogen system the correlation between the massive-martensite structures in substitutional iron based alloys and interstitial massive martensites had not been pointed out spite of the work of Scheil[85,86] and Mehl[87,88,89] on low carbon iron-based martensites which clearly pointed to a variety of possible microstructures. An investigation of the literature showed that the massive-martensite structure had been observed but not recognised or identified in the interstitial iron-carbon and iron-boron systems. Figures[33,34,35] illustrate the microstructural similarity of iron-nitrogen, iron-carbon[44] and iron-boron[90] massive martensites.

To test whether in fact this quenched product is martensite the surfaces of prepolished specimens containing about 0.2^{w}/o nitrogen were examined with oblique illumination.

Figure 36 shows surface relief corresponding to the shear plates. It can be seen that these interwoven plates do not cross the original austenite grain boundaries, which have been revealed in this specimen by thermal grooving during the nitriding process.

As the nitrogen content is increased to 0.37^{w}/o nitrogen the single phase supersaturated massive martensite is still present. (Figure 37)

Prepolished surfaces continue to show surface relief, this is shown in Figure 38. Interference patterns of the surface tilts were taken for this 0.37^{W}/o nitrogen alloy, using a two beam interferometer employing light of 5,640A^{o}. The interferogram corresponding to the field of view in Figure 38 is given in Figure 39. From the smooth contours of the interference fringes it can be seen that the shear plates of the massive martensite have a rounded profile, while the relatively wide spacing and wavy appearance of the fringes indicate that the surface erruptions are not very high. A detailed study of the height of these shear markings and of the angle of shear is being made by R.G. Bryans[91] using interferometry on both binary substitutional and binary interstitial massive martensites. Preliminary studies show that for massive martensites the angle of shear is about 3^{o} and that the height of the ridges is generally not greater than 5000A^{o}.

Figures 40 and 41 are of 0.54^{W}/o and 0.65^{W}/o nitrogen alloys respectively. These are single phased. X-ray diffraction showed that they still have a body centred cubic structure. They do not appear to have exactly the same metallographic form as the alloys with lower nitrogen content. The structure seems more fragmented and the massive blocks are no longer clearly discernable.

Examination of prepolished surfaces show that the surface relief markings still have the same appearance as the surface markings on the lower nitrogen alloys but quite often they form a Widmanstatten structure. A photomicrograph of an obliquely illuminated prepolished surface of an alloy containing 0.54^{W}/o nitrogen after transforming to martensite is illustrated in Figure 42. A Widmanstatten structure is present indicating shear on $\{111\}_{\gamma}$ planes. The corresponding interferogram is given in Figure 43. Again the fringes show that the martensite plates at the surface have a rounded profile and that the height of the surface eruptions is about the same as in the 0.37^{W}/o nitrogen alloy.

Figure 44 is a photomicrograph of a 1.2^{W}/o nitrogen alloy. There is distinct difference between its appearance and that of Figure 41 for a 0.64^{W}/o nitrogen alloy. The 1.2^{W}/o nitrogen alloy contains regions of retained austenite and the martensite is more acicular. This difference becomes even more marked in Figure 45 which is of a 1.8^{W}/o nitrogen alloy. The martensite plates are clearly acicular and even though this particular specimen has not been tempered to darken the martensite plates, regions of retained austenite are readily visible.

Figures 46 and 47 illustrate the general metallographic

structure of alloys containing 2.1^{W}/o and 2.3^{W}/o nitrogen respectively. These specimens had been tempered lightly at about 225^{o} C to darken the martensite plates. The acicular plates are surrounded by a matrix of untransformed austenite and their appearance is exactly the same as those found in high carbon steels. Alloys in this composition range have considerable amounts of retained austenite even after quenching to liquid nitrogen. This can be seen in Figure 48 for a 2.4^{W}/o nitrogen alloy, which has been tempered lightly and etched in nital. The white regions are the untransformed austenite.

Figure 49 is a low-magnification photomicrograph of a prepolished surface of a 2.35^{W}/o nitrogen alloy that had been quenched to 10^{o} C. It illustrates the surface upheaval of the few acicular martensite plates that are present in the austenite matrix. Figure 50 is the interferogram corresponding to the field of view in Figure 49. From the shape and form of the fringes it can be seen that the contour of the acicular martensite plates is quite sharp, whereas the massive martensite plates had a rounded profile. The close spacing of the fringes indicates that the height of the shear markings is relatively large. Again R.G. Bryans[91] is currently undertaking a detailed study of the form and height of these shear markings as well as the angle of shear. His initial work has shown

that for acicular martensite the shear angle is about 11° and the height of the surface eruptions is usually as great as 2.5μ . Figures 51 and 52 are a similar pair of photographs to Figures 49 and 50 but at a high magnification for the same alloy after it had been quenched to liquid nitrogen temperature, bringing about further transformation of the austenite to martensite.

Alloys containing more than 2.35^{W}/o nitrogen are fully austenitic on quenching to room temperature. Figure 53 is a photomicrograph of an iron - 2.5^{W}/o nitrogen alloy after quenching to 10° C showing the completely austenitic structure. There are a large number of annealing twins present indicating a relatively low stacking fault energy. This is in keeping with the observations of Nutting and Dulieu[92] that nitrogen lowers the stacking fault energy of the austenite. To date no quantitative measurements have been made on the series of alloys used in the present work.

An examination of prepolished surfaces of high nitrogen alloys of a composition such that their M_s is at or a little below room temperature showed that annealing twins and grain boundaries can act as nucleation sites for martensite plates. Figure 54 which is a photomicrograph of a prepolished surface of a 2.4^{W}/o

nitrogen alloy quenched to 10° C, shows several austenite grains some containing slip lines, presumably on $\{111\}$ planes in $\langle 110 \rangle$ directions. Acicular plates of martensite have nucleated at several points on the grain boundary and on the annealing twins.

6.4. Conclusions.

All the following conclusions refer to quenched-iron-nitrogen alloys.

1. Alloys containing very small amounts of nitrogen have a massive ferrite structure.

2. Alloys containing between 0.1^{W}/o and 0.4^{W}/o nitrogen have a massive-martensite structure.

3. Alloys containing nitrogen in the range 0.4^{W}/o to 0.7^{W}/o have a structure which closely resembles but is not exactly the same as the structure usually described as massive-martensite but they are still single phased. They do however, have the same form of surface relief on prepolished surfaces, as massive martensite, but the structure tends to be arranged in a Widmanstatten fashion.

4. At about 0.9^{W}/o nitrogen austenite can be detected in the quenched structure and the martensite plates are acicular.

5. Between 1.4^{W}/o and 2.35^{W}/o nitrogen there is essentially

no change in morphology except for an increased proportion of retained austenite at the higher nitrogen contents.

6. Alloys containing more than 2.4 w/o nitrogen are fully austenitic.

7. Annealing twin interfaces in the austenite and grain boundaries can not act as nuclei for acicular martensite plates.

7. MORPHOLOGY OF IRON-NITROGEN MARTENSITE II

7.1 Thin Film Electron Microscopy

7.1.1 Introduction

The first thin film electron microscopy investigation of the morphology of interstitial ferrous martensites was by Pitsch[3,4] who worked with very thin evaporated films of iron. These were heated to temperatures in the gamma field and carburised with methane or nitrided with ammonia-hydrogen mixtures and subsequently quenched to produce martensite. These alloys had interstitial contents greater than about $2.8\frac{a}{100}$ and hence the bulk form of these materials would have a metallographic structure consisting of a mixture of acicular martensite and retained austenite.

Pitsch[4] found that these alloys were made up of grains containing very thin long fibre crystals, a photograph of the structure can be seen in Figure 2 of Section 1. These fibre crystals were found to exist in two orientations which were twin related to each other. The twin plane was $\{112\}_{\alpha'}$ and the fibre axis $\langle 111\rangle_{\alpha'}$ for both the iron nitrogen and iron-carbon martensites. The austenite-martensite orientation was found for both systems to be $[\bar{1}10]_{\gamma} \parallel [11\bar{1}]_{\alpha'}$ and $(110)_{\gamma} \parallel (112)_{\alpha'}$

This is different to the Kurdjumov-Sachs relationship[93]

$\left([\bar{1}10]_\gamma \parallel [11\bar{1}]_{\alpha'} \quad \text{and} \quad (11\bar{1})_\gamma \parallel (101)_{\alpha'}\right)$

It is probable, although it has not been proved, that the Kurdjumov-Sachs orientation relationship holds also for bulk iron-nitrogen martensite. This difference between the orientation relationships is explained by Pitsch on the assumption that there is less elastic constraint to the growth of martensite plates in thin films.

This work was closely followed by that of Kelly and Nutting[94] who prepared thin films of a range of iron-carbon martensites. Starting from bulk material 1mm thick they used an electro jet machining technique[95] which thinned the specimens down to about 50-100μ, these were then electropolished, using chromic and acetic mixtures down to foils less than 2000A^{o} thick.

They found that the internal structure of low carbon martensite, that is massive martensite, consisted of needles or laths a few microns long and that the longstudinal axes of these laths were predominately parallel to $\langle 111\rangle_{\alpha'}$ They also showed that the austenite martensite orientation relationship is the same as the Kurdjumov-Sachs relationship found in bulk material. Quite often the laths were found assembled in the form of a "sheet". The laths had a completely dislocated substructure.

Occasionally the low carbon martensite contained plates which were internally twinned as a result of the inhomogeneous shear taking place by twinning rather than by slip. The volume fraction of internally twinned plates increased as the carbon content increased but with carbon contents less than about 0.6^{W}/o carbon. Kelly and Nutting found that the substructure of the martensite consisted predominately of dislocated laths. In one particular "sheet" of laths Kelly found the laths to be twin orientated. This, however, was only found on one occasion. Later Speich and Swann[96], showed that the laths of massive martensite in iron-nickel-carbon alloys are quite frequently twin orientated. The twin-related cells are probably a result of adjacent regions adopting different variants of the Kurdjumov-Sachs orientation relationship to minimize the shape change leading to a lower strain energy condition.

Optical microscopy has shown that when the carbon content of the binary iron-carbon martensite is greater than about 0.6^{W}/o the martensite is in the form of acicular plates. Electron microscopy of thin films of high carbon martensites confirms this platelike structure and shows further that the substructure of the plates usually consists of fine internal twinning. Kelly and Nutting[94] have shown by selected area electron diffraction

that the fine twinning occurs on $\{112\}_{\alpha'}$. The twin width can be quite variable between 100A° and about 900A° and with an average value of 500A°.

Wayman[136] has shown that in iron-nickel-carbon alloys where the M_s is about room temperature the martensite plates can have an internally twinned substructure in the centre of the plate around the mid-rib and the outer regions of such plates can have a dislocated substructure.

No work has been reported on the electron metallography of iron-nitrogen martensite thinned from bulk material.

In the present work on iron-nitrogen martensite considerable difficulties have been encountered in the preparation of consistent and reproducible thin foils, particularly with alloys having a high nitrogen content.

7.2. Experimental Procedure.

All the alloys used in the electron microscopy experiments were rapidly quenched from the nitriding temperature into brine, followed by a subzero quench into liquid nitrogen. Several techniques were tried to produce thin films of the quenched iron-nitrogen alloys, using as starting material sheet specimens about 0.006" thick. None of the methods gave more than 10% success.

Two basic electropolishing techniques were used;

the washer technique[97,98] and the window technique[99]. A variety of electropolishing solutions were used and these together with the optimum operating conditions, and the degree of success of each method are listed in Table 7.

(a). The washer technique is a modified form of the Bollman method[97]. The specimen is placed between stainless steel washers each containing a 0.5" diameter hole. The cathode consists of two stainless steel points and the distance between the points and the specimen can be varied. Initially the distance is set at about 1 cm to produce a uniform overall thining of the specimen, but later this is reduced to 2 mm. and the points are offset from the centre of the specimen. Polishing is continued until perforation occurs. A second hole is then produced diametrically apposite the first hole and the foils are cut from the bridge between the two holes. After the specimen has been washed to remove the electrolyte.

(b). The Window Technique was developed by Nicholson, Thomas and Nutting[99] and was initially used for aluminium alloys. It consists in lacquering the edges of a thin sheet of specimen and mounting it vertically with a vertical cathode, which in this case is the stainless steel beaker containing the electropolishing solution.

Preferential thinning occurs at the top edge, so the specimen is rotated through 90° and after a minute or so polishing is continued. A further two rotations are made resulting in the unlacquered area being uniformly thinned, to about 0.001". The polishing is continued and perforation occurs at the top edge of the lacquer coating and advance downwards. When perforation has extended about half-way down, the specimen is removed and washed, and foils are cut from the edge of the hole.

The foils were mounted on grids in A.E.I. EM6 microscope operated at 100kv. To ensure as clean a surface as possible the specimens were examined immediately after preparation, but traces of oxide were noticed on some foils. Selected area diffraction was carried out using a 0.5μ aperture and with a magnification setting of 50,000 times. The microscope was calibrated for rotation of the image relative to the diffraction pattern using crystals of molybdenum trioxide[100].

7.3 Results and Discussion

At 0.3^{W}/o nitrogen the martensite is made up of 'sheaves' containing individual laths a few microns long. The general structure of the martensite is illustrated in Figure 55. The thickness of the laths is quite variable

as can be seen from Figure 57, from a maximum of 2μ to about 0.3μ, with an average of 1μ. It is not know definitely that these individual laths correspond to the shear plates found on prepolished surfaces of massive martensite. The correlation between their dimensions however is such that there is a high probability that they do correspond. From Figure 57 it can be seen that the laths fit together in such a manner as to completely fill space. This is achieved by a dovetailing or tapering of the ends of the individual laths. Figure 56 illustrates the sharp boundary between two sheaves of martensite laths. The individual laths have a densely dislocated substructure and at this composition no trace of internal twinning was observed. The selected area electron diffraction pattern from the large plate in Figure 57 is reproduced in Figure 58. The foil orientation is approximately $(\bar{1}3\bar{1})$.

Kelly[94] found Widmanstatten precipitates which formed during the quench in the low carbon martensite laths. There was however, no trace of precipitates in the low nitrogen alloys.

The structure of 0.42 w/o nitrogen alloys was the same as that of the 0.3 w/o alloy consisting of dislocated laths which were quite often arranged in 'sheaves'.

Figure 59 is of a 0.42^{W}/o nitrogen alloy and Figure 60 is the corresponding electron diffraction pattern from the large martensite lath, which has an orientation(133) No trace of internal twinning was found in the specimens examined.

At 0.65^{W}/o nitrogen the laths seem rather finer and more fragmented. (Figures61 and 62). A similar observation was made with optical metallography at about this composition. Figure 63 shows that there are a few martensite plates present which are internally twinned, the twin spacing being of the order of 200A^{o}.

At 1.1^{W}/o nitrogen a large proportion of the plates are internally twinned. Some of the twins are relatively coarse with a spacing of 500A^{o}, while some have a spacing of only 200A^{o} Figures 64 and 65. The twins showed a reversal of contrast when a dark field image was obtained by placing the objective aperture, over oné of the diffraction spots from the twins. The twin contrast could be removed by tilting the foil in the electron beam.

At 1.4^{W}/o nitrogen the fine structure of the martensite plates is predominately internal twinning. The twins usually completely cross the plate at an angle of about 50^{o} to the major axis, this can be seen in Figure 66. Figure 67 is a high magnification photographs from

a large martensite plate showing very fine uniform twinning each twin plate being only 100A° wide. The electron diffraction pattern corresponding to Figure 67 is reproduced in Figure 68 and it shows streaking which is a further indication of the fineness of the twins. Analysis of the diffraction pattern shows that the maxtrix plane contains (112) (202) and $(1\bar{1}0)$ reflections making the orientation of the foil approximately $(11\bar{1})$. The $\frac{c}{a}$ ratio obtained from the d spacings of these reflections is 1.05 ± .01 which corresponds to a nitrogen content of about 1.5^{w}/o. The streaks on the diffraction pattern lie in a direction about 55° to $[110]_{\alpha'}$ and 34° to $[112]_{\alpha'}$. Therefore, the direction of the streaks is $\langle 112\rangle_{\alpha'}$. This direction is perpendicular to a $\langle 111\rangle_{\alpha'}$ close packed plane of atoms. The $\langle 111\rangle_{\alpha'}$ is parallel to the traces of the twins in the corresponding electron micrograph after rotation has been allowed for. Hence the streaking is normal to the fine twins.

Although the high nitrogen alloys consisted almost entirely of twinned plates, infrequently a completely dislocated plate was found. Usually these were relatively small plates embedded in a matrix of retained austenite. A good example can be seen in Figure 69.

It is extremely difficult to prepare foils from alloys containing more than 1.4^{w}/o nitrogen since there

is a preferential attack of the retained austenite and as a result the foils readily form an excess of holes. An example of this preferential attack can be seen in Figure 70 which is of a specimen from a 2.4^{w}/o nitrogen alloy. The electron-micrograph also shows that the martensite is still internally twinned and that there is a co-operative growth of the two martensite plates.

It is therefore noticed that the electron metallography of iron-nitrogen martensite is identical to that of iron-carbon martensite. The low nitrogen and low carbon massive martensites both form dislocated laths and quite often the laths form into "sheaves". No cases of the laths being twin related were observed but in all probability as in the massive martensite of the iron-carbon system this twinned relation will sometimes occur. Acicular martensites are usually internally twinned, though occasionally dislocated plates are observed. Because of difficulties in preparing iron-nitrogen martensite foils with substantial amount of retained austenite, it has not been possible to determine the austenite-martensite orientation relationship.

7.4 Conclusions

1. Quenched iron-nitrogen alloys which from optical metallography have a massive structure, have an electron

metallographic structure consisting of highly dislocated individual laths interwoven in the form of sheaves which completely fill space.

2. Occasionally an internally twinned plate is observed with the low nitrogen martensites.

3. There is transition from lath type martensite to platelike martensite at about 0.6^{w}/o to 0.7^{w}/o nitrogen.

4. The acicular martensite observed in optical metallographic studies of high nitrogen alloys has a platelike electron metallographic structure.

5. The high nitrogen martensite plates are usually internally twinned, although occasionally plates with a dislocated substructure are observed.

8. THE MARTENSITE TRANSFORMATION TEMPERATURE.

8.1 Introduction

One of the most important features of a martensitic transformation is the temperature M_s at which the martensitic product first appears on continuously cooling the parent phase. M_s is not the equilibrium temperature (T_o) at which the free energy of the austenite equals the free energy of the martensite but some lower temperature where a sufficient driving force is available to bring about the transformation.

Previous workers have established that the characteristics of the start of transformation in iron carbon alloys are;

1. The transformation temperature can not be suppressed by increasing the cooling rate.(101)
2. All alloying elements except Cobalt and Aluminium lower M_s.(102)
3. The transformation only occurs during cooling.
4. Below T_o the transformation temperature is raised by small amounts of the plastic deformation of the parent phase.(103 & 104)
5. Increasing the austenitizing temperature by about 300° C raises the M_s 20-30° C, in low alloy steels.(105)

6. Pressures in the order of 42 K bars lower the M_s temperature by about 200° C.(106)

8.2. Techniques for Determining M_s

Several techniques including metallography, magnetic analysis, X-ray diffraction, thermal analysis and electrical resistivity have been employed to determine the M_s temperature in iron-carbon alloys. Each method depends on the change of a physical property at the onset of the transformation.

8.2.1 Metallography

A metallographic technique devised by Greninger and Troiano(107) is particularly useful at temperatures below 300° C. A series of iron-carbon alloys is austenitised at a suitable temperature, usually 50° C above the $\gamma / \alpha+\gamma$ boundary, and quenched to different temperatures in the estimated region of M_s and then reheated. The alloys are subsequently quenched into water. The tempered martensite can be detected metallographically. The temperature of the initial quench which first produces martensite is M_s. Alternatively the percentage of martensite can be determined by X-ray diffraction or point counting, at eachof the

initial quench temperatures. Then by extrapolation, the temperature at zero martensite is the M_s temperature.

8.2.2 Magnetic analysis.

Magnetic analysis, although of limited application, has been developed so that it is extremely accurate. Austenite is paramagnetic and martensite is ferromagnetic. Szombatfalvy[108] has shown that on the formation of martensite during cooling, magnetic intensity and permeability change of two or three orders of magnitude respectively and hence the M_s temperature is easily identified.

8.2.3. X-ray diffraction

X-ray diffraction techniques for the determination of M_s depend on a change of crystal structure at the transformation temperature. This technique also is of limited application since without special high temperature X-ray equipment it can only be used with alloys which have M_s below room temperature. About 5% transformation must occur before it can be detected and consequently, M_s must be found by extrapolation. Unlike the magnetic method this technique is not limited to ferrous alloys and it can be used as a check on resistivity and thermal

analysis techniques.

8.2.4. Thermal Analysis

Thermal analysis has been one of the more successful techniques that have been applied to the determination of transformation start temperatures in iron-carbon alloys. Portevin and Garvin[109] in 1919 during the thermal analysis of steels, found that when a sufficiently rapid cooling rate was employed the high temperature A_r' point (the temperature at which fine pearlite first forms) was eliminated and another arrest at a much lower temperature, termed $A_{r''}$ was observed. The $A_{r''}$ point is the M_s temperature and the arrest occurs due to the evolution of heat at the start of the transformation. Esser and Bungardt[110] have shown that the heat evolved during the austenite to martensite transformation in a 1.4^W/o carbon alloy is 11.0 calories/gram.

The work by Greninger[107] on the determination of M_s in iron-carbon alloys by the detection of thermal arrests is the most reliable published and the M_s temperatures reported agree well with earlier data determined by other methods. The procedure adopted by Greninger was as follows. Specimens of iron-carbon alloys 0.039 inches square and 0.010 inches thick were austenitised in a heating coil of platinum 20% rhodium in a helium

atmosphere. The temperature of the specimen was recorded by a 40 gauge Chromel-Alumel thermocouple spot welded on each flat side of the specimen. The output of the thermocouple was fed to a precision torsion galvanometer and the signal recorded on a high speed drum camera. After austenitising for about 10 minutes the heating filament was broken and simultaneously a high pressure blast of helium was introduced causing the specimen to be uniformly cooled below M_s. The temperature-time curve during the quench was continuously recorded on the camera which had previously been calibrated. The $A_{r''}$ point was determined as the temperature at which there was a sudden change of slope due to the evolution of heat at the start of the martensite reaction. The cooling rate of the specimens at 550° C ranged from 200° C /second to 4000° C /second. The quenching experiments were performed on several specimens of each alloy, the scatter of results was usually about ± 8°C. The M_s was found to decrease from 490° C for a 0.19 w/o carbon alloy to 150° C for a 1.4 w/o carbon alloy. Greninger confirmed his results using the Greninger Troiano metallographic technique on a 0.57 w/o carbon and a 0.84 w/o carbon alloy. The thermal analysis results by Greninger are presented in Figure 71. Since 1942 the thermal analysis technique has been used by several investigators including Gilbert and Owen[81]

and Sivanson and Parr[111], both of whom studied iron-nickel alloys using an A.C. self resistance heating method for austenitising in a vacuum and then quenching with helium.

8.2.5. Electrical Resistivity.

A.W. Mc Reynolds[112] in 1946 was the first to apply electrical resistivity techniques to the determination of high temperature M_s points in iron-carbon alloys. The alloys, in the form of 0.026" diameter wire, were austenitised in a high vacuum and quenched with helium. The resistance and temperature were simultaneously recorded; the resistance on a photographic film and the temperature on a high speed recorder. Analysis of these time-temperature and time-resistance curves, enabled resistance versus temperature to be plotted and the onset of the transformation was taken to be the temperature at which the curve deports from linearity. McReynold's result for a 0.4 w/o carbon alloy is given in Figure 72. There is a decrease in resistance on cooling from the face-centred austenite to the body-centred martensite, of about 35% for complete transformation.

8.3 M_s Temperatures In The Iron-Nitrogen System.

Only metallographic techniques have been used to study

M_s temperatures in iron-nitrogen alloys. The only reliable M_s temperature recorded was determined by Bose and Hawkes[1], (to be 35°C.) for a eutectoid alloy containing 2.35 w/o nitrogen.

8.4. Experimental Methods.

8.4.1. Introduction

Initial experiments in the present work showed that alloys containing more than 2.35 w/o nitrogen were fully austenitic at room temperature. This was easily demonstrated because the alloys were non-ferromagnetic and gave X-ray diffraction patterns corresponding to a face-centred cubic lattice. It was decided to use the thermal analysis technique for low nitrogen alloys which have an M_s temperature above about 150° C and a resistivity method for those alloys with an M_s at lower temperatures. The continuous cooling and resistivity data has been supplemented by metallography and X-ray diffraction.

The specimens for both techniques were prepared by the controlled nitriding of 3 inch loops of AC N2 pure iron wire 0.010" diameter. The nitriding procedure is given in Section 2. The specimens were quenched from the austenitising temperature into brine at about 20°C,

without removing them from the ammonia-hydrogen atmosphere, this produced homogeneous alloys. Up to about 0.6^{W}/o nitrogen the alloys were fully martensitic. At greater nitrogen contents the alloys contained progressively more retained austenite, until at about 2.4^{W}/o nitrogen, they were fully austenitic.

8.4.2. Thermal Arrest Technique

In the case of iron-carbon alloys austenitisation prior to the M_s determination can be carried out either in a vacuum or in an inert atmosphere. This however was not possible in the case of iron-nitrogen alloys because extensive loss of nitrogen occurs even in short terms at high temperatures.(19) Consequently austenitisation was carried out in an Ammonia-hydrogen atmosphere of a predetermined composition corresponding to that required to establish equilibrium at the alloy composition and austenitising temperature. This equilibrium nitriding atmosphere must of necessity be only approximate because the dissociation conditions of the ammonia are different to thosein which the specimen was originally prepared in a Vachrome wound A.C. Heating furnace.

The apparatus which was designed for these experiment is shown diagramatically in Figure 73. Straight 2½" lengths off the arms of the 3" loops were suspended under

slight spring tension between a pair of jeweller's pin chucks. These were attached to insulated $\frac{1}{8}$" diameter stainless steel rods which also acted as conductors for the 50 cycle/second A.C. which was used for heating the specimen to the austenitising temperature. In the original design a 0.002" diameter Chromel-Alumel thermocouple was used for measuring the temperature, but this gave erroneous readings due to nitrogen pick-up. Therefore a 0.002" diameter platinum-platinum 13% rhodium thermocouple was spot welded to the centre of the specimen. These fine leads were attached to 0.010" diameter wires of the same composition which were led out of the specimen holder via two lengths of stainless steel. The complete specimen holder was inserted in a glass tube 22 inches long fitted with a B 34 socket. A photograph of the specimen holder and chamber is given in Figure 74. The glass tube has inlet and outlet parts for the nitriding gases and a specially designed nozzle which is inserted about $\frac{1}{4}$" above the specimen and the thermocouple. This nozzle admits a uniform blast of cooling gas when a magnetic valve is opened. The potential output from the thermocouple was led to a Honeywell Brown high-speed continuously recording potentiometric unit. The recorder

had a response time of ¼ second for a full scale deflection and a range of 0-10 millivolts. Hence on a platinum-platinum-13% rhodium thermocouple millivolt scale a full scale deflection corresponds to about 1000° C and cooling rates of up to 4000° C per second can be followed. A very high chart speed 20 inches per minute was used for most runs in order to obtain a reasonable scale on the time axis. After austenitising for 1-2 minutes at temperatures between 890° C and 950° C the A.C. current was switched off and a blast of hydrogen admitted through the magnetic valve to uniformly cool the specimen. The output of the thermocouple was continuously recorded during the quench. By varying the hydrogen pressure from zero to 10 lbs per square inch gauge pressure, cooling rates between 400° C and 4000° C per second were obtained.

The specimens were extremely brittle and quite often they broke during the mounting and spot welding operations but normally two or three quenching curves were recorded for each specimen. To aid the accurate location of the martensite arrest points a series of standard cooling curves of 0.010" diameter platinum, which has no transformation within the temperature range being studied, were prepared. The appropriate standard curve was then superimposed on the curve of the alloy being studied and the $A_{r''}$ point could be detected with considerably more

accuracy than was possible by mere inspection. This method was particularly useful for cooling velocities greater than 1000° C per second. The original nitrogen analysis was confirmed by a bulk analysis on the specimens after the above treatment.

8.4.3. Resistivity experiments.

It was seen earlier that if sufficient nitrogen is present then the M_s temperature is so reduced that alloys containing more than 2.35 w/o nitrogen are fully austenitic even after quenching to room temperature. Thus it is not possible to determine the M_s by the thermal analysis method. Instead four three inch loops specimens were prepared at a series of four compositions greater than 2.35 w/o nitrogen. One specimen was for X-ray diffraction one for chemical analysis and two for resistivity measurement of the M_s temperature. The specimens were quenched from room temperature into constant temperature baths and the resistance of the specimens was measured after the temperature had been raised back to room temperature. It was assumed that any change in resistance can be associated with the transformation to martensite. The onset of martensite formation was detected by observing a change in slope of the temperature resistance curve.

The loop specimens were held in pin chucks and 0.002" diameter potential leads of Chromel wire, spot welded about 5 inches apart. The specimen holder and resistance circuit used in these experiements are diagramatically illustrated in Figure 77. The potential across the specimen was measured on a Pye Universal precision potentiometer and the current at each potential reading was measured across a standard 1 ohm resistance. The constant temperature baths for temperatures down to -100° C were made by cooling alcohol with liquid nitroge and those down to -140° C by similarly cooling iso-pentone in a vacuum flask. The temperature was measured with a calibrated copper-constantan thermocouple. After about two seconds the specimen was at temperature since it had very little thermal capacity but the specimen was immersed in the refrigerant for about two minutes. The cooling bath was then removed and the temperature of the specimen allowed to return to room temperature. The potential drop across the specimen was then measured after about 10 minutes, by which time it had attained a constant temperature. One specimen of each composition was quenched to few degrees above the experimentally determined M_s temperature and a Debye Sherrer pattern taken. No body-centred tetragonal lines

were observed for any of the specimens.

8.5 Results.

8.5.1 High temperature M_s results.

The average M_s values and the average cooling rates and austenitising temperatures for all the alloys used in the thermal analysis experiments are given in Table
Figure 75 shows the millivolt time tracings of a series of cooling curves for alloys in the composition range 0.17^{W}/o nitrogen to 1.9^{W}/o nitrogen. All the curves except that for N 90 show the $A_{r''}$ arrest only. Specimen N 90 with 1.9^{W}/o nitrogen shows both the $A_{r'}$ and $A_{r''}$ arrests. Figure 76 gives two of the cooling curves of a 0.44^{W}/o nitrogen alloy together with a standard cooling curve of a 0.010" diameter platinum wire. Figure 71 shows the average transformation temperatures as a function of interstitial atoms per hundred iron atoms and also the temperature scatter band for each alloy.

8.5.2. Low temperature M_s results.

The M_s temperatures for four alloys obtained by resistivity are given in Table 9 . The error is about $\pm$ 5^{o} C.

A series of X-ray diffraction patterns for specimen N 103 containing 2.45^{W}/o nitrogen were taken at room temperature after the alloy had been quenched to 20° C; 6° C; -15°C and -25° C, these are shown in Figure 78 and the corresponding resistance curve is given in Figure 79, showing that the M_s temperature is -20° C ± 5° C.

The M_s temperatures for the four alloys are plotted in Figure 71 as a function of interstial content.

8.6. Discussion

The M_s points obtained by thermal analysis have an error of about ± 10° C. This scatter can be accounted for by the slight inhomogeneities arising during specimen preparation and by a slight disturbance of the equilibrium nitrogen concentration during the austenitising process. The error in the experimental method accounts for about half of the total error.

The transformation temperature curve in Figure 71 is drawn through 545° C, the M_s temperature for pure iron determined by Owen and Gilbert[81]. Higher M_s values for pure iron have been determined by J. Parr[111].

Figure 71 shows the variation of transformation temperature in degrees centigrade with interstitial atoms per 100 iron atoms for both the results of

A.R. Greninger[107] on iron-carbon martensite and for the present work on iron-nitrogen martensite. The iron-nitrogen transformation temperature curve has very much the same shape as the iron-carbon curve up to $7\frac{a}{100}$ but it lies at slightly higher temperatures. The difference between the carbon and nitrogen curves increases from about 25° C at low concentrations up to 60° C at $7\frac{a}{100}$. The curve is approximately linear in the range 1 to $7\frac{a}{100}$, the M_s temperature decreasing 25° C per 0.1 w/o nitrogen. From the resistivity results it can be seen that the curve is no longer linear in the high nitrogen range and the rate of fall of M_s temperature with interstitial content increases. For a 2.7 w/o nitrogen alloy the M_s temperature is about -120° C. It might be expected, by reference to the iron-nickel-carbon system, that the "burst"[113] type of martensite reaction might occur at these very low temperatures. The X-ray diffraction experiments indicated that there was a marked increase in the variation of volume fraction of martensite per degree of cooling, but no direct evidence of an autocatalytic burst reaction was obtained.

In low interstitial iron-carbon alloys there is a large decrease in resistance accompanying the transformation to martensite. It was found that on

transforming the austenites with a high nitrogen concentration to martensite an un-anticipated increase in resistance of the order of 3-4 percent was observed, corresponding to about 40 percent transformation. A critical examination of the limited resistivity data that is available for transformation in iron-carbon alloys shows that there is a decrease in the change of resistivity at M_s, with increasing carbon content (112 & 114). Extrapolation of this data to a hypothetical carbon content of 2.1 w/o ($10\frac{a}{100}$) shows that in this alloy system also, the change in resistance accompanying transformation changes sign at high interstitial concentrations. This decrease in resistance change at M_s with increasing carbon content suggests that the rate of increase of resistivity of martensite with increasing carbon content is greater than that of austenite. This hypothesis was tested by making measurements of absolute resistivity at a constant temperature of iron-nitrogen martensite and iron-nitrogen austenite. A series of both cubic and tetragonal martensites were prepared and quenched to -196° C. The specimens in the form of either 0.008" or 0.010" diameter wires about three inches long. The resistivity was measured at 20° C using a circuit similar to that in Figure 77. The alloys with less than 0.7 w/o nitrogen, contain virtually zero retained austenite

after quenching to -196° C. Alloys containing greater amounts of nitrogen have progressively increasing retained austenite contents after quenching to -196° C. The resistivity of the austenite was determined for two high-nitrogen alloys at 20° C as 68.8μohm cm. for a 2.45^{W}/o nitrogen alloy and 72.1μohm cm. for a 2.6^{W}/o nitrogen alloy. A third value for the austenite can be deduced by extrapolation of high temperature resistivity data on pure iron, to 20° C. This value for pure iron is 61μohm cm.(115) This resistivity data for both the austenite and the austenite and martensite mixtures are plotted in Figure 80, as a function of interstitial contents. The relationship for the austenite is linear and the fractional change in resistivity per $1\frac{a}{100}$ is approximately 0.9μohm cm. at room temperature. This value is of the same order as the fractional change in resistivity per $1\frac{a}{100}$ of fully austenitic iron carbon alloys at 950° C, which is 1.2μohm cm. (116)
Initially the resistivity of the fully martensitic alloys is also linear but at about $3\frac{a}{100}$ the graph deviates from linearity. After this composition the observed resistivity corresponds to that of a mixture of martensite and retained austenite. The relationship connecting resistivities of individual components of a mixture, with the total

resistivity is

$$\ln \rho = C_{\alpha'} \ln \rho_{\alpha'} + C_{\gamma} \ln \rho_{\gamma} \qquad 8.1$$

Where $\rho_{\alpha'}$ and ρ_{γ} are the individual resistivities of the two phases martensite and austenite respectively. While $C_{\alpha'}$ and C_{γ} are the volume fractions of martensite and austenite respectively. The total resistivity of the mixture is ρ Hence,

$$\rho = \rho_{\alpha'}^{C_{\alpha'}} \times \rho_{\gamma}^{C_{\gamma}} \qquad 8.2$$

and from a knowledge of the fractions of martensite and austenite and the linear variation of resistivity with interstitial content for the austenite, the resistivity $\rho_{\alpha'}$ of the martensite in the mixture can be deduced. This is shown as a dotted line in Figure 80. This crosses the austenite resistivity line between 9 and $10\frac{a}{100}$, thus providing clear evidence supporting the suggestion that the change in sign is due to a difference in the variation of resistivity of austenite and martensite with nitrogen content. A change in the slope of the martensite resistivity curve occurs at an interstitial content corresponding approximately with the transition from cubic to tetragonal martensite.

8.7 Conclusions.

1. The shape of the curve of transformation temperature as a function of interstitial content, in the iron-nitrogen system is very similar to that for the iron-carbon system in the range $0-7\frac{a}{100}$.

2. The M_s temperatures for the iron-nitrogen alloys are a little higher than for the corresponding iron-carbon alloys.

3. The M_s temperature of iron-nitrogen alloys decreases as the nitrogen content increases. In the range $1-7\frac{a}{100}$ the decrease in M_s temperature per $0.1^{w}/o$ nitrogen is about 25^{o} C.

At high concentrations the rate of decrease with nitrogen content is greater.

4. Alloys containing more than $2.4^{w}/o$ nitrogen are fully austenitic at room temperature.

5. A large decrease in resistivity occurs on transforming low nitrogen alloys from austenite to martensite. On increasing the nitrogen content this resistivity drop diminishes until at about $9.5\frac{a}{100}$ there is a change to an increase in resistance which becomes larger as the nitrogen content is further increased.

9. THERMODYNAMICS OF IRON-NITROGEN MARTENSITE.

9.1 Introduction

A knowledge of the free-energy change associated with the transformation of face centred-cubic austenite to body-centred cubic or tetragonal martensite enables the equilibrium temperature T_o and the driving force at M_s to be determined. Thus, it is an important part of the theory of the martensite transformation. There have been a number of estimates of the free energy difference between austenite and martensite as a function of the carbon content of iron-carbon alloys and there is a reasonable measure of agreement but some problems still remain. It is proposed to critically review the application of thermodynamics to the martensite transformation in the iron-carbon system, to extend the study to cover iron-nitrogen alloys and to compare the results obtained from the two systems.

9.2 Zener Analysis

From a knowledge of the equilibrium solubilities of carbon in austenite and ferrite and the free energies of pure austenite and ferrite as a function of temperature. Zener[117] in 1946, was able to deduce the temperature T_o at which the free energy of the two phases is equal, as a

function of carbon content of the alloy. Then, by assuming a constant elastic strain energy, independent of composition of -290 cals $mole^{-1}$ of martensite, an approximate theoretical M_s versus carbon content curve was fitted to that for the known transformation temperatures. The Zener analysis is repeated here utilising more reliable data for the solubilities of carbon in ferrite and austenite as a function temperature.(118, 119) An elastic strain energy ranging from -290 to -355 cals $mole^{-1}$ rather than a constant -290 cals $mole^{-1}$ independent of composition, was found to give a better fit of the theoretical M_s curve with the experimental M_s curve obtained by Greninger.(101)

From X-ray diffraction experiments reported earlier in this thesis it is found that the average lattice distortion of martensite produced by an interstitial nitrogen atom is the same as that produced by a carbon atom. Thus if the Zener analysis is applied to the iron-nitrogen system agreement between the theoretical and experimental M_s temperatures should be obtained as was in fact found, if the same variation of elastic strain energy with concentration is used. That is -290 to -360 cals $mole^{-1}$ in the range 0 to $6\frac{a}{100}$.

9.2.1. Alpha-gamma equilibrium

Assuming a dilute solution

$$\frac{C_i^{\alpha}}{C_i^{\gamma}} = \beta_i \exp\left\{\frac{\Delta G_i}{RT}\right\} \qquad 9.1$$

ΔG_i is the change in free energy on transferring one mole of i from α to γ phase, i.e. $\Delta G^{\alpha \rightarrow \gamma}$, i represents components 1,2,3 etc., Ci is the concentration in mole fractions and β_i is a numerical constant equal to unity for substitutional alloys and to 3 when the solute is interstitial.(117)

If i represents either carbon or nitrogen atoms in solution in iron

$$\frac{C_i^{\alpha}}{C_i^{\gamma}} = 3 \exp\left\{\frac{\Delta G_i}{RT}\right\} \qquad 9.2.$$

Thus from Equation 9.2, $\Delta G_i^{\alpha \rightarrow \gamma}$ at any one temperature can be obtained from C_i^{α} and C_i^{γ}, the equilibrium concentrations in the respective phases.

For iron-nitrogen (12) at the eutectoid temperature of 590° C (863° K)

$$C_N^{\alpha} = 0.1^{w}/o = 0.4^{a}/o$$

$$C_N^{\gamma} = 2.35^{w}/o = 8.75^{a}/o$$

Therefore, from Equation 9.2,

$$\Delta G_N^{\alpha \rightarrow \gamma} = -7{,}167 \text{ cals mole}^{-1} \qquad 9.3$$

For iron-carbon[118,119] at the eutectoid temperature of 727° C (1000°K)

$$C_c^{\alpha} = 0.02^{w}/o \simeq 0.095^{a}/o$$

$$C_c^{\gamma} = 0.765^{w}/o \simeq 3.45^{a}/o$$

Therefore

$$\Delta G_c^{\alpha \rightarrow \gamma} = -9{,}321 \text{ cals mole}^{-1} \qquad 9.4$$

For a martensite transformation, there will be no change in composition or positional entropy. Hence, following Zener[117], the free-energy of the iron atoms and their associated interstitial atoms must be identical in the two phases at T_o.

At the temperature T_o for Fe/C system

$$G_{Fe}^{\gamma} + G_c^{\gamma} C_c = G_{Fe}^{\alpha} + G_c^{\alpha} C_c \qquad 9.5$$

For Fe/N system

$$G_{Fe}^{\gamma} + G_N^{\gamma} C_N = G_{Fe}^{\alpha} + G_N^{\alpha} C_N \qquad 9.6$$

From Equations 9.4 and 9.5

$$G_{Fe}^{\gamma} - G_{Fe}^{\alpha} = 9{,}321 C_c \qquad 9.7$$

From Equations 9.3 and 9.6

$$G_{Fe}^{\gamma} - G_{Fe}^{\alpha} = 7,167\ C_N \qquad 9.8$$

The quantity $G_{Fe}^{\gamma} - G_{Fe}^{\alpha}$ is given in Table 10 as a function of temperature and from Equations 9.7 and 9.8 T_o may be obtained as a function of carbon or nitrogen concentration. These values are given in Table 11. A plot of the concentrations C_N and C_c in Table 11 against temperature gives the variation of the value of T_o with interstitial solute concentration for the iron-nitrogen and iron-carbon respectively. (Figure 81) On transforming to martensite, the M_s temperature must be appreciably below T_o to provide sufficient driving force to overcome the elastic strain energy associated with the formation of martensite. Suppose ΔE is the elastic strain energy per mole of martensite formed. Then equations 9.7 and 9.8 become

$$G_{Fe}^{\gamma} - G_{Fe}^{\alpha} = 9,321\ C_c + \Delta E \qquad 9.9$$

$$G_{Fe}^{\gamma} - G_{Fe}^{\alpha} = 7,167\ C_N + \Delta E \qquad 9.10$$

Rewrit ing these equations

$$C_c = \frac{\Delta G^{\gamma \rightarrow \alpha}_{Fe}}{9321} - \frac{\Delta E}{9321} \qquad 9.11.$$

$$C_N = \frac{\Delta G^{\gamma \rightarrow \alpha}_{Fe}}{7167} - \frac{\Delta E}{7167} \qquad 9.12$$

The effect of including ΔE into equations 9.11 and 9.12 is to displace the curves relating temperature and concentration to lower concentrations and temperatures. Zener chose $\Delta E = -290$ cals mole^{-1} independent of concentration to make the theoretical curve relating M_s temperature and carbon content to coincide with the experimental M_s curve. However, a much better fit to the experimental M_s curve in the range 0-7$\frac{a}{o}$ is obtained in the present calculations if we choose ΔE in Equation 9.11 so that it increases from 290 cals mole^{-1} at 0^a/o carbon to 360 cals mole^{-1} at 7^a/o carbon. The variation of ΔE with temperature, to make the M_s predicted by the corrected Zener theory coincide with the experimentally determined M_s is given in Table 12. In the iron-nitrogen system coincidence between the experimental and theoretical M_s curves as a functions of composition are also obtained when approximately the same variation of ΔE with

temperature is used as in the iron-carbon system. The only difference is that in the iron-nitrogen system the range of solubility of the interstitial solute is appreciably greater and martensite can be formed in alloys containing as much as 10^{a}/o nitrogen. Thus the range of variation of ΔE with nitrogen concentration has to be extended and values of $\Delta E = -400$ cals $mole^{-1}$ are approached in the most concentrated alloys. The data used to calculate the theoretical M_s temperatures curves as a function of interstitial concentration from equations 9.11 and 9.12 are given in Table 12. The theoretical M_s curves as functions of composition and the experimental M_s data are presented in Figure 81 for both the iron-carbon and the iron-nitrogen systems.

9.3 Fisher Model

The Zener analysis, although interesting because of its simplicity, is incomplete. In the determination of T_o and $\Delta G^{\gamma \rightarrow \alpha'}$ it does not take into account the structure of the martensite which may be either body-centred cubic or ordered body-centred tetragonal according to the carbon content and the temperature of transformation. It was Zener himself in 1946[59] who showed that iron-carbon martensite had an ordered body-centred tetragonal lattice below a critical temperature,

$$T_c = 28{,}000\ C_c \qquad 9.13.$$

and a body-centred cubic lattice above this temperature T_c. A detailed calculation of equation 9.13 for the iron-nitrogen system is given in Appendix 2 and a detailed discussion of the significance of Zener ordering is presented in the general discussion of this thesis. Fisher[121] has shown that the ordering is accompanied by a decrease in free energy

$$\Delta G_* = 2.39 \times 10^{-8}\ V_o\ \Delta g_* \qquad 9.14$$

cals per gram atom.

V_o is the volume corresponding to a mole of lattice sites and Δg_* is the decrease in free energy per unit volume on ordering, as derived from the Zener ordering analysis in Appendix 2. ΔG_* is a function of temperature and composition and of the strain associated with the transfer of a carbon atom from one <001> interstice to one at right angles to it. Because the carbon and nitrogen atoms in the martensite are the same size the value ΔG_* is expected to be the same for both the iron-carbon and the iron-nitrogen systems.

Fisher has incorporated this change in free energy

on ordering in a determination of the free energy change accompanying the martensite transformation in plain carbon steels. His analysis utilizes the activity data of carbon in austenite, by Smith[122] and the free-energy data of Zener[117] and Johansson[123] for the allotropic ferrite to austenite change in pure iron. A similar determination of the free energy change accompanying the austenite to martensite transformation in the iron-nitrogen system will be presented using the solubility data of nitrogen gas in alpha iron at one atmosphere[124] and the activity of nitrogen in gamma iron as determined by Atkinson[13] using ammonia-hydrogen mixtures. Following J.C. Fisher[121], for martensitic transformations in the iron-nitrogen system.

$$\Delta G^{\gamma\to\alpha} = C_{Fe}\left[RT \ln\left(\frac{\gamma^{\alpha}_{Fe}}{\gamma^{\gamma}_{Fe}}\right) + \Delta G^{\gamma\to\alpha}_{Fe}\right] + C_N RT \ln\left(\frac{\gamma^{\alpha}_{N}}{\gamma^{\gamma}_{N}}\right) \qquad 9.15$$

Where γ^{α}_{Fe} , γ^{γ}_{Fe} , γ^{α}_{N} , γ^{γ}_{N} are activity coefficients. The approximation $\gamma^{\gamma}_{Fe} = \gamma^{\alpha}_{Fe} = 1$ cannot be appreciably in error, especially since the ratio is taken. Then Equation 9.15 reduces to

$$\Delta G^{\gamma\to\alpha} = C_{Fe}\,\Delta G^{\gamma\to\alpha}_{Fe} + C_N RT \ln\left(\frac{\gamma^{\alpha}_{N}}{\gamma^{\gamma}_{N}}\right) \qquad 9.16$$

Johansson[123] and Zener[117] have calculated $\Delta G^{\gamma\to\alpha}_{Fe}$

from the specific heat data of Austin[126] and it is tabulated as a function of temperature in Table 10. The activity coefficients relative to nitrogen gas dissolved in gamma and alpha iron vary with temperature according to the relationships,

$$\frac{d \ln \gamma_N^{\gamma}}{d\left(\frac{1}{T}\right)} = \frac{\Delta H_N^{\gamma}}{R} \qquad 9.17$$

$$\frac{d \ln \gamma_N^{\alpha}}{d\left(\frac{1}{T}\right)} = \frac{\Delta H_N^{\alpha}}{R} \qquad 9.18$$

Where ΔH_N^{γ} and ΔH_N^{α} are the heats of solution of nitrogen gas in gamma and alpha iron. Assuming the values of ΔH to be independent of nitrogen concentration and temperature, Equations 9.17 and 9.18 on integration become

$$\ln \gamma_N^{\gamma} = \frac{\Delta H_N^{\gamma}}{RT} + I_1 \qquad 9.19$$

$$\ln \gamma_N^{\alpha} = \frac{\Delta H_N^{\alpha}}{RT} + I_2 \qquad 9.20$$

Where I_1 and I_2 are intergration constants.

Thus

$$RT \quad \ln\left(\frac{\gamma^{\alpha}_{N}}{\gamma^{\gamma}_{N}}\right) = \Delta H_N^{\alpha} - \Delta H_N^{\gamma} + RT\Delta I \qquad 9.21.$$

D. Atkinson has shown from his work on the nitriding of austenite with ammonia that

$$\Delta H_N^{\gamma} = -3{,}000 \text{ cals per gram atom} \qquad 9.22.$$

ΔH_N^{α} can be deduced by applying the Von't Hoff equation to the solubility of nitrogen in iron at one atmosphere.

$$d\,\frac{\ln C_N}{dT} = \frac{\Delta H_N^{\alpha}}{RT^2} \qquad 9.23.$$

Which on intergration becomes

$$\ln C_N = -\frac{\Delta H_N^{\alpha}}{RT} + I_3 \qquad 9.24$$

Where I_3 is another intergration constant. A plot of ln C_N versus $\frac{1}{T}$ enables ΔH_N^{α} to be obtained from the slope of the resultant straight line. The solubility data used, is that given in Figure 4 of Section 1. Which gives

$$\Delta H_N^{\alpha} = 6820 \text{ cals per gram atom} \qquad 9.25$$

Substituting Equations 9.22 and 9.25 into Equation 9.21.

$$RT \ln\left(\frac{\gamma^{\alpha}_{N}}{\gamma^{\gamma}_{N}}\right) = 9820 + RT\Delta I \qquad 9.26$$

It is now necessary to evaluate ΔI in Equation 9.26. Consider the distribution of nitrogen at equilibrium in the two phase $\alpha + \gamma$ region,

$$\Delta \bar{G}_N^{\gamma} = \Delta \bar{G}_N^{\alpha}$$

and

$$RT \ln \gamma_N^{\gamma} C_N = RT \ln \gamma_N^{\alpha} C_N^{\alpha} \qquad 9.27$$

Thus

$$\frac{\gamma_N^{\alpha}}{\gamma_N^{\gamma}} \simeq \frac{C_N^{\gamma}}{C_N^{\alpha}} \qquad 9.28$$

From the equilibrium boundaries of the metastable iron-nitrogen phase diagram as determined by Paranjpe.[12]

(at 810°C) $C_N^{\gamma} = 1.88 \times 10^{-2}$, while from Rawlings[14] internal friction data at 810° C $C_N^{\alpha} = 0.105 \times 10^{-2}$.

Therefore at 810° C,

$$\frac{C_N^{\gamma}}{C_N^{\alpha}} = 17.83 \qquad 9.29.$$

From Equations 9.27, 9.28 and 9.29

$$RT \ln\left(\frac{\gamma_N^{\alpha}}{\gamma_N^{\gamma}}\right) = 6,199 \qquad 9.30$$

Substitute equation 9.30 into 9.26

$$\Delta I = -3.34 \qquad 9.31$$

and equation 26 becomes,

$$C_N \; RT \ln\left(\frac{\gamma_N^{\alpha}}{\gamma_N^{\gamma}}\right) = C_N \; (9820-3.34T) \qquad 9.32$$

Therefore the terms in Equation 9.16 can be evaluated and the value of $\Delta G^{\gamma \rightarrow \alpha'}$ determined as a function of temperature and composition, but Equation 9.16 was obtained by an extrapolation which effectively assumes that the distribution of nitrogen in ferrite remains completely random at low temperatures. However, we have seen that spontaneous ordering of the carbon in ferrite takes place below the temperature

$$T_c = 284 x \ ^{o}K$$

Where x is in $\frac{a}{100}$ Equation 9.13 will be equally applicable to the ordering of both nitrogen and carbon to form a b.c.t. lattice from a b.c.c. lattice, because both interstitials have the same effective size in martensite. The change in free-energy ΔG_* associated with this b.c.c. to b.c.t. transition must be included in Equation 9.16. For the free energy change associated with the austenite to martensite transformation,

$$\Delta G^{\gamma \rightarrow \alpha'} = C_{Fe} \Delta G_{Fe}^{\gamma \rightarrow \alpha} + C_N (9820-3.34T) + \Delta G_* \quad 9.33.$$

The three terms on the right hand side of Equation 9.33 are listed in Tables 13,14,15 and $\Delta G^{\gamma \rightarrow \alpha'}$ for the iron-nitrogen system as a function of temperature and composition is presented in Figure 82.

The above Fisher treatment has been repeated for the iron-carbon martensite transformation and the corresponding free energy change as a function of temperature and carbon concentration is plotted in Figure 83.

When $\Delta G^{\gamma \rightarrow \alpha'}$ is zero the free energy of the austenite and martensite phases is equal, so from the data in Figures 82 and 83 the variation of T_o with nitrogen and carbon content can be deduced. These results are presented in Figure 84 together with the corresponding M_s curves as a function of composition. T_o for the iron-nitrogen system falls between 20-70° K higher than T_o for the iron-carbon system. Similarly the M_s temperatures for iron-nitrogen alloys lie somewhat higher than those for the corresponding iron-carbon alloys. At high nitrogen contents the rate of fall of T_o with increasing nitrogen concentration decreases, but a similar levelling off is not observed in the iron-carbon system because the solubility range is more restricted. From Figures 82,83 and 84 the free-energy change at M_s, the driving force, as a function of temperature for both iron-carbon and iron-nitrogen, alloys can be deduced. Over the complete range of nitrogen concentrations in the iron nitrogen alloys the driving force at M_s increases from about -290 cals $mole^{-1}$ to

to -520 cals mole^{-1} as the transformation temperature is correspondingly lowered from 800° K to 250° K. Similarly, the driving force in the iron-carbon system increases from -300 cals mole $^{-1}$ to -450 cals mole $^{-1}$ as the transformation temperature decreases from 800° K to 350° K. Figure 85 shows the variation of the driving force at M_s as a function of absolute temperature and Figure 86 shows the variation of the driving force at M_s as a function of composition for both the iron-carbon and the iron-nitrogen systems. Up to about 5^a/o a linear relationship between the free energy change and the interstitial content is observed.

9.4 Original Cohen Model.

Cohen, Machlin and Paranjpe[127] in 1950 estimated $\Delta G^{\gamma \rightarrow \alpha'}$ at M_s for the iron-carbon system by a method somewhat similar to that used by Fisher.[121] Perhaps surprisingly, Cohen et al found that the driving force at M_s is independent of composition over most of the range for iron-carbon alloys and is -290 cals mole^{-1} which is the same as the value originally deduced by Zener. As can be seen from Figure 87, this model predicts a slight decrease in the driving force at M_s at high carbon contents. This is the reverse to that found for both the iron-carbon and the iron-nitrogen systems using the revised Zener model and the Fisher analysis.

This trend is accentuated when considering high interstitial contents. Although the Cohen analysis, because of its similarity to the Fisher analysis, has not been worked out in detail, it is clear that when it is applied to the iron-nitrogen system at very high nitrogen contents the theoretical T_o is below the experimental M_s. This is impossible from the definition of T_o. This anomaly is illustrated for the iron-nitrogen system in Figure 88. The main differences between the Fisher and the Cohen analyses is that, instead of using the idea that the ordered b.c.t. structure is favoured at low temperatures and high carbon concentrations, Cohen assumed that the disordered b.c.c. structure is the more stable arrangement under all conditions. The elastic strain energy term was obtained directly from X-ray lattice parameter measurements using isotropic elastic constants.

It would therefore appear that the Zener idea of a transition temperature from b.c.c. to b.c.t. is correct and that the b.c.t. structure is the stable form at certain temperatures and compositions. If this concept is included in the Cohen model then the results of the Cohen analysis and the Fisher analysis are virtually identical. That is both the iron-nitrogen and iron-carbon systems show an increased driving force at M_s as the interstitial content is increased and also the same variation

of T_o with interstial content.

9.5. Geometric Model by Kaufman, Radcliffe and Cohen.[128]

The thermodynamic properties of interstitial solid solution have been treated statistically from a geometric point of view[123,129-132]. Scheil[130,131] has applied the results of this geometric model to the analysis of the activity measurements obtained by Smith[122] on austenitic iron-carbon alloys. These measurements were made in the ranges 800° C $\leq$ T $\leq$ 1200° C and $0.0007 \leq C_c \leq 0.07$ and it was found that within these limits an exclusion parameter $z^{\gamma} = 5$ gave the best fit. Kaufman, Radcliffe and Cohen[128] adopting this value of $z^{\gamma} = 5$ for the austenitic phase in the geometric model, and utilising Smith's activity data, derived the following expression for the free energy change accompanying the austenite to martensite transformation.

$$\Delta G^{\gamma\rightarrow\alpha} = (1-C_c)\Delta G_{Fe}^{\gamma\rightarrow\alpha} + C_c\,(15{,}580 - 5.76T) - RT\left[C_c \ln\left(\frac{3-C_c(3+z^{\alpha})}{1-6C_c}\right) + \frac{1-x}{5}\ln\left(\frac{1-6C_c}{1-C_c}\right) - \frac{3(1-C_c)}{z^{\alpha}}\ln\left(\frac{3-C_c(3+z^{\alpha})}{3(1-C_c)}\right)\right] \qquad 9.34$$

Z^{α} is the unknown exclusion parameter of the ferrite. Because the term in brackets containing Z^{α} is insensitive to the value of Z^{α} adopted provided it lies between 1 and 10, an average value of $Z^{\alpha} = 5$ was taken by Kaufman et al.

In order to obtain an expression for the free energy change associated with the transformation to martensite, the idea of Cohen[127] and Kaufman and Cohen[133] that the b.c.c. structure is the most stable form under all conditions of temperature and composition has been abandoned in the K-R-C[128] analysis. The ideas of Zener[117] and Fisher[121] concerned with ΔG_*, the free energy change associated with the ordering to a body centred tetragonal lattice, are incorporated in the K-R-C geometric model, thus,

$$\Delta G^{\gamma \rightarrow \alpha'} = \Delta G^{\gamma \rightarrow \alpha} + \Delta G_* \qquad 9.35$$

From this model it is deduced that the driving force at M_s is more or less constant at -265 cals $mole^{-1}$, independent of composition over the usual range of carbon concentrations iniron-carbon alloys. If, However, the model is extended to higher carbon concentrations it is seen that a lower driving force at M_s is predicted. This is in disagreement

with the predictions of Fisher's model where a greater driving force at M_s is required for high carbon contents. It is however in agreement with the original Cohen model in which the erroneous assuption was made that the body centred cubic structure was the more stable at all temperatures and compositions.

In the K-R-C analysis it is suggested that an exclusion parameter of $Z^{\gamma} = 5$ should also apply to the iron-nitrogen system but this is not supported by Atkinson's work. Atkinson[13] has compared his measurements of the activity of nitrogen in iron-nitrogen alloys with the predictions of the geometric model[130] and has found that the best fit occurs with an exclusion parameter for the austenite of $Z^{\gamma} = 4$. The choice of $Z^{\gamma} = 4$ is supported by the fact that the experimentally observed f.c.c. nitride is Fe_4N which has a value of $Z = 4$. Using the value of $Z^{\gamma} = 4$ the geometric model is now applied to the iron-nitrogen system. The free energy of the austenite G^{γ} containing interstitial nitrogen can be written in terms of the partial molar values

$$G^{\gamma} = (1-C_N)\,\bar{G}^{\gamma}_{Fe} + C_N\,\bar{G}^{\gamma}_{N} \qquad 9.36$$

A value of $\bar{G}_N^{\gamma}$ has been derived by Atkinson[13] using nitride as the standard state (G_N^S)

$$\bar{G}_N^{\gamma} - G_N^S = RT \ln a_N^{\gamma} \qquad 9.37$$

$$\bar{G}_N^{\gamma} - G_N^S = RT \ln \left(\frac{C_N}{1-5C_N} \right) - 3420 + 6.65T \qquad 9.38$$

While $\bar{G}_{Fe}^{\gamma}$ can be found from standard geometric thermodynamics (130 and 131) as

$$\bar{G}_{Fe}^{\gamma} - G_{Fe}^{\gamma} = \frac{RT\, n}{Z^{\gamma}} \ln \left\{ \frac{n - C_N(n+Z^{\gamma})}{n(1-C_N)} \right\} \qquad 9.39$$

n = number of interstitial sites per host lattice atom.

Now for iron-nitrogen austenite n = 1, $Z^{\gamma} = 4$

Therefore Equation 9.39 becomes

$$\bar{G}_{Fe}^{\gamma} - G_{Fe}^{\gamma} = \frac{RT}{4} \ln \left\{ \frac{1-5\,C_N}{1-C_N} \right\} \qquad 9.40.$$

Putting Equations 9.38 and 9.40 into Equation 9.36 obtains an expression for the free energy of the austenite,

$$G^{\gamma} = (1-C_N)\left[G_{Fe}^{\gamma} + \frac{RT}{4} \ln\left\{ \frac{(1-5C_N)}{(1-C_N)} \right\} \right] + C_N \left[G_N^S + RT \ln\left\{ \frac{C_N}{1-5C_N} \right\} - 3,420 + 6.65T \right] \qquad 9.41.$$

An Equation similar to Equation 36 can be written for the ferrite.

$$G^{\alpha} = (1-C_N)\ \bar{G}^{\alpha}_{Fe} + C_N\ \bar{G}^{\alpha}_{N} \qquad 9.42.$$

For ferrite Z^{α} is unknown and n = 3.

Therefore from Equation 9.39 in terms of ferrite.

$$\bar{G}^{\alpha}_{Fe} - G^{\alpha}_{Fe} = \frac{3}{Z^{\alpha}} RT \ln \left\{ \frac{3-C_N\ (3 + Z^{\alpha})}{3\ (1 - C_N)} \right\} \qquad 9.43.$$

The right hand side of Equation 9.43 tends to zero as C_N

Now the standard expression for $\bar{G}^{\alpha}_{N}$ can be written in the form

$$\bar{G}^{\alpha}_{N} - G^{S}_{N} = RT\ \ln\left(\frac{C_N}{3}\right) + A + BT \qquad 9.44$$

where the concentration C_N of nitrogen in ferrite is small. From a knowledge of the equilibrium solubilities of nitrogen in austenite and ferrite as a function of temperature together with Equation 9.38 the constants A and B can be evaluated. The data used in the computation of A and B is tabulated in Table 16. The 1083° K and 993° K values in Table 16. were experimentally determined by Atkinson[13], the other values were taken from the published phase diagram[12] and the $C_N^{\alpha/\alpha+\gamma}$ values were obtained by Rawlings[14].

Equation 9.44 becomes

$$\bar{G}_N^{\alpha} - G_N^{s} = RT \ln\left(\frac{C_N}{3}\right) + 4{,}365 + 7.15T \qquad 9.45$$

Therefore from Equations 9.42, 9.43 and 9.45 the free energy of the ferrite is

$$G^{\alpha} = (1-C_N)\left[G_{Fe}^{\alpha} + \frac{3RT}{Z^{\alpha}} \ln\left\{\frac{3-C_N(Z^{\alpha}+3)}{3(1-C_N)}\right\}\right] + C_N\left[G_N^{s} + RT \ln\left(\frac{C_N}{3}\right) + 4{,}365 + 7.15T\right] \qquad 9.46$$

An alternative and more exact form Equation 9.45 is

$$\bar{G}_N^{\alpha} - G_N^{s} = RT \ln\left\{\frac{C_N}{3-(3+Z^{\alpha})\ C_N}\right\} + 4{,}365 + 7.15\ T \qquad 9.47$$

If Equations 9.47 and 9.43 are put into Equation 9.42 an alternative form to Equation 9.46 for the free energy of the ferrite is obtained

$$G^{\alpha} = (1-C_N)\left[G_{Fe}^{\alpha} + \frac{3RT}{Z^{\alpha}} \ln\left\{\frac{3-C_N(Z^{\alpha}+3)}{3\ (1-C_N)}\right\}\right] + C_N\left[G_N^{s} + RT \ln\left\{\frac{C_N}{3-(3+Z^{\alpha})\ C_N}\right\} + 4{,}365 + 7.15T\right] \qquad 9.48.$$

From Equations 9.41 and 9.48 for the free energies of austenite and ferrite, the free energy change between austenite and ferrite of the same composition is

$$\Delta G^{\gamma\rightarrow\alpha} = (1-C_N)\,\Delta G_{Fe}^{\gamma\rightarrow\alpha} + C_N\,(7785 + 0.5T) - RT\left[C_N \ln\left\{\frac{3-C_N\,(3+Z^{\alpha})}{1-5C_N}\right\} + \frac{1-C_N}{4}\ln\left\{\frac{1-5C_N}{1-C_N}\right\} - \frac{3(1-C_N)}{Z^{\alpha}}\ln\left\{\frac{3-C_N\,(3+Z^{\alpha})}{3\,(1-C_N)}\right\}\right] \qquad 9.49$$

Z^{α} is the unknownexclusion parameter of the ferrite and because the term in brackets containing Z^{α} is insensitive to the value of Z^{α} adopted provided it lies between 1 and 10 an average value of $Z^{\alpha} = 5$ is taken. The term in $[\ ]$ will be written $[\Phi]$.

The first term on the right hand side of Equation 9.49 is given in Table 13 as a function of temperature and composition. The second and third terms are given in Tables 17 and 18 respectively, again as functions of nitrogen concentration and absolute temperature. For the reasons discussed previously in this section a term ΔG_* must be added to Equation 9.49 in order to obtain an expression for the austenite to martensite free energy

change $\Delta G^{\gamma \rightarrow \alpha'}$. Values of this expression ΔG_{Λ} are given in Table 15. Figure 89 shows the variation of free energy at M_s as a function of temperature and composition for the iron nitrogen system and it can be seen by comparison with Figure 83. that a virtually identical result is obtained with the K-R-C model as with the Fisher model. The driving force at M_s is given in Figure 90 and again a very similar relationship to the Fisher result is obtained. The driving force at M_s increases from -380 cals mole^{-1} at 800° K to about -600 cals mole^{-1} at 300° K. Figure 91 gives the results of the variation of T_o as a function of composition as derived by the K-R-C analysis for the iron-carbon system and also for the iron-nitrogen system. The results on the iron-nitrogen alloys show that the same variation of T_o with composition, within 50° C, is obtained from this model as with the Fisher model. While in the iron-carbon case with the geometric analysis T_o is considerably lower than the corresponding values of T_o obtained with the Fisher method. Furthermore a more or less constant driving force of -265 cals mole^{-1} independent of composition at M_s is predicted for the iron-carbon system on the K-R-C model. Recently Dr. Kaufman has stated[134] that $\Delta G^{\gamma \rightarrow \alpha}$ for the iron-carbon system need not be constant and independent of composition at M_s as he has derived in the K-R-C analysis and that the results

which he quotes in his paper were the best that could be obtained with the experimental data available and that an increased driving force at M_s is quite possible.

9.6. Summary and Conclusions.

9.6.1. Zener Model[117]

1. Using more reliable solubility data for carbon in ferrite and austenite than that available to Zener an elastic strain energy of -290 cals $mole^{-1}$ independent of composition fails to give agreement between the theoretical and experimental M_s results. Complete agreement is obtained when an elastic strain energy term increasing from -290 at $0^a/o$ carbon to -360 cals $mole^{-1}$ at $7^a/o$ carbon is used.

2. The Zener model, although satisfactory at low concentrations of nitrogen is essentially incorrect because it assumes that the elastic strain energy per mole of martensite is independent of composition. In fact at high concentrations about $10^a/o$ nitrogen, a strain energy term of about -400 cals $mole^{-1}$ is required to predict the experimental iron-nitrogen M_s values.

9.6.2. Cohen Model.[127]

1. This model when applied to the iron-nitrogen system shows that the driving force at M_s decreases as the M_s

temperature decreases and is not constant at about -290 cals mole^{-1} as deduced by Cohen.

2. The original Cohen model when applied to both the iron-carbon and iron-nitrogen systems fails to give a realistic picture of the free energy change associated with the martensitic transformation. It predicts that T_o can be lower than the experimental M_s temperature at high concentrations of nitrogen, which is impossible.

3. The main error in the Cohen analysis arises from the assumption that the b.c.c. form of martensite is the stable form under all conditionsbut the present work has shown that at high interstitial contents and low M_s temperatures, the b.c.t. structure is the more stable. Thus, any satisfactory thermodynamic model must incorporate a term describing Zener ordering of the interstitial solute atoms.

9.6.3. Fisher Model[121]

1. The Fisher model shows that T_o in the iron-nitrogen system is between 20-70° K higher than the corresponding values of T_o in the iron-carbon system.

2. The driving force at M_s increases from about -300 cals mole^{-1} at 0^a/o carbon to -450 cals mole^{-1} at 7^a/o carbon and to -550 cals mole^{-1} at 10^a/o nitrogen.

3. This increase in the driving force at M_s as the interstitial content is increased is predicted by the modified Zener analysis.

4. The thermodynamic model of Fisher, when applied to the iron-nitrogen system gives the variation of T_o with concentration to be up to 60°K higher than the corresponding iron-carbon T_o data and similarly the experimental iron-nitrogen M_s data lies about 60° K. higher. These differences of T_o and M_s between the two systems must arise from differences in the nature of the chemical solution of carbon and nitrogen in the various iron phases, rather than from the elastic strain energy associated with the alloying of iron with carbon and nitrogen.

9.6.4. Geometric K-R-C Model(128)

1. The application of the geometric model to the iron-nitrogen system results in essentially the same variation of T_o and $\Delta G^{\gamma \rightarrow \alpha'}$ at M_s, with composition as given by the Fisher analysis.

2. In the iron-carbon system the geometric model does not predict an increased driving force at M_s as the carbon content increases as was found for the other models reviewed and for the iron-nitrogen system. Rather a more or less constant driving force at M_s of -265 cals $mole^{-1}$ independent of composition is obtained.

10. GENERAL DISCUSSION.

One of the main reasons why very little previous experimentation has been carried out concerning the nature and structure of quenched iron-nitrogen alloys has been the difficulty of reproducibly obtaining homogeneous alloys in a form suitable for physical metallurgy experiments. The work in Section 2 of this thesis has established the necessary nitriding conditions in the gamma phase field to produce iron-nitrogen alloys in the form of wire or strip of any desired composition containing up to 2.7^{w}/o nitrogen. The maximum thickness of pure iron that can be nitrided by the methods described is 0.010" and consequently all the experiments in the present work have been carried out with specimens of this thickness. Yet despite this restriction the methods of specimen preparation described in Section 2 have enabled a whole range of experiments to be carried out yielding much new information on diffusionless transformations in the iron-nitrogen system. There is work in progress in the department attempting to uniformly nitride thicker sections, so that the range of experimental techniques may be extended still further.

The X-ray diffraction experiments in Section 3 showed that nitrogen has effectively the same atomic radius as carbon in both austenite and martensite. Consequently

it is expected that nitrogen is as effective as carbon in the solid solution hardening of martensite. This is despite the popular belief, arising from the experiments of Nehrenberg et al[53] which showed that nitrogen is less effective than carbon in the hardening of steel. Microhardness experiments did in fact show that the rate of hardening $\frac{dH}{dc}$ of martensite by either carbon or nitrogen was the same up to interstitial contents of about $2.5\frac{a}{100}$. The reason why the Nehrenbergs[53] results appeared to indicate that nitrogen is a less effective hardener is that nitrogen loss had occurred during the heat-treatment prior to quenching. Final nitrogen analyses were not reported. Such a nitrogen loss is expected because of the instablility of nitrogen-austenite at high temperatures and one atmosphere pressure.[12,19] The present results have shown that nitrogen is apparently less effective than carbon in hardening martensite only at high concentrations of the interstitial. However even at concentrations greater than $2.5\frac{a}{100}$ the effect is probably not real, the lower hardness in the iron-nitrogen alloys being due to the greater volume fraction of retained austenite.

The reasons why nitrogen is a more effective austenite stabiliser than carbon are not yet completely understood.

They have been discussed in Section 5, in terms of the relative effectiveness of carbon and nitrogen in immobilising martensitic strain embryos in the austenite the differences being a result of differences in the diffusion rates of the interstitials in austenite and martensite. It was concluded that on the basis of either of the current theories of stabilisation (diffusion in the austenite[64] or diffusion in the martensite[68]) the rate of diffusion of nitrogen was such that nitrogen would be more effective than carbon in stabilising the austenite. An alternative, or possibly additional, explanation of the relatively strong stabilising effect of nitrogen follows from the supposition that nitrogen lowers the stacking fault energy of the austenite. The profusion of annealing twins in iron-nitrogen austenite (Figure 53) indicates that this is a reasonable hypothesis. Dulieu and Nutting[92] have also shown that nitrogen lowers the stacking fault energy of austenite. The available evidence is that carbon has little effect or may even raise the stacking fault energy[92]. A lower stacking fault energy would cause nitrogen-austenite to work harden more rapidly than carbon austenite if, on account of the large strains associated with the austenite to martensite transformation, the third stage of work hardening is reached. Thus, the resistance to growth of new martensite plates would be increased.

There is however no direct experimental evidence to support this hypothesis.

The optical metallographic studies described in Section 6 show that low-nitrogen martensites have a structure strikingly similar to massive martensites, which in iron-nickel alloys have been the subject of much discussion recently.[41,83] Furthermore, the existance of interstitial massive martensites is not confined to iron-nitrogen alloys. As can be seen from Figures 34 and 35 the structure is also observed in iron-carbon[44] and iron-boron[90] alloys. Careful etching of massive martensite alloys reveals a substructure within the massive blocks consisting of parallel plates or laths packed in such a way as to completely fill space. It would appear from high temperature studies of iron-nickel-carbon massive martensites[91] that thes platelets grow in bursts, usually from an annealing twin or grain boundary, as the temperature is gradually lowered below M_s. Further evidence that the massive blocks are nucleated at and grow parallel to twin boundaries is provided by the observation that the longitudinal edges of the blocks are in a $\langle 111 \rangle_{\alpha'}$ direction in $\{ 110 \}_{\alpha}$ plane[91,136] It has not been established that the individual platelets grow uniquely in a $\langle 111 \rangle_{\alpha'}$ direction but quite often they appear to do so within a scatter of 5-10°.[96] From the

correlation between the dimensions of these platelets as determined from optical photomicrographs of prepolished surfaces (Figures 36 + 38) and the dimensions of the laths observed with the electron microscope of thin films of iron-nitrogen massive martensites (Figures 55-59) it appears that the two observations are of the same substructural feature.

The structure of quenched high-nitrogen alloys has also been shown to have the same morphology as quenched high-carbon alloys, that is lenticular plates of body-centred tetragonal martensite in a matrix of untransformed austenite. (Figures 64-70). The only essential difference between the two systems is that because of the high interstitial concentrations which are possible in the iron-nitrogen system, in an alloy containing sufficient nitrogen a completely austenitic structure can be retained on quenching to room temperature.

The transition from massive martensite to acicular martensite has been found to occur for both the iron-carbon and the iron-nitrogen systems at approximately the same interstitial content, $2.8\frac{a}{100}$. A corresponding transition from internally dislocated lath type martensite to internally twinned martensite is observed at about the same concentration. This transition is not sharp and quite

often it is possible to detect internally twinned plates at compositions below $2.8\frac{a}{100}$ [94] and dislocated plates in more concentrated alloys.(Figure 69). It is however, true to say that a predominance of dislocated plates exists in alloys containing less than $2.8\frac{a}{100}$ and a predominance of twinned plates at greater concentrations. In Section 3 it was also reported that at interstitial contents less than $2.8\frac{a}{100}$ the martensite has a cubic structure, while at higher concentrations binary interstitial martensites are tetragonal. Thus, an increasing the concentration of interstitial solute through $2.8\frac{a}{100}$ simultaneously there is a change in optical morphology, substructureand crystal symmetry.

As discussed earlier (Sections 9 Appendix 2) Zener[59] has shown that in iron alloys containing interstitials, there is according to the concentration of the interstitials and the temperature, an equilibrium structure for supersaturated ferrite which can be either b.c.c. or ordered b.c.t. The equation correlating the critical temperature for ordering T_c with interstitial concentration C_i for the situation of zero applied stress, as derived in Appendix 2 is

$$T_c = 0.243\ C_i E_{ool} \frac{\lambda^2}{k} \qquad 10.1$$

E_{001} is the modulus of elasticity in the [001] direction and λ is a parameter equal to the strain introduced by the transfer of 1 carbon or nitrogen atoms per unit volume from one [001] interstice to one normal to it.

This equation, when evaluated, is simply

$$T_c = 28000\ C_i \qquad 10.2$$

The M_s temperature, on the other hand, for iron-alloys decreases as the interstitial content in creases. Therefore, there is an interstitial content and a corresponding transformation temperature at which T_c and M_s are equal. At higher interstitial contents the [001] distortions will be ordered and therefore the structure will be tetragonal because M_s is below T_c, but at lower concentrations the disordered cubic structure should occur. This hypothesis can be tested. With binary iron-carbon alloys the transition point at which $M_s = T_c$ is predicted to be about $2.5\frac{a}{100}$ (Figure 92). This is in fair agreement with the value of $2.8\frac{a}{100}$ found experimentally. On this basis, the transition from b.c.c. to b.c.t. martensite is a function both of temperature and carbon content. Similarly for iron-nitrogen alloys the experimental M_s data from Section 8 as a function of temperature and concentration can be superimposed on the critical temperature curve for Zener

ordering. A value of $2.6\frac{a}{100}$ is predicted for the b.c.c. to b.c.t. transition which is once again in reasonable agreement with the experimentally observed value of $2.8\frac{a}{100}$. To test this idea still further the affect of adding substitutional alloying elements can be considered. By adding nickel to an iron-carbon alloy the M_s temperature is depressed and is shown by the iron-nickel-carbon data[102] in Figure 92 and the transition occurs at a lower carbon content. Also plotted in Figure 92 are the measurements of Winchell + Cohen[45] for a series of iron-nickel-carbon alloys in which the nickel and carbon contents were balanced to give a constant M_s. For both series of iron-nickel-carbon alloys the carbon-concentration transition predicted by the intersection of the Zener ordering curve and the curves representing the variation of M_s with carbon content is in good agreement with the minimum carbon content which is found experimentally by X-ray diffraction to give a tetragonal structure. The comparisons are set out in Table 19.

In these experiments the nickel has been varied over a considerable range of concentration but the Zener ordering curve (Figure 92) was calculated for iron-carbon and iron-nitrogen alloys with zero nickel content, Equation 10.2.

The good agreement shown in Table 19 indicates that nickel has no effect on the ordering process except through it's influence on the transformation temperature. In the Winchell and Cohen iron-nickel-carbon alloys[45] the M_s temperature is low about -35° C. When the X-ray measurements are made at about room-temperature, Zener disordering can take place in alloys with carbon contents less than $1\frac{a}{100}$. Winchell and Cohen showed that alloys with carbon contents less than $1.12\frac{a}{100}$ when transformed at -35° C and held at -100° C during the X-ray diffraction experiments had the non-equilibrium b.c.t. structure "frozen in" and yet the same alloy X-rayed at room temperature was body centred cubic. This gives an indication of the way in which the austenite to martensite transformation proceeds. It is expected that at the temperatures of interest disordering will be a slower process than the rearrangement of atoms on lattice sites by the movement through unit volume of a coherent austenite-martensite interface. Thus it is expected that at interstitial contents less than the transition concentration the face-centred cubic austenite will transform to a body-centred tetragonal structure and, provided sufficient thermal energy is available, disordering will occur at or immediately behind the interface, producing a body centred cubic structure.

In the crystallographic theories of the martensite transformation, using the notation of Bullough and Billy[140], the shape deformation F is composed of three components; a pure strain P, which is a homogeneous lattice strain converting the gamma to alpha phase (for iron alloys this is always assumed to be the Bain strain), a pure rotation R and S, a deformation which does not affect the lattice or cause a volume change.

$$F = S.R.P. \qquad 10.3.$$

Each solution defines a possible habit plane, orientation, and shape deformation. S is either a lattice shear produced by slip of a unit dislocation or possibly the equivalent of a simple shear produced by the movement of dislocations of more than one type in the interface. Alternatively, S may be described in terms of alternate twins. Further flexibility may be introduced if, following Bowles and Mackenzie[141,142], a dilation is allowed. In general and in principle the crystallographic theory gives a satisfactory description of the irrational habit planes with either the Kurdjumov-Sachs[42] or Nishiyama[143] orientations. If the alpha phase is tetragonal, symmetry considerations require the habit plane to be irrational; but, as shown by Kurdjumov and Sachs[42] a cubic lattice

can have a rational plane. They suggested that the f.c.c. to b.c.c. transformation could occur by consecutive shears $(111)_\gamma [\bar{1}\bar{1}2]_\gamma$ and $(1\bar{1}2)_\alpha [\bar{1}11]_\alpha$. The habit would then be $\{111\}_\gamma$ which is, in fact, observed, but these shears do not produce the required shape change.(141) Almost all subsequent developments of crystallographic theories have been concerned with transformations to tetragonal structures and irrational habits. However, Jaswon and Wheeler(144), introducing the concept that the habit plane is a plane which does not rotate during the transformation, showed that for transformations to a cubic lattice (incorrectly assumed to be attained only at zero carbon) $\{111\}_\gamma$ is a possible habit. Thus, in principle there is no reason why a formal crystallographic theory should not be developed to describe the transformation to cubic martensite with $\{111\}_\gamma$habit.

A change in the tetragonality of the martensite must be accommodated in the theory by changing the Bain strain P and thus a change in S.R. is expected. That is, a change in the Bain strain is accompanied by a change in orientation, habit or lattice strain, or any combination of these. The change from a cubic($\frac{c}{a}$ = 1) to a tetragonal lattice $\frac{c}{a}$ = 1.02 which occurs at $2.8\frac{a}{100}$, more or less coincides with a change

from a $\{111\}_\gamma$ habit and lattice shear by slip, to a $\{225\}_\gamma$ habit and shear by twinning. There does not appear to be a change in orientation in the iron-carbon series, although there is some doubt about the orientation adopted by high carbon alloys. The orientation relationships between the austenite and martensite have not been measured in the iron-nitrogen system, but it is expected from the similarity to the iron-carbon system that the Kurdjumov--Sachs[42] relationship $(111)_\gamma \parallel (110)_\alpha$ and $[1\bar{1}0]_\gamma \parallel [111]_\alpha$ will hold. In iron-carbon alloys a further change in habit from $\{225\}_\gamma$ to $\{259\}_\gamma$ on increasing the carbon content from 1.5 w/o to 1.8 w/o is observed. This change has been attributed to the decrease in the transformation temperature[145], but it is more likely to be due to the increase in tetragonality accompanying the increase in carbon content.[146] Although the habit planes have not yet been determined in the iron-nitrogen system it would be interesting to see if the series included $\{225\}$ going to $\{259\}$ and at the very high nitrogen contents to see if a still further deviation of the habit plane from $\{225\}$ occurs as the tetragonality is still further increased.

The change in tetragonality, habit plane and lattice shear at $2.8\frac{a}{100}$ is accompanied by a change in morphology from massive to acicular martensite. The reasons for this change are obscure. To minimise the elastic strain energy associated with a growing coherent plate, an arrangement of parallel plates growing adjacent to each other with alternate plates sheared in the opposite sense would appear to produce a situation of minimum elastic strain energy. Experimentally it has been found that adjacent lath type plates can be twin related.(96) The acicular arrangement adopted by tetragonal martensite with an irrational habit is a less obvious disposition of the plates and the formation of acicular martensite is most probably determined by the energy change associated with the growth of one plate in the elastic strain field created by a previously formed plate. Whatever the cause of the difference in morphologies, there can be little doubt that the change from virtually zero retained austenite in the massive structure, to a significant volume fraction, increasing with decreasing M_s temperature, in the acicular martensites is a direct result of the change in morphology. The elastic and plastic strains found in the untransformed gamma during the progress of the massive-martensite formation are insufficient to inhibit the nucleation of new plates

either parallel to existing packets or within the austenite volumes. On the other hand the strains in the gamma matrix of an acicular martensite prevents further nucleation even in specimens cooled well below the M_s temperature.

The occurrence of a few twinned martensite plates[94] and small volumes of tetragonality[145] in the massive martensites formed in low-carbon and low-nitrogen alloys and some dislocated martensite in high-interstial acicular martensite can be explained in terms of Zener ordering. There are two factors which could be significant. The variation of the order parameter with temperature for zero applied stress and several values of $\frac{\sigma}{\sigma_m}$ (where σ is an applied tensile stress and σ_m the tensile stress that would have to be applied to produce the same strain as that produced by a change in the order parameter from zero to unity) is shown in Figure 93. At zero applied stress, the order parameter increases from zero to 0.33 at the critical temperature, but on further cooling it increases less rapidly to unity. Thus, although at the critical temperature there is a large increase in the degree of ordering, there is a significant degree of short range disorder below the critical temperature. This could account for the local volumes of dislocated structure (Figure 69)

found in martensites with an M_s temperature below the Zener transition temperature, but, of course it does not explain ordering in massive martensites. However, a degree of ordering could be induced at temperatures above the zero-stress critical temperature by localised heterogeneous quenched in stresses, because the effect of applied stress is to smooth out the transition over an extensitive temperature range.

The Zener ordering hypothesis applied in the way described provides a rational explanation of the transition in iron-carbon and iron-nitrogen martensites but the explanation appears to be unsatisfactory when applied to iron-nickel alloys. In this system alloys with 29 to 33^a/o nickel at subzero temperatures form internally twinned acicular martensite which is not predicted by the theory. An alternative and more general hypothesis to explain the morphological transition in ferrous martensites is suggested by the thermodynamic results in Section 9. Furthermore this explanation includes the iron-nickel situation and shows that the morphological changes in the interstitial alloys may not of necessity be primarily associated with the Zener ordering transition which essentially only predicts the structural b.c.c. to b.c.t. change.

In the iron-nickel system a fairly sharp massive to acicular martensite transition takes place at about 29^{a}/o nickel and an associated dislocated to internally twinned substructure change also occurs at the same concentration[41]. Wayman[136] has shown that there is a small transition range of concentration in which the martensite plates may be partially twinned around the mid-rib and have a dislocated outer substructure. Kaufman and Cohen[133] have shown that the driving force at M_s in the iron-nickel system increases as the nickel content increases and the M_s is lowered. The driving force at the M_s temperature at which the transition from dislocated to twinned substructure occurs is about 310 cals mole^{-1}.

From the results in Section 9 it is seen that all the various thermodynamic models, except the K-R-C analysis for iron-carbon, show that there is an increase in driving force at M_s as the interstitial is increased in both the iron-carbon and iron-nitrogen systems. At an interstitial content of $2.8\frac{a}{100}$ $\Delta G^{\gamma \rightarrow \alpha}$ is approximately 310 cals mole^{-1}. It might therefore be expected that in all iron-based alloy systems a certain critical driving force at M_s of about 310 cals mole^{-1}; independent of temperature, is required to provide the elastic strain energy for twinning to replace slip as the mode of inhomogeneous deformation. Further

evidence for this idea is forthcoming from the fact that in the binary iron-chromium system the driving force at M_s for the austenite to martensite transformation is always less than the critical value of 310 cals $mole^{-1}$, (147) and acicular internally twinned martensite is not observed in this system.(40) The critical driving force of 310 cals $mole^{-1}$ occurs at about 0° C in the iron-nickel system and at about 350° C in the interstitial alloy systems and these are the temperatures at which the morphological transitions occur. This observation invalidates the proposition by P.M. Kelly(135) that the factor determining the transition is the temperature. The slip to twinning transition in the interstitial martensites is not abrupt but in the iron-nickel system the transition is fairly sharp. The difference probably arises because in the iron-nickel system near the transition composition the rate of change of the driving force at M_s with concentration is quite large, while in the iron-carbon and iron-nitrogen systems it is small.

GENERAL CONCLUSIONS.

Detailed conclusions have been given at the end of each Section. Only the major conclusions which can be drawn from the present work are presented again here.

1. The conditions necessary for the controlled and reproducible production of homogeneous iron-nitrogen alloys containing up to 2.7 w/o nitrogen, in the form of 0.010" wire or strip have been established.

2. The same linear variation of the lattice parameters of austenite and martensite with interstitial content occurs in both the iron-carbon and the iron-nitrogen systems.

3. The effective atom diameter of carbon and nitrogen in martensite is the same, consequently both interstitial elements are equally effective in the hardening and solid solution strengthening of martensite.

4. There is a transition from a body-centred cubic to a body centred tetragonal structure in rapidly quenched iron-carbon and iron-nitrogen alloys about $2.8\frac{a}{100}$. This transition can be predicted by considering the effect of interstitial concentration on the critical temperature for Zener ordering and on the M_s temperature.

5. The transition in crystal symmetry is accompanied by a change in morphology from massive to acicular martensite

and by a change in the substructures produced by the second shear, from a dislocated to a twinned structure.

6. Iron-nitrogen alloys containing more than 2.4^{w}/o nitrogen are fully austenitic after quenching to room temperature.

7. The high density of annealing twins in iron-nitrogen austenite observed metallographically, suggests that nitrogen lowers the stacking fault energy of austenite.

8. Nitrogen stabilises austenite more effectively than carbon. This results in a greater volume fraction of austenite being retained in quenched iron-nitrogen alloys, than in the corresponding iron-carbon alloys.

9. Massive martensite which is metallographically similar to massive martensite in substitutional alloys, is formed in rapidly quenched dilute alloys of iron-nitrogen iron-carbon or iron-boron.

10. Both the optical and electron metallographic structures of quenched iron-nitrogen and iron-carbon alloys are identical over corresponding range of composition.

11. The M_s temperature for an iron-nitrogen alloy is up to 70° C higher than that for the corresponding iron-carbon alloy.

12. The rate of increase of electrical resistivity with interstitial content is much greater for martensite than for austenite.

13. There is good agreement between the thermodynamic model for the variation of T_o with nitrogen concentration proposed by Fisher and that due to Kaufman, Radcliffe and Cohen when applied to the iron-nitrogen system. Both models show also that the driving force at M_s in the iron-nitrogen system increases from 290 cals mole $^{-1}$ at $0^w/o$ nitrogen to about 500 cals mole^{-1} at $2.6^w/o$ nitrogen. For the iron carbon system similar predictions are forthcoming from the Fisher model, but the K-R-C analysis gives a roughly constant value of $\Delta G^{\gamma \rightarrow \alpha'}$ at M_s.

APPENDIX 1.

Theory of the X-ray determination of retained austenite by integrated intensities.

If a mixture of martensite and austenite is irradiated with X-rays, each crystallite will diffract in accordance with the Bragg law. The diffracted energy at each Bragg angle from a polycrystalline sample may be written for given camera and exposure conditions as

$$I_x = \overline{K} \frac{1}{V_x^2} F^2 \; m \; (L.P) e^{-2m} \; C_x \; A(\theta) \qquad A_1.1.$$

I_x = Integrated intensity per unit length of diffraction line for a particular diffraction line of a substance x in arbitary units.

V_x = volume of unit cell

F = structure factor per unit cell

M = Multiplicity factor of diffracting plane.

L.P. = Lorentz and polarisation factor.

e^{-2m} = Debye-Waller temperature factor.

C_x = Volume fraction of substance irradiated.

$A(\theta)$ = sample absorption factor

(θ) = Bragg angle.

$\overline{K}$ = A constant.

Equation $A_1.1$ reduces to

$$I_x = \overline{K} R C_x A(\theta) \qquad A_1.2$$

where $$R = \frac{1}{\sqrt{2}} F^2 m (L.P) e^{-2m}$$

Volume of the unit cell The volume of the unit cells of austenite and martensite were determined from the observed variation of the lattice parameters of nitrogen martensite and austenite as a function of nitrogen content, presented in Section 3 of the thesis.

Structure Factor For the b.c.t. structure, where the unit structure has one atom at the centre of the unit cell and one atom at the corner of the unit cell (one eighth of 8 corner atoms) making a total of 2 atoms per unit cell. The equivalent point coordinates are 0,0,0, and $\frac{1}{2},\frac{1}{2},\frac{1}{2}$, the structure factor is therefore

$$F = \sum f \exp 2\pi i (hu + kv + lw)$$
$$= f \exp 2\pi i (h_o + k_o + l_o) + f \exp 2\pi i (h_{\frac{1}{2}} + k_{\frac{1}{2}} + l_{\frac{1}{2}})$$
$$= f \left(1 + \exp \pi i (h+k+l)\right)$$

When h + k + l is even F = 2f (f atomic scattering factor) and when h + k + l is odd no lines appear.

For the f.c.c. austenite lattice The equivalent point coordinates of the four atoms belonging to the unit cell are 0,0,0, ; $\frac{1}{2},\frac{1}{2},0$; $\frac{1}{2},0,\frac{1}{2}$, $0,\frac{1}{2},\frac{1}{2}$,. Since in the iron

lattice all the atoms are equivalent and have a scattering factor of f, the structure factor is

$F = 4f$ when h k l are all odd or all even

and $F = 0$ when h k l are mixed.

In the calculation of the effective structure factor a correction for dispersion must be made to the values of the scattering factor f tabulated by Taylor[76]. In the following experiments Cobalt $K\alpha$ is used and the wavelength of Cobalt $K\alpha$ radiation is very close to that of the absorption edge of iron. The correction, which has been tabulated in Taylor[76], takes the form

$f = f_o - \Delta f.$

f = effective atomic scattering factor

f_o = usual atomic scattering factor

Δf = decrement of the atomic scattering factor due to interaction with K electrons. With $Co K\alpha$ the dispersion is quite large $f = 4.0$ units.

Hence for b.c.t. lattice $F = 2(f_o - 4)$

and for the f.c.c. lattice $F = 4(f_o - 4)$

Multiplicity factor This is defined as the number of different planes of a particular form having the same spacing ($\{100\}$ in a cubic system m = 6). The values of m for the f.c.c. and b.c.t. phases were obtained from "The Interpretation of X-Ray Diffraction Photographs."[125]

The Lorentz Polarisation Factor For radiation which has not been crystal monochromated,

$$L.P = \frac{1 + \cos^2\theta}{\sin^2\theta \cos\theta}$$

and the values of L P are tabulated in Cullity[26].

Absorption Factor For a given cylindrical specimen the relative absorption increases as θ decreases, hence it is necessary to use reflections with only a limited spread in θ. When a diffractometer is used it is best to use as high θ lines as possible since absorption which is difficult to calculate, will be small and can be neglected.

Temperature Factor Thermal agitation decreases the intensity of a diffracted beam and the intensity decreases as the temperature is raised. For a constant temperature, thermal vibration causes a greater decrease in the reflected intensity at high angles rather than at low angles. This temperature effect and the previously discussed absorption effect in cylindrical specimens depend on angle in opposite ways and to a first approximation cancel each other out. This is particularly true if the comparison of intensities is is limited to lines of a restricted range of θ. When a diffractometer with a flat specimen is used the

temperature factor must be included in the calculation of the 'R' factor and the value of e^{-2m} is given as a function of $\frac{\sin\theta}{\lambda}$ in Cullity[26].

The reduced Equation $A_2.2$ may be written out in terms of austenite denoted by the subscript γ and martensite denoted by the subscript α', neglecting absorption.

$$I_\gamma = \overline{K} R_\gamma C_\gamma \qquad A_1.\ 3$$

$$I_{\alpha'} = \overline{K} R_{\alpha'} C_{\alpha'} \qquad A_1\ 4$$

Division of these two equations yields

$$\frac{I_\gamma}{I_{\alpha'}} = \frac{R_\gamma C_\gamma}{R_{\alpha'} C_{\alpha'}} \qquad A_1\ 5$$

The value of $\frac{C_\gamma}{C_{\alpha'}}$ can be obtained from the measurement of the integrated intensities I_γ and $I_{\alpha'}$ and from the calculation of R_γ and $R_{\alpha'}$. Once $\frac{C_\gamma}{C_{\alpha'}}$ is found the value of C_γ can be obtained from the additional relationship, $C_\gamma + C_{\alpha'} = 1$, when only martensite and austenite exist in the specimen. It is therefore possible to make an absolute measurement of the austenite content in the quenched iron nitrogen alloys by a direct comparison of the integrated intensity of an austenite line with the integrated intensity of a martensite line.

APPENDIX 2.

The calculations of the equilibrium conditions of temperature and interstitial concentration for the formation of either body-centred cubic or body-centred tetragonal martensite by the analysis of Zener[59] are set out.

Introduction

Following the initial observation by Fink and Campbell[120] that freshly quenched high carbon martensites have a body-centred tetragonal structure, numerous workers have made similar observations. It has often been assumed that all of the interstitial martensites are body-centred tetragonal of increasing tetragonality as the interstitial content is increased.[45] In contradiction to this assumption interstitial martensites with a cubic symmetry have been reported, including observations by Honda[24] of martensites in the binary iron-carbon system, by Maxwell[2] in the iron-nitrogen system and by Dijkstra.[25] The ranges of composition and M_s temperature in which cubic martensites are formed in the iron-nitrogen, iron-carbon and iron-nickel carbon alloys have been defined by the present investigation.

The question arises whether the cubic martensite is the result of a tempering process, such as occurs

relatively quickly at temperatures around 100° C and above, by which precipitation of a carbide or nitride phase takes place or, alternately, whether the tetragonality is lost by disordering of the aligned ⟨001⟩ tensile strains produced in the iron lattice by the interstitial atoms. The lattice disordering must involve the jumping of interstitial atoms into neighbouring sites. In fact, when the quenching rate is slow there is time for diffusion and the loss of tetragonality is due to tempering. This has been demonstrated by Kelly,[39] Aborn[44] and Baker[43] each of whom have demonstrated the existence of precipitates in slowly quenched low carbon martensites. However, specimens quenched very rapidly show no signs of precipitates either in iron-carbon martensites[44] or in the present work on iron-nitrogen martensites and yet such specimens are body centred cubic. It is postulated that in the latter case Zener disordering occurs.

In 1946 Zener[59] deduced the equilibrium conditions for the preferential distribution of carbon atoms amongst the octahedral sites to form a body-centred tetragonal lattice. The tetragonality arises from the carbon atoms spending a much longer time in the interstitial positions with tetragonal axes parallel to the lattice tetragonal axis than in other interstitial positions.

Zener in his analysis of the stability of the preferred distribution and therefore of the orthogonality of the lattice found that there exists a critical temperature T_c above which the equilibrium condition is the random distribution of interstitial carbon atoms and below which it is a preferred distribution. The equilibrium distribution is a function only of temperature, interstitial concentration, the elasticity modulus of the iron lattice and the strain associated with the transfer of an interstitial atom from one octahedral interstice to one at right angles to it. Because carbon and nitrogen have the same effective diameter in martensite the Zener analysis will be equally applicable to both.

Calculation of the Critical ordering temperature as a function of Composition.

A ferrite lattice containing interstitial nitrogen will automatically acquire the structure which renders its free energy a minimum.

The free energy per unit volume of the lattice is

$$G = U - TS - e\sigma \qquad A_2.1$$

where U = the internal energy

S = the entropy per unit volume

σ = tensile stress

e = tensile strain

In the computation of the strain e, the reference configuration is taken as that in which σ is zero and in which the distribution of the nitrogen atoms is random. When the free energy is a minimum

$$\delta G = 0 \qquad A_2.2$$

where δ refers to any small change of internal parameters which leaves the stress σ unchanged. This variation will be taken as the transfer of a nitrogen atom from an interstitial position with the tetragonal axis normal to the preferred axis (n position) to an interstitial position with the tetragonal axis parallel to this direction (p position). If N_n and N_p represent the number of nitrogen atoms per unit volume in these two types of position, respectively, the variation δ is

$$\delta N_p = 1, \quad \delta N_n = -1 \qquad A_2.3$$

and the corresponding variation in energy U is

$$\delta U = U_p - U_n + \sigma \delta e \qquad A_2.4$$

where U_p and U_n refer to the energy of a nitrogen atom in a p and n position respectively. The equilibrium Equation $A_2.2$ becomes,

$$U_p - U_n = T \delta S \qquad A_2.5$$

An estimate of the left hand side of Equation $A_2.5$ can be made if it is assumed that it is a function of the

tensile strain e, irrespective of how this strain is obtained; e.g. by a tensile stress or by a preferred distribution. We start with a random distribution and with no applied stress. The material is then subjected to a tensile stress along a lattice principal axis to produce a strain e, the distribution of nitrogen remaining random. The internal energy is thereby raised by the amount $\frac{1}{2} E_{100} e^2$. Next, keeping the strain constant, all the carbon atoms are moved to p positions. The change in internal energy is

$$\Delta U = \frac{2}{3} N (U_p - U_n) \qquad A_2 \cdot 6$$

N = total number of nitrogen atoms per unit volume. The total change in energy is therefore

$$\Delta f = \frac{1}{2} E_{100} e^2 + \frac{2}{3} N(U_p - U_n) \qquad A_2 \cdot 7$$

The final stress necessary to maintain the strain e will be zero if $\frac{\delta \Delta f}{\delta e}$ is zero, that is when

$$E_{100} e + \frac{2}{3} N \frac{\delta}{\delta e} (U_p - U_n) = 0 \qquad A_2 \cdot 8$$

For small strains, $U_p - U_n$ can be taken as a linear function of the strain, so Equation $A_2 \cdot 8$ reduces to

$$U_p - U_n = -E_{100} \lambda e \qquad A_2 \cdot 9$$

where $\lambda = \frac{e}{\frac{2}{3} N}$ and $N_p = N$

The quantity λ may be interpreted as the strain introduced by the transfer of one nitrogen atom per unit volume from an n to a p position. When deriving equation $A_2.9$ it was assumed that order is complete ($N_p = N$) but, since $U_p - U_n$ is a linear function of e, it must be of general validity.

The right-hand side of Equation $A_2.5$, the change in entropy associated with the transfer of a nitrogen atom from an n to a p position, can be shown by the standard methods of statistical mechanics to be given by

$$\delta S = - k \ln \frac{2N_p}{N_n} \qquad A_2.10$$

Expressing the entropy change in terms of a parameter that changes from zero, in the case of random distribution, to unity, in the case where all the nitrogen atoms are in p positions.

$$z = \frac{3}{2} \left[\frac{N_p}{N} - \frac{1}{3} \right] \qquad A_2.11$$

Hence equation $A_2.10$, in terms of this order parameter, is

$$\delta S = -k \ln \left[\frac{1 + 2z}{1 - z} \right] \qquad A_2.12$$

Combining Equations $A_2.5$ and $A_2.12$ gives

$$E_{100}{}^{\lambda}e = kT \ln\left[\frac{1+2z}{1-z}\right] \qquad A_2.13$$

When there is no tensile stress present the strain is proportional to the order parameter

$$e = \frac{2}{3} N\lambda z \qquad A_2.14$$

In this case the order parameter itself may be interpreted as the ratio of the actual tetragonality divided by the maximum tetragonality which occurs in the case of complete order. Substitution of Equation $A_2.14$ into $A_2.13$ gives

$$\left[\frac{2E_{100}N\lambda^2}{3kT}\right]Z = \ln\left[\frac{1+2z}{1-z}\right] \qquad A_2.15.$$

Zener showed graphically, from Equation $A_2.15$, that at all temperatures T above a critical value T_c the only possible value of the order parameter is $Z = 0$, corresponding to a random distribution of the interstial atoms in p and n positions and that at T_c, $Z = 0.33$. Therefore as the temperature is slowly lowered, the order parameter Z suddenly changes from 0 to 0.33, when the critical temperature is reached. The gradual increase

of Z as the temperature is further lowered is shown in Figure 93 of Section 10, (the case of zero applied tensile stress) obtained by graphically solving Equation $A_2.15$. At T_c the product $Z^{-1} \ln\left\{\frac{(1+z)}{(1-z)}\right\}$ has a value of 2.75. Therefore the critical temperature is given by,

$$T_c = 0.243\ NE_{100}\ \lambda^2/k \qquad A_2.16.$$

This critical temperature can be expressed in terms of interstial atoms per 100 iron atoms by making the substitutions,

$$N = 8.4 \times 10^{20}\ x \qquad \text{where x is in } \frac{a}{100}$$

$$E_{100} = 1.3 \times 10^{2} \text{ dynes per sq. cm.}$$

$$\lambda = 1.22 \times 10^{-23}$$

$$k = 1.39 \times 10^{-16}$$

The result is

$$T_c = 284 \times {}^{o}K \qquad A_2.17.$$

This equation is presented graphically in Figure 92 of Section 10 for iron-carbon and iron-nitrogen alloys.

REFERENCES

1. B. N. Boae and M. F. Hawkes, Trans. A.I.M.E., 1950 188, p. 307.
2. D. Maxwell and K. H. Jack, private communication.
3. W. Pitsch, Phil. Mag. 1959, 4, p.577.
4. W. Pitsch, J.I.M. 1959, 87, p.444.
5. A. Fry, Krupp. Mh. 1923, 4, p.138.
6. F. Osmond, Bull. Soc. d'Encour 1895 (iv), 10, p.496.
7. A. Fry, Stahl u. Eisen 1923, 43, p.1271.
8. S. Epstein, Trans. A.S.S.T., 1929, 16, p.19.
9. O. Eisenhut and E. Kaupp, Ztsch. Electrochemie, 1930 37, p.392.
10. G. Hägg, Ztsch, phys. chemie, 1930, 8. p.455.
11. E. Lehrer, Ztsch, Electrochemie, 1930, 37, p.460.
12. V. G. Paranjpe et al. Trans. A.I.M.E. 1950, 188, p.261.
13. D. Atkinson, Ph.D. Thesis, University of Liverpool, 1965.
14. R. Rawlings and D. Tambini, J.I.S.I. 1956, 184, p.302.
15. K. H. Jack, Proc. Roy.Soc. (A) 1951, 208. p.200.
16. K. H. Jack, ibid 1951, 208, p.216.
17. I. Ye Kontorovich and L. G. Yemel Ianova, Fiz, Metal. Metalloved, 1960, 9 no. 2, p.216.
18. R. M. Hudson, Trans. A.I.M.E. 1963, 227, p.695.
19. M. Akamoto, R. Tanaku, T. Naito and R. Fuyimoto Tetsu-to-Hagne, 1961, 2, p.25.

20. 'The Determination of Nitrogen in Steel'. B.I.S.R.A. special report, No. 62, 1958.

21. N. J. Petch, J.I.S.I. 1942, 145, p.111.

22. N. J. Petch, ibid 1943, 147, p.221.

23. H. Lipson and A.M.B. Parker, ibid, 1944, 149, p.123.

24. K. Honda and Z. Nishiyama, Sci. Rep. Tokohu Imp. Univ. 1932, 21, p.299.

25. L. J. Dijkstra, Trans. A.I.M.E. 1949, 185, p.252

26. B. D. Cullity, 'Elements of X-Ray diffraction' Addison-Wesley Publishing Co. Inc. 1956.

27. J. B. Nelson and D. P. Riley, Proc. Roy Soc. (A), 1945. 57, p.160.

28. C. S. Roberts, Trans. A.I.M.E., 1953, 196, p.203.

29. M. Cohen, J.I.S.I. 1963, 201, p.833.

30. D. Atkinson, T. Bell + D. Brough, J.I.S.I. Aug. 1965, p.836.

31. R. Speiser, J. W. Spretnak and W. S. Taylor, Trans. A.S.M. 1954-46, p.1168.

32. J. Prescott, 'Applied Elasticity', Dover Pub. N.Y. 1946, chapter 12.

33. J. D. Fast and M. B. Verijp J.I.S.I., 1954, 176, p.24.

34. C. M. Zener, 'Elasticity and Anelasticity of Metals', University of Chicago Pres. Chicago Ill. 1948.

35. J. Smith and H. G. Van Bueren, Philips Research Report 1954, 9, p.460.

36. J. L. Snoek, Physica. 1941, 8, p.711.

37. D. Polder, Philips Research Report, 1945, 1, p.5.

38. P. M. Kelly, and J. Nutting, I.S.I. Special Report No. 93, 1965, p.95.

39. P. M. Kelly, 'Electron Miscroscopy and Strength of Crystals' Interscience Publishers 1963, Chapter 21, p.917.

40. S. V. Radcliffe and M. Schatz, Nature 1963, 163, p.4902.

41. W. S. Owen, E. A. Wilson and T. Bell, Second International Materials Symposium, University of California, 1964 chapter 5 p.167.

42. G. V. Kurdjumov, J.I.S.I. 1960, 195, p.26.

43. A. J. Baker et al. 'Electron Microscopy and Strength of Crystals', Interscience Publishers 1963, p. 899.

44. R. A. Aborn, Trans. A.S.M. 1950 48, p.51.

45. P.G. Winchall and M. Cohen, 'Electron Microscopy and Strength of Crystals', Interscience Publishers 1963, p.995.

46. C. Wert, Trans. A.I.M.E., 1950, 188, p.1242.

47. E. T. Stephenson, Trans. A.S.M.1962, 55, p.625.

48. A. J. McEvily, R. C. Ku and T. L. Johnston - to be published.

49. M. J. Roberts and W. S. Owen, I.S.I. Special Report No. 93 1965, p.58.

50. E. C. Bain and H.W. Paxton, 'Alloying Elements in Steel'.

51. P. G. Winchell and M. Cohen, Trans. A.S.M. 1962, 55; p.347.

52. M. J. Roberts, Ph.D. Thesis, University of Liverpool 1966.

53. A. E. Nehrenberg, P. Payson and P. Lillys, Trans. A.S.M. 1955, 47, p.785.

54. B. L. Averbach, L. S. Castleman and M. Cohen, ibid. 1950, 42, p.112.

55. B. L. Averbach and M. Cohen, Trans. A.I.M.E. 1948, 176. p. 401.

56. R. A. McCune, 'Proceedings of the 11th Annual Conference on the Application of X-ray Analysis', Pittsburg, 1962, 6, p. 85.

57. R. F. Bunshah and R. F. Mehl, Trans. A.I.M.E. 1953, 197. p. 1251

58. M. G. H. Wells, Acta Met. 1964, 12, p. 389.

59. C. M. Zener, Trans. A.I.M.E. 1946, 167, p.550.

60. C. Crussard, ibid, 1946, 167, p. 590.

61. P.H. Kelly and J. Nutting, J.I.S.I., 1961, 197, p. 199.

62. J. Philibert, Comp. Renal, 1955, 240, p. 190.

63. L. C. Chang. J. Appl. Physics, 1952, 23, p. 727.

64. E. R. Morgan and T. Ko, Acta. Met. 1953, 1, p.36.

65. S. C. Das Gupta and B. S. Lement, Trans. A.I.M.E., 1953, p. 198, p. 530.

66. E. P. Klier and A. R. Troiano, ibid. 1945, 162, p. 175.

67. D. J. De. Lazaro, M. Hansen, R. E. Riley and W. Rostoker, ibid, 1952, 194, p. 265.

68. J. Woodila, P. G. Winchell and M. Cohen, ibid. 1959, 215, p. 849.

69. H. Knapp and V. Dehlinger, Acta. Met. 1956, 4, p. 289.

70. F. C. Frank, ibid, 1953, 1. p. 15.

71. E. G. Ramachandran and C. Dasarathy, ibid, 1960, 8, p.729.

72. J. K. Stanley, Trans. A.I.M.E. 1949, 185, p. 752.

73. C. A. Wert, Phys. Rev. 1950. 79, p. 601.

74. C. Wells and R. F. Mehl, Trans. A.I.M.E. 1960, 140, p.279.

75. W. Geller and T. H. Seen, Arch. Eisenhuttenweren, 1950, 21, p. 423.

76. A. Taylor 'X-ray metallography' Wileys N.Y. 1961.

77. L. S. Darken, R.P. Smith and R.W. Filer, Trans. A.I.M.E. 1951, 191, p.1174.

78. A. B. Greinger, Trans. A.I.M.E. 1939, 133, p. 204.

79. D. Hull and R. D. Garwood, J.I.M. 1957-8, 86, p.485.

80. J. B. Massalski, Acta. Met. 1958, 6, p. 243.

81. A. Gilbert and W. S. Owen, ibid, 1962, 10, p.45.

82. M. Cohen et al. 'Perspectives in metals research' Office of naval research, U.S. Navy, 1961, p.315.

83. W. S. Owen and E. A. Wilson, I.S.I. Special Report No. 93, p. 90.

84. G. V. Kurdjumov Probe met. fiz. met. 1952.

85. F. Forster and E. Scheil, Z. Metallkunde, 1936, 28, p. 245.

86. Ibid, 1940, 32, p. 165.

87. R. F. Mehl, and D. W. Smith, Trans. A.I.M.E. 1934, 113, p. 203.

88. R. F. Mehl and B. Derge, ibid, 1937, 125, p. 482.

89. R. F. Mehl, C. S. Barrett and D. W. Smith ibid, 1933, 105 p. 215.

90. C. C. McBride, J. W. Spretnak and R. Speiser, Trans. A.S.M. 1954, 46, p.449.

91. R. G. Bryans, Ph.D. Thesis, University of Liverpool, 1966

92. J. Nutting and D. Dulieu, I.S.I. Special Report No. 86. p. 140.

93. G. Kundjumov and G. Sachs, Z. Physik, 1930, 64, p.325.

94. P. M. Kelly and J. Nutting, Proc. Roy. Soc. (A), 1960, 259, p. 45.

95. P. M. Kelly and J. Nutting, G.I.S.I. 1959, 192, p.246.

96. G. R. Speich and P. R. Swann, ibid, 1965, 203, p.480.

97. W. Bollman, Phys. Rev. 1956, 103, p.1588.

98. P. M. Kelly and J. Nutting. J.I.M. 1959, 87, p.385.

99. R. B. Nicholson, G. Thomas and J. Nutting, Brit. J. Appl. Physics, 1959, 10, p.255.

100. 'Electron Microscopy of thin crystals', Butterworths 1965.

101. A. B. Greninger, Trans. A.S.M. 1942,,30, p.1.

102. P. Payson and C. H. Savage, ibid, 1943, 33, p.261.

103. J. F. Breedis and W. D. Robertson, Acta. Met. 1963, 11. p. 547.

104. H. C. Fielder, B. L. Averbach and M. Cohen, Trans. A.S.M. 1955, 47, p.269.

105. A. S. Sastri and D. R. F. West, J.I.S.I. 1965, 203, p.138.

106. S. V. Radcliffe and M. Schatz, Acta. Met. 1962, 10, p.201.

107. A. B. Greninger and A. R. Troiano, Trans. A.S.M., 1940, 29. p. 537.

108. A. Szombatfalvy, Acta. Techn. Acad. Sci. Hung., 1964 48, p. 143.

109. A. M. Portevin and M. Garvin, J.I.S.I. 1919, 99, p. 469.

110. H. Esser and W. Bungardt, Archiv für das Eisenhüttenwesen 1934, 7, p.533.

111. W. D. Swann and J. G. Parr, J.I.S.I., 1964, 202, p.105.

112. A. W. McReynolds, J. Appl. Phys. 1946. 17, p.823.

113. J. C. Bockros and E. R. Parker, Acta. Met. 1963, 11, p. 1291.

114. S. V. Radcliffe, Ph.D. Thesis, University of Liverpool, 1955.

115. G. W. C. Kaye and T. H. Laby, 'Tables of Physical and Chemical Constants', (11th Ed) 1956.

116. E. Griffiths, 'Physical Constants of some commercial steels at elevated temperatures E.D. by BISRA London 1953, Butterworths Scientific Pub.

117. C. M. Zener, Trans. A.I.M.E. 1946, 167, p. 513.

118. M. Hansen - 'Constitution of Binary Alloys', p. 353. McGraw-Hill Book Co. Inc. 1958.

119. M. G. Benz and J. F. Elliott, Trans. A.I.M.E. 1961, 221, p.323.

120. W. L. Fink and E. D. Campbell Trans. A.S.S.T. 1926, 9, p. 717.

121. J. C. Fisher, Metals Transactions, 1949, 185, p. 688.

122. R. P. Smith, Jnl. Am. Chem. Soc. 1946, 68, p.1163.

123. C. H. Johansson, Archiv. Für das Eisenhüttenwesen, 1937, 11, p. 241.

124. L. S. Darken, R. W. Gurry Physical Chemistry of Metals Chapt. 15, McGraw-Hill Publishing Co. Ltd., London, 1953.

125. Henry, Lipson and Wooster 'The Interpretation of X-ray Diffraction Photographs' 1951.

126. J. B. Austin, Jnl. Ind. and Eng. Chem. (1932) 24, p.1225.

127. M. Cohen, E. S. Machlin and V. J. Paranjpe, Thermodynamics in Metallurgy, A.S.M. Cleveland, 1949, p. 242.

128. L. Kaufman, S.V. Radcliffe and M. Cohen, Trans. Met. Soc. Symposium, 'The Decomposition of Austenite by diffusional processes' 1960, pp.313-351.

129. H. Dunwald and C. Wagner, Z. Anorg. Chem., 1931, 199. p. 231.

130. E. Scheil, Archiv. für des Eisenhuttenwesen, 1959, 30, p. 315.

131. E. Scheil, ibid. 1951, 22, p. 37.

132. R. Speiser and J. W. Spretnak, Trans. A.S.M. 1955, 47, p. 493.

133. L. Kaufman and M. Cohen, Progress in metal physics 19, 7, p.493.

134. L. Kaufman, I.S.I. Special report no. 93, p. 48.

135. P. M. Kelly. Electron Microscopy and Strength of crystals G. Thomas and J. Washburn Eds. N.Y. 1963, p.995.

136. C. M. Wayman, I.S.I. Special Report No. 93, p. 153.

137. G. Hagg, J.I.S.I. 1934, 130, p.439.

138. A. Ivenson and G. Kurdjumov, Zhur. Fiz. Khim, 1930, 1, p. 41.

139. M. Cohen, Trans. A.I.M.E., 1962, 224, p. 638.

140. R. Bullough and B. A. Bibby, Proc. Phys. Soc. 1956, 69B p. 1276.

141. J. S. Bowles and J. K. Mackenzie, Acta. Met. 1954, 2, p. 129.

142. ibid, 1954, 2, p. 224.

143. Z. Nishiyama Sci. Repts. Tokohu, Imp. Univ. 1934, 23, p. 637.

144. M. A. Jaswon and J. A. Wheeler, Acta. Crystal 1948, 1. p. 216.

145. G. V. Kurdjumov and L.I. Lysak. J.I.S.I. 1947, 156, p. 29.

146. M. S. Wechsler, D. S. Lieberman and T. A. Read, Trans. A.I.M.E. 1953, 197, p. 1503.

147. L. Kaufman, ibid. 1959, 215, p. 218.

LIST OF TABLES.

11. Concentration dependence of T_o for the iron-carbon and the iron-nitrogen systems (Zener model).
12. The data used to calculate the theoretical M_s temperature curves for iron-carbon and iron-nitrogen martensites. (Zener model).
13. The variation of $-C_{Fe}\, G_{Fe}^{\gamma \rightarrow \alpha}$ with absolute temperature and composition.
14. Evaluation of C_N (9,820 -3.34T) as a function of absolute temperature and nitrogen concentration.
15. The variation of the decrease in free energy $-\Delta G_*$ associated with Zener ordering in iron-carbon and iron-nitrogen alloys, with absolute temperature and interstitial content.
16. Data used in the computation of the constants in equation 9.44 The equilibrium solubilities of nitrogen in austenite and ferrite as a function of absolute temperature
17. Evaluation of C_N (7785 + 0.05T) as a function of temperature and nitrogen concentration.
18. Evaluation of $- RT[\Phi]$ as a function of temperature and nitrogen concentration.
19. Predicted and experimental interstitial concentration for the transition from cubic to tetragonal martensite.

TABLE I.

Analysis and Heat Treatment of Starting Material

Material Number	BISRA Code Number	Form	Heat Treatment	Initial %C	Final %C	$w_o O_2$	$w_o N_2$
1	A C N 2	Wire	110 hours at 750°C in wet H_2	0.015	0.008	0.006	0.002
2	A C N 2	Strip	170 hours at 950°C in wet H_2	0.0177	0.0047	0.007	0.002
3	V 8 1 O	Wire		0.004	0.004	0.007	
4	A J N 3	Strip		0.004	0.004	0.002	

TABLE 2.

Data used in the Nelson Riley extrapolation for the determination of the austenite and martensite lattice parameters of an iron-2.35W/o nitrogen alloy.

$hkl_{\alpha'}$	hkl_{γ}	4 θ cm	θ°	$\sin^2\theta$	d	a_{γ}	$\frac{1}{2}\left[\frac{\cos^2\theta}{\theta} + \frac{\cos^2\theta}{\sin\theta}\right]$	$a_{\alpha'}$	$c_{\alpha'}$
111	101	10.125	25.31	0.1827	2.0922	3.6262	1.881	2.8429	3.0988
	110	10.595	26.49	0.1990	2.0053		1.764	2.8375	3.0935
200		11.835	29.59	0.2430	1.8114	3.6243	1.498		
	002	14.100	35.25	0.3331	1.5498		1.120	2.8500	3.0996
	200	15.570	38.92	0.3943	1.4236		0.927	2.8472	3.1042
220		17.690	44.22	0.4863	1.2825	3.6302	0.701		
	112	18.735	46.84	0.5321	1.2262		0.607	2.8486	3.0997
	211	19.840	49.60	0.5799	1.1745		0.522	2.8453	3.0970
311		21.940	54.85	0.6685	1.0939	3.6308	0.376		
222	202	23.475	58.69	0.7299	1.0469	3.6292	0.290	2.8436	3.0997

TABLE 3.

Calculated radii of Interstitial Solute atoms in Austenite.

System	Reference	Interstitial Hole Diameter Å	$\bar{x}$	a_o Å	Δa_o Å	2 Δ R	radius of solute atom Å
Fe - C	Roberts(28)	1.042	1×10^{-2}	3.555	9.2×10^{-3}	0.439	0.74
Fe - N	Present Results	1.045	1×10^{-2}	3.564	7.7×10^{-3}	0.368	0.71

TABLE 4.

Data used for the determination of the retained austenite content of Specimen N63 containing 2.1W/o nitrogen.

Lattice parameter of austenite a_o= 3.63 Å Lattice parameters of martensite C_o= 3.074, a_o= 2.852

θ	hkl	sin θ/λ	fo	f	F^2	m	v^2	L.P.	I	R
35.64	002 α'	0.325	15.02	11.02	485	2	625.5 α'	3.994	127	6.20
38.91	200 α'	0.350	14.45	10.45	437	4	625.5 α'	3.405	243	9.35
44.28	220 γ	0.393	13.46	9.46	1432	12	2279 γ	2.870	223	21.61
47.21	112 α'	0.412	13.05	9.05	328	8	625.5 α'	2.750	250	11.53
49.61	211 α'	0.436	12.70	8.70	303	16	625.5 α'	2.729	422	21.2

TABLE 5.

Intensity measurements on specimen N63 obtained with the diffractometer.

hkl	I	R	e^{-2m}	Corrected R value
220γ	210	21.61	0.890	19.2
112α′	260	11.53	0.880	10.2
211α′	380	21.20	0.875	18.5

TABLE 6.

The diffusivities of carbon, nitrogen and hydrogen in Austenite and Ferrite.

Diffusivity (cm^2/sec)	At 20° Centigrade.	Reference Number.
$D_C^{\gamma} = 7.0 \times 10^{-2} \exp^{-32,000/RT}$	$D_C^{\gamma} = 9.55 \times 10^{-26}$	74
$D_N^{\gamma} = 2.0 \times 10^{-2} \exp^{-28,000/RT}$	$D_N^{\gamma} = 2.69 \times 10^{-22}$	77
$D_H^{\gamma} = 1.1 \times 10^{-2} \exp^{-9.950/RT}$	$D_H^{\gamma} = 4.2 \times 10^{-10}$	75
$D_C^{\alpha} = 2.0 \times 10^{-2} \exp^{-20,100/RT}$	$D_C^{\alpha} = 2.0 \times 10^{-17}$	72 & 73
$D_N^{\alpha} = 6.6 \times 10^{-3} \exp^{-18,600/RT}$	$D_N^{\alpha} = 8.8 \times 10^{-17}$	76
$D_H^{\alpha} = 2.2 \times 10^{-3} \exp^{-2,900/RT}$	$D_H^{\alpha} = 1.5 \times 10^{-5}$	75

TABLE 7.

Electropolishing techniques for producing thin foils of iron-nitrogen martensite.

Technique	Composition of Electrolyte	Polishing conditions			Remarks	Degree of Success	
		Cathode	Voltage	Temp °C		< 0.6 W/o N	> 0.6 W/o N
Washer	135 cc. of glacial acetic acid. 26 g. of chromic acid 7 cc. of water.	Stainless Steel	25-30	<30	Wash in acetic acid, then alcohol	None	None
	Saturated solution of chromic oxide in orthophosphoric acid.	Stainless steel points	15	<40	Stir the electrolyte, Wash with water then Methanol.	Moderate	None
Washer	10% solution of perchloric acid in isopropyl alcohol	Stainless steel points	20-30	not critical	Stir the electrolyte, Wash in methanol	Limited	Limited
Window	10 parts glacial acetic acid/one part perchloric acid	Stainless steel beaker	25-30	<20	Stir the electrolyte, Wash in Acetic Acid then alcohol.	Moderate	Moderate

TABLE 8.

The Average Ms values and the average cooling rates and Austenitising temperatures for all the alloys used in the Thermal analysis experiments.

Alloy No.	Weight percent N	Interstitial atoms per 100 Fe atoms	Average Ms °C	Average Austenitising temperature °C	Average Cooling rate at 600°C
N 84	0.17	0.68	515	927	2,600
N 81	0.44	1.80	417	885	1,440
N 82	0.55	2.00	412	870	2,220
N 76	0.62	2.48	389	885	1,710
N 80	0.67	2.68	353	888	1,700
N 78	0.75	3.00	350	870	1,290
N 75	0.82	3.28	324	852	960
N 99	0.94	3.76	334	860	1,300
N 74	1.22	4.90	263	780	1,050
N106	1.64	6.70	155	950	1,270
N 90	1.90	7.70	133	820	825

TABLE 9.

Ms Temperature as a function of composition, as determined by the resistivity technique.

Specimen Number	Weight % Nitrogen	Interstitial atoms per 100 Fe atoms	M_s ($\pm$ 5°C)	X ray (f.c.c. lines only)(°C)
N 94	2.36	9,7	-1	0
N103	2.45	10.0	-21	-15
N 95	2.50	10.3	-29	-20
N 96	2.65	10.8	-100	-90

TABLE 10.

Mean interpolated values of the free energy difference between, γ - iron and α - iron calculated by Johanson[123] and Zener[117] from the specific heat data of Austin[126]

T°K	$-\Delta G_{Fe}^{\gamma \rightarrow \alpha}$ cals mole^{-1}
200	1109
250	1062
300	1007
350	946
400	880
450	811
500	738
550	663
600	591
650	521
700	449
750	377
800	308
850	243
900	180
950	121
1000	75
1050	42
1100	22
1180	0
1200	-4
1250	-10

TABLE 11.

Concentration dependence of To for the iron-carbon and the iron-nitrogen systems (Zener model)

T°K	$C_c \times 10^2$	$C_n \times 10^2$
200	11.9	15.5
300	10.8	14.1
400	9.4	12.3
500	7.9	10.3
600	6.3	8.3
700	4.8	6.3
800	3.3	4.3
850	2.6	3.4
900	1.9	2.5
950	1.3	1.7
1000	0.8	1.0
1050	0.5	0.6
1100	0.1	0.3
1180	0.0	0.0

TABLE 12.

The Data used to calculate the Theoretical Ms Temperature Curves for Iron-Carbon and Iron-Nitrogen Martensites (Zener Model)

T°K	$-\Delta G_{Fe}^{\gamma \rightarrow \alpha}$	$-\Delta E_{Fe/N}$	$-\Delta E_{Fe/c}$	$\Delta G - \Delta E_{Fe/N}$	C_N $^{\alpha}/_{o}$	$\Delta G - \Delta E_{Fe/C}$	C_c $^{\alpha}/_{o}$
200	1109	400	—	-709	9.9	—	—
300	1007	385	355	-622	8.7	-652	7.0
400	880	365	350	-515	7.2	-530	5.7
500	738	340	340	-398	5.6	-398	4.3
600	591	320	320	-271	3.8	-271	2.9
700	449	310	310	-139	1.9	-139	1.5
750	377	300	300	-77	1.1	-77	0.8
800	308	290	290	-18	0.3	-18	0.2

TABLE 13.

The Variation of $-C_{Fe}\ G_{Fe}^{\gamma \rightarrow \alpha}$ with Absolute Temperature and Composition.

	TEMPERATURE °K									
C_{Fe}	300	400	500	600	700	800	900	1000	1100	1200
0.996	1003	877	735	589	447	307	179	75	22	-4.0
0.985	992	867	727	582	442	303	177	74	22	-3.9
0.977	984	860	721	577	439	301	176	73	22	-3.9
0.969	976	853	715	573	435	299	174	73	21	-3.9
0.962	969	846	710	569	431	296	173	72	21	-3.8
0.946	953	833	698	559	425	291	170	71	21	-3.8
0.932	939	820	688	551	419	287	168	70	21	-3.7
0.909	915	800	671	537	408	280	164	68	20	-3.6
0.900	906	792	664	532	404	277	162	68	20	-3.6

TABLE 14.

Evaluation of $C_N(9{,}820 - 3.34T)$ as a function of Absolute Temperature and Nitrogen Concentration.

		TEMPERATURE ^{o}K									
w/o N	C_N	300	400	500	600	700	800	900	1000	1100	1200
0.1	0.004	35	34	33	31	30	29	27	26	25	23
0.4	0.015	132	127	122	117	112	107	102	97	92	87
0.6	0.023	203	195	188	179	172	164	157	149	142	134
0.8	0.031	273	263	253	242	231	222	211	200	191	180
1.0	0.038	335	322	310	297	284	272	259	246	234	221
1.4	0.054	476	458	440	422	404	386	368	350	332	314
1.8	0.068	599	577	554	532	508	486	463	440	419	395
2.45	0.091	802	772	741	711	680	650	620	589	560	529
2.70	0.100	882	848	815	782	748	715	681	648	615	581

TABLE 15.

The Variation of the Decrease in Free Energy $-\Delta G$ Associated with Zener Ordering in Iron-Carbon and Iron-Nitrogen Alloys with Absolute Temperature and Interstitial Content.

TEMPERATURE °K

C_N	300	400	500	600	700	800	900	1000	1100	1200
0.004	-1	-2	-4	-5	-6	-8	-8	-10	-11	-13
0.015	2	0	0	-1	-1	-1	-2	-2	-2	-3
0.031	30	23	19	12	6	5	4	3	0	-2
0.038	52	43	35	27	20	13	7	2	1	0
0.054	122	110	98	88	75	63	52	42	32	23
0.068	209	194	179	164	149	134	120	106	92	78
0.091	404	384	365	345	325	306	284	266	246	227

TABLE 16.

Data used in the computation of the constants in Equation 9.44 The Equilibrium solubilities of nitrogen in Austenite and Ferrite as a function of Absolute Temperature.

$T^{o}K$	$C_N^{\alpha/\gamma+\alpha}$	$C_N^{\alpha+\gamma/\gamma}$	$A + BT$ cals $mole^{-1}$
1083	.00102	.0150	12,096
1073	.00116	.0175	12,032
993	.00214	.0380	11,492
973	.00240	.0450	11,332
863	.00400	.0880	10,504

TABLE 17.

Evaluation of C_N (7785 + 0.5T) as a function of temperature and Nitrogen Concentration.

		TEMPERATURE °K									
W/o N	C_N	300	400	500	600	700	800	900	1000	1100	1200
0.1	0.004	32	32	32	32	32	33	33	33	33	34
0.4	0.015	119	120	120	121	122	123	123	124	125	125
0.6	0.023	183	184	185	186	187	189	189	191	192	193
0.8	0.031	246	248	249	251	252	254	256	257	259	260
1.0	0.038	302	303	305	307	309	311	313	315	316	319
1.4	0.054	429	431	434	437	439	442	445	447	450	453
1.8	0.068	540	543	547	551	554	558	561	564	568	571
2.45	0.091	722	727	731	736	740	745	750	754	759	763
2.7	0.100	794	799	804	809	814	819	824	829	834	839

TABLE 18.

Evaluation of - RT [ø] as a function of temperature and nitrogen concentration.

		TEMPERATURE °K									
w/o N	C_N	300	400	500	600	700	800	900	1000	1100	1200
0.1	0.004	3	4	5	5	6	7	8	9	10	11
0.4	0.015	8	11	13	16	19	22	25	27	30	33
0.6	0.023	16	21	26	32	37	42	48	53	58	64
0.8	0.031	21	28	34	41	48	55	62	69	76	83
1.0	0.038	26	35	43	52	60	69	78	86	95	104
1.4	0.054	38	51	63	76	88	101	114	126	139	152
1.8	0.068	47	63	79	94	110	126	141	158	173	189
2.45	0.091	64	85	107	128	149	170	191	213	234	256
2.70	0.100	75	100	125	150	175	200	225	250	275	300

TABLE 19.

Predicted and Experimental Interstitial Concentration for Transition from Cubic to Tetragonal Martensite.

Series	Predicted Transition Interstitial Concentration $\alpha/100$	Experimental Value Interstitial Concentration at Transition	Reference
Iron-carbon	2.5	2.8	42, 137, 138, 139
Iron-nitrogen	2.6	2.8	Present results
Iron-19% Nickel-Carbon	1.5	1.45	102
Iron-nickel-carbon, constant $M_s(-35^{o}C)$	0.93	1.12	45

LIST OF FIGURES.

12. The variation of the lattice parameter of iron-nitrogen austenite with increasing interstitial content.
13. The variation of the c and a lattice parameters of iron-carbon and iron-nitrogen martensites with increasing interstitial content.
14. Variation of the lattice parameter ratio $\frac{c}{a}$, for iron-carbon and iron-nitrogen martensites, with increasing interstitial content.
15. Debye Sherrer X-ray diffraction patterns of iron-nitrogen martensites with increasing nitrogen concentration.
16. Diffractometer tracings of the $\{110\}_{\alpha'}$, $\{200\}_{\alpha'}$, $\{211\}_{\alpha'}$ reflections for a series of iron-nitrogen martensites.
    1. 0.00^{W}/o nitrogen; b.c.c. reflections
    2. 0.30^{W}/o nitrogen; b.c.c. reflections
    3. 0.64^{W}/o nitrogen; b.c.c. reflections
    4. 0.71^{W}/o nitrogen; b.c.t. reflections
17. The Nelson-Riley extrapolation for the determination of the austenite and martensite lattice parameters of an iron -2.35^{W}/o nitrogen alloy.
18. The variation of hardness with nickel content for iron-nickel alloys. After Owen, Wilson and Bell.[41]

19. Curves for the conversion of Reichart microhardness scale readings, for a constant 80 gram load, into Vickers Hardness Numbers.

20. The variation of the hardness of iron-nitrogen and iron-carbon[40] martensites with interstitial content.

21. The variation of the flow stress σ_f, of quenched iron-carbon-nickel alloys as a function of the square root of the atom fraction of carbon. After Roberts.[51]

22. Variation of the 0.2% flow stress with the square root of the atom fraction of interstitial solute, for iron-nitrogen and iron-nickel-carbon martensites.

23. Variation of the volume percent retained austenite at -196° C with interstitial content for iron-nitrogen and iron-carbon alloys.

24. Intensity versus Bragg angle curve of specimen N 63 containing 2.1 w/o nitrogen, obtained from the microphotometer tracing of the corresponding Debye Sherrer X-ray diffraction pattern.

25. Curve for converting microphotometer deflections into intensites and the corresponding graduated intensity film.

26. Diffractometer tracing of specimen N 63 containing 2.1 w/o nitrogen.

27. Typical equiaxed alpha structure; F_e - 4.0[a]/o Ni, thermally etched to reveal austenite boundaries, quenched, and subsequently etched to reveal ferrite boundaries.[83] x 880

28. Typical massive-martensite structure. Quenched iron - 23.8[a]/o nickel.[41] x 350.

29. Surface shears on a pre-polished specimen of iron - 15[a]/o nickel transformed to massive martensite at 338° C.[41] x 850.

30. Acicular martensite in F_e - 31[w]/o Ni - 0.3[w]/o C, electro etched in perchloric-acetic acid solution[49] x 1000

31. Typical massive in an iron -0.08[w]/o nitrogen alloy, quenched into brine at room temperature, etched in alcoholic ferric chloride x 220

32. Massive martensite in an iron -0.17[w]/o nitrogen alloy quenched into brine at room temperature, etched in picral-2% nital solution. x 200

33. Massive martensite in an iron -0.17[w]/o nitrogen alloy quenched into brine at room temperature, etched in picral-2% nital solution. x 550

34. Massive martensite in a quenched low carbon steel.[44] x 550

35. Massive martensite in an iron-boron alloy quenched from the $\alpha + \gamma$ region.[90] x 450 (white regions are ferrite.)

36. Prepolished surface of an iron -0.17^{W}/o nitrogen alloy quenched into brine. Oblique illumination illustrating the surface relief effect of massive martensite. x 350

37. Iron -0.37^{W}/o nitrogen massive martensite quenched into brine at room temperature, etched in picral-2% nital solution x 540.

38. Prepolished surface of an iron - 0.37^{W}/o nitrogen alloy quenched into brine. Oblique illumination x 700

39. Interferogram corresponding to Figure 38.

40. Iron - 0.54^{W}/o nitrogen alloy quenched into brine and further cooled to -196^{o} C. Etched in 2% nital x 750.

41. Iron -0.65^{W}/o nitrogen alloy quenched into brine and further cooled to -196^{o} C. Etched in 2% nital x 750

42. Prepolished surface of an iron -0.54^{W}/o nitrogen alloy quenched into brine. Oblique illumination x 1000.

43. Interferogram corresponding to Figure 42.

44. Iron - 1.2^{W}/o nitrogen alloy quenched into brine and etched with 5% nital x 620.

45. Iron -1.85^{W}/o nitrogen alloy quenched into brine and etched with 5% nital x 750.

46. Iron -2.1^{W}/o nitrogen alloy quenched into brine and further cooled to -196^{o} C, lightly tempered and etched with 2% nital x 500

47. Iron -2.3^{W}/o nitrogen alloy quenched into brine and further cooled to 0^{o} C, lightly tempered and etched with 2% nital x 550.

48. Iron -2.4^{W}/o nitrogen alloy quenched into brine and further cooled to -196^{o} C, lightly tempered at 225^{o} C and etched in 2% nital. x 750.

49. Prepolished surface of an iron -2.35^{W}/o nitrogen alloy quenched into brine and further quenched to 0^{o} C. There are a few acicular martensite plates present in a matrix of austenite. Oblique illumination x 400

50. Interferogram corresponding to Figure 49.

51. Prepolished surface of an iron 2.35^{W}/o nitrogen alloy quenched into brine and further cooled to -196^{o} C. Oblique illumination. x 1000.

52. Interferogram corresponding to Figure 51.

53. Iron -2.5^{W}/o nitrogen alloy quenched to 10^{o}C, showing a fully austenitic structure. Electropolished and etched in 5% perchloric-acid acetic solution. x 300

54. Prepolished surface of an iron -2.4^{W}/o nitrogen alloy quenched to 10°C. Oblique illumination x 350.

55. Electron micrograph of iron -0.3^{W}/o nitrogen martensite, illustrating general lath type structure. x 30,000.

56. Electron micrograph of iron -0.3^{W}/o nitrogen martensite illustrating the sharp boundary between two "sheaves" of laths. x 30,000

57. Electron micrograph of iron -0.3^{W}/o nitrogen martensite, illustrating the variation in lath thickness and the dovetailing of individual laths. x 30,000.

58. Selected area electron diffraction patterns of the large lath in Figure 57. Foil orientation ($\bar{1}3\bar{1}$)

59. Electron micrograph of iron -0.42^{W}/o nitrogen martensite.

60. Selected area electron diffraction pattern of the large lath in Figure 59. Foil orientation is approximately (133).

61. Electron micrograph of iron -0.65^{W}/o nitrogen martensite, showing small interwoven dislocated laths. x 40,000

62. Electron micrograph of iron -0.65^{W}/o nitrogen martensite illustrating general lath type structure. x 40,000.

63. Electron micrograph of an iron -0.65^{W}/o nitrogen martensite. There are a few internally twinned martensite plates present x 50,000.

64. Electron micrograph of iron -1.1^{W}/o nitrogen martensite showing a large martensite plate which has coarse internal twinning, with a spacing of about 500A^{o}. x 60,000

65. Electron micrograph of an 1.1^{W}/o nitrogen martensite. x 50,000.

66. Electron micrograph of iron 1.4^{W}/o nitrogen martensite. The fire structure of the martensite is predominately internal twinning. x 50,000.

67. Electron micrograph of a large iron -1.4^{W}/o nitrogen martensite plate, showing fine internal twinning 100^{o}A thick. x 100,000.

68. Selected area electron diffraction pattern corresponding to Figure 67. Foil orientation is approximately (11$\bar{1}$)and the streaking is at right angles to the fine twins.

69. Electron micrograph of an iron -1.4^{W}/o nitrogen alloy showing a dislocated martensite plate, embedded in a matrix of retained austenite. x 90,000.

70. Electron micrograph of an iron -2.4^{W}/o nitrogen alloy, showing two internally twinned martensite plates and preferential attack of the surrounding retained austenite has resulted in holes. x 60,000.

71. Variation of M_s temperature with interstitial content for iron-nitrogen and iron-carbon alloys.

72. The variation of resistivity with temperature for an iron- 0.4^w/o carbon alloy, on transforming from austenite to martensite. After McReynolds.(112)

73. Diagramatic representation of the apparatus used in the determination of M_s temperatures by thermal analysis.

74. Photograph of the gas quenching chamber and specimen holder.

75. Tracings of a series of cooling curves of iron-nitrogen alloys containing between 0.17^w/o to 1.9^w/o nitrogen.

76. Two cooling curves of an iron -0.44^w/o nitrogen alloy together with a standard cooling curve of platinum.

77. Diagram of the specimen holder and resistance circuit used for low temperature M_s determinations.

78. A series of X-ray diffraction patterns of an iron-2.35^w/o nitrogen alloy, showing no transformation to martensite until -25^{o}C.

79. Resistance curve corresponding to the specimen from Figure 78, showing an increase in resistance on transforming to martensite from austenite.

80. Variation of resistivity at 20°C, as a function of nitrogen content for iron-nitrogen austenite, and iron-nitrogen martensite-austenite mixtures.

81. Variation of T_o and the theoretical M_s temperature as a function of interstitial content for both iron-carbon and iron-nitrogen alloys. (Modified Zener model).

82. Variation of $\Delta G^{\gamma \rightarrow \alpha'}$ with temperature and composition for the iron-nitrogen system(Fisher model).

83. Variation of $\Delta G^{\gamma \rightarrow \alpha'}$ with temperature and composition for the iron-carbon system. (Fisher Model).

84. Variation of T_o and experimental M_s with interstitial content for the iron-carbon and iron-nitrogen systems. (Fisher Model)

85. Variation of $\Delta G^{\gamma \rightarrow \alpha'}$ at M_s with temperature for iron-carbon and iron-nitrogen alloys. (Fisher Model)

86. Variation of $\Delta G^{\gamma \rightarrow \alpha'}$ at M_s with composition for iron-carbon and iron-nitrogen alloys. (Fisher Model).

87. Variation of $\Delta G^{\gamma \rightarrow \alpha'}$ with temperature and composition for the iron-carbon system (original Cohen model[127])

88. Variation of $\Delta G^{\gamma \rightarrow \alpha'}$ with temperature for iron-nitrogen alloys. (original Cohen model[127]).

89. Variation of $\Delta G^{\gamma \rightarrow \alpha'}$ with temperature and composition for the iron-nitrogen system. (K-R-C model[128])

90. Variation of $\Delta G^{\gamma \rightarrow \alpha'}$ at M_s with temperature for the iron-nitrogen and iron-carbon systems.

91. Variation of T_o with composition for iron-carbon and iron-nitrogen alloys (K-R-C model[128]).

92. Variation of M_s temperatures and critical temperature for Zener ordering with interstitial content for iron-carbon, iron-nitrogen and some iron-nickel-carbon alloys.

93. The dependence of Zener ordering on temperature and applied stress.

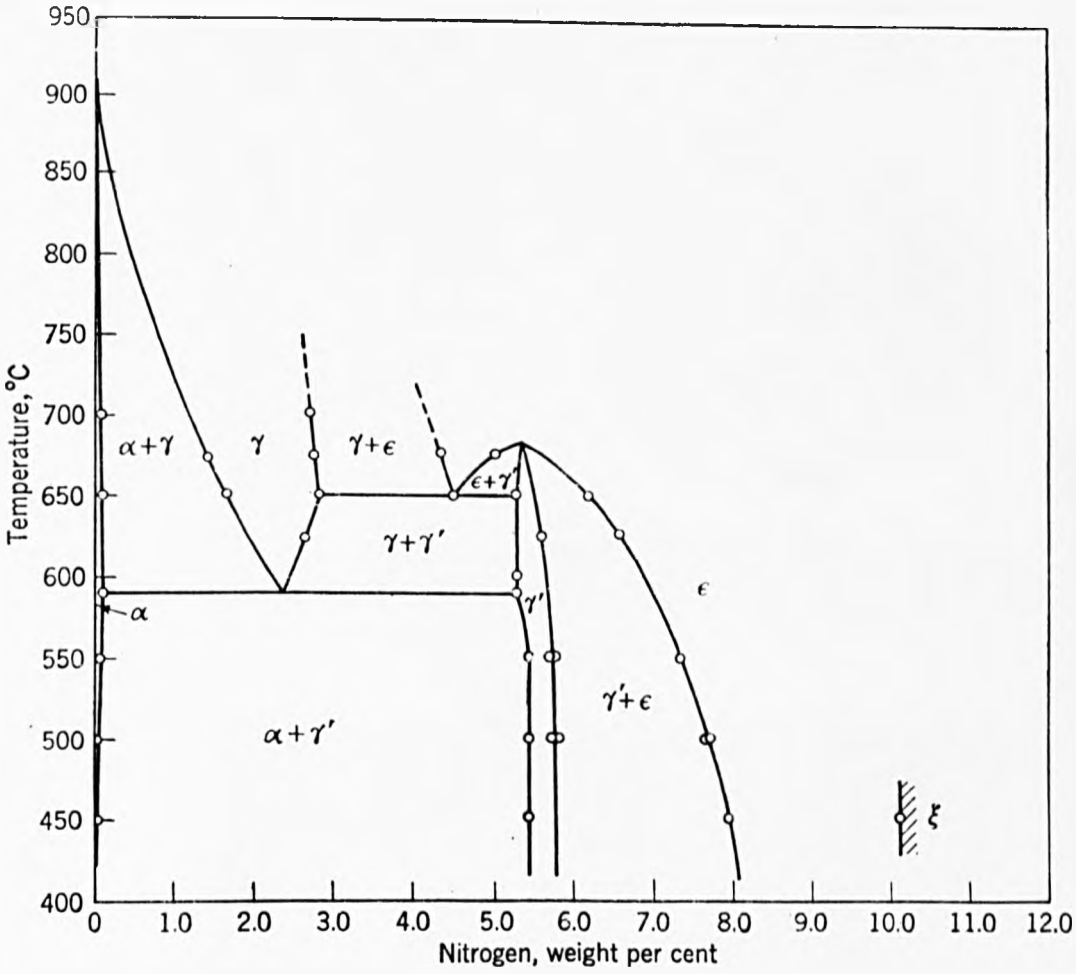

FIG.1 THE IRON-NITROGEN METASTABLE PHASE DIAGRAM ACCORDING TO PARANJPE, COHEN, BEVER AND FLOE (12)

Figure 2.

Transmission electron micrograph of a quenched iron -1.5 W/o nitrogen alloy. After Pitsch.[4]
×40,000

Figure 3.

Electron diffraction pattern corresponding to Figure 2.

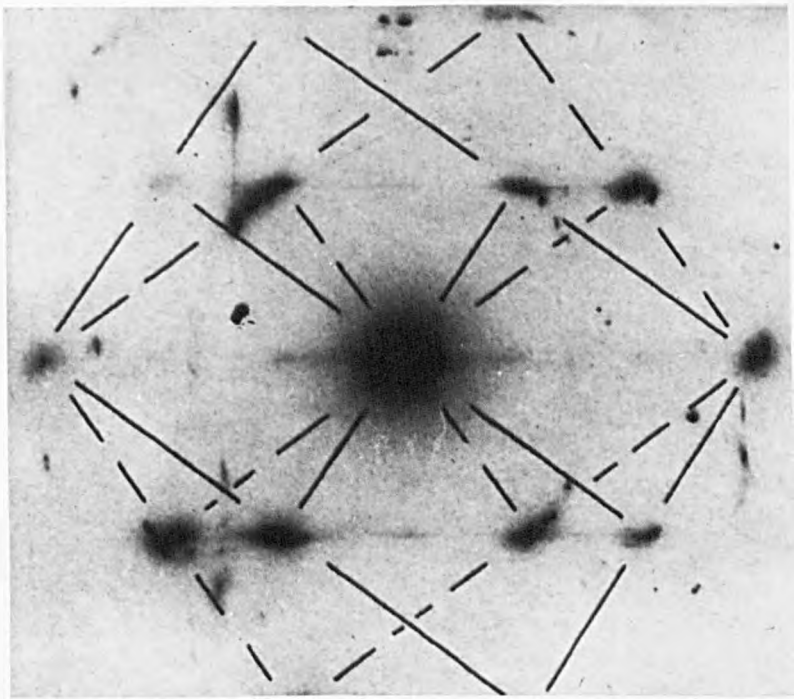

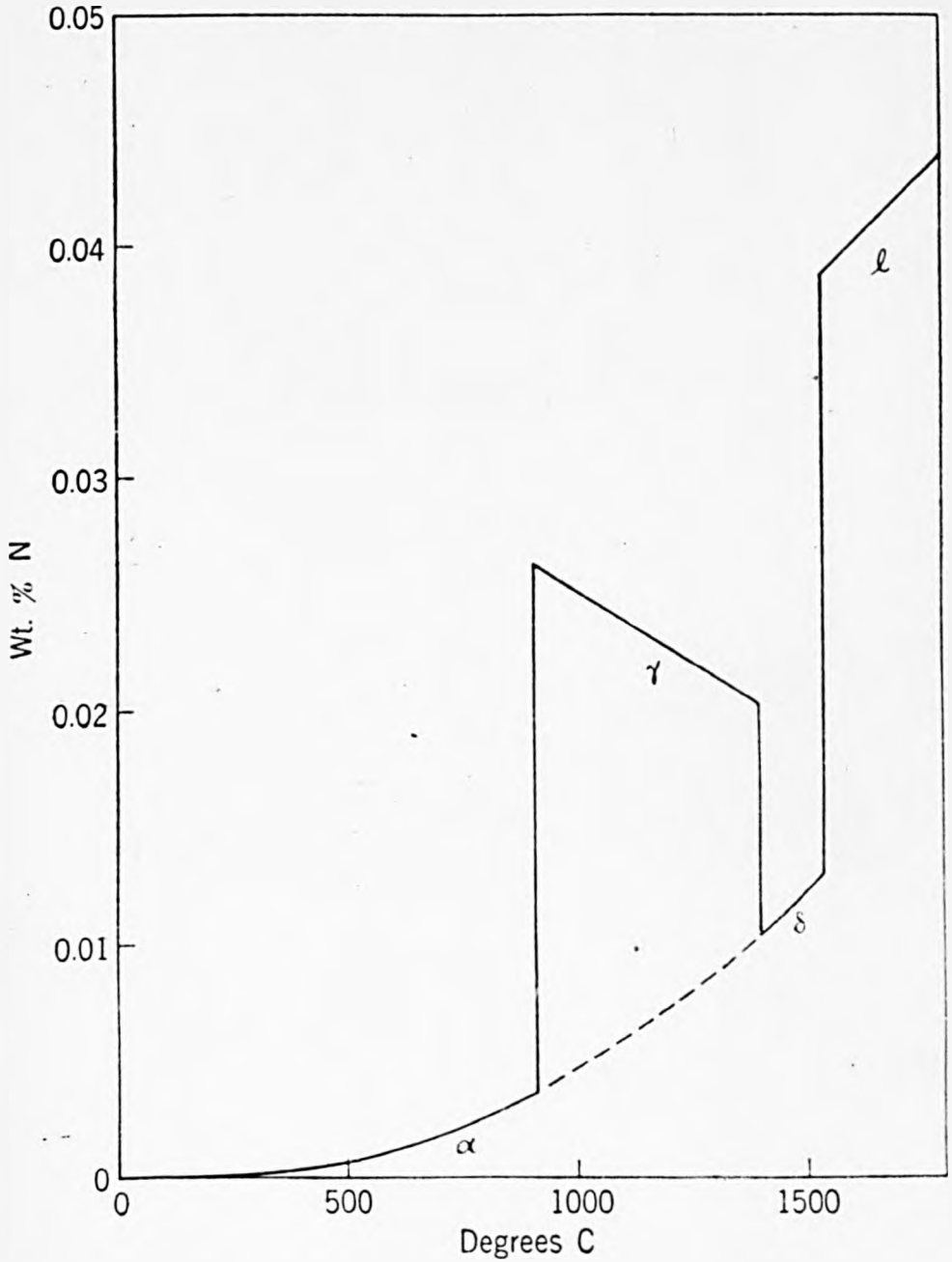

FIGURE 4. SOLUBILITY OF NITROGEN GAS AT 1 ATMOSPHERE IN IRON AS A FUNCTION OF TEMPERATURE (124)

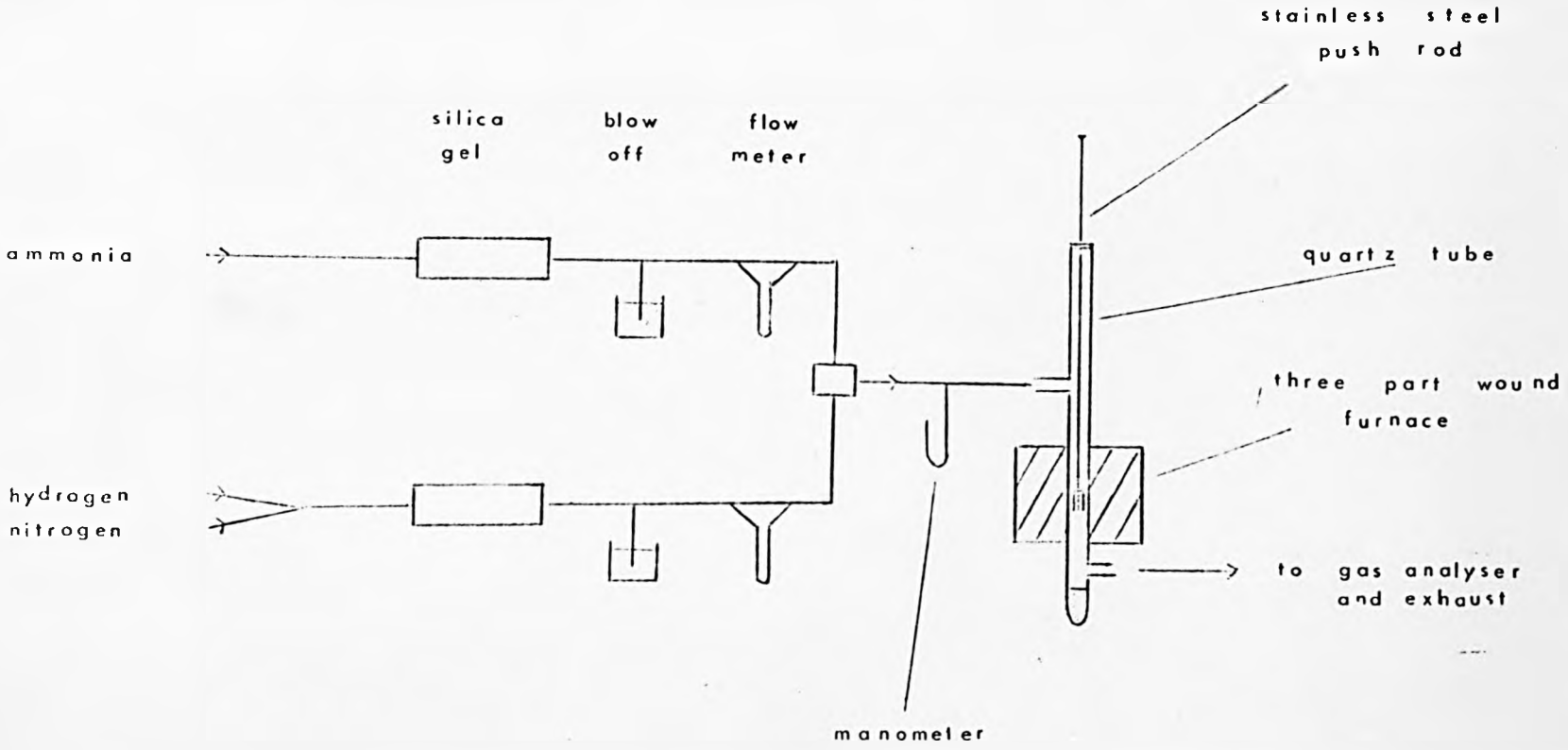

FIGURE 5 NITRIDING APPARATUS

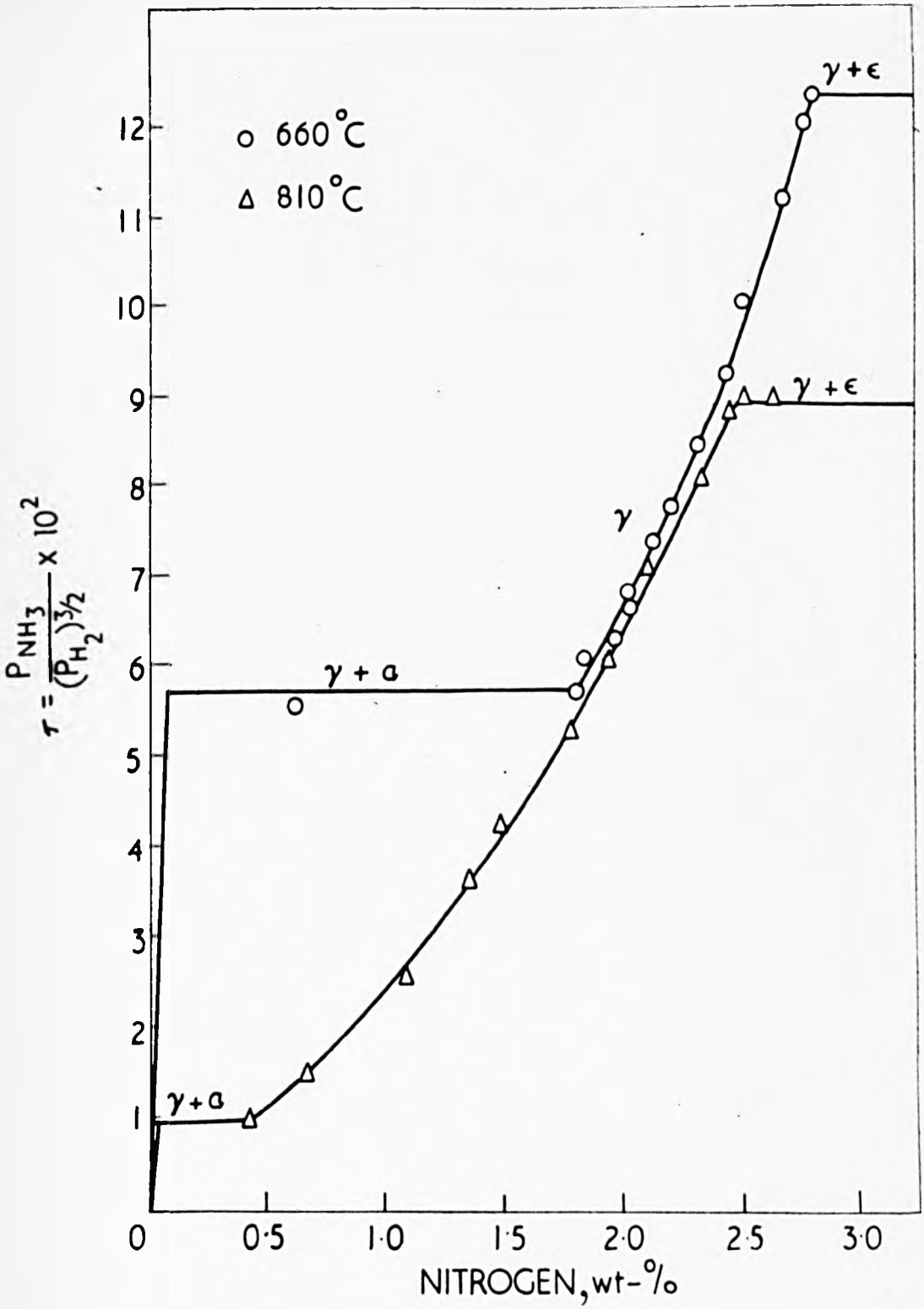

FIGURE 6. VARIATION OF NITRIDING POTENTIAL AS A FUNCTION OF NITROGEN CONCENTRATION [30]

Figure 7.

Iron -1.8^{w}/o nitrogen alloy which has been slack quenched showing grain boundary transformation product. Etched in 2% nital x 360

Figure 8.

Single stage carbon replica of the grain boundary transformation product in Figure 7. x 9,000

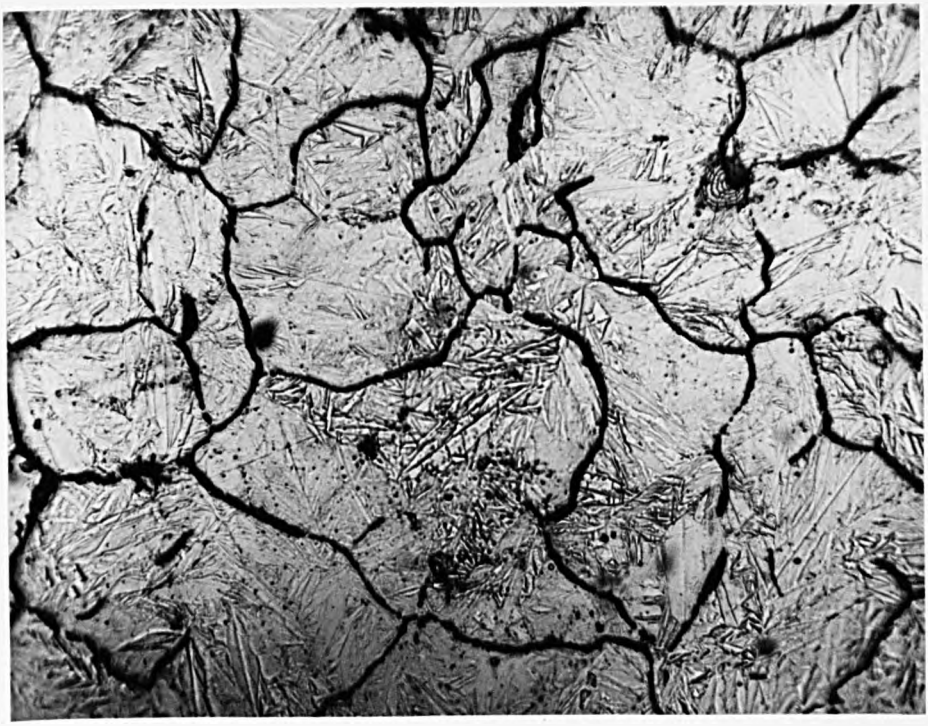

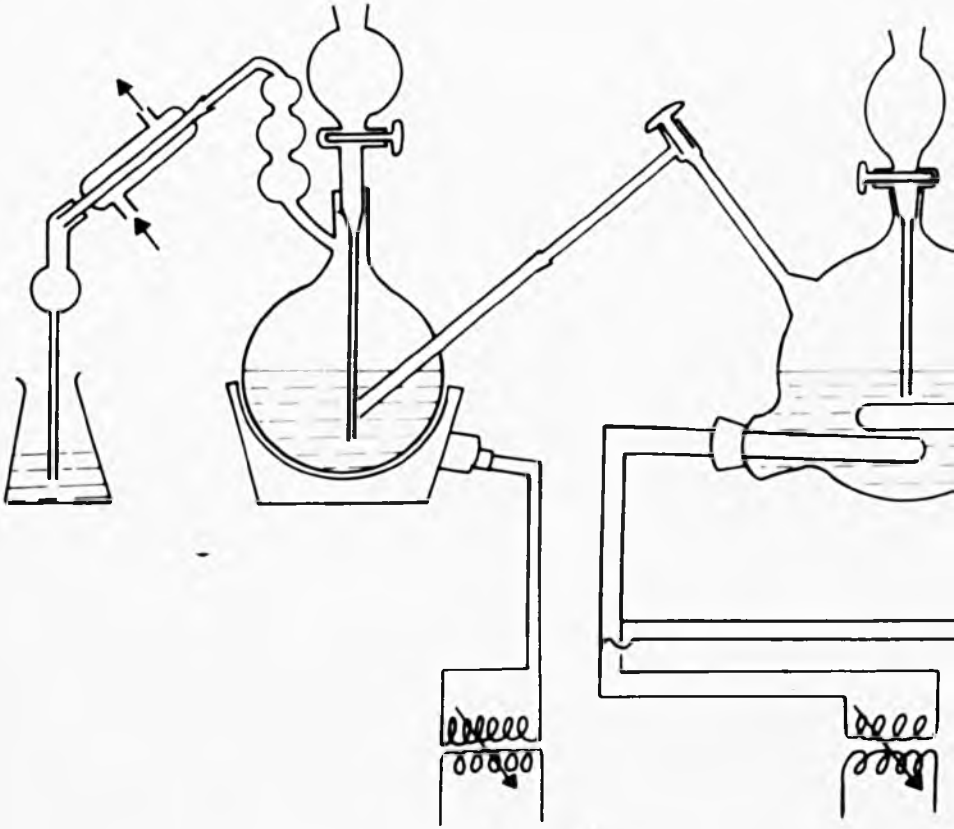

FIGURE 9. KJEHDAL STEAM – DISTILLATION

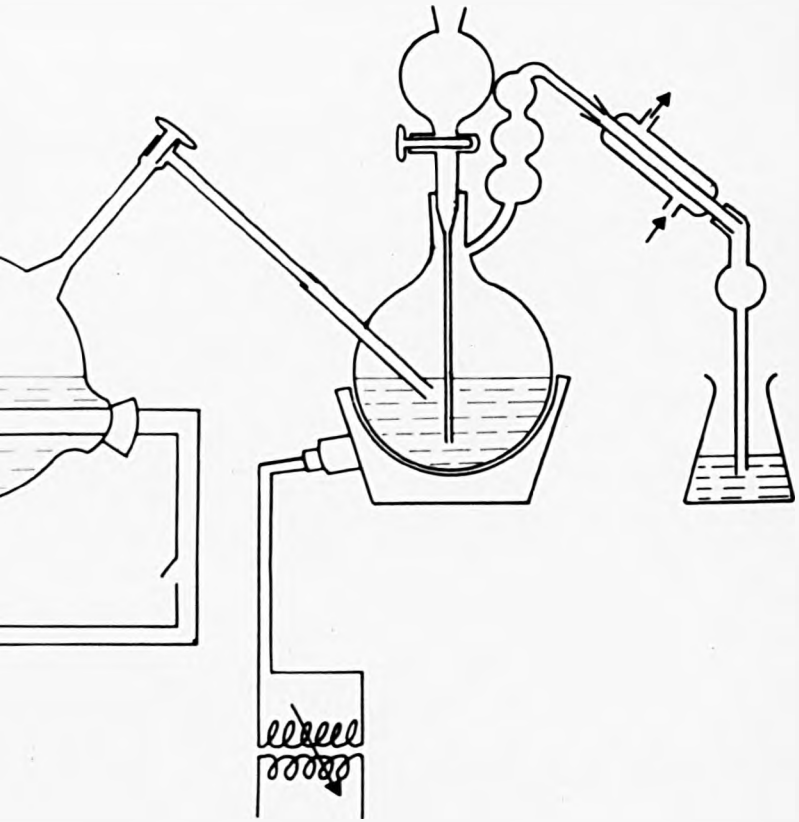

APPARATUS

Figure 10.

The crystal structure of austenite showing the carbon atoms in the octohedral interstices. After N.J. Petch[21].

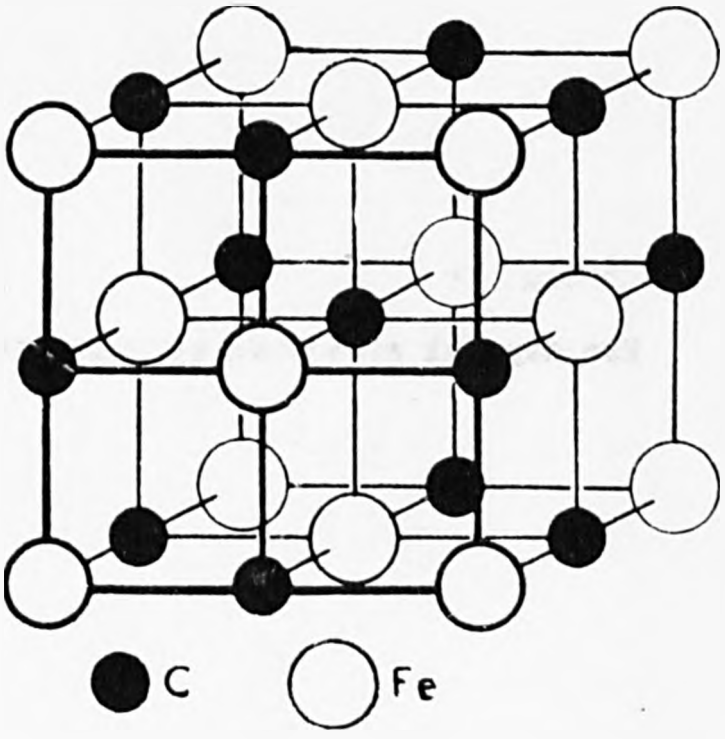

FIGURE 10.

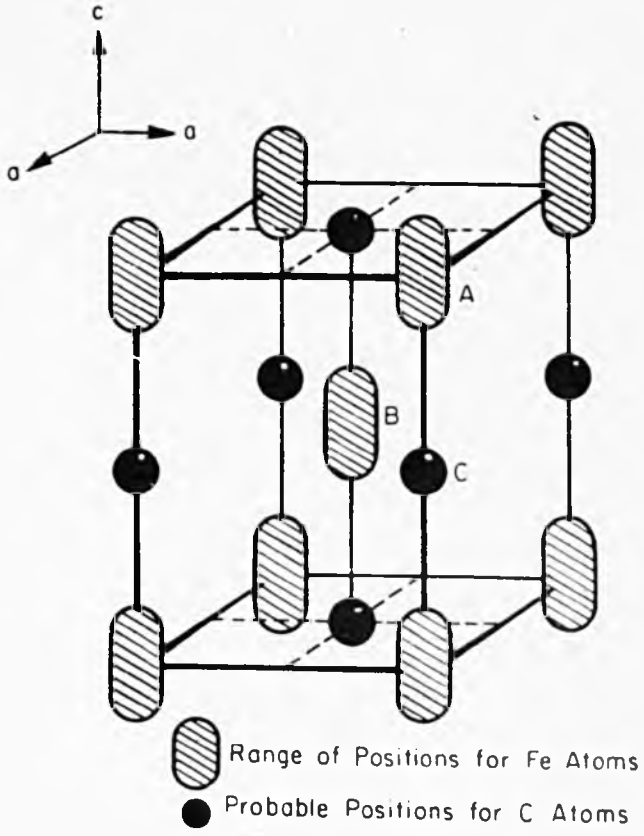

Figure 11. The structure of tetragonal martensite, showing random displacements of the iron atoms by interstitial carbon. (Lipson and Parker.)[23]

Figure 12.

The variation of the lattice parameter of iron-nitrogen austenite with increasing interstitial content.

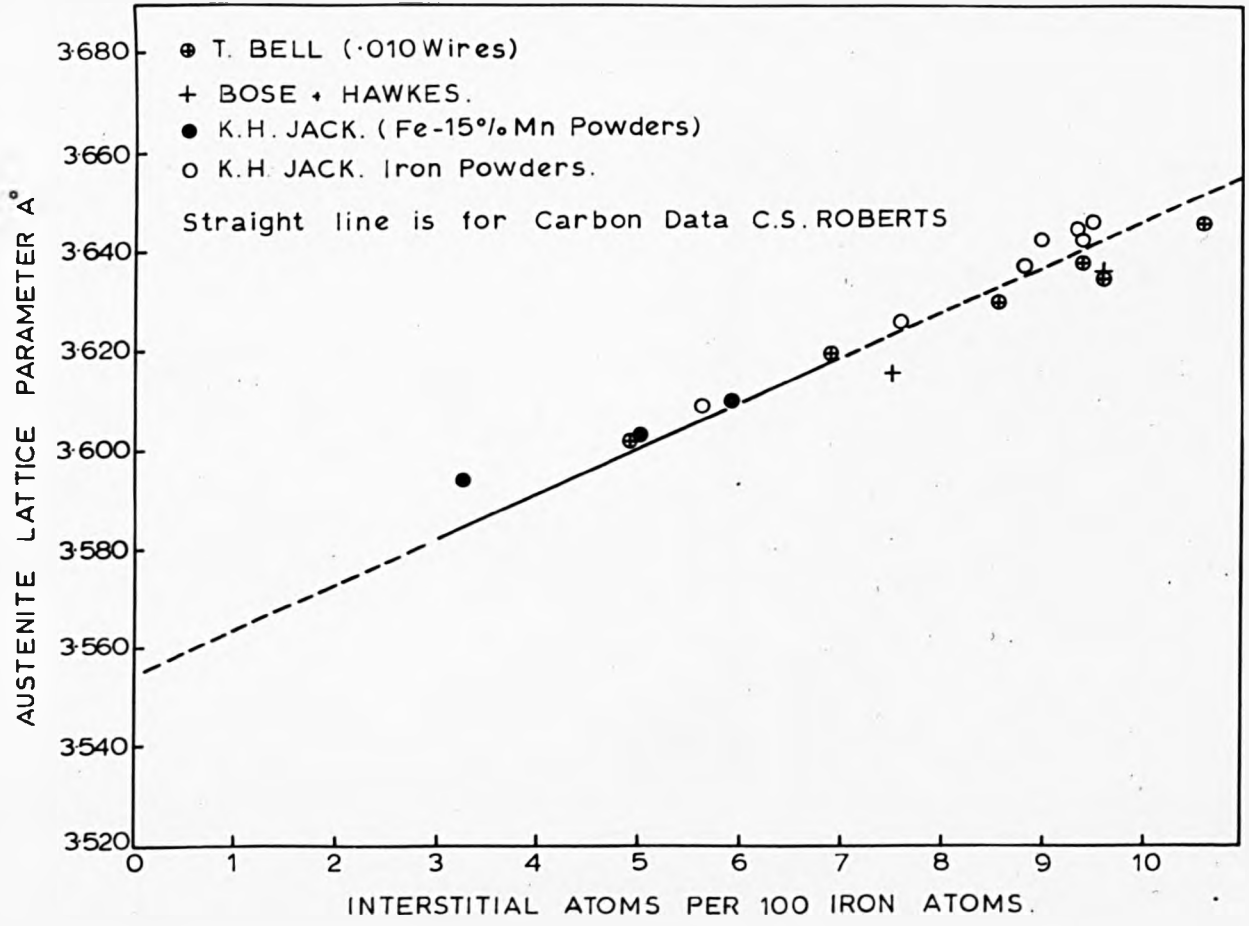
⊕ T. BELL (·010 Wires)
+ BOSE + HAWKES.
● K.H. JACK. (Fe-15% Mn Powders)
o K.H. JACK. Iron Powders.
Straight line is for Carbon Data C.S. ROBERTS
AUSTENITE LATTICE PARAMETER A°
3·680
3·660
3·640
3·620
3·600
3·580
3·560
3·540
3·520
0
1
2
3
4
5
6
7
8
9
10
INTERSTITIAL ATOMS PER 100 IRON ATOMS.

FIGURE 12.

Figure 13.

The variation of the c and a lattice parameters of iron-carbon and iron-nitrogen martensites with increasing interstitial content.

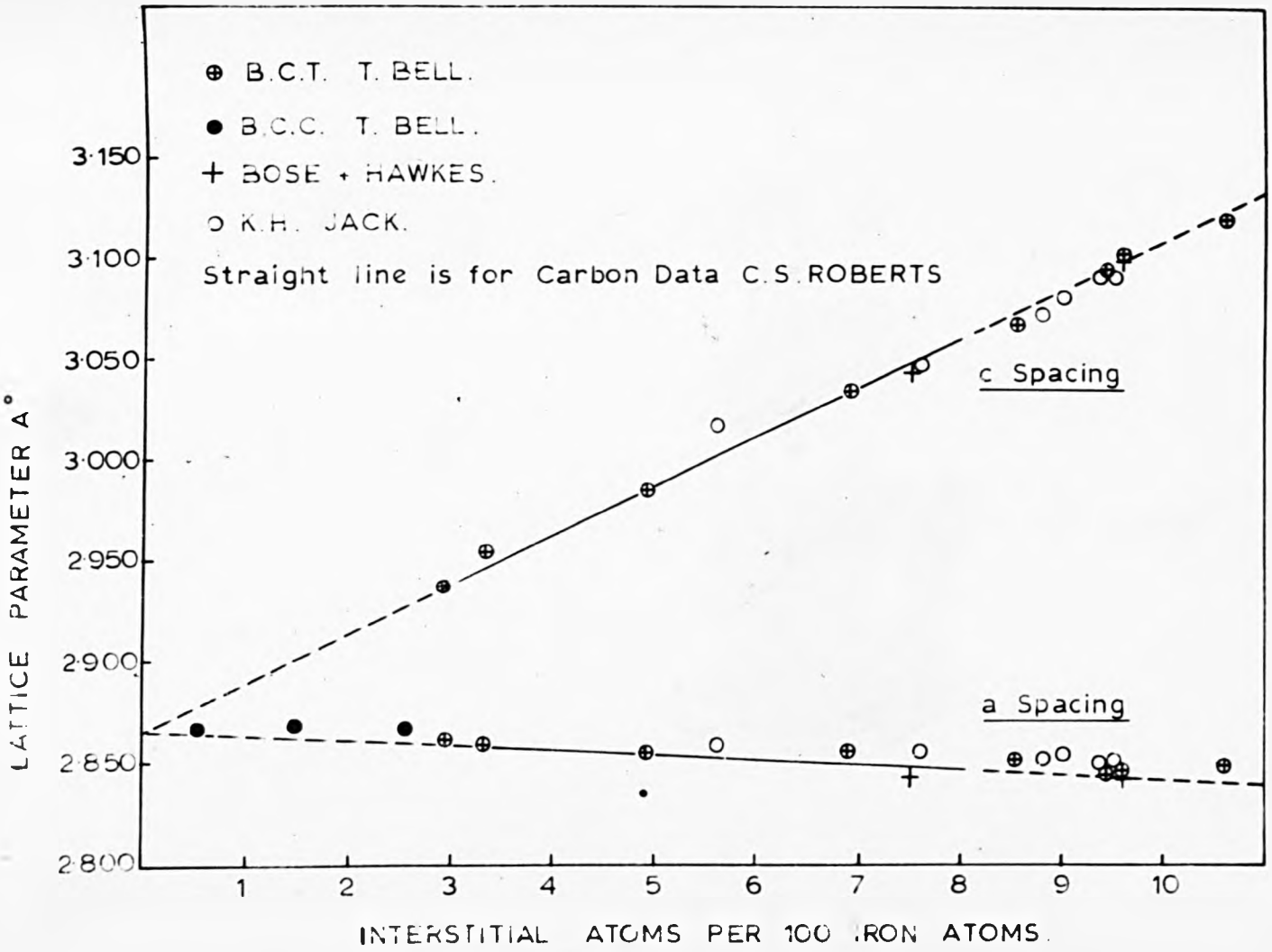
⊕ B.C.T. T. BELL.
● B.C.C. T. BELL.
+ BOSE + HAWKES.
○ K.H. JACK.
Straight line is for Carbon Data C.S.ROBERTS
c Spacing
a Spacing
LATTICE PARAMETER A°
3·150
3·100
3·050
3·000
2·950
2·900
2·850
2·800
1
2
3
4
5
6
7
8
9
10
INTERSTITIAL ATOMS PER 100 IRON ATOMS.

FIGURE 13.

Figure 14.

Variation of the lattice parameter ratio $\frac{c}{a}$, for iron-carbon and iron-nitrogen martensites, with increasing interstitial content.

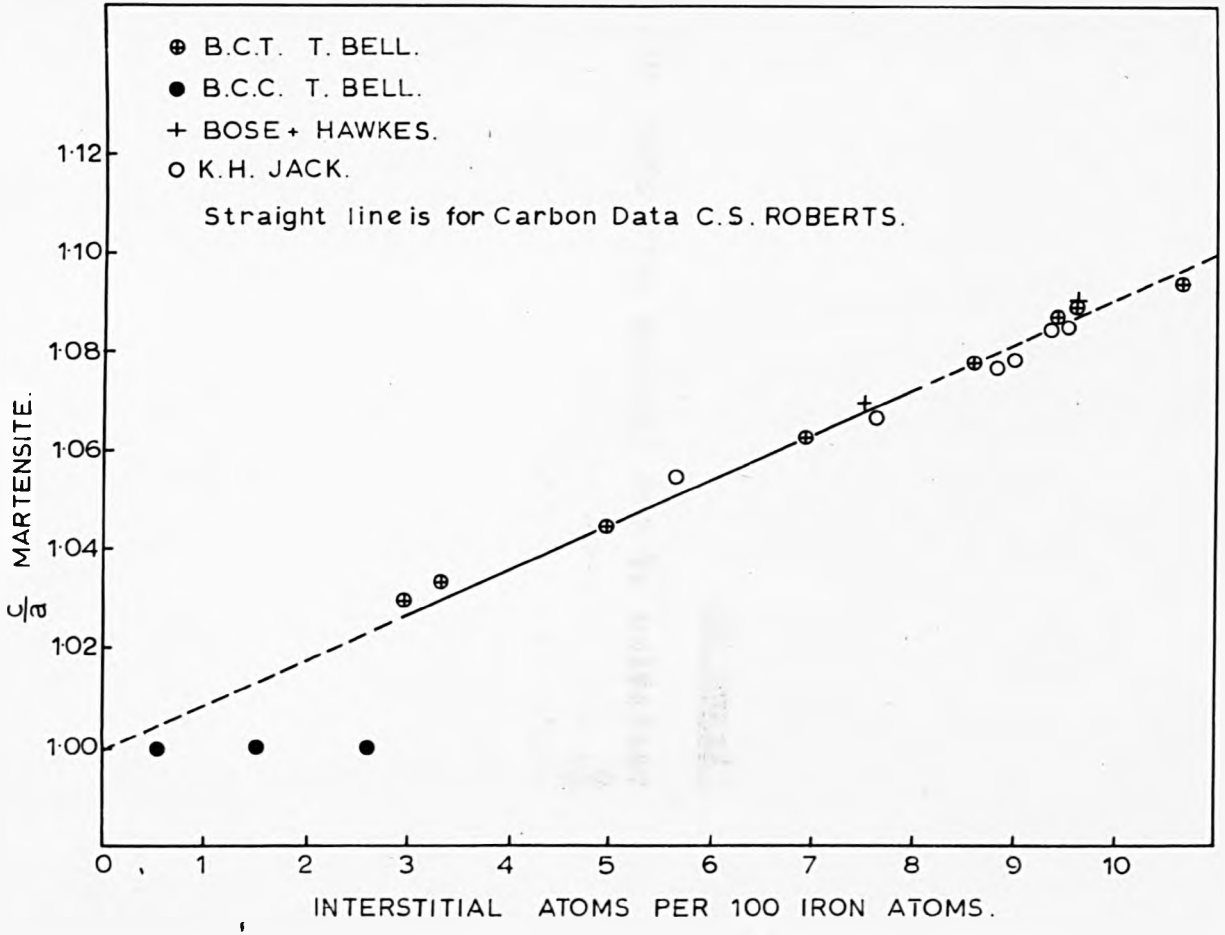
⊕ B.C.T. T. BELL.
● B.C.C. T. BELL.
+ BOSE + HAWKES.
o K.H. JACK.
Straight line is for Carbon Data C.S. ROBERTS.
c/a MARTENSITE.
1·12
1·10
1·08
1·06
1·04
1·02
1·00
0
1
2
3
4
5
6
7
8
9
10
INTERSTITIAL ATOMS PER 100 IRON ATOMS.

FIGURE 14.

Figure 15.

Debye Sherrer X-ray diffraction patterns of iron-nitrogen martensites with increasing nitrogen concentration.

FIGURE 15.

.010" wire specimens quenched -196°C. Austenite reflections marked with dotted lines and martensite reflections with full lines.

Figure 16.

Diffractometer tracings of the $\{110\}_{\alpha'}$ $\{200\}_{\alpha'}$ $\{211\}_{\alpha'}$ reflections for a series of iron-nitrogen martensites.

1. 0.00^{w}/o nitrogen; b.c.c. reflections
2. 0.30^{w}/o nitrogen: b.c.c. reflections
3. 0.64^{w}/o nitrogen; b.c.c. reflections
4. 0.71^{w}/o nitrogen; b.c.t. reflections

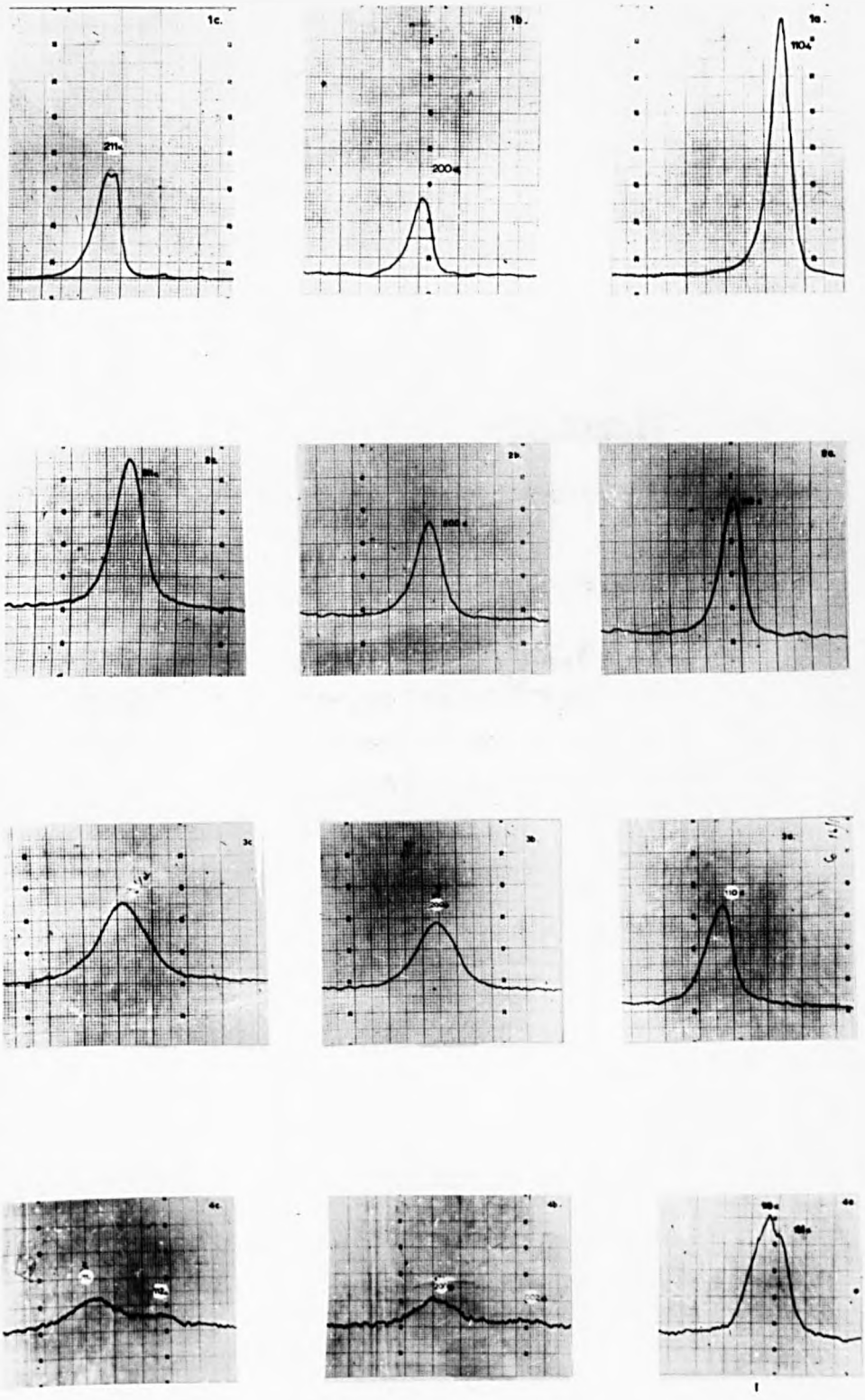

FIGURE 16

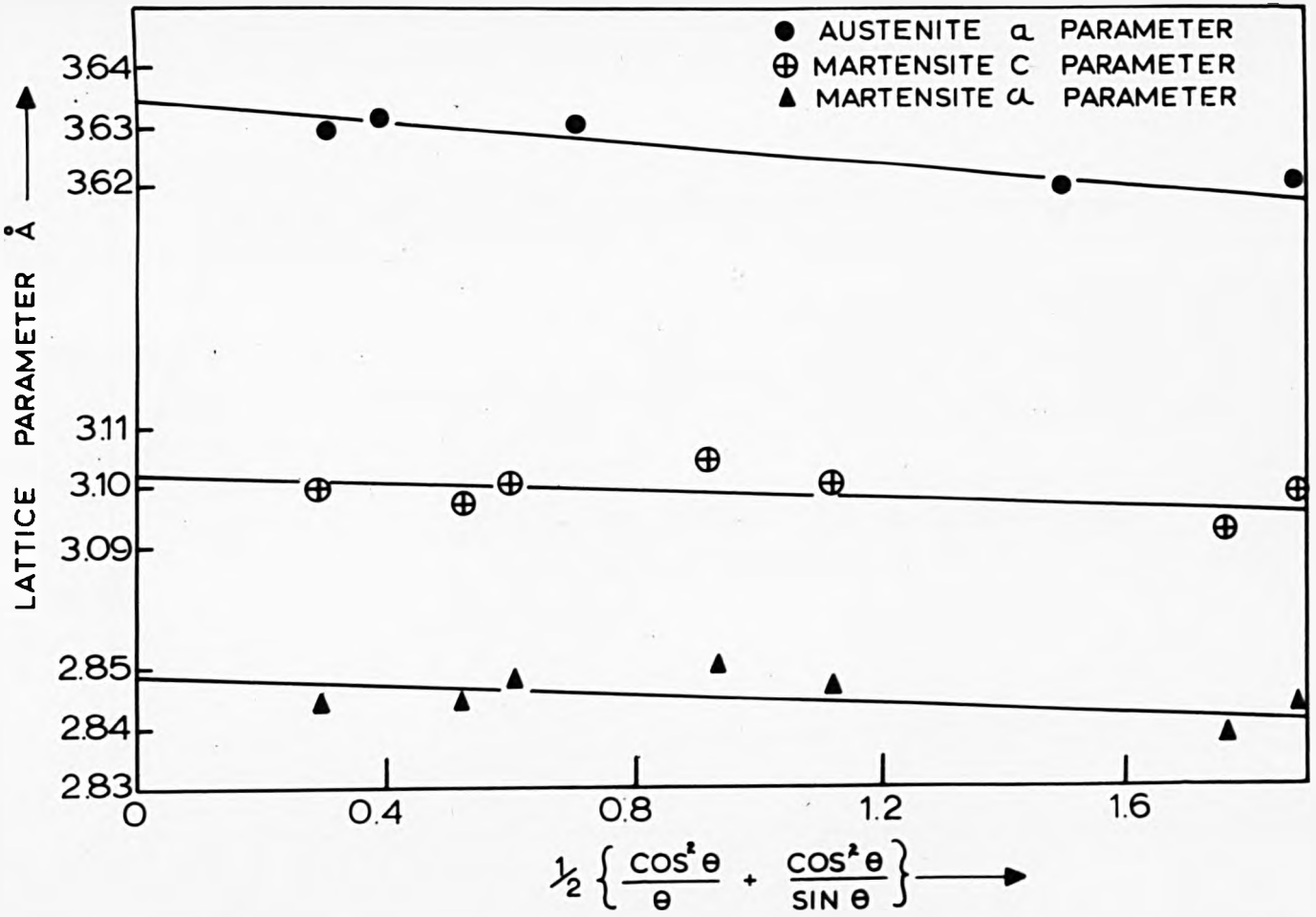

Figure 17. THE NELSON - RILEY EXTRAPOLATION FOR THE DETERMINATION OF THE AUSTENITE AND MARTENSITE LATTICE PARAMETERS OF AN IRON - 2.35 WEIGHT PER CENT NITROGEN ALLOY.

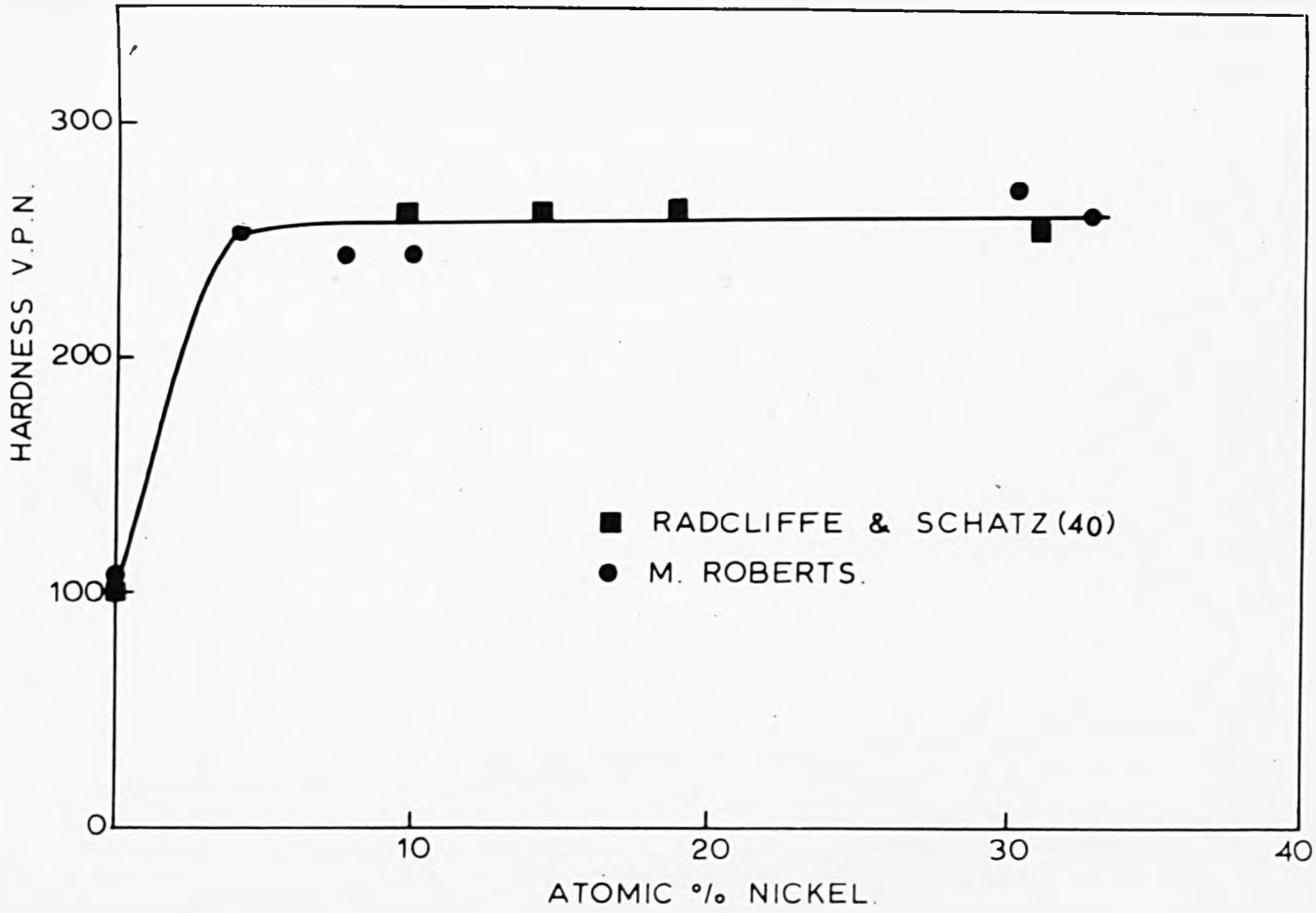

Figure 18. Composition dependence of hardness for a series of iron-nickel alloys quenched into liquid nitrogen.

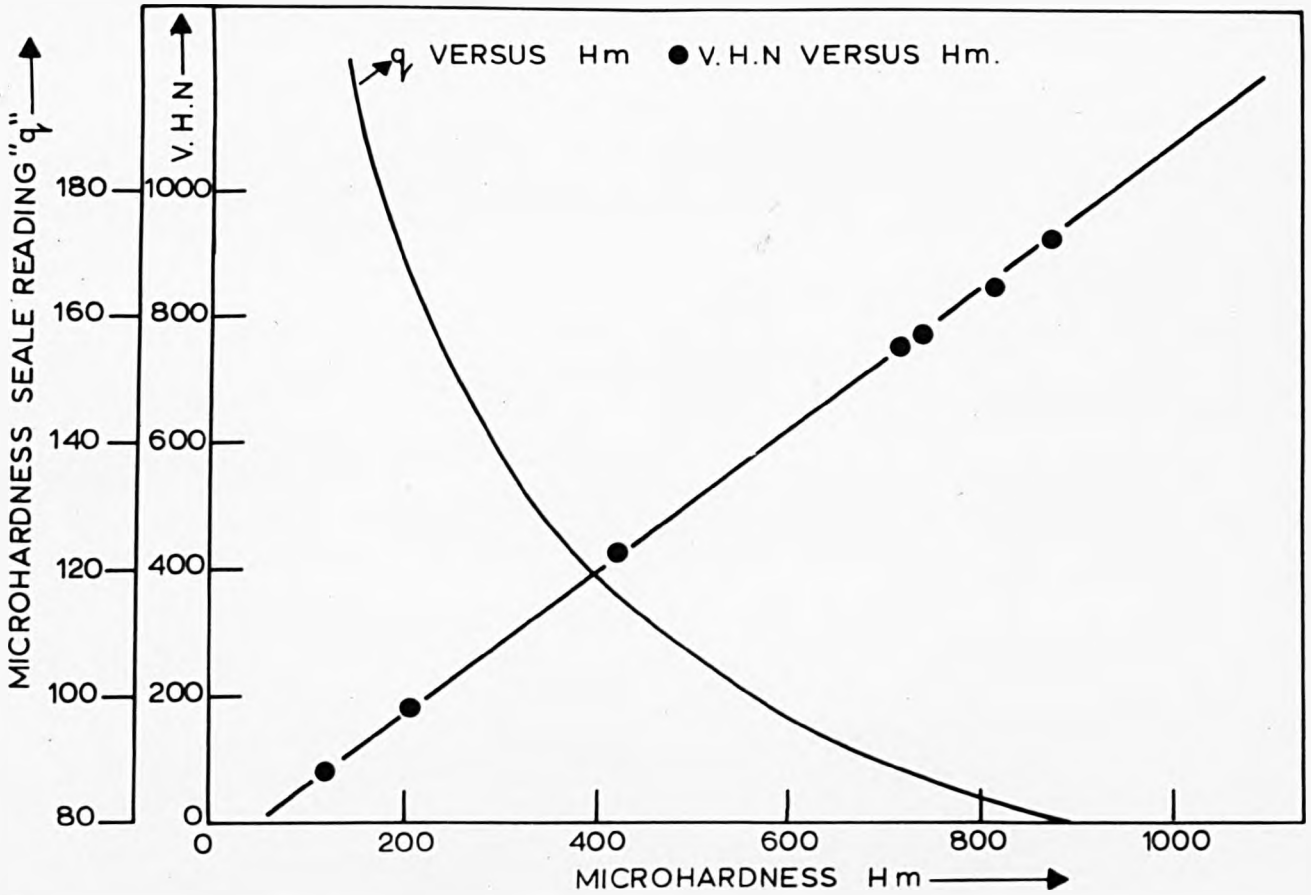

Figure 19. CURVES FOR THE CONVERSION OF REICHART MICROHARDNESS SCALE READINGS INTO VICKERS HARDNESS NUMBERS.

Figure 20.

The variation of the hardness of iron-nitrogen and iron-carbon[40] martensites with interstitial content.

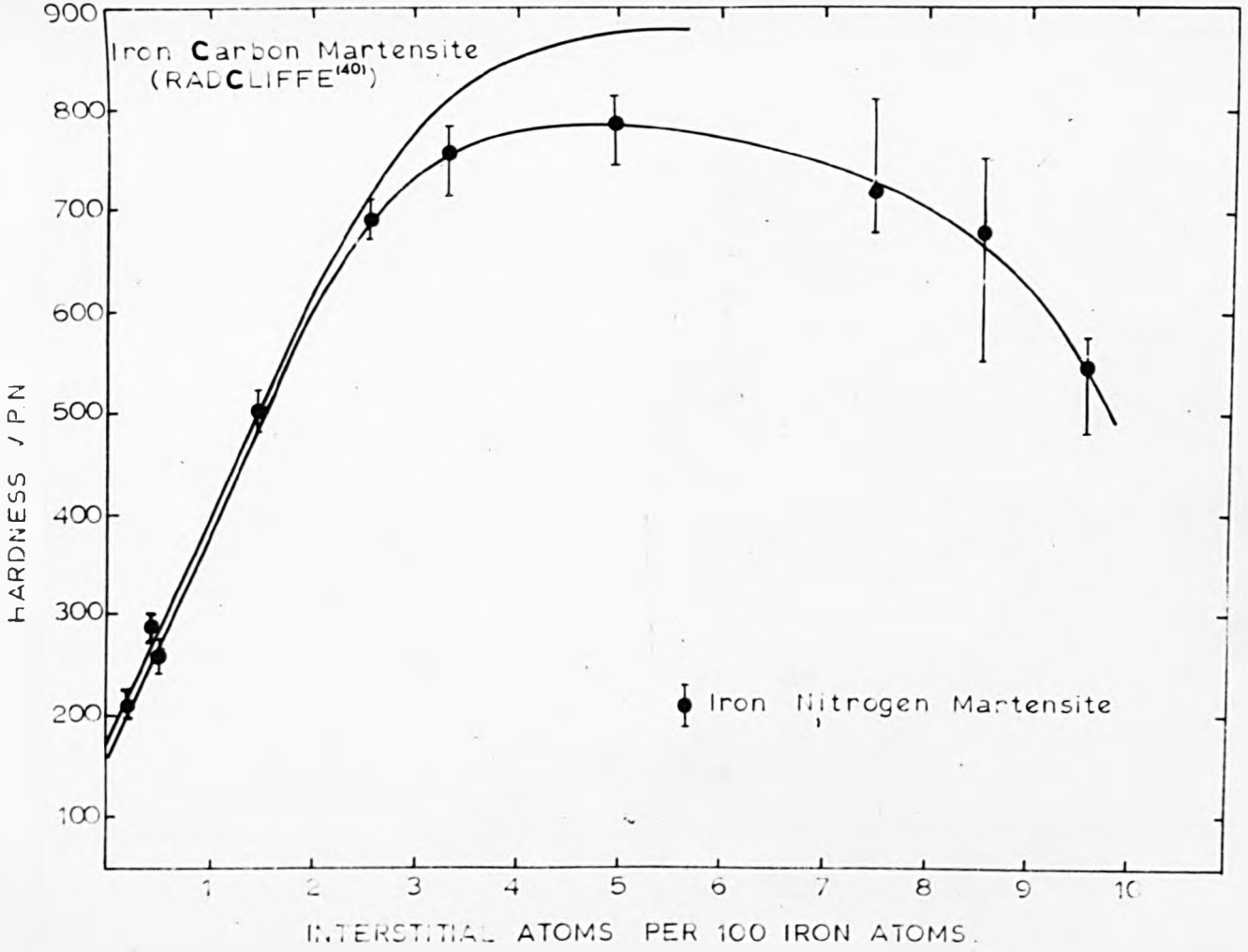
Iron Carbon Martensite
(RADCLIFFE[40])
Iron Nitrogen Martensite
HARDNESS / P.N
900
800
700
600
500
400
300
200
100
1
2
3
4
5
6
7
8
9
10
INTERSTITIAL ATOMS PER 100 IRON ATOMS.

FIGURE 20.

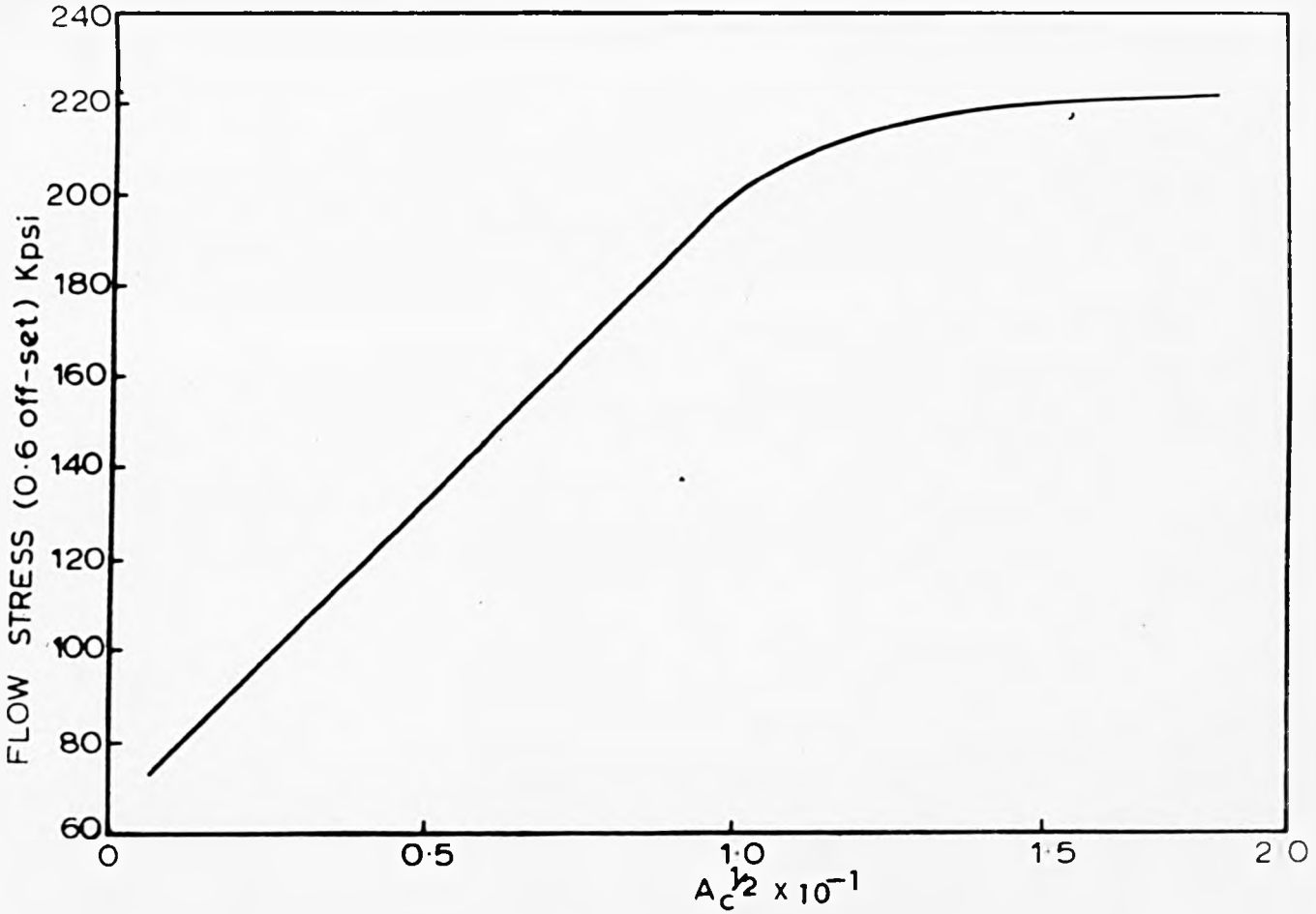

Figure 21 Variation of the flow stress (0.6% offset) with the square root of the atomic fraction of carbon (A_c) for a series of iron-nickel-carbon alloys. Data from Winchell and Cohen (51).

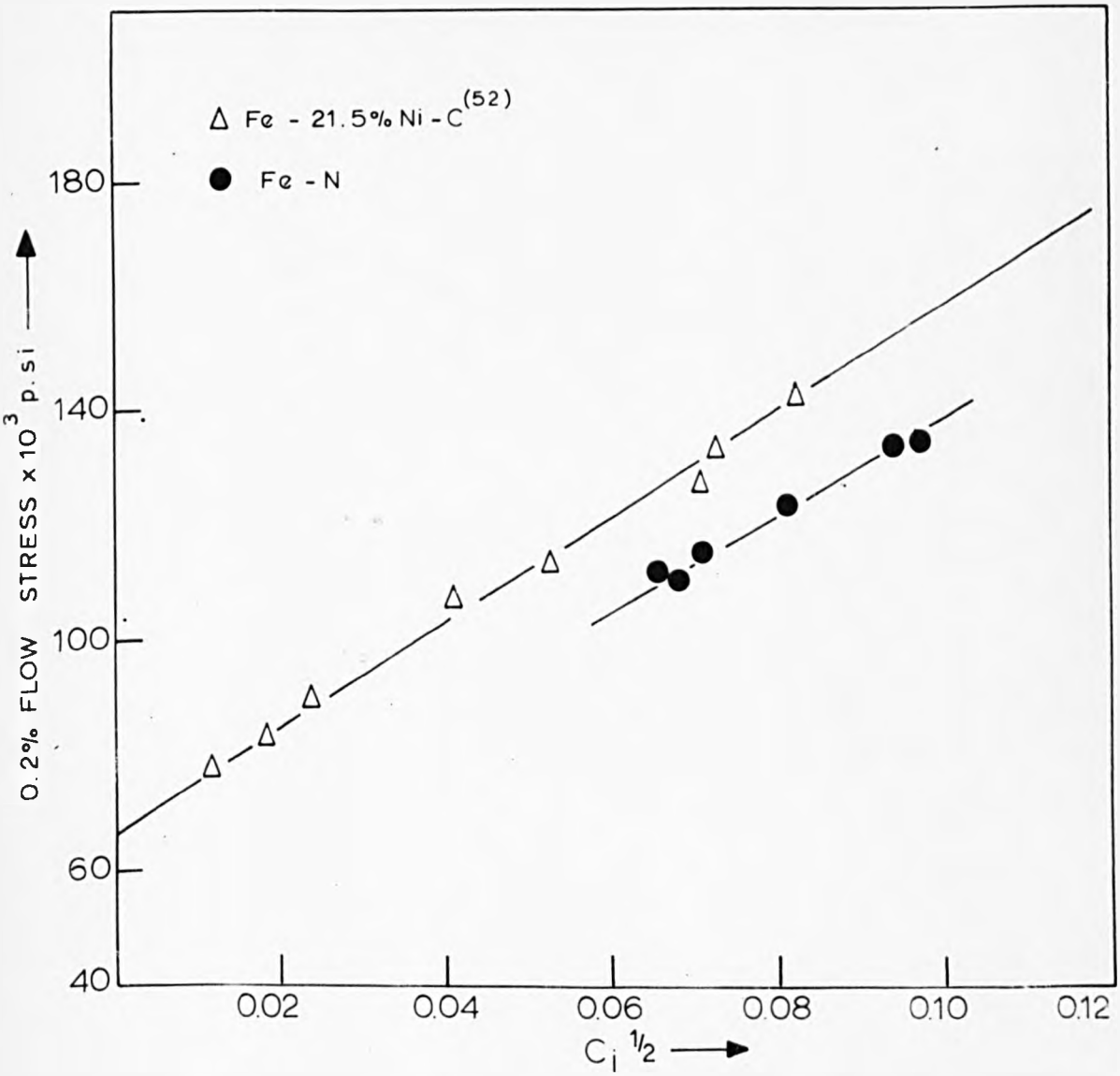

Figure 22 VARIATION OF THE 0.2% FLOW STRESS WITH THE SQUARE ROOT OF THE ATOMIC FRACTION OF INTERSTITIAL SOLUTE, FOR IRON - NITROGEN AND IRON - NICKEL - CARBON MARTENSITES.

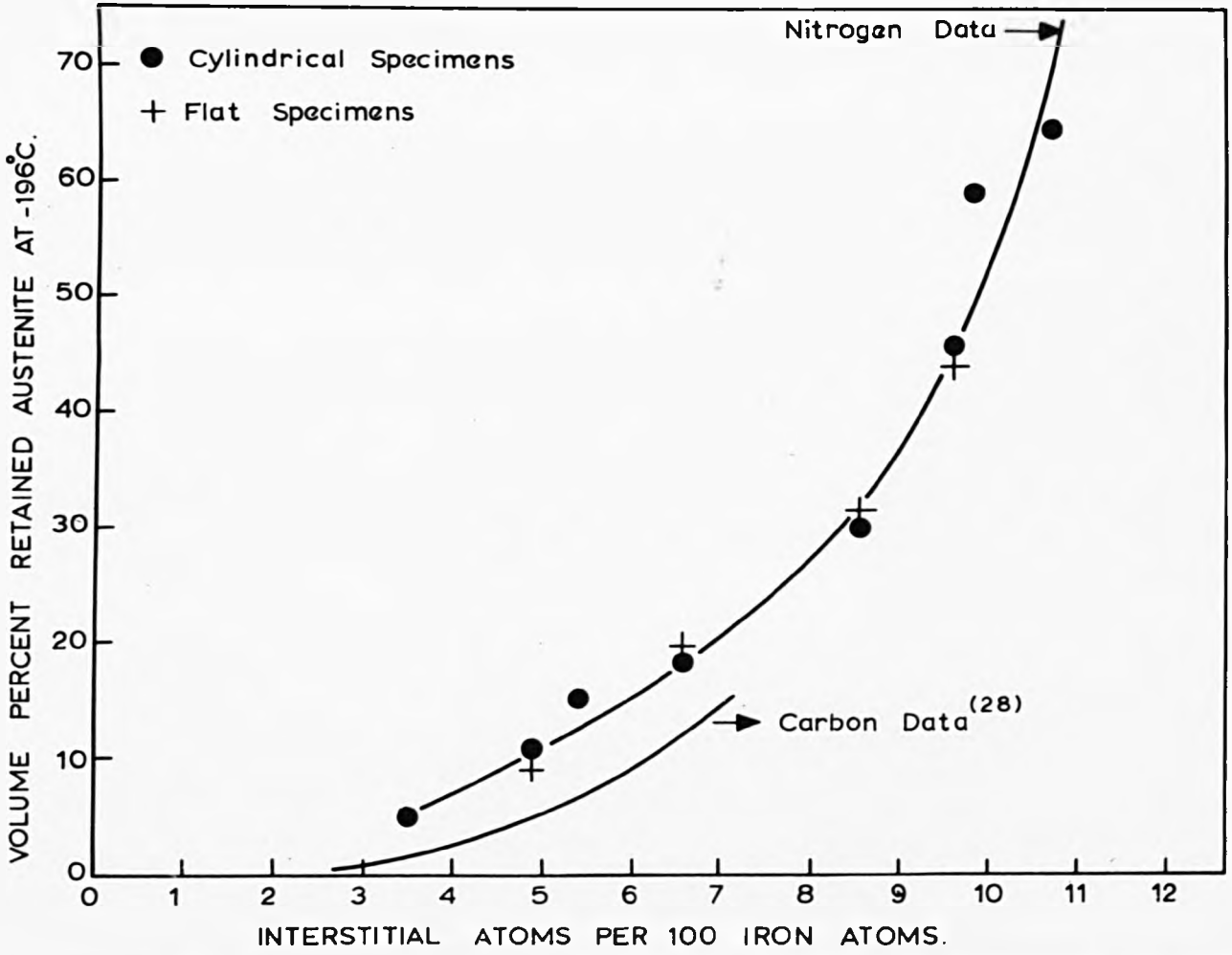

Figure 23. VARIATION OF VOLUME PER CENT RETAINED AUSTENITE AT -196°C. WITH INTERSTITIAL CONTENT FOR IRON NITROGEN AND IRON CARBON ALLOYS.

Figure 24.

Intersity versus Bragg angle curve of speciman N 63 containing 2.1^{W}/o nitrogen, obtained from the microphotometer tracing of the corresponding Debye Sherrer X-ray diffraction pattern.

Figure 26.

Diffractometer tracing of specimen N 63 containing 2.1^{W}/o nitrogen.

FIGURE 24

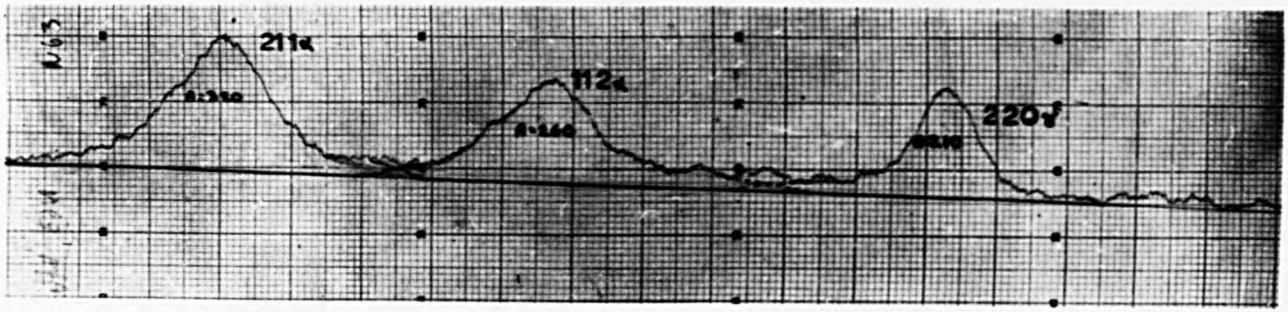

FIGURE 26

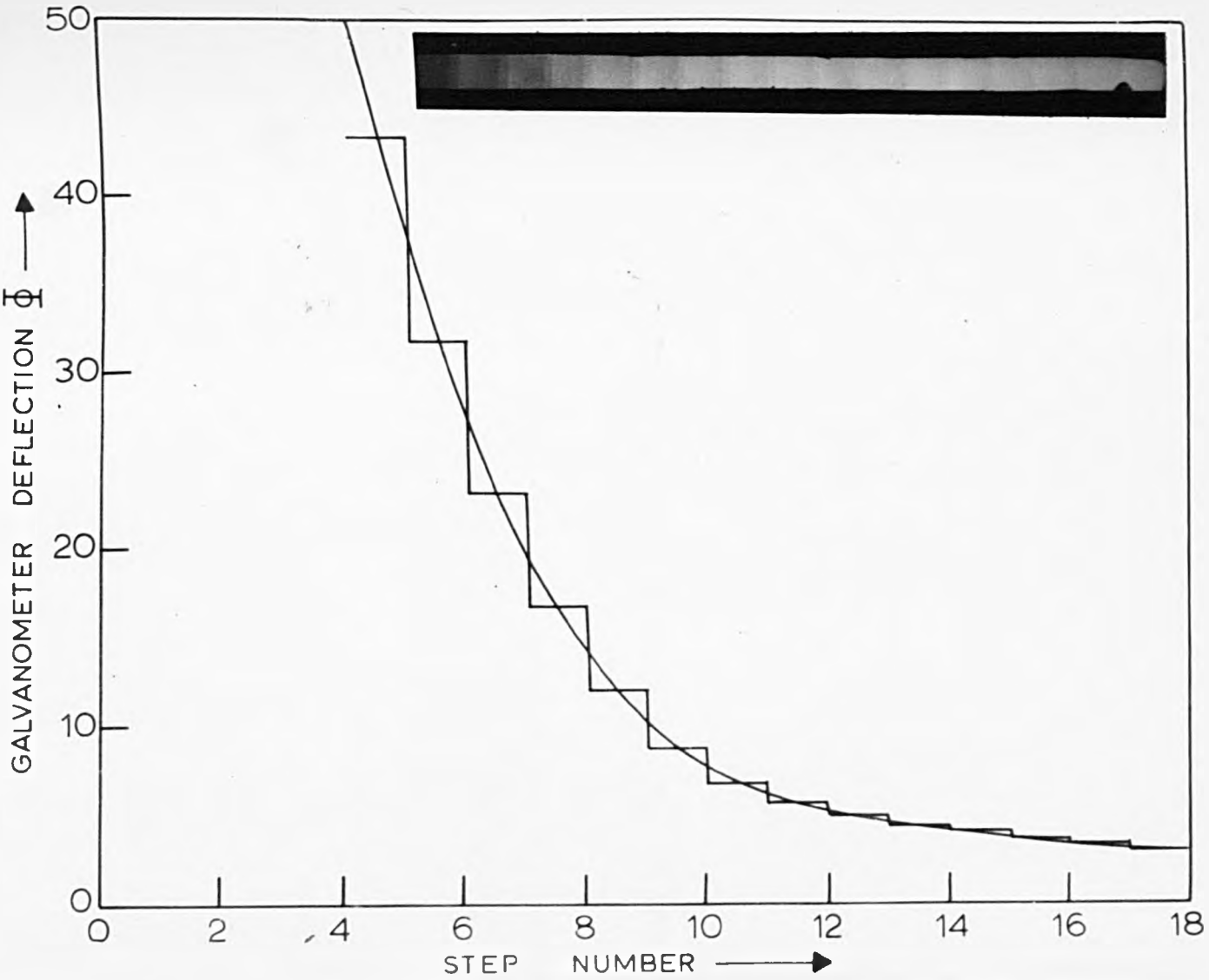

Figure 25. CURVE FOR CONVERTING MICROPHOTOMETER DEFLECTIONS INTO INTENSITIES AND THE CORRESPONDING FILM OF GRADUATED INTENSITIES.

Figure 27.

Typical equiaxed alpha structure; Fe -4.0[a]/o Ni; thermally etched to reveal austenite boundaries, quenched, and subsequently etched to reveal ferrite boundaries.(83)

x 880

Figure 28.

Typical massive-martensite structure. Quenched iron -23.8[a]/o nickel.(41)

x 350

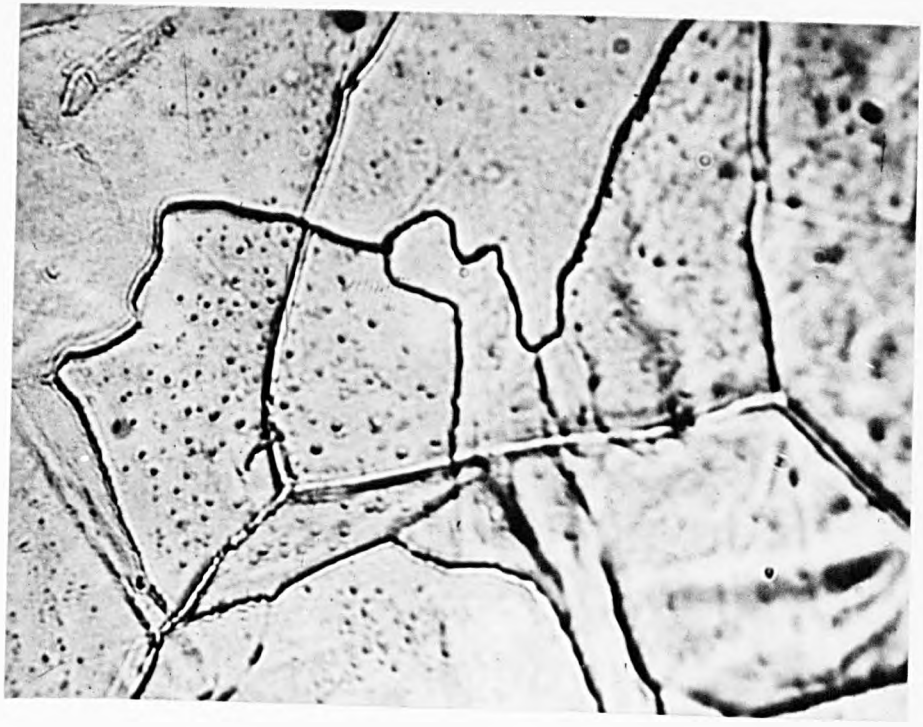

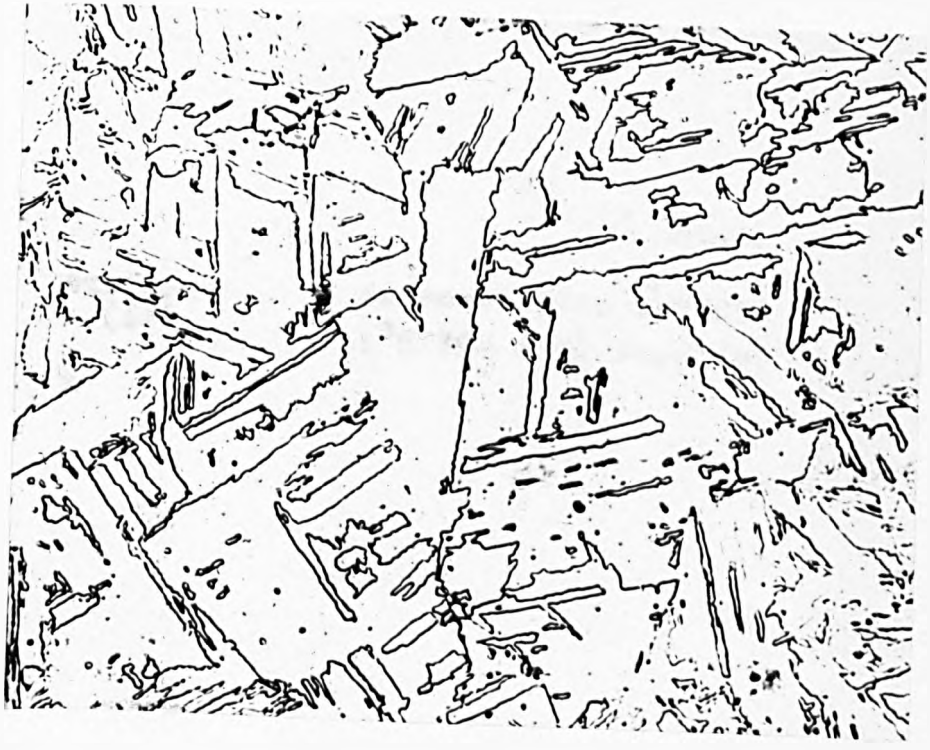

Figure 29.

Surface shears on a pre-polished specimen of iron -15^{a}/o nickel transformed to massive martensite at 338° C.[41]

x 850

Figure 30.

Acicular martensite in Fe -31^{w}/o Ni -0.3^{w}/o C; electro etched in perchloric-acetic acid solution[49]

x 1000

Figure 31.

Typical massive in an iron -0.08^{W}/o nitrogen alloy, quenched into brine at room temperature, etched in alcoholic ferric chloride

x 220

Figure 32.

Massive martensite in an iron -0.17^{W}/o nitrogen alloy quenched into brine at room temperature, etched in picral-2% nital solution.

x 200

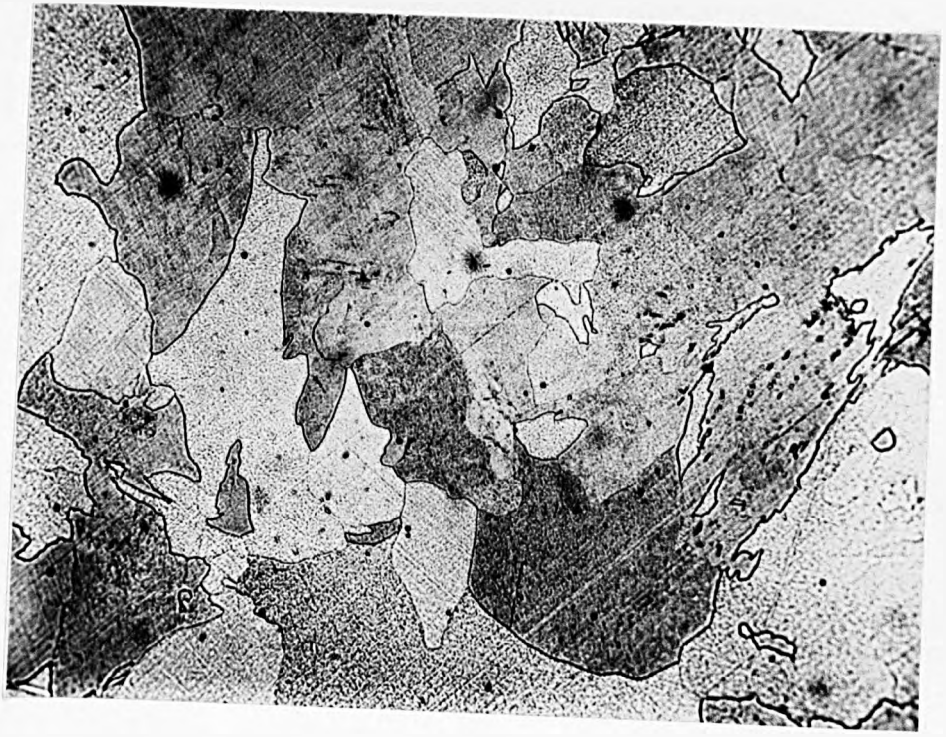

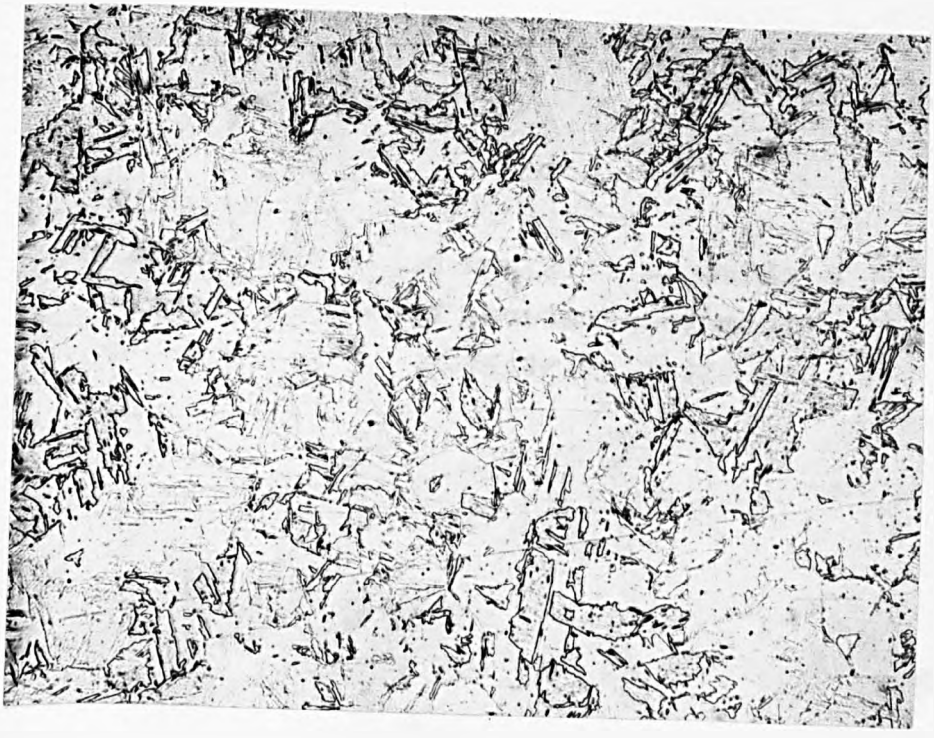

Figure 33.

Massive martensite in an iron -0.17^{w}/o nitrogen alloy quenched into brine at room temperature, etched in picral - 2% nital solution.

x 550

Figure 34.

Massive martensite in a quenched low carbon steel[44]

x 550

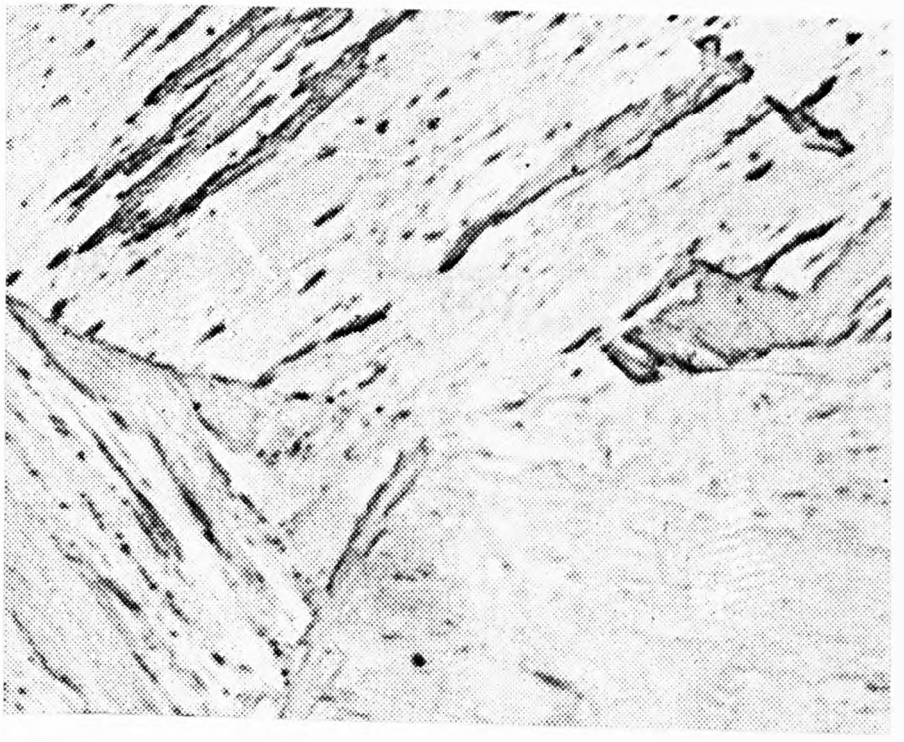

Figure 35.

Massive martensite in an iron-boron alloy quenched from the + region[90].
(white regions are ferrite.)

x 450

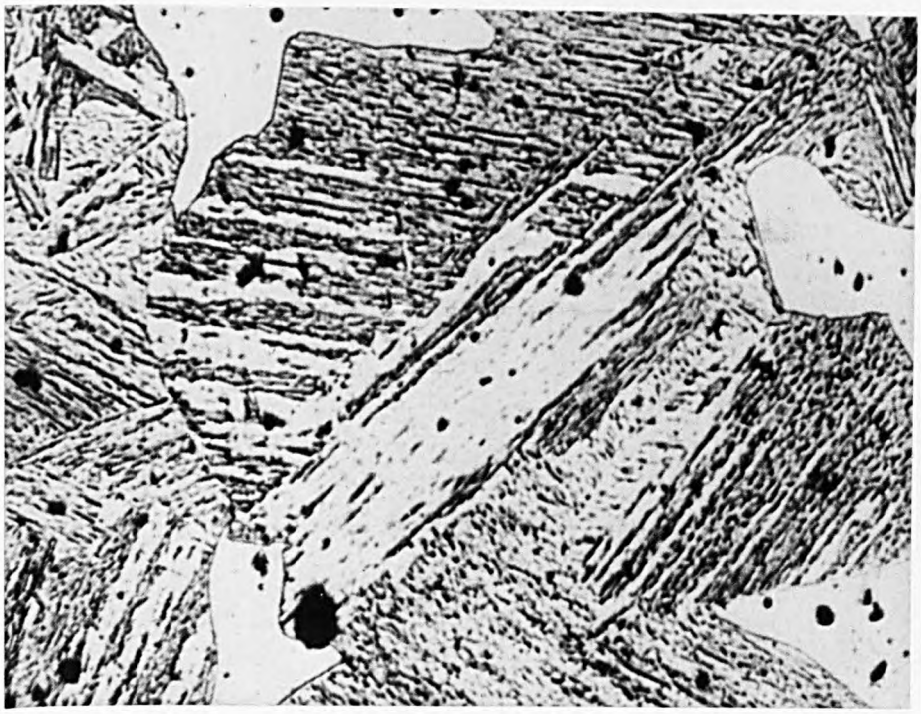

Figure 36.

Prepolished surface of an iron -0.17^{w}/o nitrogen alloy quenched into brine. Oblique illumination illustrating the surface relief effect of massive martensite.

x 350

Figure 37.

Iron -0.37^{w}/o nitrogen massive martensite quenched into brine at room temperature, etched in picral -2% nital solution

x 540

Figure 38.

Prepolished surface of an iron -0.37^{W}/o nitrogen alloy quenched into brine. Oblique illumination

x 700

Figure 39.

Interferogram corresponding to Figure 38.

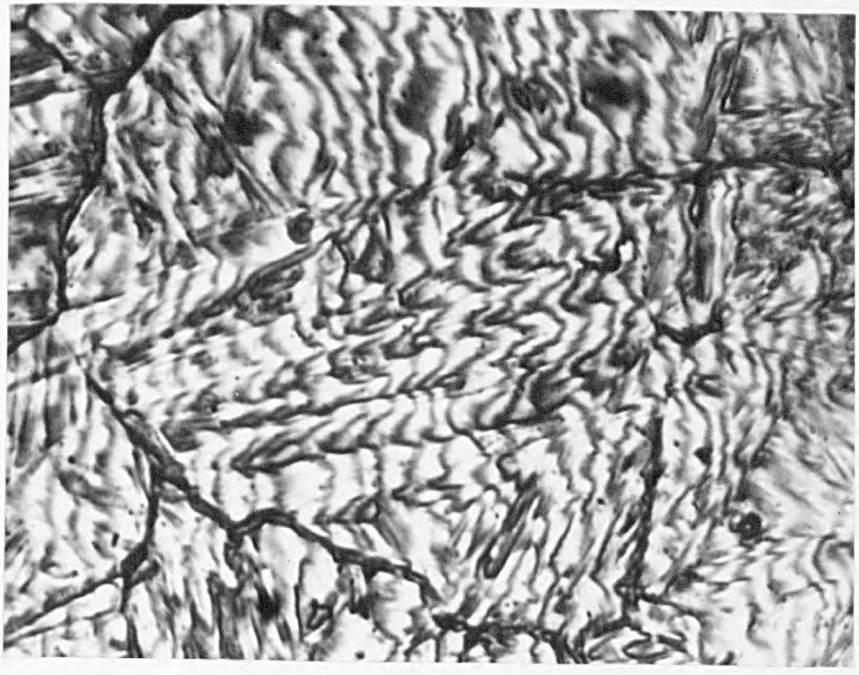

Figure 40.

Iron -0.54^{w}/o nitrogen alloy quenched into brine and further cooled to -196° C. Etched in 2% nital

x 750

Figure 41.

Iron -0.65^{w}/o nitrogen alloy quenched into brine and further cooled to -196° C. Etched in 2% nital

x 750

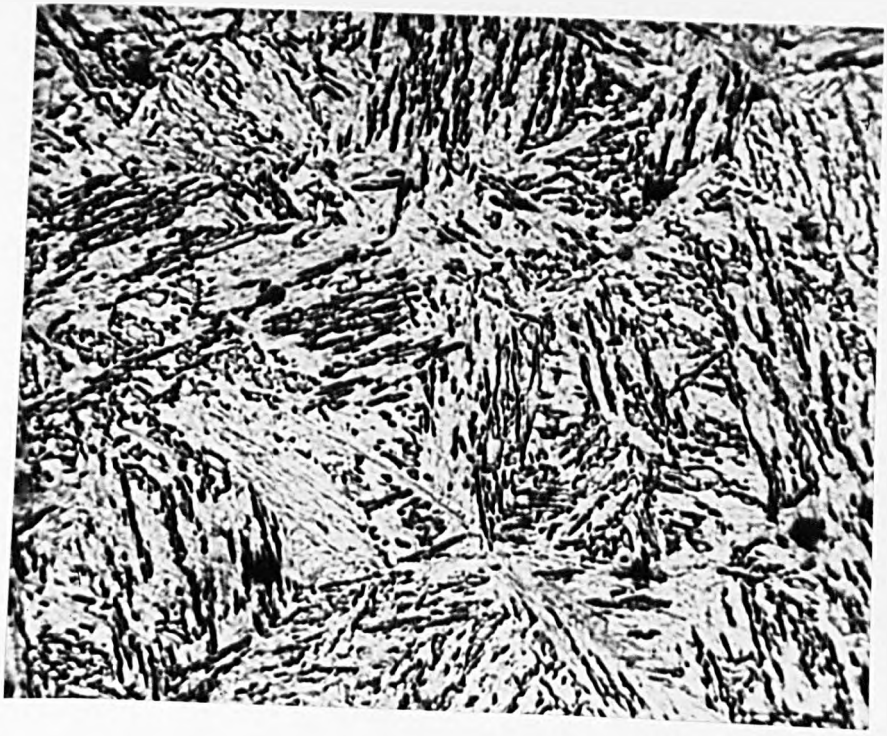

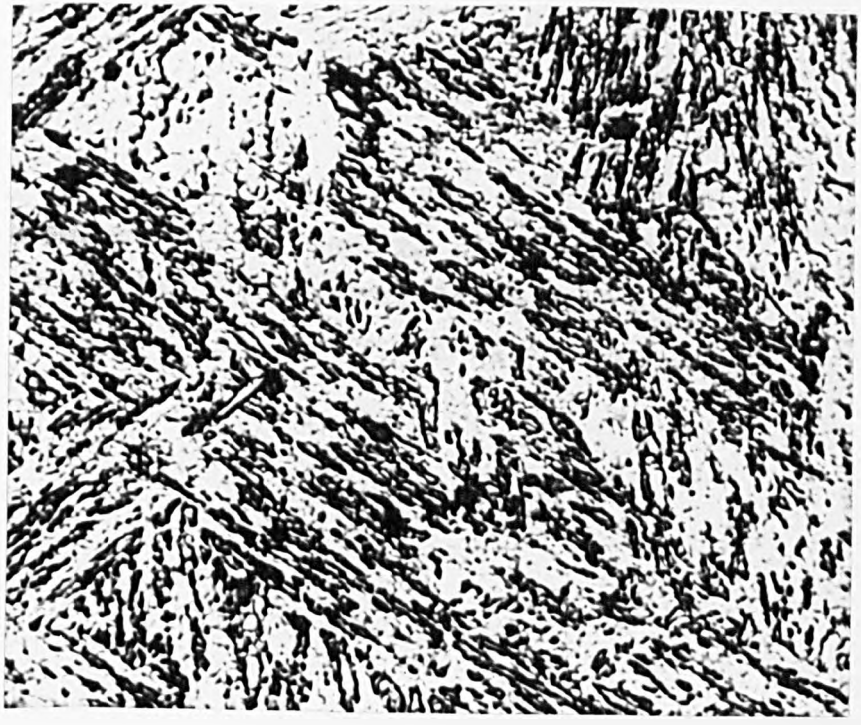

Figure 42.

Prepolished surface of an iron -0.54^{W}/o nitrogen alloy quenched into brine. Oblique illumination

x 1000

Figure 43.

Interferogram corresponding to Figure 42.

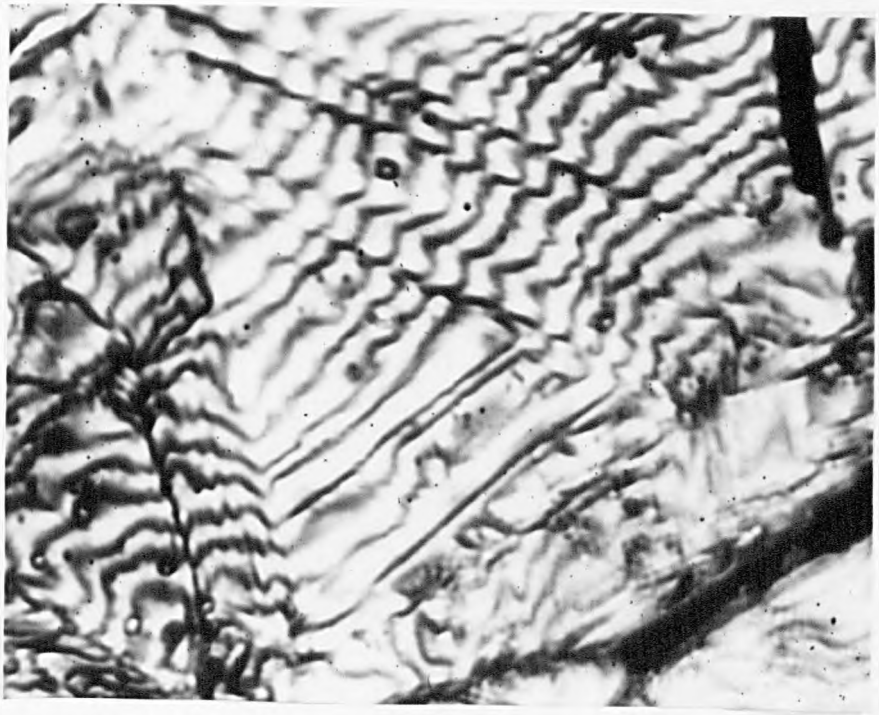

Figure 44.

Iron -1.2^{W}/o nitrogen alloy quenched into brine and etched with 5% nital

x 620

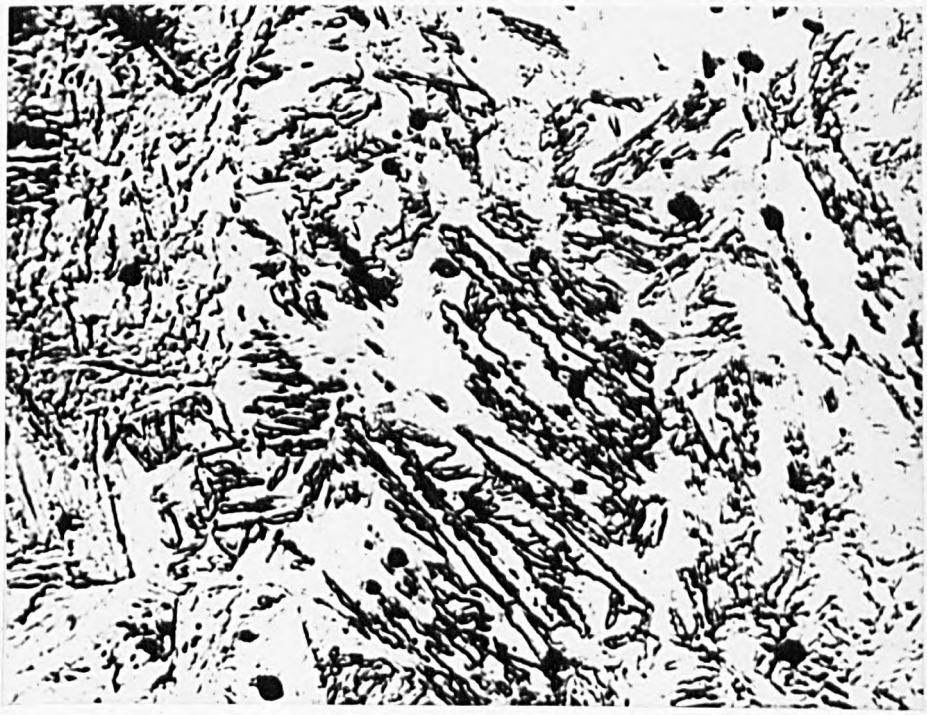

Figure 45.

Iron -1.85^{W}/o nitrogen alloy quenched into brine and etched with 5% nital

x 750

Figure 46.

Iron -2.1^{W}/o nitrogen alloy quenched into brine and further cooled to -196^{o}C, lightly tempered and etched with 2% nital

x 500

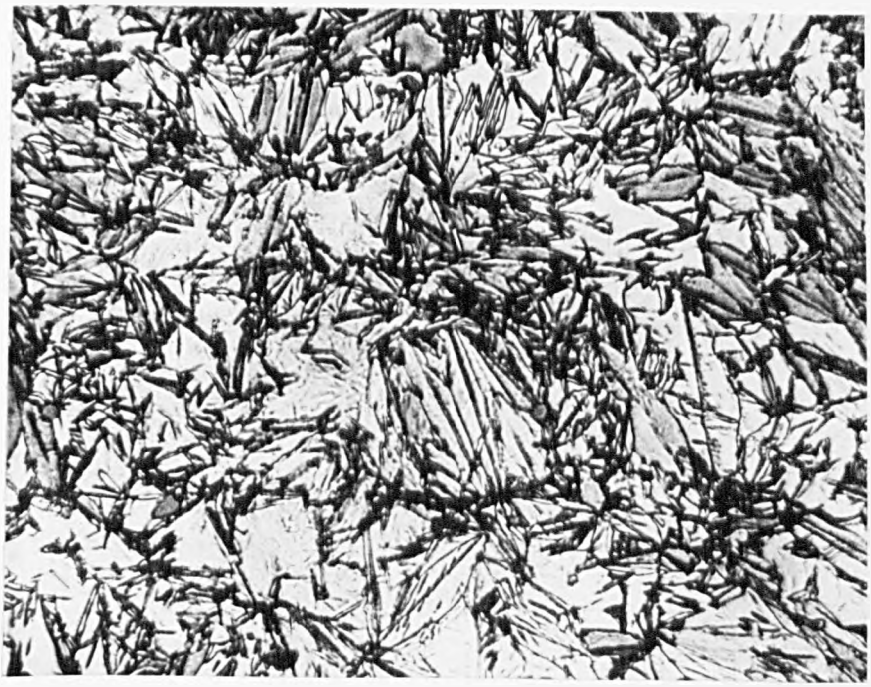

Figure 47.

Iron -2.3^{W}/o nitrogen alloy quenched into brine and further cooled to 0^{o}C, lightly tempered and etched with 2% nital

x 550

Figure 48.

Iron -2.4^{W}/o nitrogen alloy quenched into brine and further cooled to -196^{o} C, lightly tempered at 225^{o} C and etched in 2% nital.

x 750

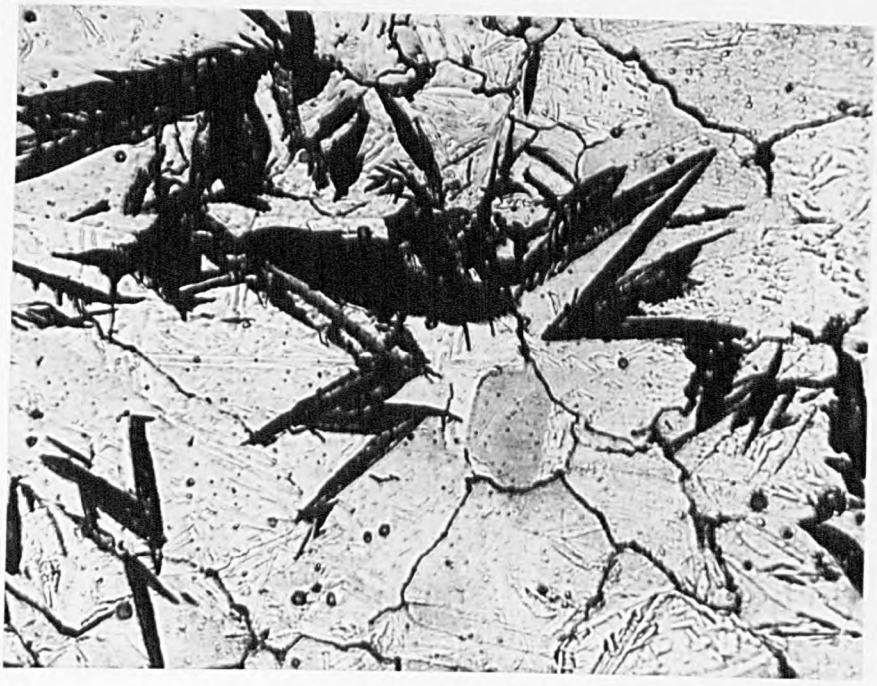

Figure 49.

Prepolished surface of an iron -2.35^{w}/o nitrogen alloy quenched into brine and further quenched to 0^{0}C. There are a few acicular martensite plates present in a matrix of austenite. Oblique illumination.

x 400

Figure 50.

Interferogram corresponding to Figure 49.

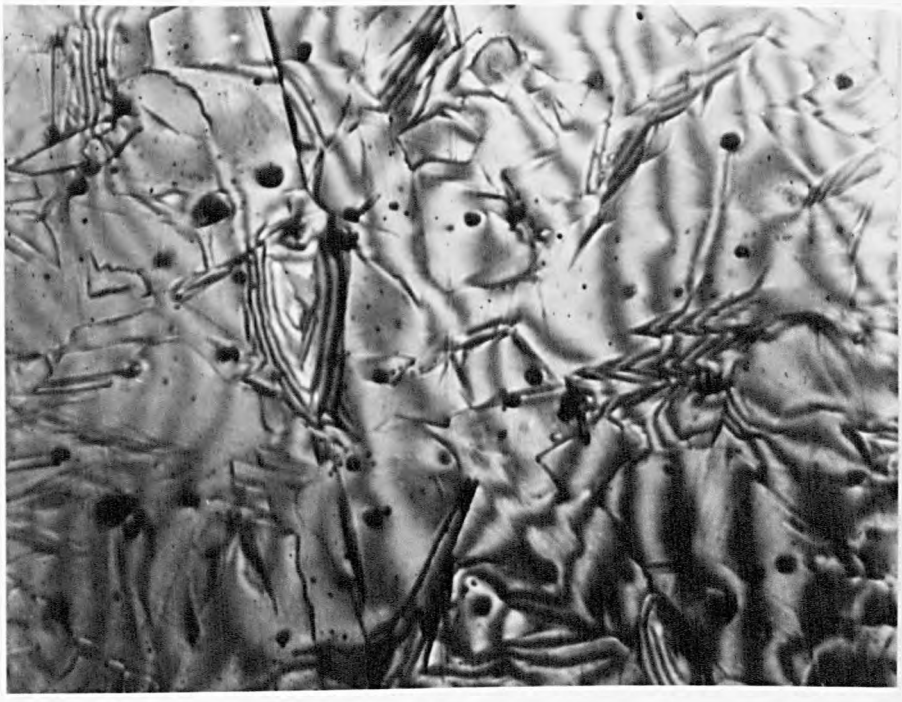

Figure 51.

Prepolished surface of an iron 2.35 w/o nitrogen alloy quenched into brine and further cooled to -196° C. Oblique illumination.

x 1000

Figure 52.

Interferogram corresponding to Figure 51.

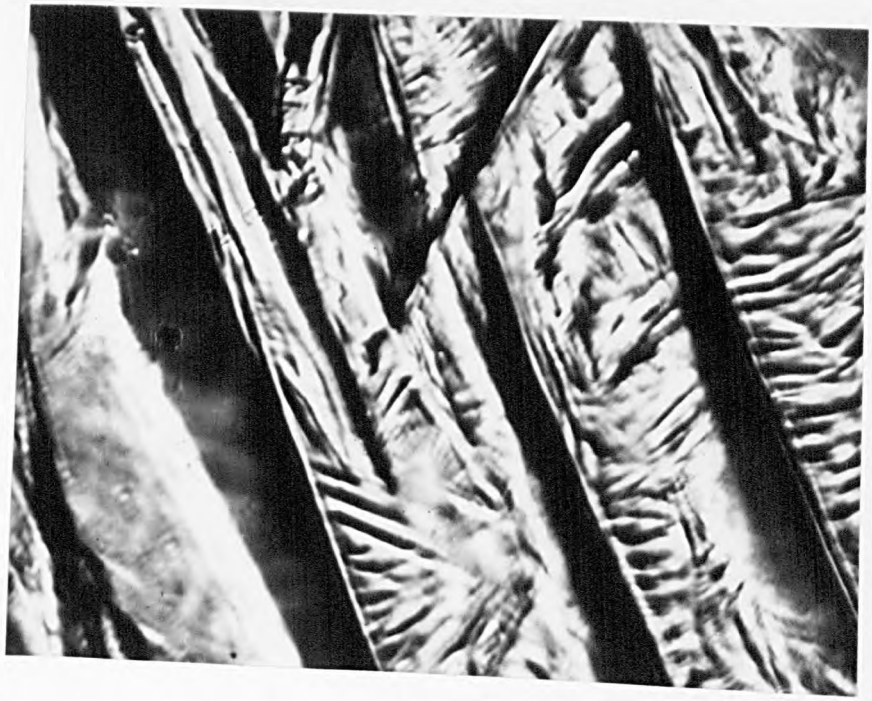

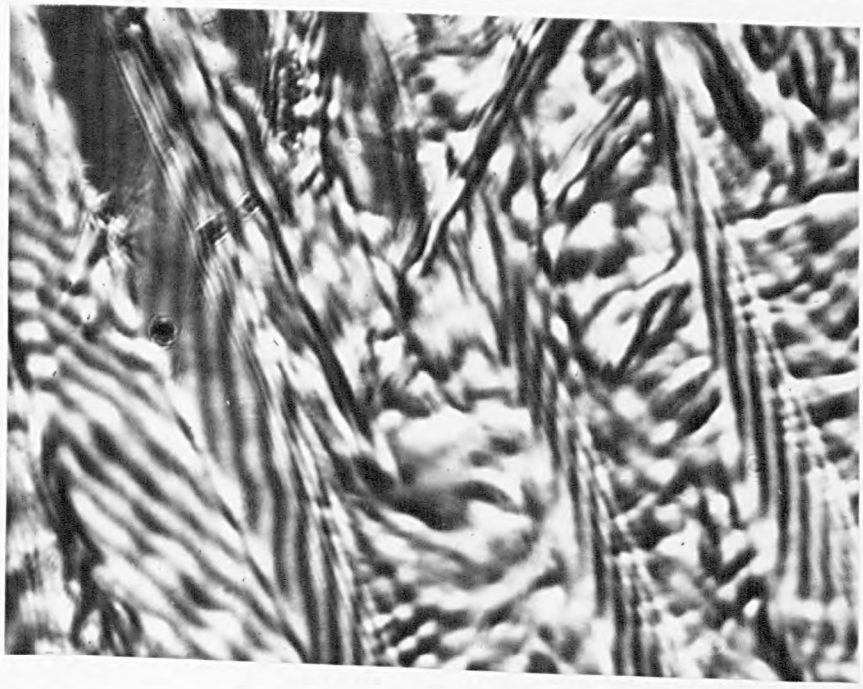

Figure 53.

Iron -2.5^{w}/o nitrogen alloy quenched to 10^{o} C, showing a fully austenitic structure. Electropolished and etched in 5% perchloric-acetic acid solution.

x 300

Figure 54.

Prepolished surface of an iron -2.4^{w}/o nitrogen alloy quenched to 10^{o} C. Oblique illumination

x 350

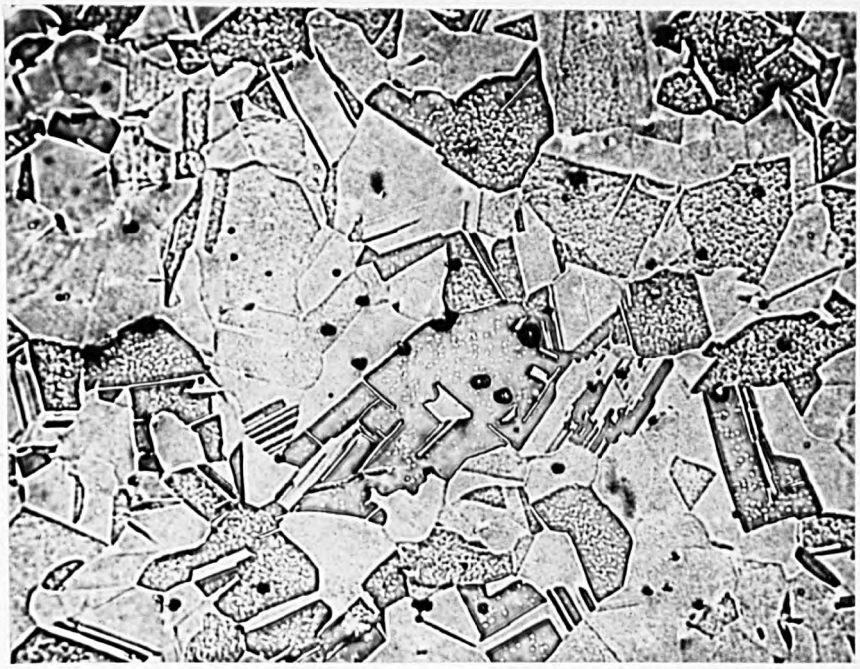

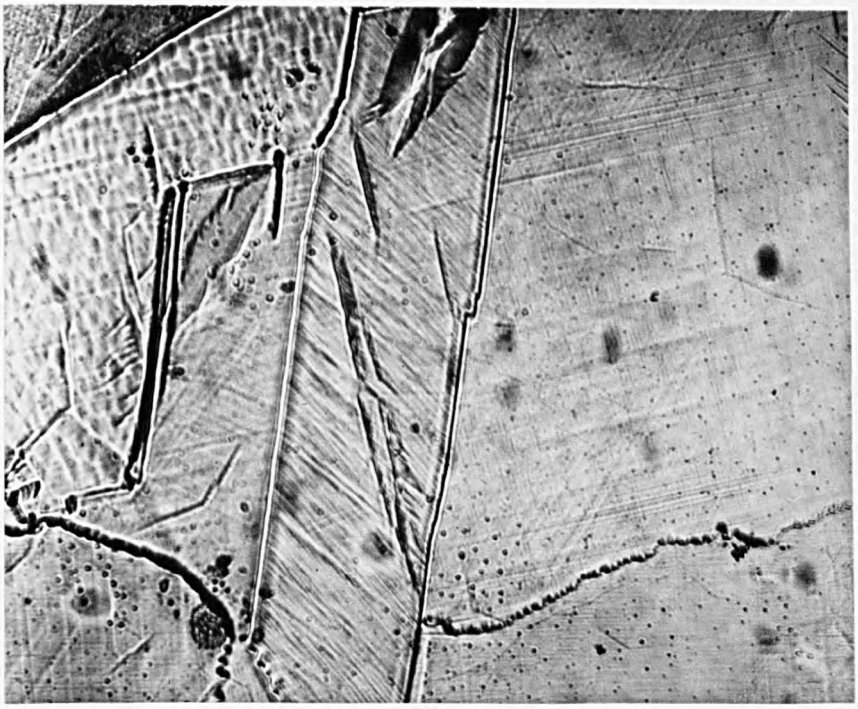

Figure 55.

Electron micrograph of iron -0.3^{W}/o nitrogen martensite, illustrating general lath type structure.

x 30,000

Figure 56.

Electron micrograph of iron -0.3^{W}/o nitrogen martensite illustrating the sharp boundary between two "sheaves" of laths.

x 30,000

Figure 57.

Electron micrograph of iron -0.3^{w}/o nitrogen martensite, illustrating the variation in lath thickness and the dovetailing of individual laths.

x 30,000

Figure 58.

Selected area electron diffraction pattern of the large lath in Figure 57. Foil orientation ($\bar{1}3\bar{1}$)

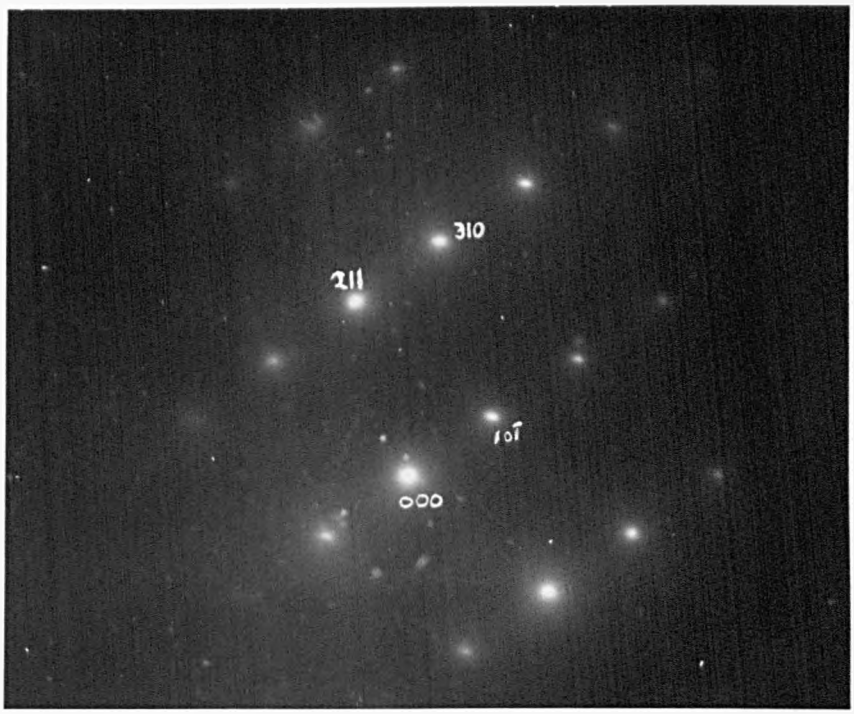
310
211
101
000

Figure 59.

Electron micrograph of iron -0.42^{w}/o nitrogen martensite.

Figure 60.

Selected area electron diffraction pattern of the large lath in Figure 59. Foil orientation is approximately (133).

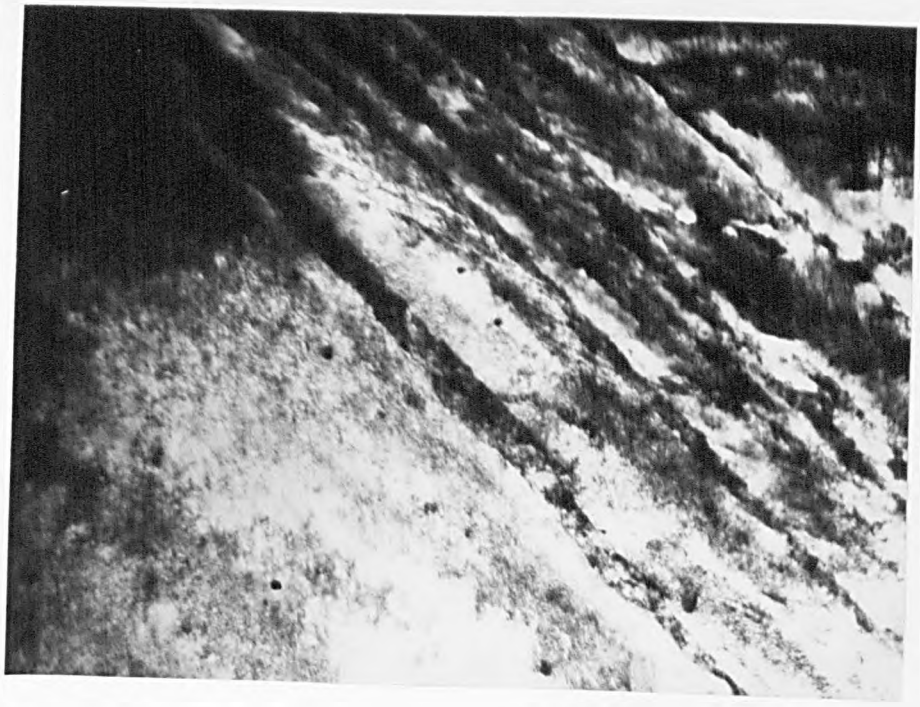

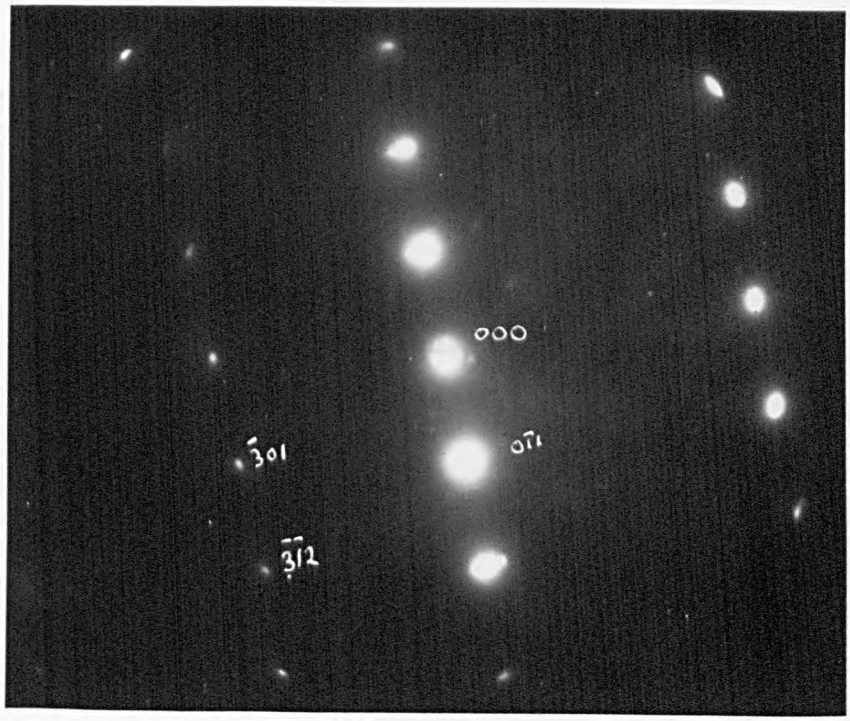
000
$\bar{3}01$
$0\bar{1}1$
$\bar{3}\bar{1}2$

Figure 61.

Electron micrograph of iron -0.65^{W}/o nitrogen martensite, showing small interwoven dislocated laths.

x 40,000

Figure 62.

Electron micrograph of iron -0.65^{W}/o nitrogen martensite illustrating general lath type structure.

x 40,000

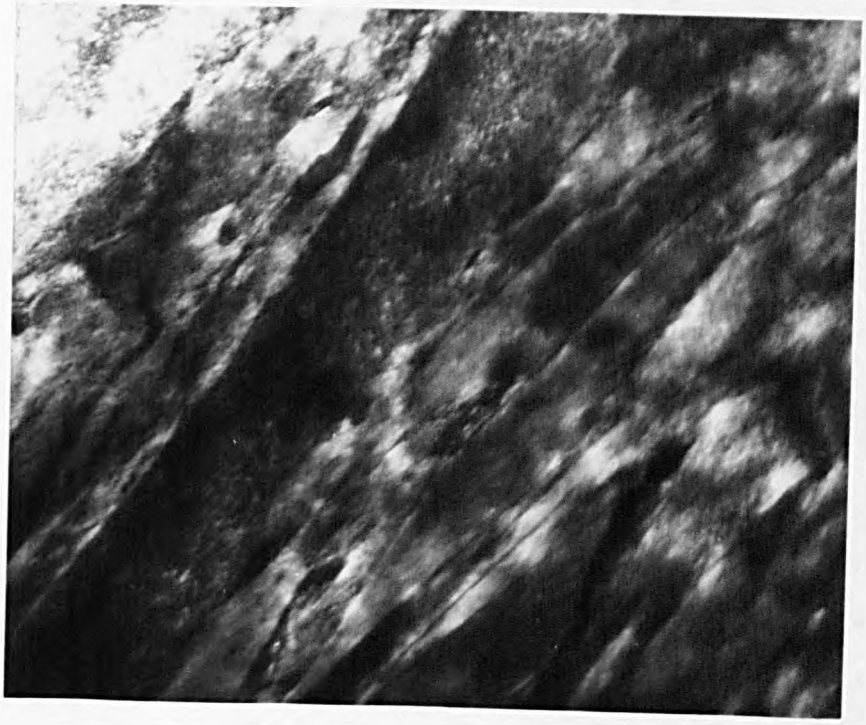

Figure 63.

Electron micrograph of an iron -0.65^{W}/o nitrogen martensite. There are a few internally twinned martensite plates present.

x 50,000

Figure 64.

Electron micrograph of iron -1.1^{W}/o nitrogen martensite showing a large martensite plate which has coarse internal twinning, with a spacing of about 500A^{o}

x 60,000

Figure 65.

Electron micrograph of an 1.1^{W}/o nitrogen martensite.

x 50,000

Figure 66.

Electron micrograph of iron 1.4^{W}/o nitrogen martensite. The fine structure of the martensite is predominately internal twinning.

x 50,000

Figure 67.

Electron micrograph of a large iron - 1.4 w/o nitrogen martensite plate showing fine internal twinning 100°A thick.

x 100,000

Figure 68.

Selected area electron diffraction pattern corresponding to Figure 67. Foil orientation is approximately $(11\bar{1})$ and the streaking is at right angles to the fine twins. Planes underlined are twin reflections.

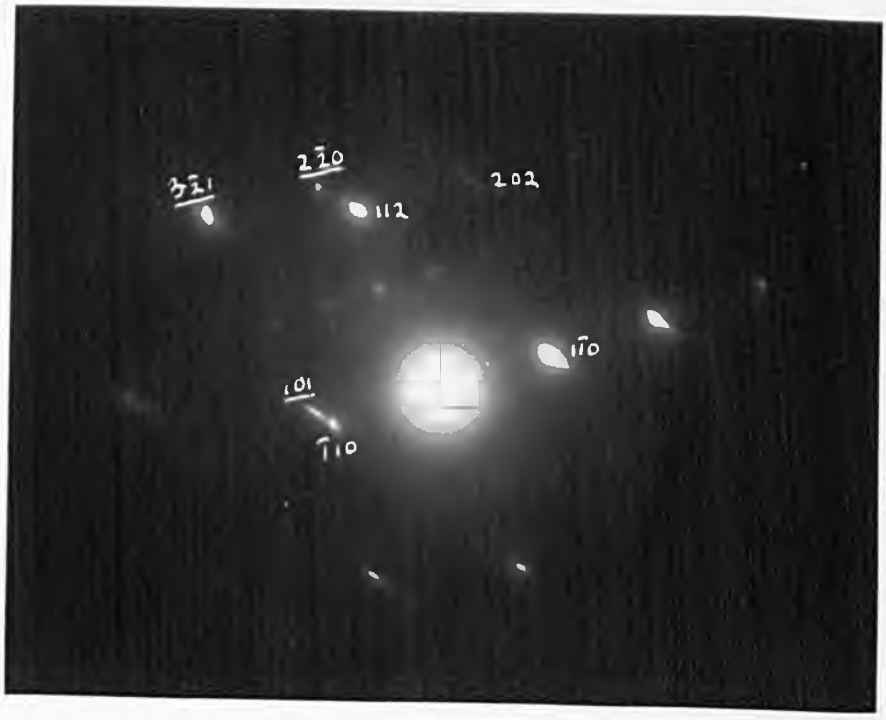
3$\bar{3}$1
2$\bar{2}$0
112
202
1$\bar{1}$0
101
$\bar{1}$10

Figure 69.

Electron micrograph of an iron -1.4^{W}/o nitrogen alloy showing a dislocated martensite plate, embedded in a matrix of retained austenite.

x 90,000

Figure 70.

Electron in micrograph of an iron -2.4^{W}/o nitrogen alloy, showing two internally twinned martensite plates preferential attack of the surrounding retained austenite has resulted in holes.

x 60,000

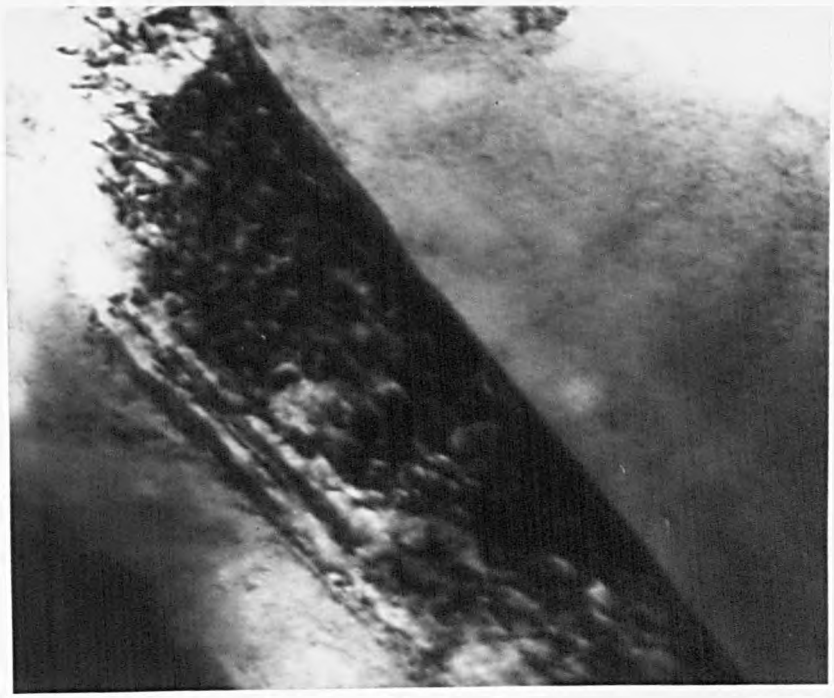

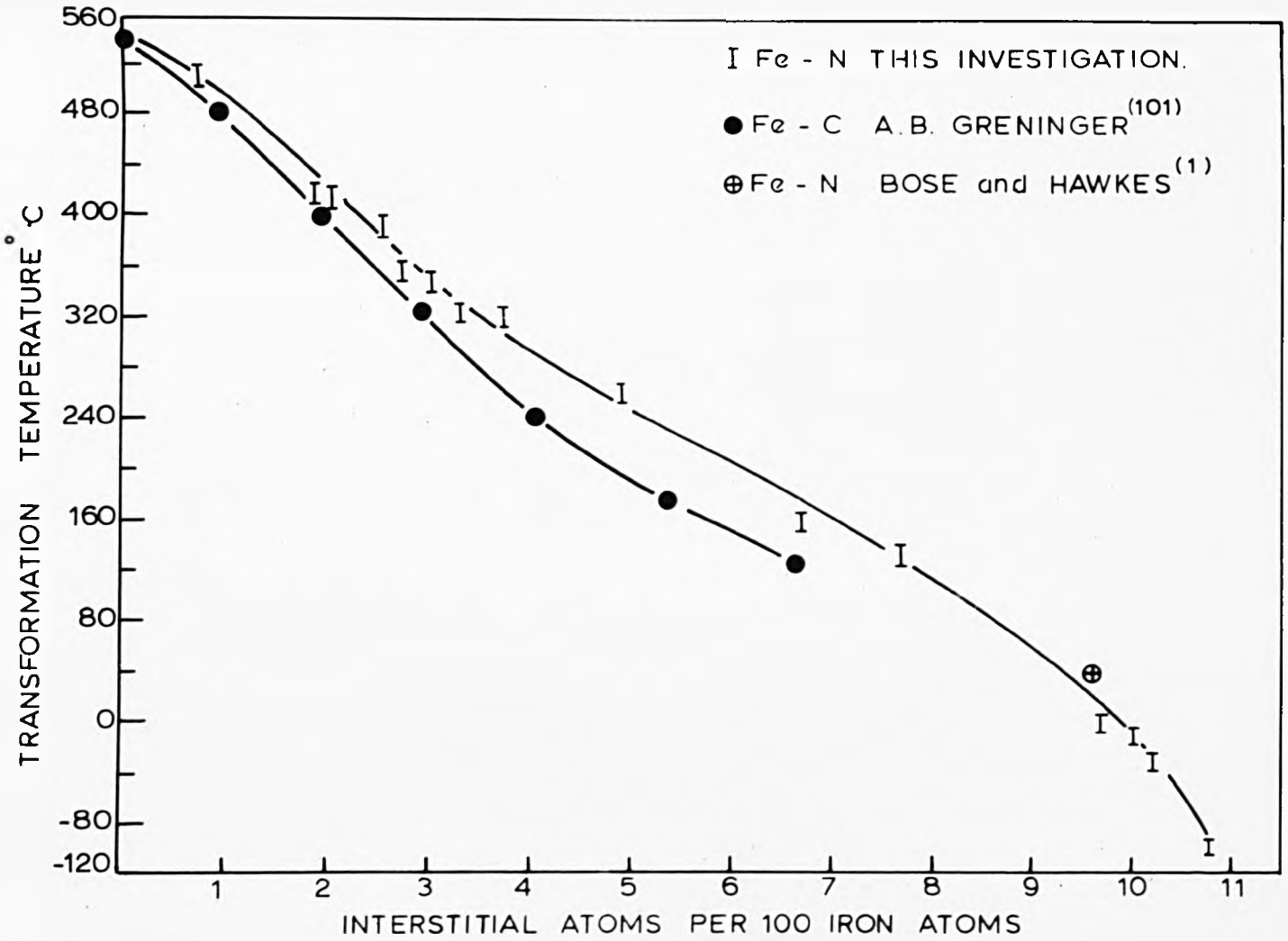

Figure 71. VARIATION OF M_s TEMPERATURE WITH INTERSTITIAL CONTENT FOR IRON - NITRCGEN AND IRON CARBON ALLOYS

Figure 72.

The variation of resistivity with temperature for an iron -0.4 w/o carbon alloy, on transforming from austenite to martensite. After McReynolds (112)

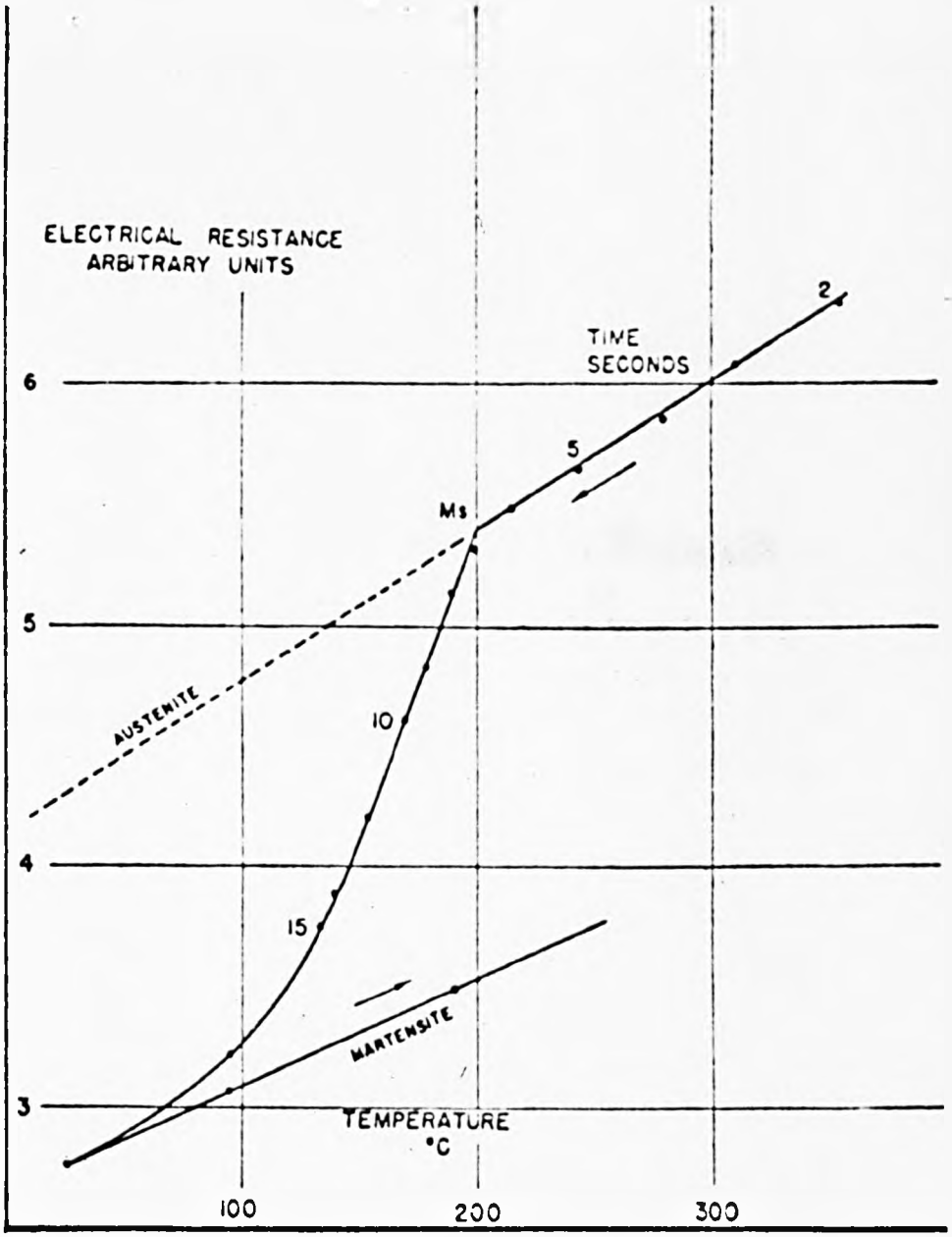
ELECTRICAL RESISTANCE
ARBITRARY UNITS
TIME
SECONDS
2
5
Ms
10
15
AUSTENITE
MARTENSITE
6
5
4
3
TEMPERATURE
°C
100
200
300

Figure 73.

Diagramatic representation of the apparatus used in the determination of M_s temperatures by thermal analysis.

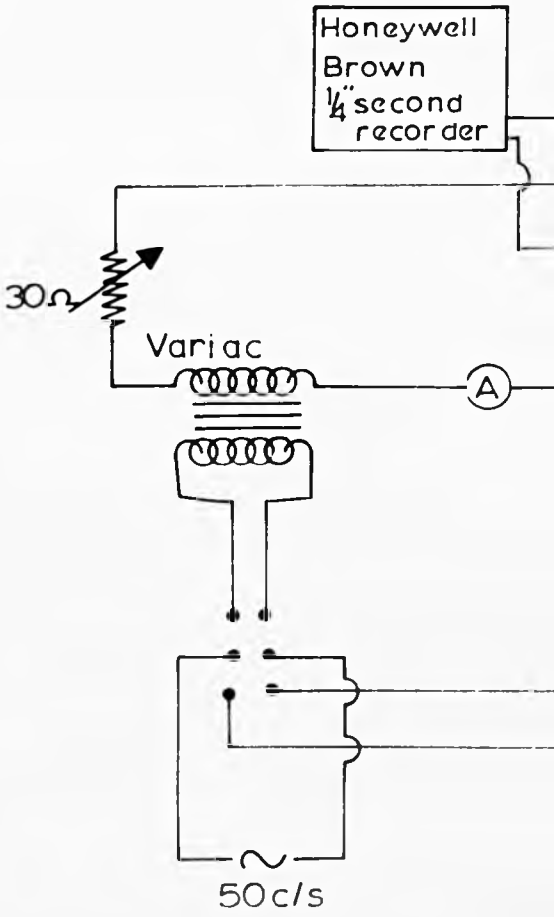
Honeywell
Brown
¼" second
recorder
30Ω
Variac
A
50c/s

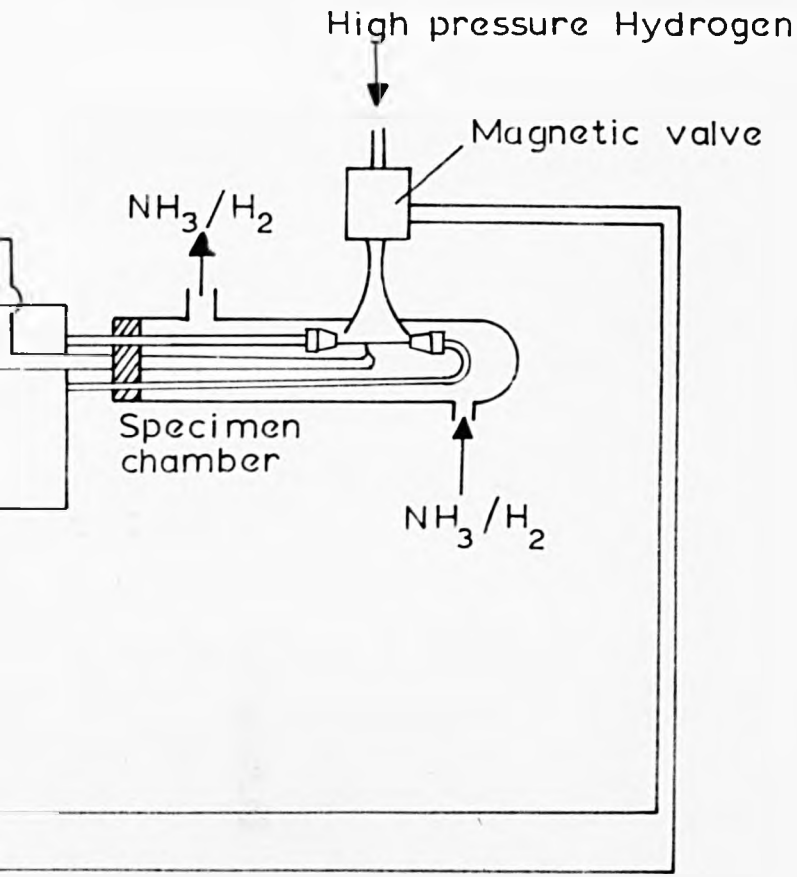
High pressure Hydrogen
Magnetic valve
NH_3/H_2
Specimen chamber
NH_3/H_2

Figure 74.

Photograph of the gas quenching chamber and specimen holder.

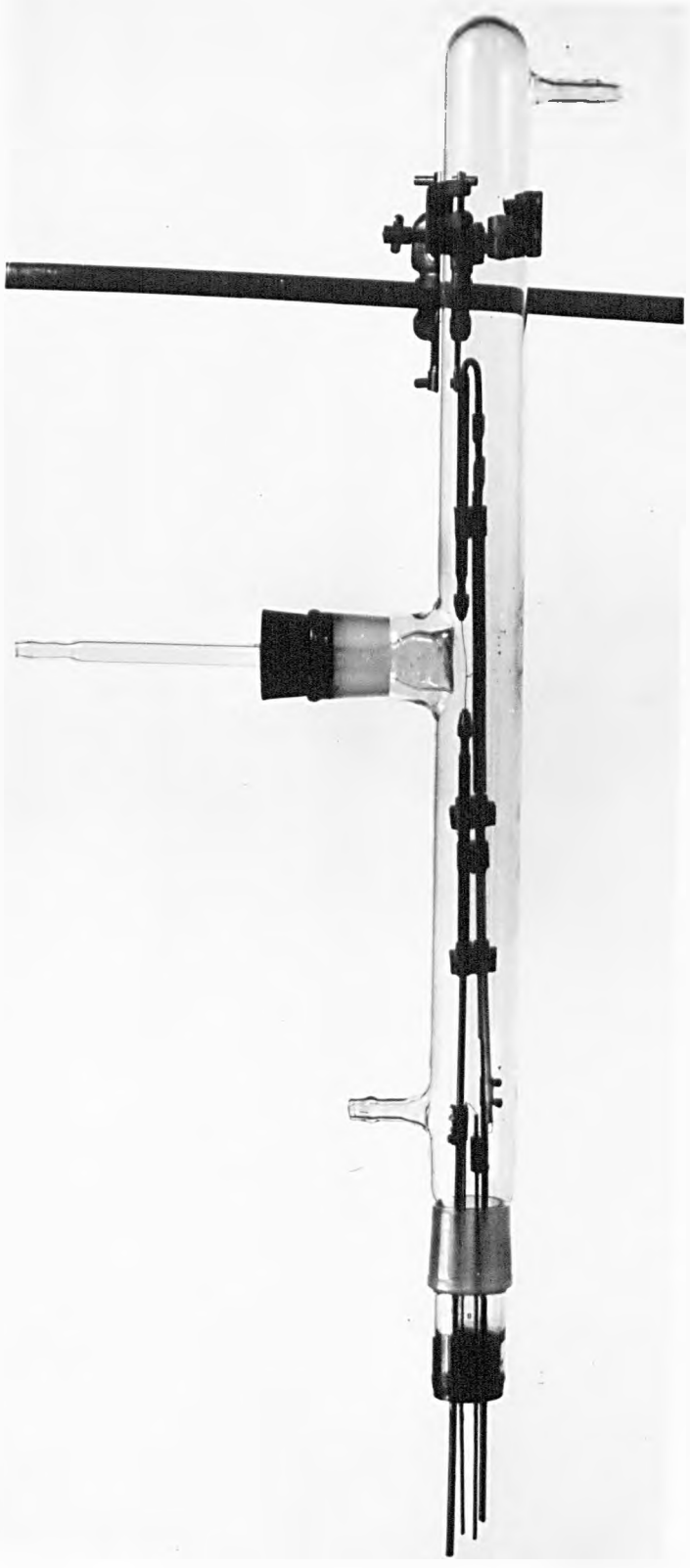

Figure 75.

Tracings of a series of cooling courves of iron-nitrogen alloys containing between 0.17^{w}/o to 1.9^{w}/o nitrogen.

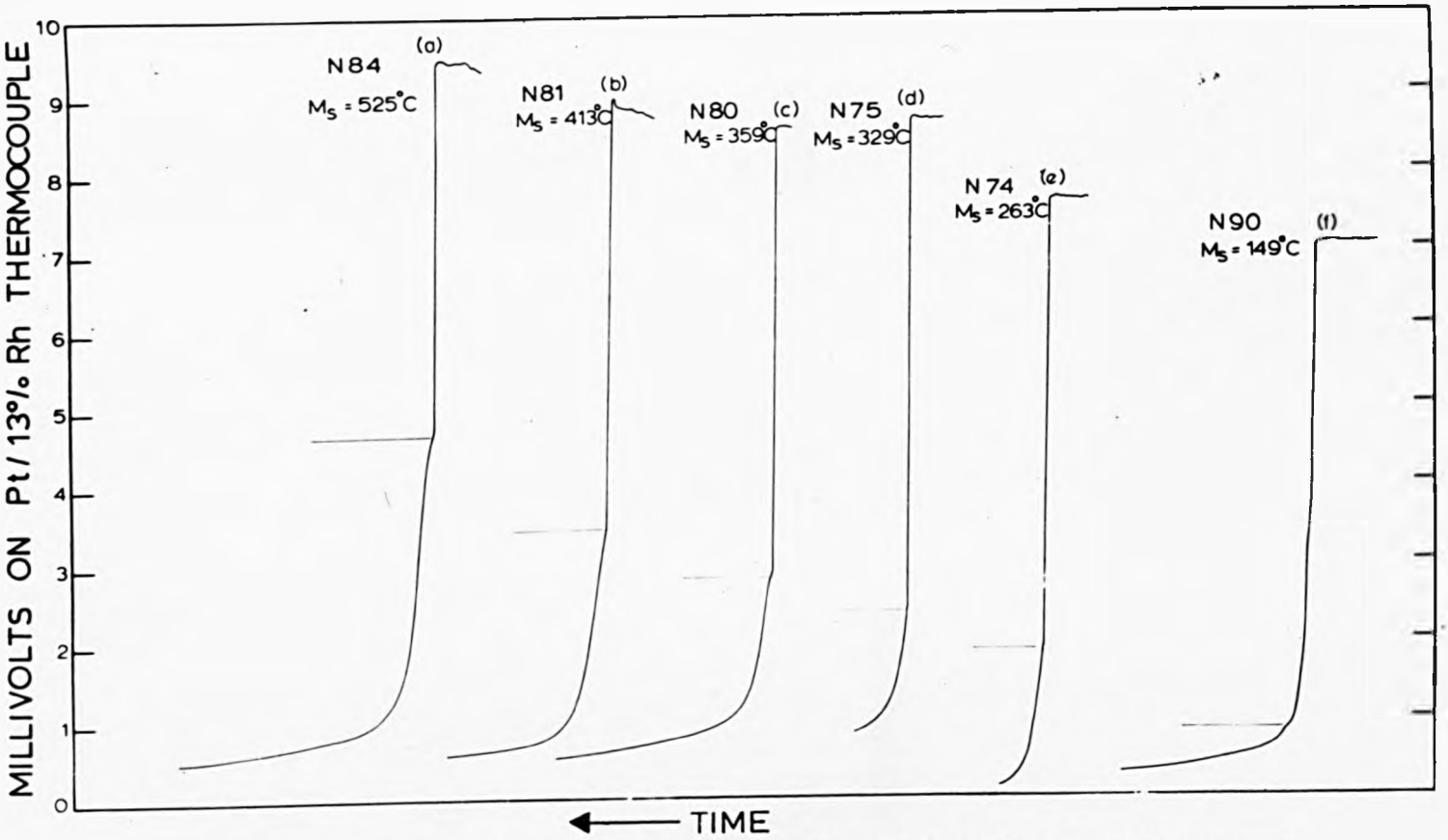

(a), (b), (c) and (f) 1 Inch 3 seconds (d) and (e) 1 Inch 7.5 seconds.

Figure 76.

Two cooling curves for an iron -0.44^{W}/o nitrogen alloy together with a standard cooling wave of platinum.

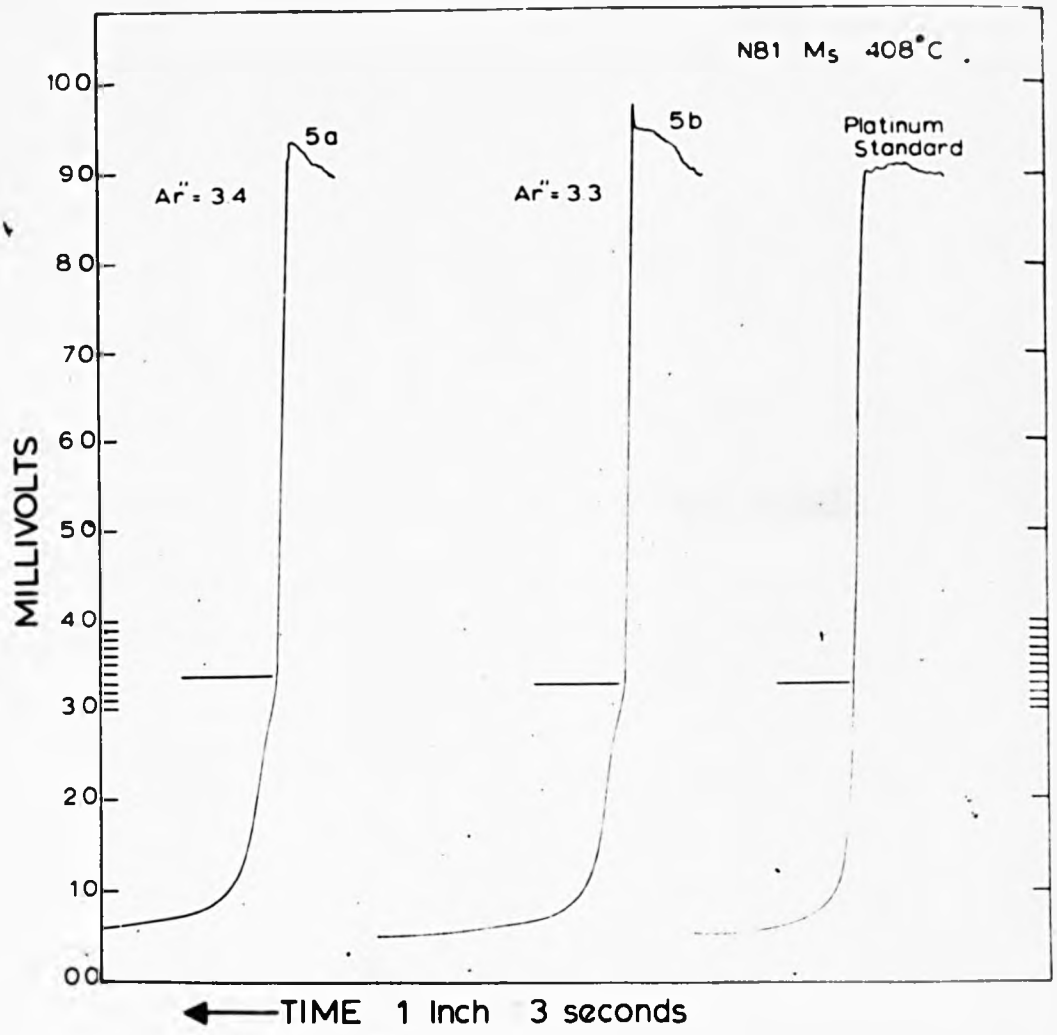
N81 Ms 408°C
100
90
80
70
60
50
40
30
20
10
00
MILLIVOLTS
5a
Ar'' = 3.4
5b
Ar'' = 3.3
Platinum Standard
TIME 1 Inch 3 seconds

Figure 77.

Diagram of the specimen holder and resistance circuit used for low temperature M_s determinations.

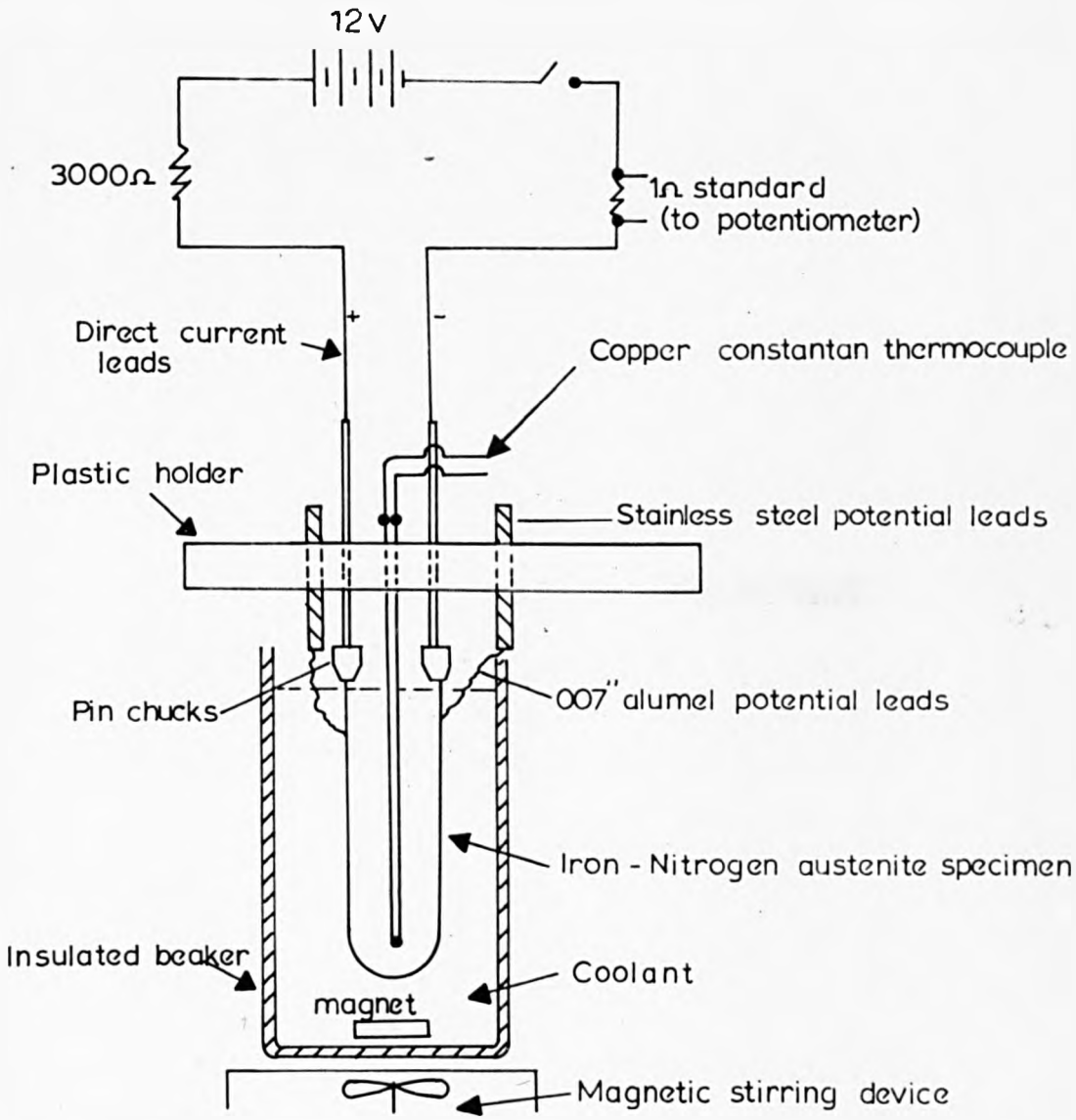
12 v
3000Ω
1Ω standard
(to potentiometer)
Direct current
leads
+
-
Copper constantan thermocouple
Plastic holder
Stainless steel potential leads
Pin chucks
007" alumel potential leads
Iron - Nitrogen austenite specimen
Insulated beaker
Coolant
magnet
Magnetic stirring device

Figure 78.

A series of X-ray diffraction patterns of an iron -2.35^{w}/o nitrogen alloy, showing no transformation to martensite until -25^{o} C.

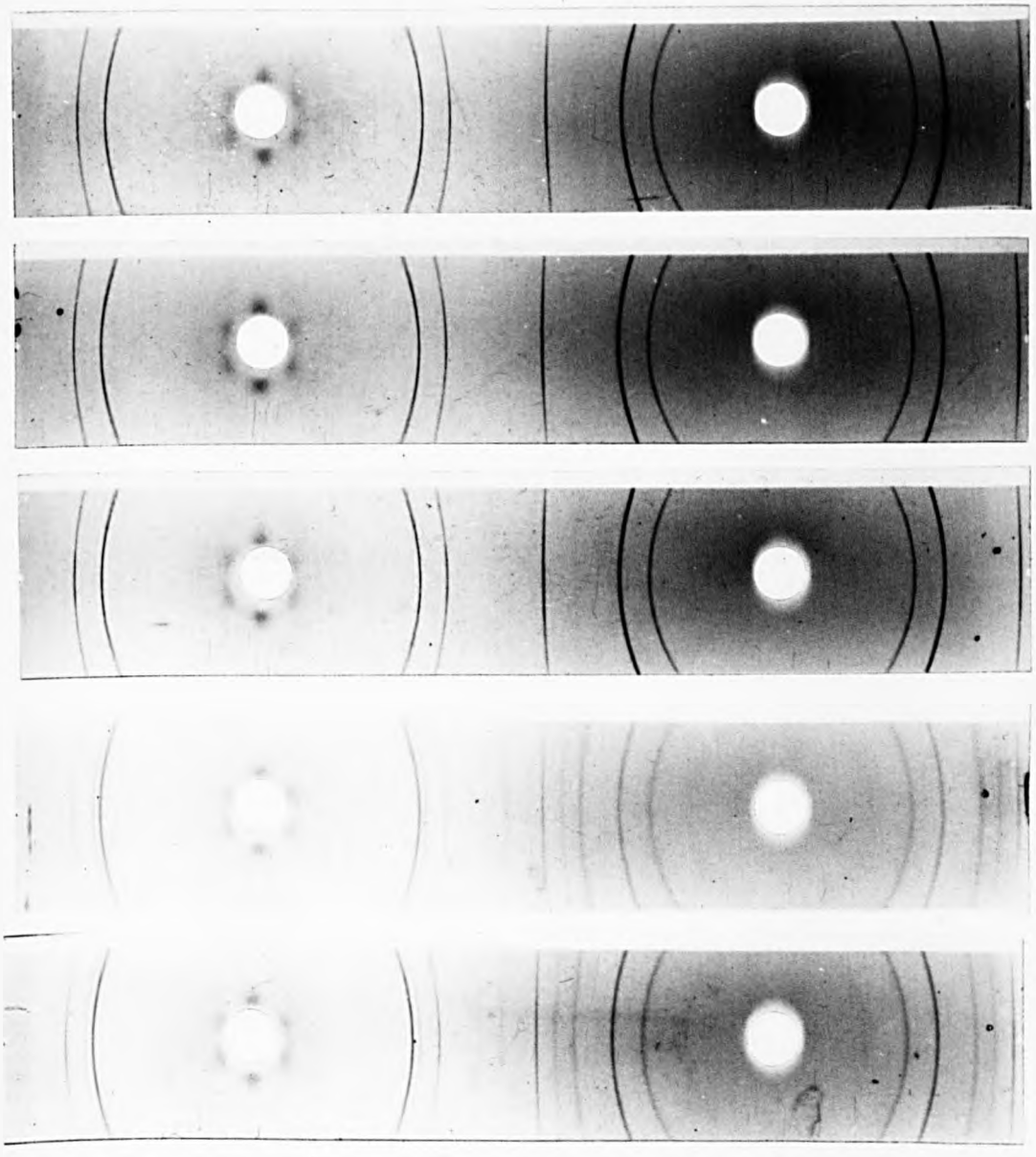

X-ray diffraction photographs of a 2.45% nitrogen alloy quenched to the temperatures indicated. Photographs N_{os}, 1 2 and 3 show f.c.c austenite lines only. No 4 shows b.c.t. lines due to martensite as well as retained austenite (iron $k\alpha$ radiation; manganese filter)

Figure 79.

Resistance curve corresponding to the specimen from Figure 78, showing an increase in resistance on transforming to martensite from austenite.

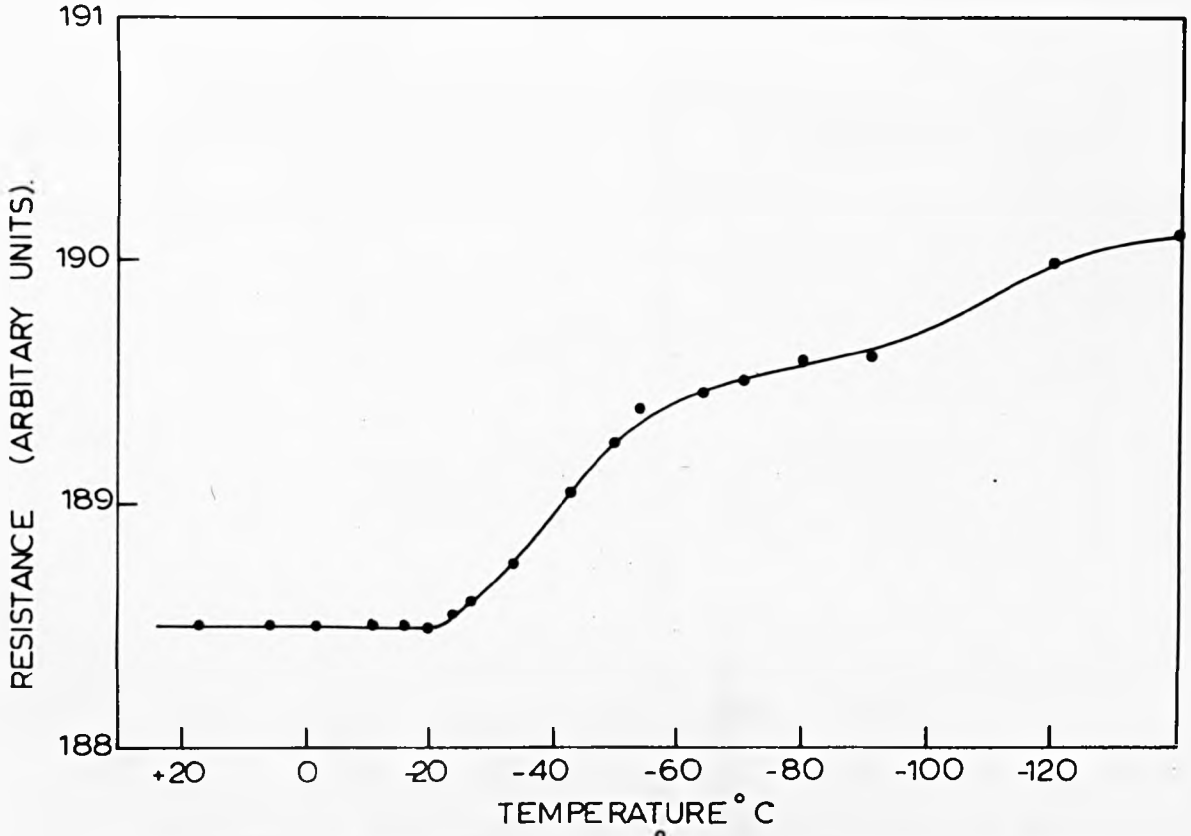

Variation of resistance at 20°C as a function of quenching temperature for Iron - 2.45 weight percent Nitrogen alloy.

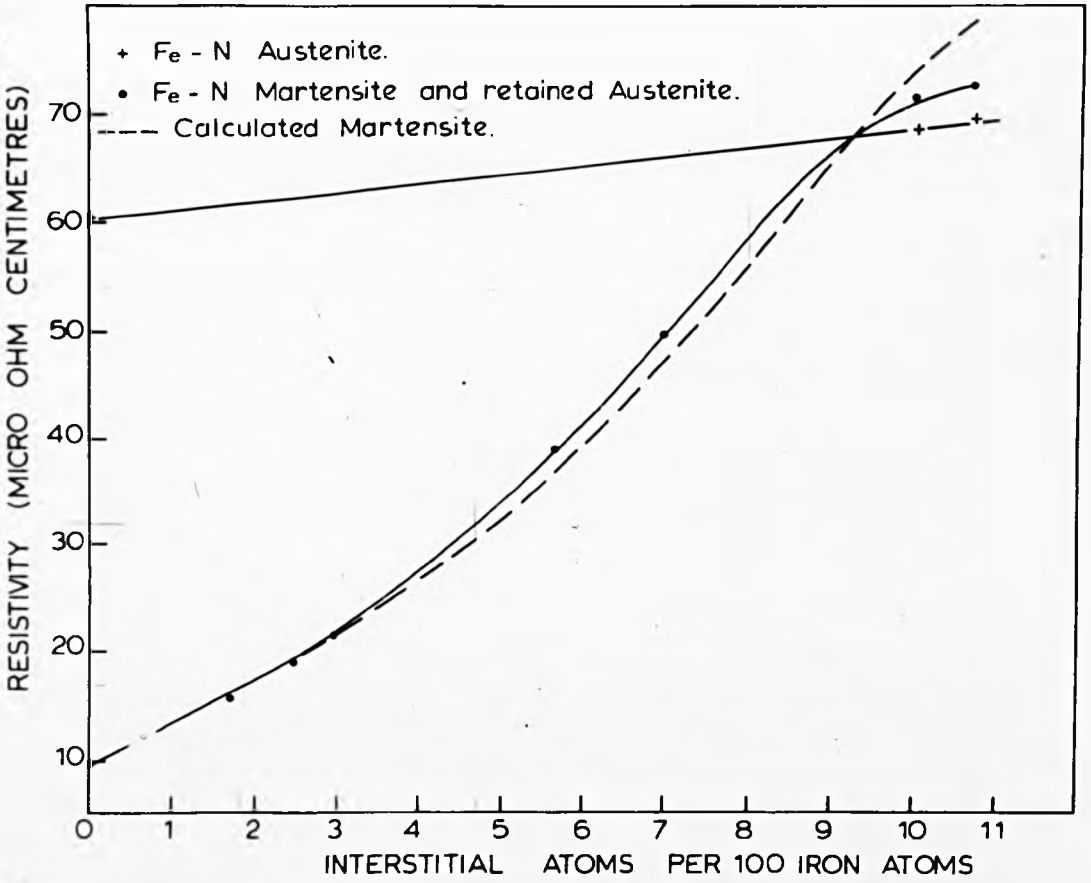

FIGURE 80 Resistivity of Fe - N Austenite and Fe - N Austenite - Martensite mixtures at 20°C, as a function of interstitial content.

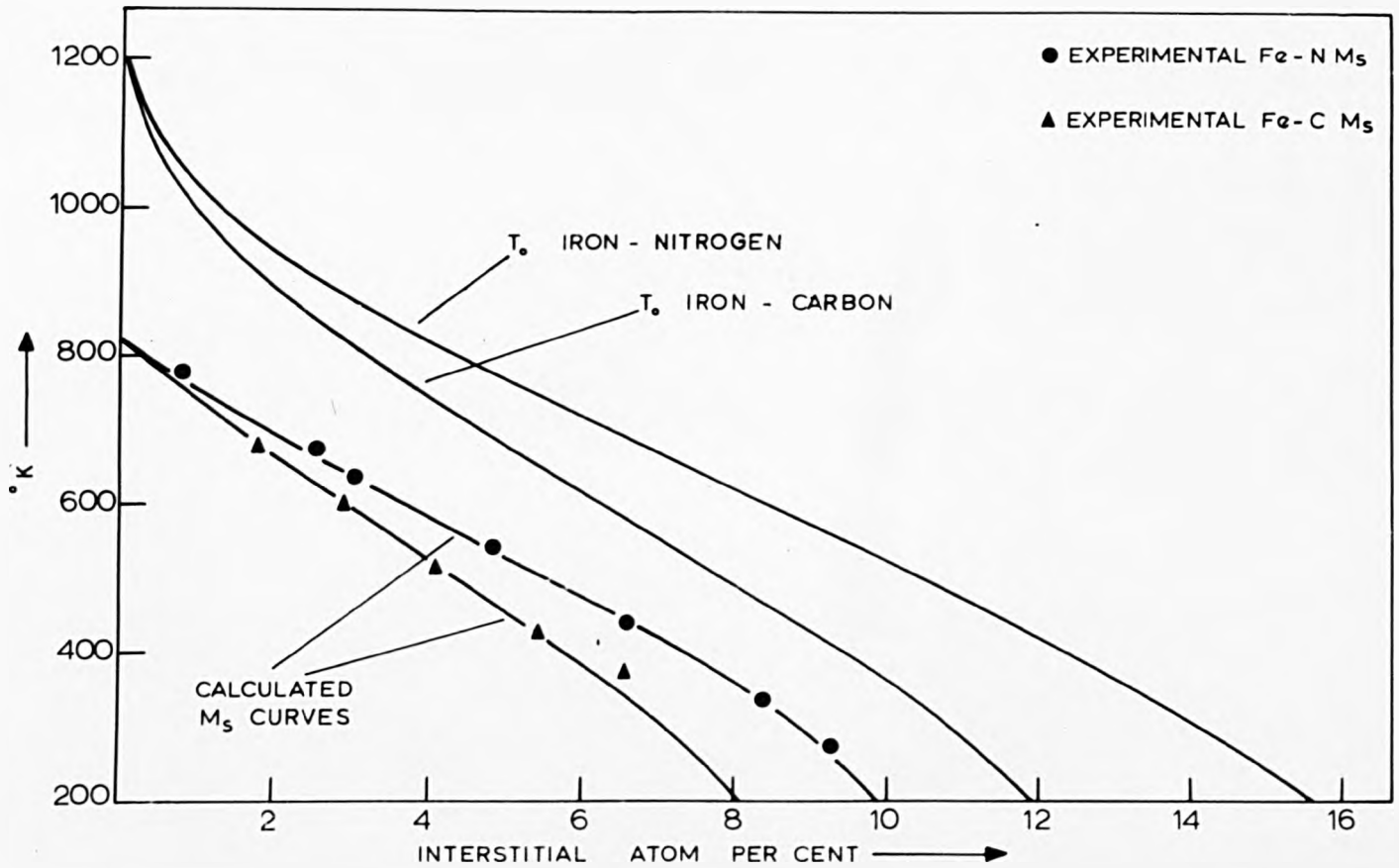

Figure 81 VARIATION OF T_0 AND OF THE THEORETICAL AND EXPERIMENTAL M_S TEMPERATURE WITH INTERSTITIAL CONTENT FOR IRON - CARBON AND IRON - NITROGEN SYSTEMS (ZENER MODEL).

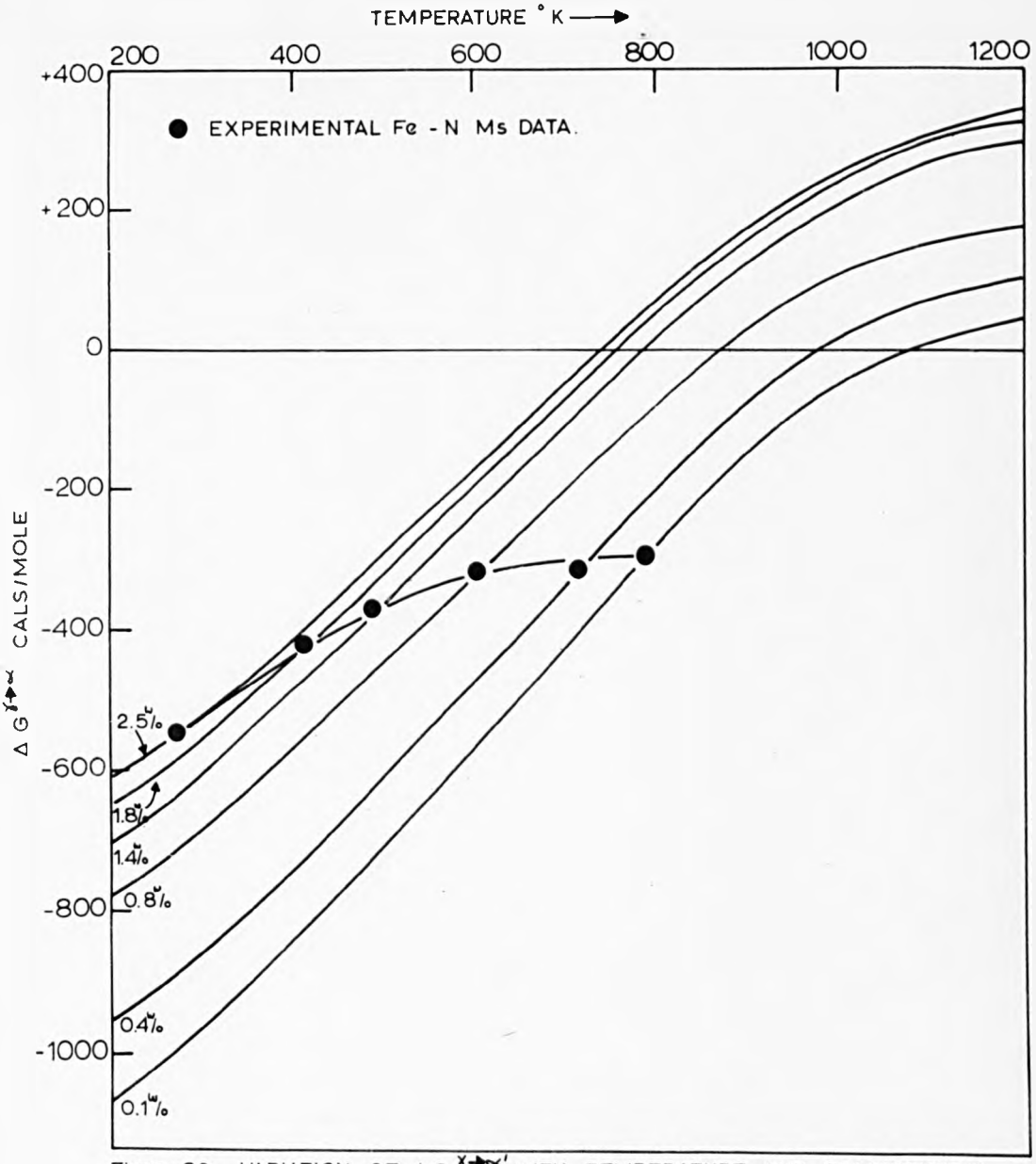

Figure 82. VARIATION OF $\Delta G^{\gamma \rightarrow \alpha'}$ WITH TEMPERATURE AND COMPOSITION FOR THE IRON - NITROGEN SYSTEM (FISHER MODEL).

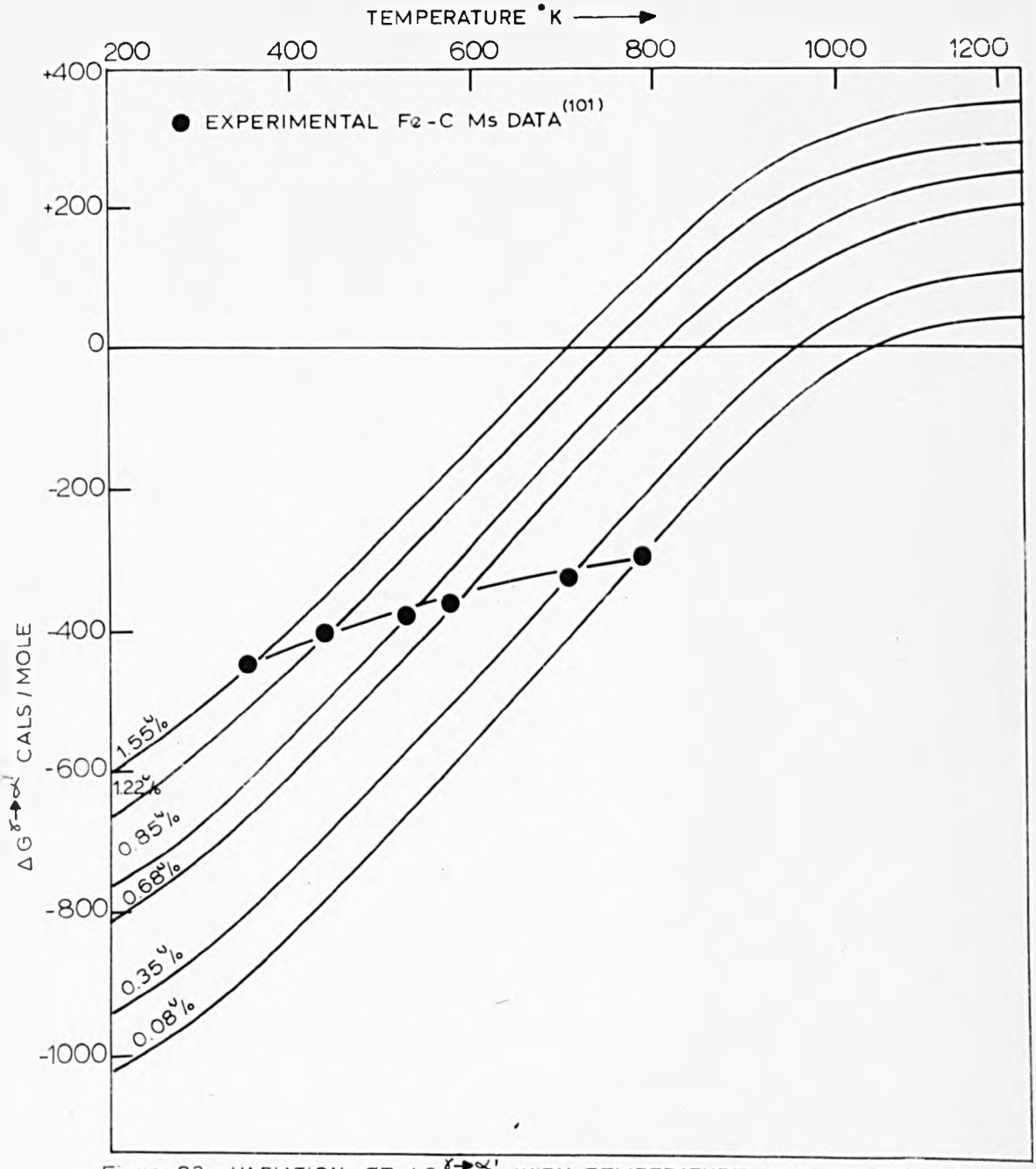

Figure 83. VARIATION OF $\Delta G^{\gamma \rightarrow \alpha'}$ WITH TEMPERATURE AND COMPOSITION FOR THE IRON - CARBON SYSTEM (FISHER MODEL).

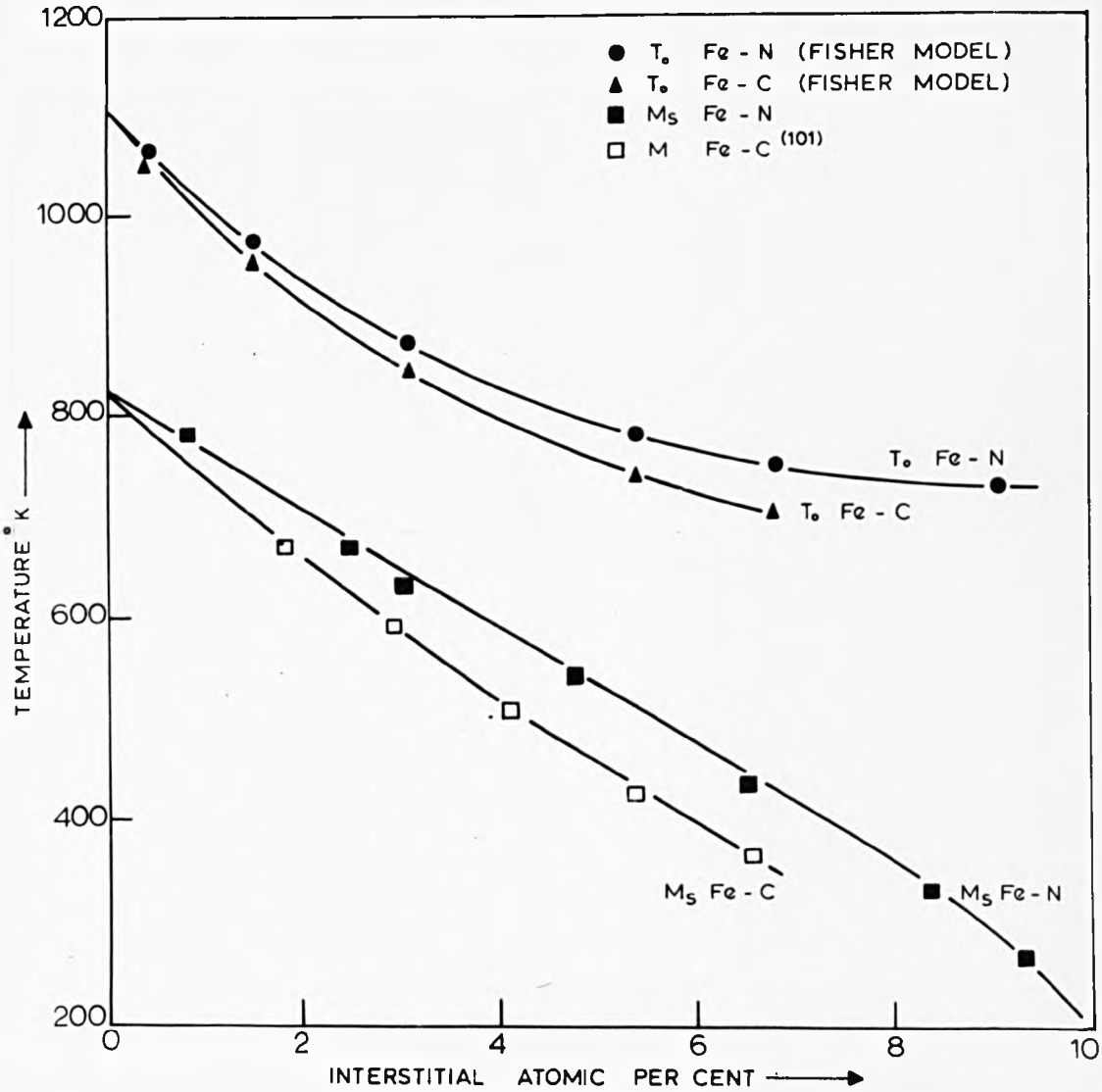

Figure 84. VARIATION OF T_o AND EXPERIMENTAL M_S WITH INTERSTITIAL CONTENT FOR THE IRON - CARBON AND IRON - NITROGEN SYSTEMS.

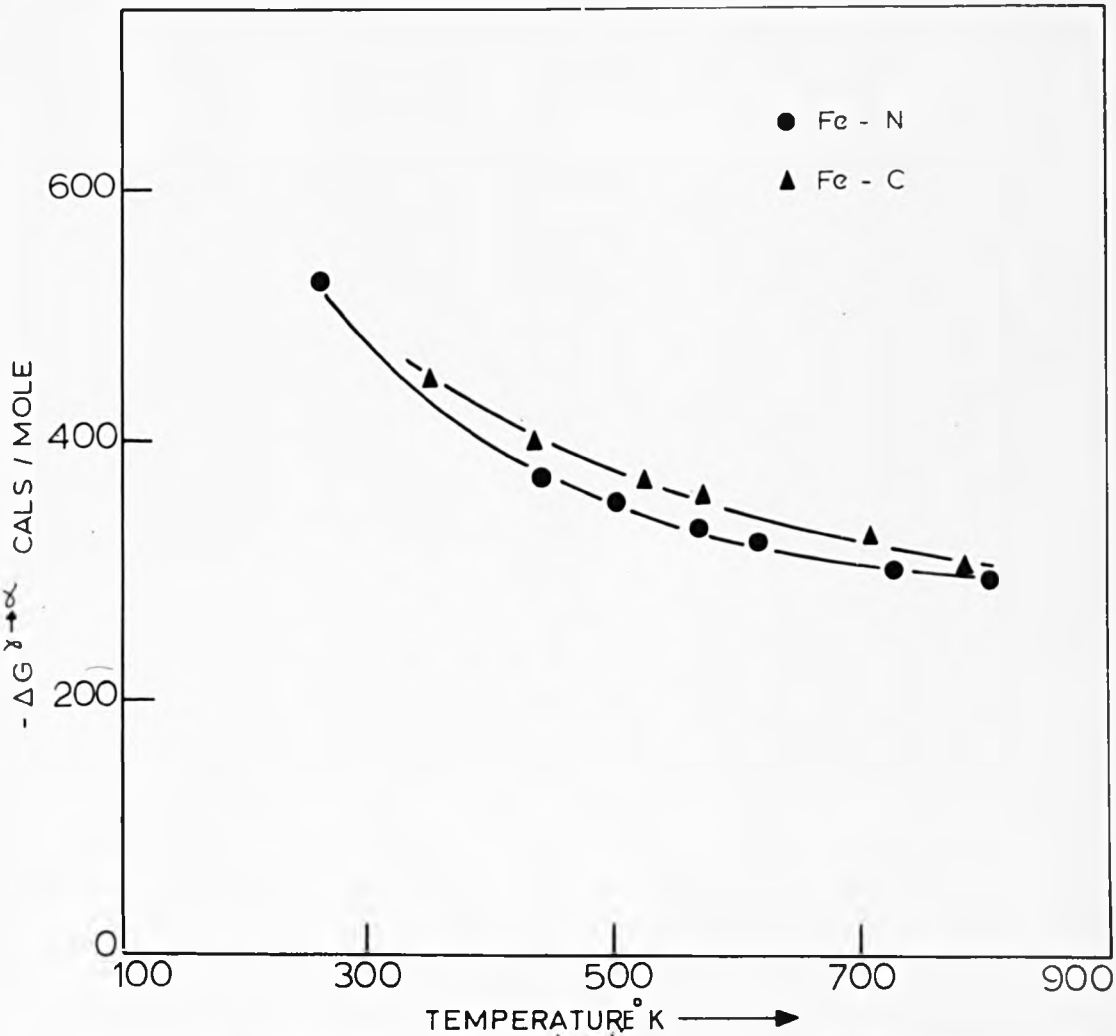

Figure 85. VARIATION OF $\Delta G^{\gamma \rightarrow \alpha}$ AT Ms WITH TEMPERATURE FOR IRON - CARBON AND IRON - NITROGEN ALLOYS (FISHER MODEL).

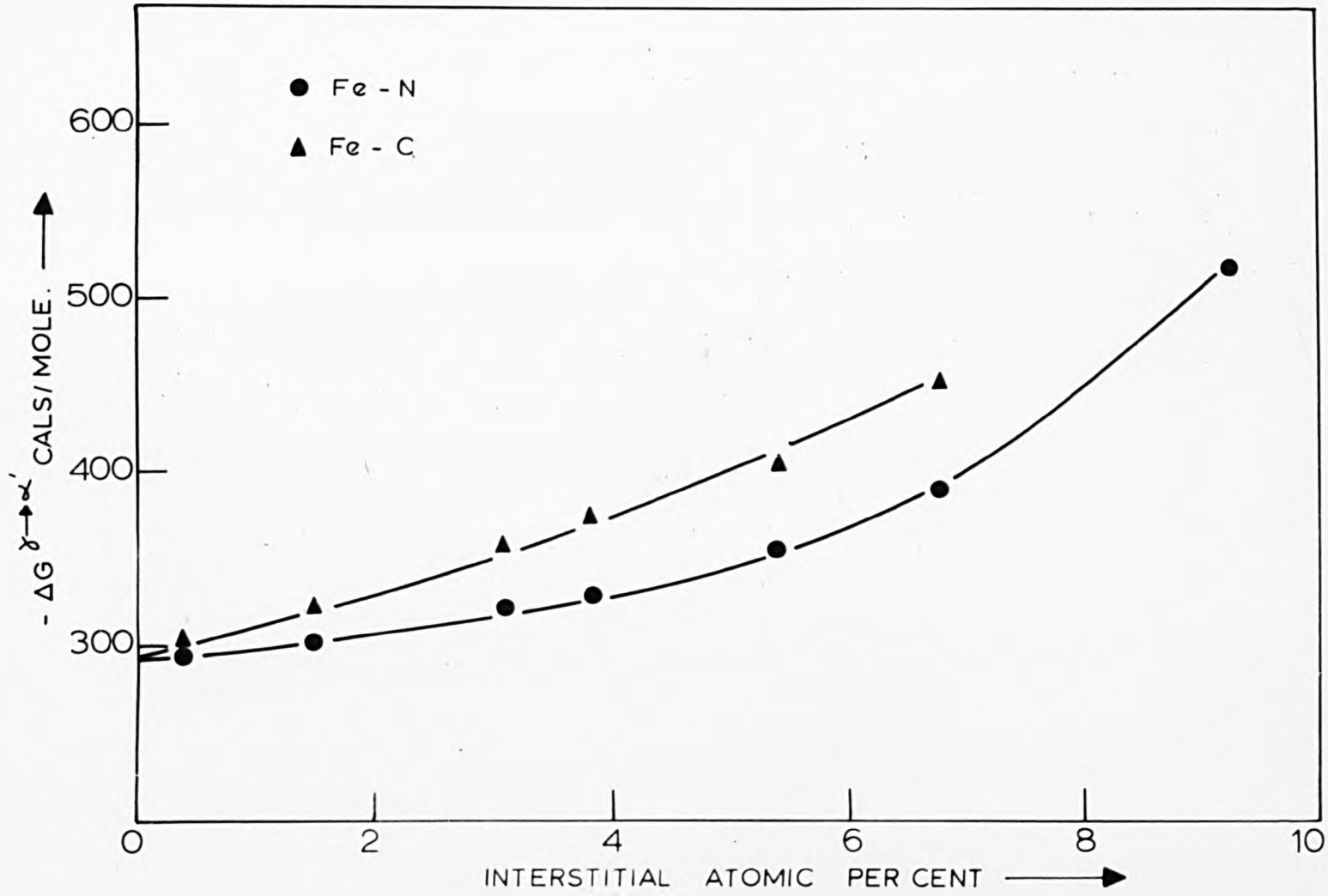

Figure 86. VARIATION OF $\Delta G^{\gamma \rightarrow \alpha'}$ AT M_s WITH COMPOSITION FOR IRON-CARBON AND IRON-NITROGEN ALLOYS (FISHER MODEL).

Figure 87.

Variation of $\Delta G^{\gamma \rightarrow \alpha'}$ with temperature and composition for the iron-carbon system (original Cohen model[127])

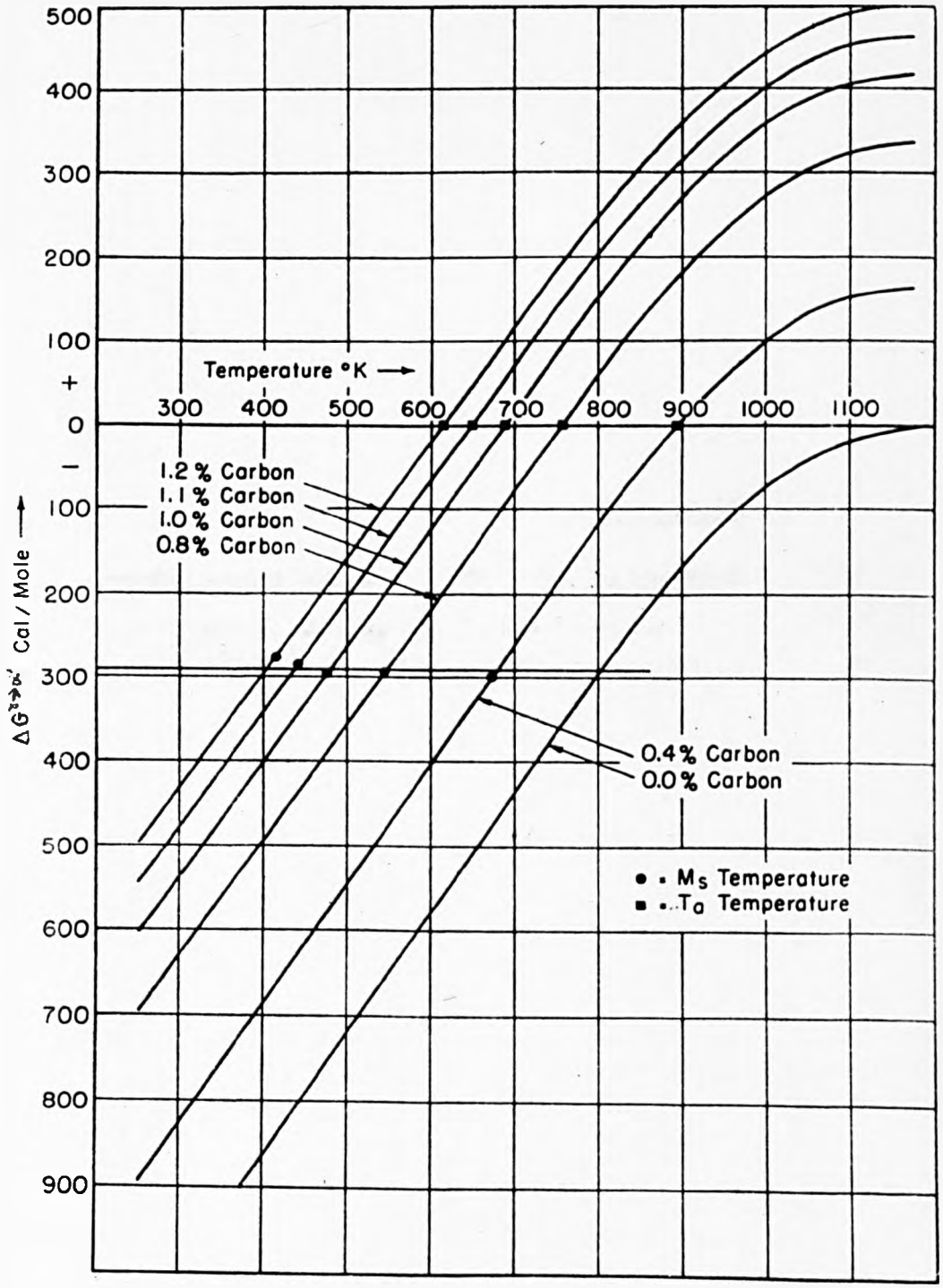
500
400
300
200
100
+
0
−
100
200
300
400
500
600
700
800
900
Temperature °K →
300
400
500
600
700
800
900
1000
1100
ΔG Cal / Mole
1.2 % Carbon
1.1 % Carbon
1.0 % Carbon
0.8 % Carbon
0.4 % Carbon
0.0 % Carbon
● = Ms Temperature
■ = To Temperature

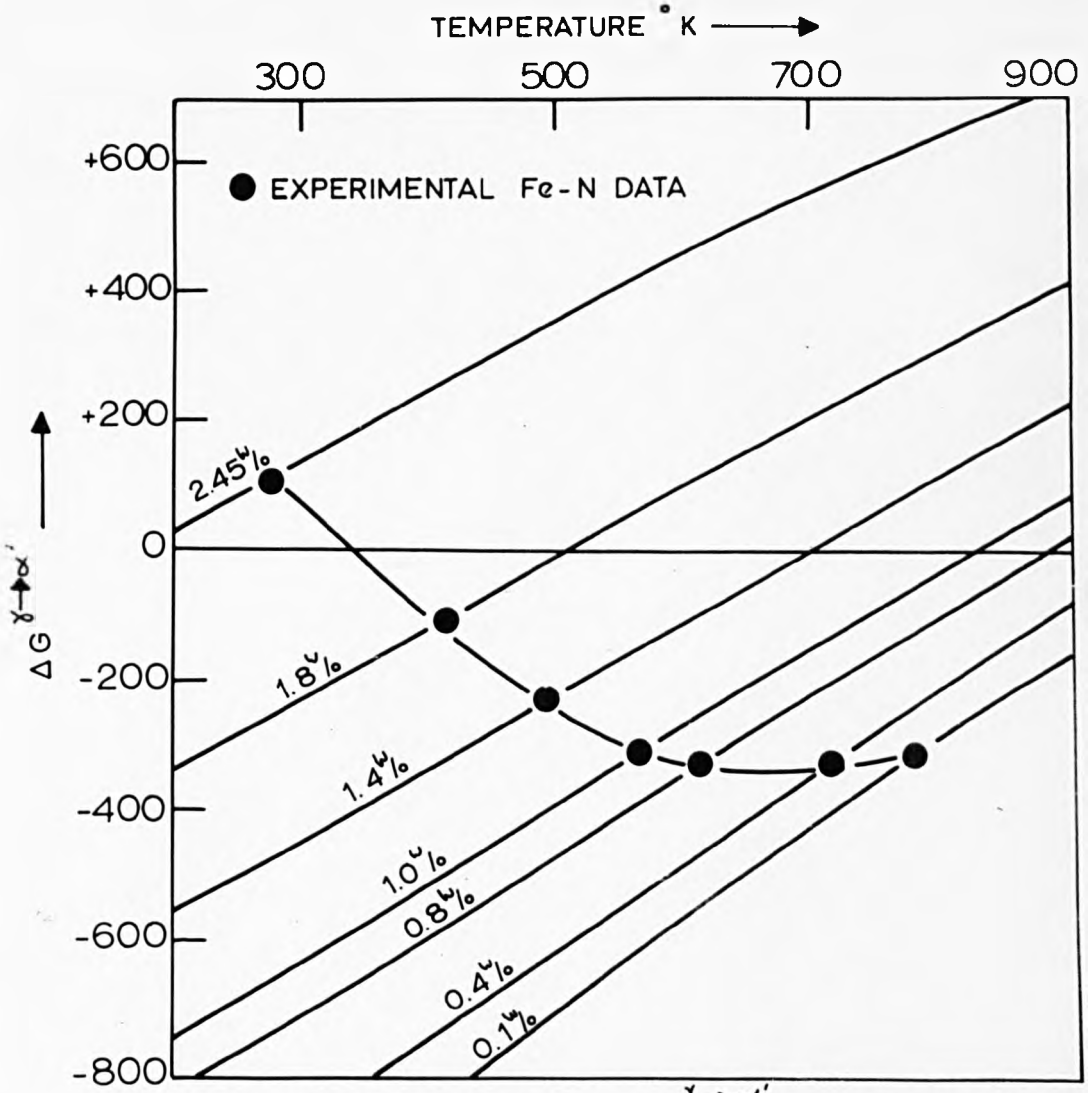

FIGURE 88. VARIATION OF $\Delta G^{\gamma \rightarrow \alpha'}$ WITH TEMPERATURE FOR IRON - NITROGEN ALLOYS (ORIGINAL COHEN MODEL[127])

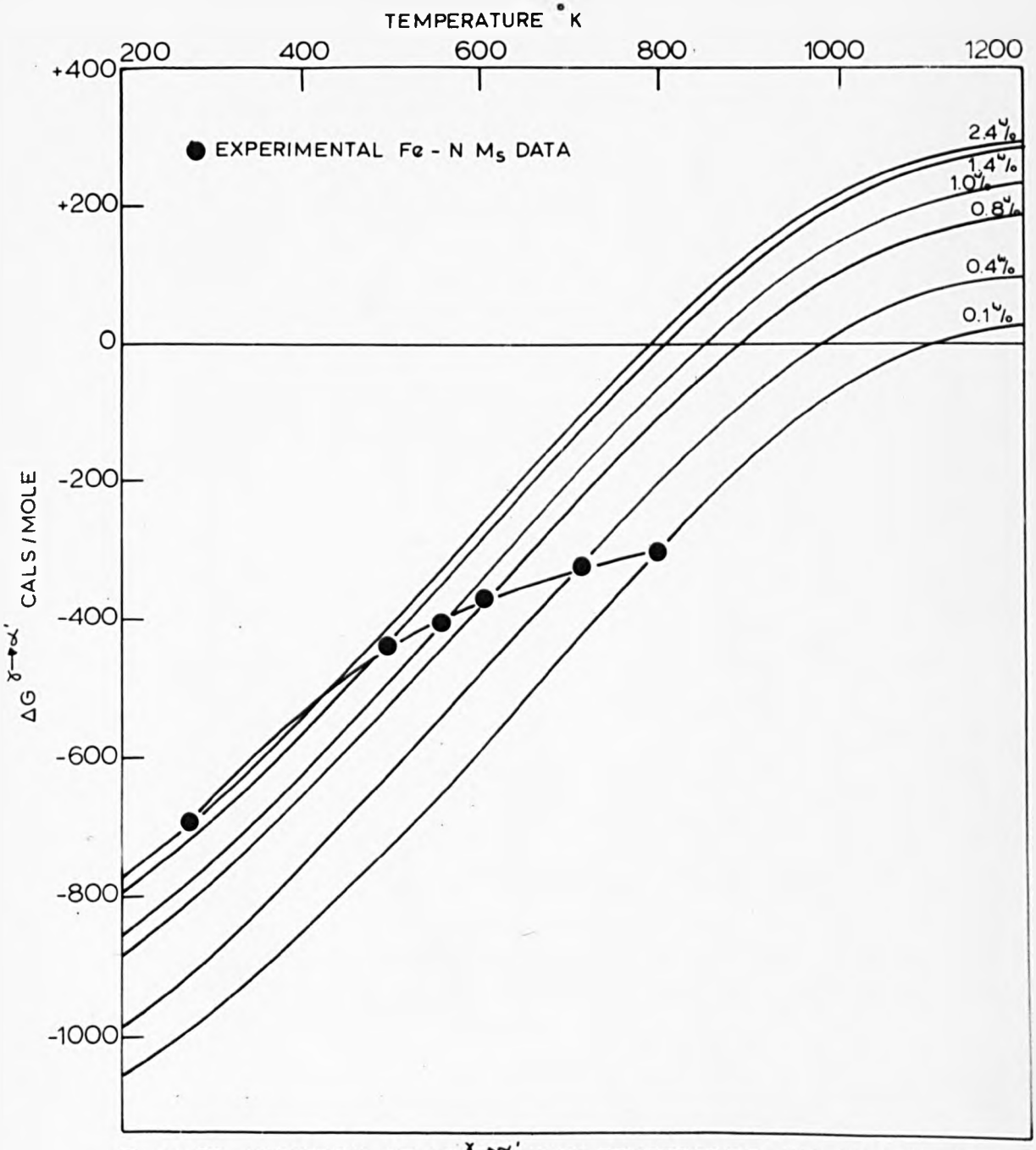

Figure 89. VARIATION OF $\Delta G^{\gamma \rightarrow \alpha'}$ WITH TEMPERATURE AND COMPOSITION FOR THE IRON - NITROGEN SYSTEM (K-R-C MODEL[128]).

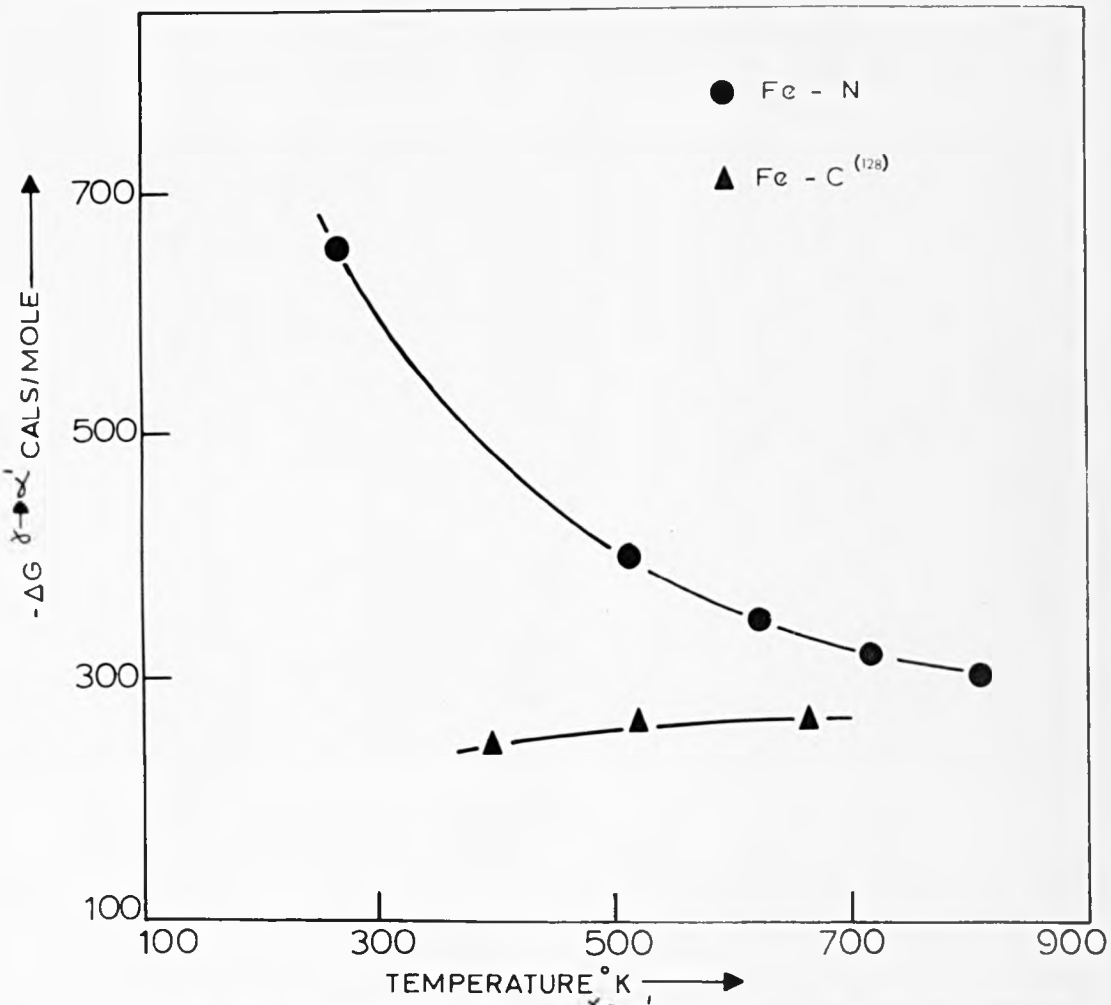

Figure 90. VARIATION OF $\Delta G^{\gamma \rightarrow \alpha'}$ AT M_S WITH TEMPERATURE FOR IRON - NITROGEN AND IRON - CARBON ALLOYS (GEOMETRIC K - R - C MODEL[128]).

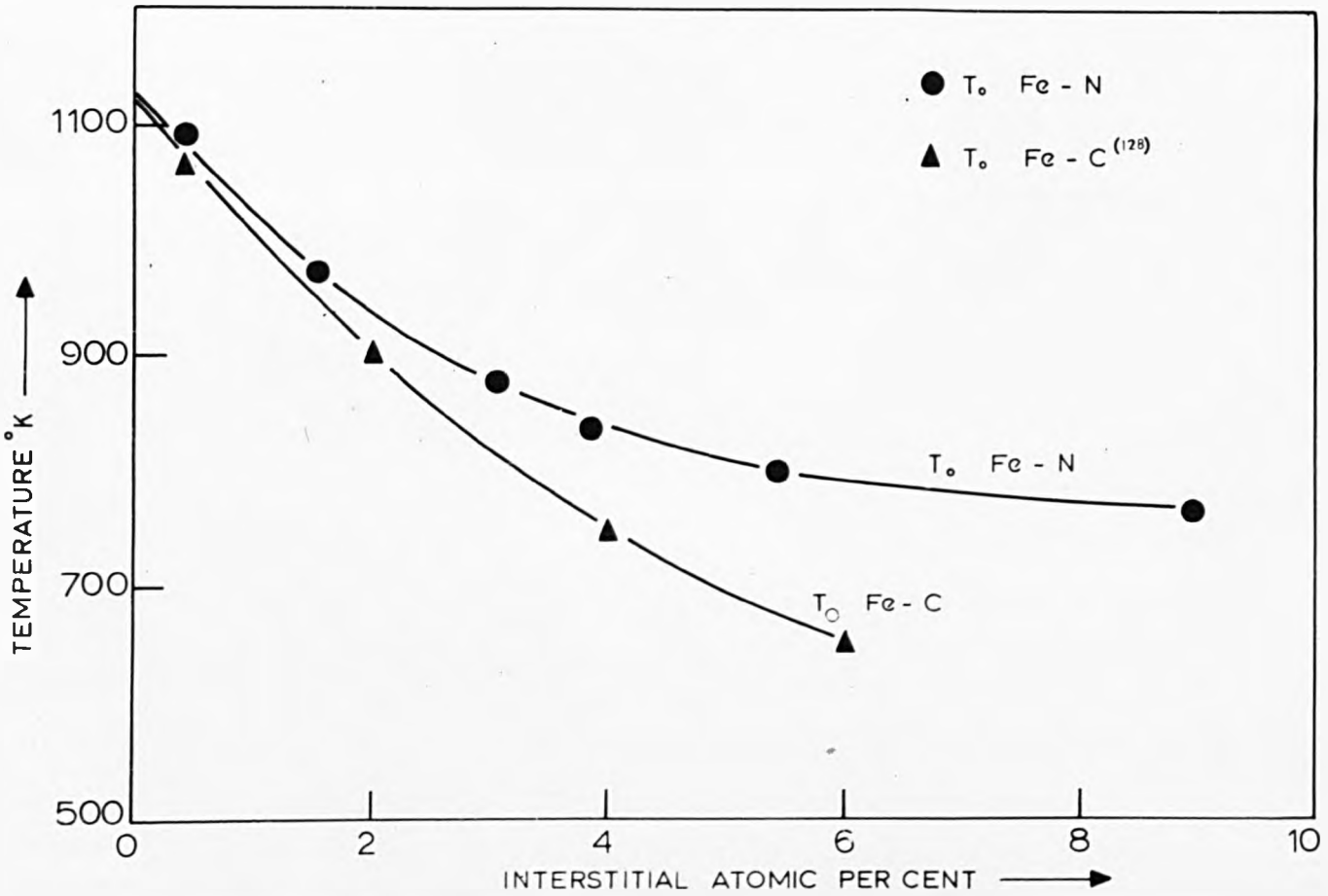

Figure 91. VARIATION OF T_0 WITH COMPOSITION FOR IRON - CARBON AND IRON - NITROGEN ALLOYS (GEOMETRIC K - R - C MODEL[128])

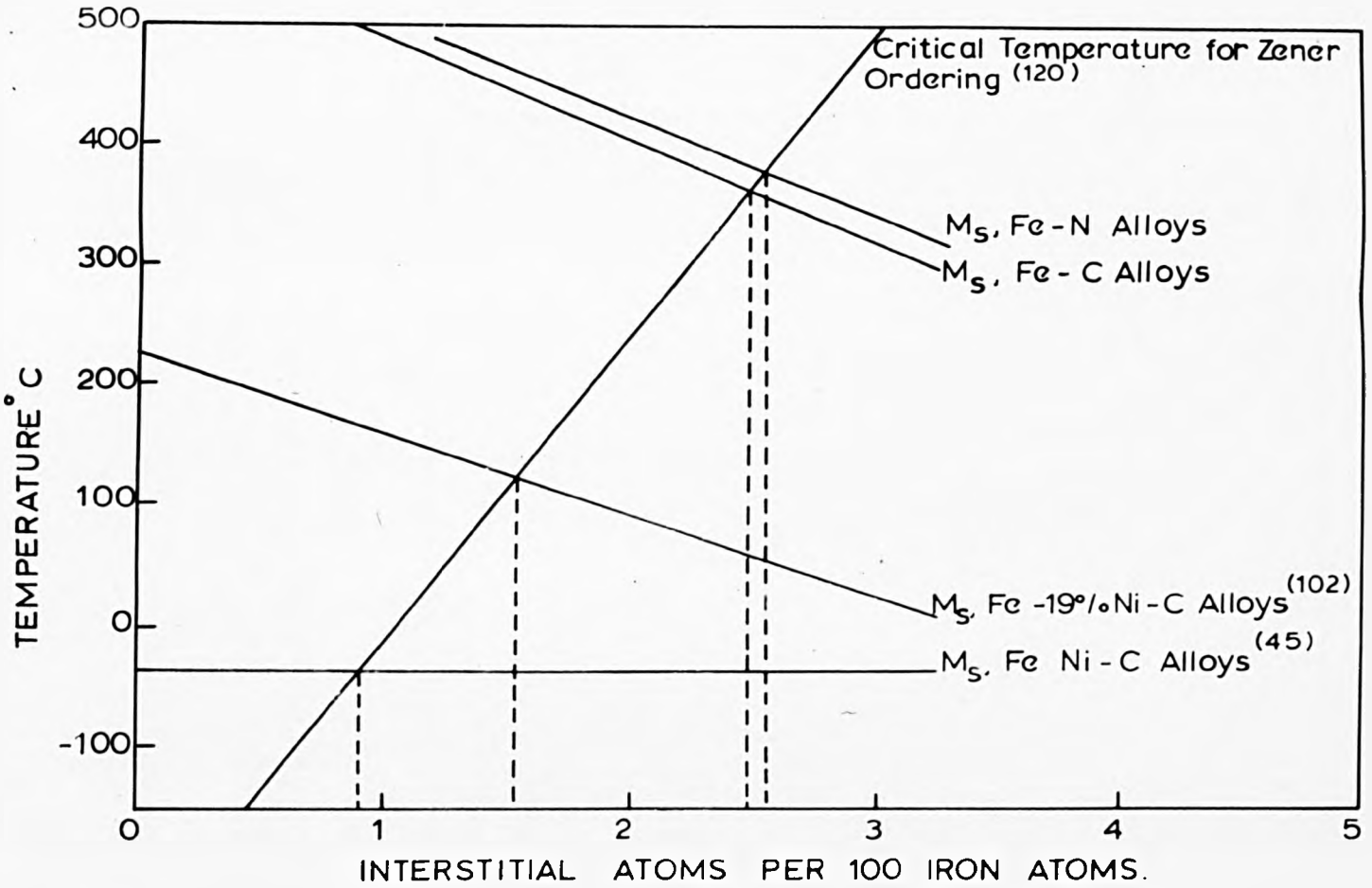

Figure 92. VARIATION OF M_s TEMPERATURES AND THE CRITICAL TEMPERATURE FOR ZENER ORDERING WITH INTERSTITIAL CONTENT FOR IRON-CARBON, IRON NITROGEN AND SOME IRON-NICKEL-CARBON ALLOYS.

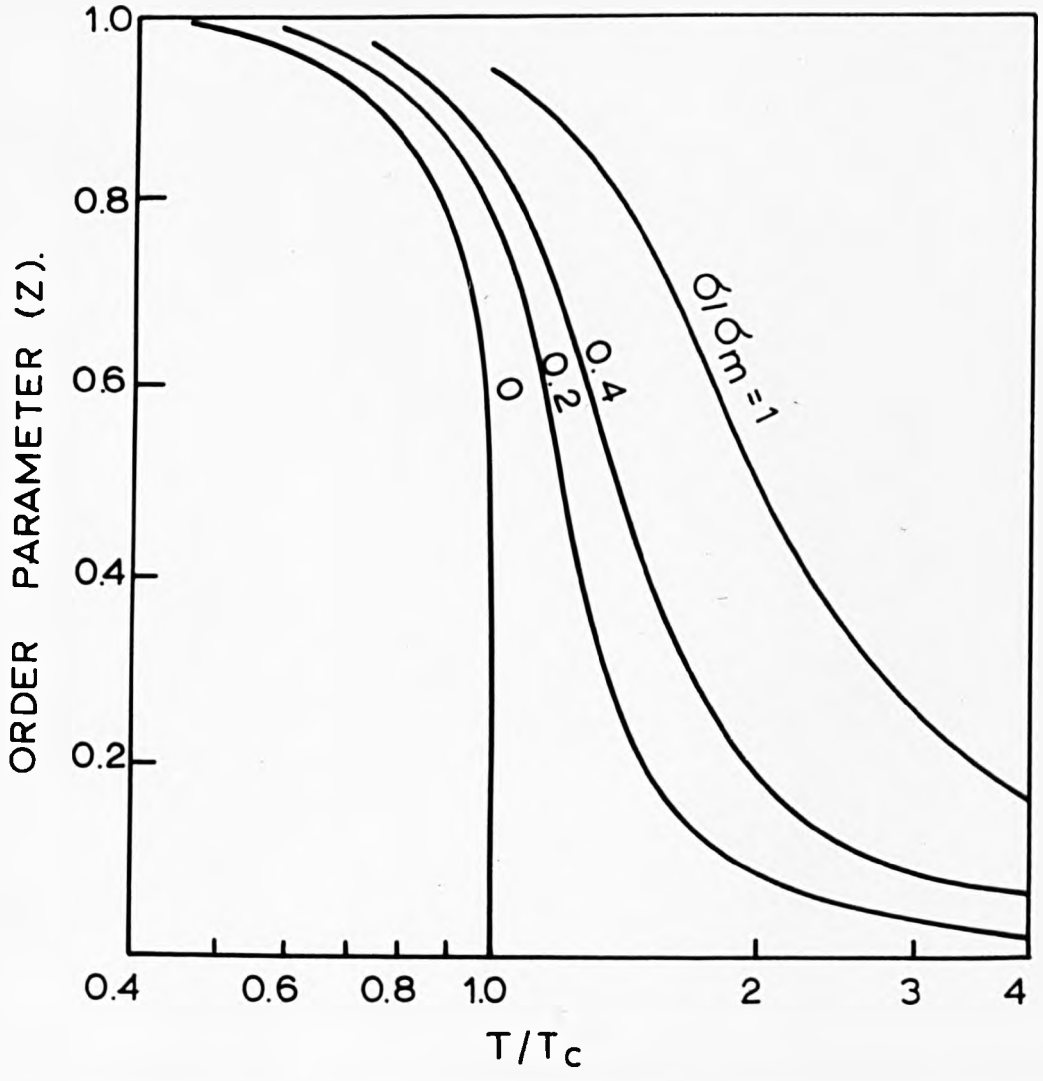

Figure 93. THE DEPENDENCE OF ZENER ORDERING ON TEMPERATURE AND APPLIED STRESS[120]